

22)

New Scaffolds for Molecular Recognition

by

Ken Shimizu
B.A. Chemistry
Cornell University, Ithaca NY

submitted to the Department of Chemistry
in partial fulfillment of the requirements
for the degree of
Doctor of Philosophy

at the
Massachusetts Institute of Technology
September 1995

© 1995 Massachusetts Institute of Technology
All rights reserved



Signature of Author.....

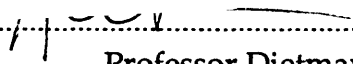
Department of Chemistry
August 25, 1995

Certified by.....



Professor Julius Rebek, Jr.
Thesis Supervisor

Accepted by.....



Professor Dietmar Seyferth
Chairman, Departmental Committee on Graduate Students

MASSACHUSETTS INSTITUTE
OF TECHNOLOGY

SEP 12 1995

Science

LIBRARIES

This doctoral thesis has been examined by a committee on the Department of Chemistry as follows

Professor S. Masamune.....

Chairman

Professor J. Rebek, Jr.....

Thesis Supervisor

Professor S. Virgil

to Linda

New Scaffolds for Molecular Recognition

by Ken D. Shimizu

Submitted to the Department of Chemistry on August 25, 1995 in partial fulfillment of the requirements for the degree of a Doctor of Philosophy in Chemistry.

Abstract

A new family of molecular scaffolds was designed and synthesized for applications in molecular recognition. The rigidity of all the scaffolds was based on a N_{imide}-C_{aryl} bond which showed restricted rotation at ambient temperatures. The conformational restriction led to the synthesis and isolation of the corresponding C- and S-shaped conformers. In addition, the imide linkage was easily formed, and through the modular assembly of xanthene, naphthalene, perylene and anthranilic acid components, a whole array of molecules with different convergent shapes and sizes was prepared.

The C- and S-shaped conformers were identified by x-ray crystallography and bridging experiments. The convergent and divergent shapes of each scaffold led to contrasting properties. The C-shaped isomer, in particular, was able to bind guests, alter the selectivity of a reaction and perform catalysis. The convergent C-shaped scaffold was also utilized as a ligand to bind alkali metals and noble metals between two nitriles in an unusual *trans*- geometry.

A second molecular recognition system was also developed which could self-assemble. A calix[4]arene was synthesized which dimerized to form a large cavity capable of encapsulation. This new self-assembling capsule relies on a novel array of eight ureas hydrogen bonded in a circular fashion. The resulting cavity was of sufficient size to bind guests such as ethyl benzene and *p*-xylene.

Finally, a xanthene tetraacid was synthesized which could be selectively mono- and di- functionalized. The polyfunctionalized molecule has shown utility as a core for a new solution based strategy of combinatorial libraries.

Thesis Supervisor: Professor Julius Rebek, Jr.
Title: Camille Dreyfus Professor of Chemistry

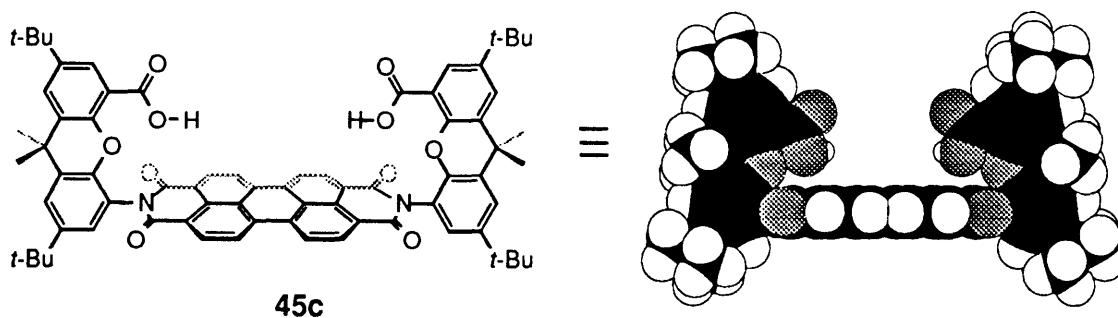
Preface

'I do my best work at night.'

-Mae West

The focus of the research presented in this thesis is the design and synthesis of new molecular scaffolds. The unique architectures and stringent steric requirements made the synthesis of scaffolds like **45c** extremely challenging. The price of admission was high, but the show was a good one. Once synthesized, the scaffolds turned out to have remarkable properties which often necessitated ingenuity to understand and to exploit. These beautiful molecules have provided me much food for thought and fodder for my frustrations.

This research has been performed under the guidance of Professor Julius Rebek, Jr., to whom I owe much. His patience and faith have allowed my development as a scientist. He encouraged participation in all aspects of a project from a molecule's conception 'in silico' to probing its properties in solution. I have particularly appreciated his brain over brawn approach to chemistry and his uncommon recognition of its human aspect.



In addition, the work presented in this thesis owes much to many co-workers, past and present: To James Nowick, for work on the xanthene tetraacid; To Torrin Dewey, for work on the perylene scaffolds and crystallography; To Takashi Oi, for applications of the perylene scaffolds; And to Blake and Linda, Roland, Anthony and Alex with whom both coffee and chemistry became addictions.

Ken D. Shimizu

Table of Contents

Abstract.....	7
Preface.....	9
Table of Contents.....	11
Chapter I An Introduction to Molecular Recognition.....	15
1.1 Introduction.....	15
1.2 Common Building Blocks.....	16
1.3 Macrocycles and Clefts.....	20
1.4 Preorganization and Structural Rigidity.....	20
1.5 Modular Synthesis and Solubility.....	21
1.6 Non-Covalent Interactions.....	23
1.7 Applications.....	29
Chapter II Synthesis of C- and S-Shaped Perylene Scaffolds.....	37
2.1 Introduction.....	37
2.2 Background.....	38
2.3 Synthesis of the Xanthene U-Turn.....	42
2.4 Perylene Cleft Assembly.....	46
2.5 Functionalization of Perylene Scaffolds.....	49
2.6 Monofunctionalization.....	52
2.7 Outlook.....	54
2.8 Experimental.....	55
Chapter III Synthesis of C- and S-Shaped Naphthalene Scaffolds.....	65
3.1 Introduction.....	65
3.2 Background.....	66
3.3 Assembly of the Xanthene Derived Naphthalene Scaffolds.....	67

3.4	Assembly of Anthranilic Acid Derived Scaffolds.....	68
3.5	Assembly of a Hybrid Scaffold.....	70
3.6	Functionalization of Naphthalene Scaffolds.....	71
3.7	Outlook.....	73
3.8	Experimental Section.....	74
Chapter IV	Structure and Properties of the New Diimide Scaffolds.....	79
4.1	Introduction.....	79
4.2	Background.....	79
4.3	Origins and Barrier of Restricted Rotation.....	81
4.4	Assignment of Perylene Isomers.....	84
4.5	Assignment of Naphthalene Isomers.....	88
4.6	Dimensions of the C-Shaped Isomers.....	91
4.7	Binding Properties of Perylene Clefs.....	93
4.8	Properties of the Naphthalene Scaffolds.....	97
4.9	Outlook.....	99
4.10	Experimental.....	101
Chapter V	Metal Binding: A Calcium Ionophore and a <i>trans</i>-Spanning Dinitrile Ligand.....	105
5.1	Introduction.....	105
5.2	Background.....	106
5.3	Alkaline Metal Binding.....	110
5.4	A <i>trans</i> -Dinitrile Ligand.....	113
5.5	Outlook.....	120
5.6	Experimental.....	121
Chapter VI	A Self-Assembling Molecular Container.....	125
6.1	Introduction.....	125
6.2	Background.....	126
6.3	Design.....	131
6.4	Synthesis of Calix[4]arene Tetraurea 140.....	136

6.5 Assembly.....	137
6.6 Encapsulation.....	141
6.7 Discussion.....	145
6.8 Cavity Size and Shape.....	148
6.9 Outlook.....	151
6.10 Experimental.....	152
Chapter VII A Selectively Functionalizable Molecular Scaffold with Four Carboxylic Acid Sites.....	157
7.1 Introduction.....	157
7.2 Background.....	157
7.3 Synthesis.....	158
7.4 Outlook.....	160
7.5 Experimental.....	161
Appendix I(crystal data).....	165

Chapter I

An Introduction to Molecular Recognition

1.1 INTRODUCTION

Few molecules are islands unto themselves, and thus, many of the important properties of matter are the direct consequence of **intermolecular** interactions. Melting point, viscosity, and solubility are just a few of the more common examples. Non-covalent interactions are also prevalent in biological systems and are found in enzymes, DNA, proteins, antibodies, membranes and receptors. The remarkable specificity, reaction control, and rate accelerations observed in Nature are also the result of intermolecular interactions. All of these examples illustrate the importance of molecular recognition to the properties of life and matter and provide pressing reasons for studying how molecules interact.

Almost 100 years earlier, Emil Fischer used the analogy of a lock and key to describe the receptor-guest interaction.¹ Yet, until recently little had been known about "intermolecular" bonds. The reasons probably lie in the relatively weak nature of non-covalent interactions, leading to structures of fleeting stability. The modern field of molecular recognition began in 1967 with Pedersen's synthesis of crown ethers. These man-made macrocyclic receptors were capable of binding alkali metals with amazing efficiency and selectivity.² Since then, synthetic receptors such as crown ethers, calixarenes, and Kemp's triacid have all become commercially available and have even found utility as synthetic reagents. The field has also accumulated a number of names including: host-guest chemistry and supramolecular chemistry. In 1987, the emerging multi-disciplinary field was acknowledged with a Nobel Prize.³

¹ Fischer, E. *Ber. Dtsch. Chem. Ges.* **1894**, *27*, 2985.

² a) Pedersen, C. J. *J. Am. Chem. Soc.* **1967**, *89*, 7017. b) Pedersen, C. J. *J. Am. Chem. Soc.* **1967**, *89*, 2495.

³ a) Cram, D. J. *Angew. Chem.* **1988**, *100*, 1041. b) Lehn, J.-M. *Angew. Chem.* **1988**, *100*, 91. c) Pedersen, C. J. *Angew. Chem.* **1988**, *100*, 1053.

Applications for molecular recognition are still emerging as the ground rules of how molecules interact becomes clearer. In general, these have fallen under three general headings:

- 1) Biomimetics and molecular devices.
- 2) Non-covalent synthesis.
- 3) Responsive host-guest systems.

Already, the study of synthetic receptors has led to a better understanding of drug design, DNA structure and protein folding. More recently the development of molecular devices capable of sensing, photo switching,⁴ separation,⁵ motion⁶ and transport⁷ have become a major focus of the field.

This introductory chapter will seek to highlight some general aspects of molecular recognition which have recently come to light, utilizing examples from the literature. This survey is by no mean comprehensive, for which there are existing review articles.⁸

1.2 COMMON BUILDING BLOCKS

At the heart of most molecular recognition systems lies a rigid molecular scaffold. They serve the vital role of positioning functionality at precise distances and orientations. Nature has taken a similar approach and utilizes peptide, carbohydrate, and nucleoside frameworks. However, these complex macromolecular structures are difficult to synthesize, redesign and study.

⁴ Irie, M.; Kato, M. *J. Am. Chem. Soc.* **1985**, *107*, 1024-1028.

⁵ Atwood, J. L.; Koutsantonis, G. A.; Raston, C. L. *Nature* **1994**, *368*, 229-231.

⁶ Taylor, E. W. *Science* **1993**, *261*, 35-36.

⁷ Chia, P. S. K.; Lindoy, L. F.; Walker, G. W.; Everett, G. W. *J. Am. Chem. Soc.* **1991**, *113*, 2533.

⁸ For reviews on molecular recognition and supramolecular chemistry see: a) Seel, C.; Vögtle, F. *Angew. Chem., Int. Ed. Engl.* **1992**, *31*, 528-549. b) Vögtle, F. *Supramolecular Chemistry*; John Wiley and Son: Chichester, 1993. c) Diederich, F. *Cyclophanes*; RSC: Cambridge, 1991. d) *Frontiers in Supramolecular Organic Chemistry and Photochemistry*; Schneider, H.-J.; Dürr, H., Ed.; VCH: New York, 1991. e) Dugas, H. *Bioorganic Chemistry: A Chemical Approach to Enzyme Action*; second ed.; Springer-Verlag: New York, 1989.

Consequently, smaller synthetic frameworks have been developed for use as artificial receptors and catalysts. No longer limited to natural products, the number of potential hosts is greatly expanded. The precise connectivity of atoms is no longer important. Instead, the overall three-dimensional structure is of paramount importance. The development of computational molecular modeling has been extremely helpful in visualizing three dimensional geometries and in predicting intermolecular complementarity. However this tool is still arguably inaccurate and high level calculations inaccessible to the normal organic chemist. Thus, the resulting 'in silico' structures must be taken with certain caveats.

Ones' imagination is still limited by a receptor's synthetic feasibility. Commonly, molecular scaffolds have stringent geometric constraints and often pack a large amount of functionality into a small area. These attributes make their syntheses extremely challenging. For this reason, once a scaffold's synthesis has been established and its conformation determined, the molecules are used repeatedly. Table I-1 lists and Figure I-1 illustrates some of the more common frameworks utilized in molecular recognition. In general, these scaffolds share some common traits:

- 1) A concave shape to focus functionality inwards.
- 2) Preorganization so that functionality spends most of its time in the desired conformation.
- 3) Structural rigidity to prevent the collapse of the binding pocket.
- 4) An adaptable modular synthesis.
- 5) Solubility in an appropriate solvent in which the desired non-covalent interactions are potent.

The challenge is to design a structure possessing all of the above attributes and to do so with an economy of structure and synthesis. In practice, one must sometimes sacrifice one characteristic to incorporate another. However, the complete lack of any one of these traits will hamper the binding abilities of a synthetic receptor often to the degree that binding is not observed. A variety of strategies have been developed to tailor each of these desirable characteristics into a molecular receptor, and these will be examined in the following sections.

building block	researcher(s)	molecule in Figure 1
aza-crown ethers	F. Vögtle ⁹	c
bis-arylporphyrins	J. K. M. Sanders ¹⁰	b
calixarenes	C. D. Gutsche ¹¹ D. Reinhoudt ¹² S. Shinkai ¹³	f
crown ethers	D. Cram ¹⁴ J.-M. Lehn ¹⁵ Pedersen ¹⁶	c
cyclodextrins	M. Bender ¹⁷ R. Breslow ¹⁸ I. Tabushi ¹⁹	a
cyclophanes	F. Dieterich	e
cycloveratrilenes	A. Collet ²⁰	d
2,6-diaminopyridines	A. Hamilton ²¹	k
glycourils	R. Nolte ²²	h
Kemp's triacids	J. Rebek, Jr. ²³	g
1,10-phenanthroline	J. P. Sauvage ²⁴	j
Tröger's bases	C. Wilcox ²⁵	i

Table I-1. Common building blocks in molecular recognition.

- ⁹ Ebmeyer, F.; Vögtle, F. *Angew. Chem.* **1989**, *101*, 95.
- ¹⁰ Anderson, S.; Anderson, H. L.; Sanders, J. K. M. *Acc. Chem. Res.* **1993**, *26*, 469-475.
- ¹¹ (a) Gutsche, C. D. *Progr. Macrocyclic Chem.* **1987**, *3*, 93. (b) Gutsche, C. D. *Calixarenes*; Royal Society of Chemistry: Cambridge, 1989.
- ¹² Dijkstra, P. J.; Brunink, J. A. J.; Bugge, K.-E.; Reinhoudt, D. N.; Harkema, S.; Ungaro, R.; Ghidini, E. *J. Am. Chem. Soc.* **1989**, *111*, 7567.
- ¹³ Shinkai, S.; Araki, K.; Matsuda, T.; Nishiyama, N.; Ideda, H.; Takasu, I.; Iwamoto, M. *J. Am. Chem. Soc.* **1990**, *112*, 9053.
- ¹⁴ Cram, D. J. *Angew. Chem.* **1988**, *100*, 1041.
- ¹⁵ Lehn, J.-M. *Angew. Chem.* **1988**, *100*, 91.
- ¹⁶ Pedersen, C. J. *J. Am. Chem. Soc.* **1967**, *89*, 7017.
- ¹⁷ Bender, M. L.; Komiyama, M. *Cyclodextrin Chemistry*; Springer: New York, 1978.
- ¹⁸ Breslow, R. *Science* **1982**, *218*, 532.
- ¹⁹ Tabushi, I. *Pure & Appl. Chem.* **1986**, *58*, 1529.
- ²⁰ Collet, A. *Tetrahedron* **1987**, *43*, 5725-5759.

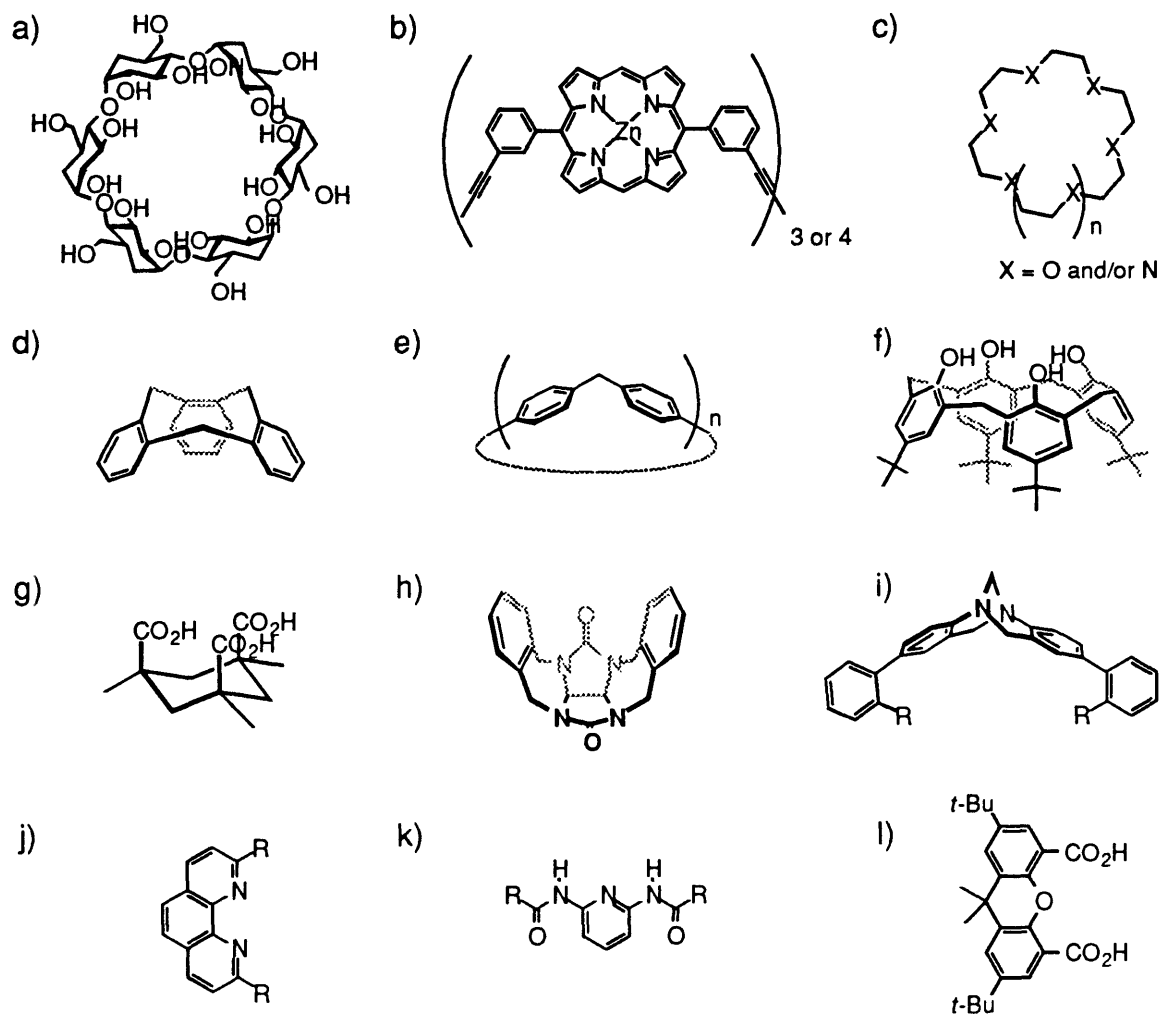


Figure I-1. Common scaffolds in molecular recognition.

- 21 Chang, S.-K.; Van Engen, D.; Fan, E.; Hamilton, A. D. *J. Am. Chem. Soc.* **1991**, *113*, 7640.
- 22 a) Smeets, J. W. H.; Sijbesma, R. P.; Niele, F. G. M.; Spek, A. L.; Smeets, W. J. J.; Nolte, R. J. M. *J. Am. Chem. Soc.* **1987**, *109*, 928. b) Sijbesma, R. P.; Kentgens, A. P. M.; Lutz, E. T. G.; van der Maas, J. H.; Nolte, R. J. M. *J. Am. Chem. Soc.* **1993**, *115*, 8999-9005. c) van Nunnen, J. L. M.; Stevens, R. S. A.; Picken, S. J.; Nolte, R. J. M. *J. Am. Chem. Soc.* **1994**, *116*, 8825-8826.
- 23 Rebek, J., Jr. *Angew. Chem. Int. Ed. Engl.* **1990**, *29*, 245-255.
- 24 Dietrich-Buchecker, C. O.; Guilhem, J.; Pascard, C.; Sauvage, J. P. *Angew. Chem., Int. Ed. Engl.* **1990**, *29*, 1154.
- 25 Webb, T. H.; Wilcox, C. S. *J. Org. Chem.* **1990**, *55*, 363

1.3 MACROCYCLES AND CLEFTS

Synthetic receptors fall into two general topologies: macrocycles and molecular clefts (also referred to as molecular 'tweezers' and/or 'clips'). Both topologies possess the desired concave shape and both position functionality in a convergent fashion. Whether by accident or design both structures can be visualized as two-dimensional simplifications of the three-dimensional bowl-shaped cavities of enzymes and antibodies (Figure I-2).

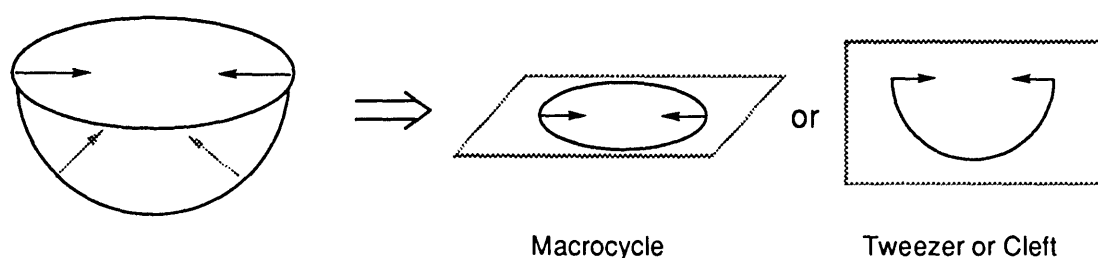


Figure I-2. Schematic representations of a three-dimensional binding pocket and two-dimensional simplifications.

Macrocycles have been extremely successful and were the dominant molecular architecture in earlier molecular recognition studies. Cyclic structures such as cyclophanes, calixarenes, cyclodextrins and cyclotrimerelanes all possess hydrophobic cavities to complex organic guests. Polar functionalities can also be organized in a circular manner as exemplified by crown ethers, aza crowns and phenanthraline based systems which bind metals and ammonium ions.

On the other hand, acyclic clefts, clips, and tweezers must position functionality through a rigid C-shape. Clips and tweezers generally contain two aromatic surfaces which 'pinch' aryl guests between them, whereas clefts organize polar functionality capable of hydrogen bonding or metal coordination.

1.4 PREORGANIZATION AND STRUCTURAL RIGIDITY

For both macrocycles and clefts, proper preorganization can significantly augment binding strengths. This conformational fixing is achieved via covalent

and non-covalent restraints. Still's acyclic crown ether analog **1** is an excellent example of both organizational strategies. Non-covalent interactions have been carefully incorporated into **1**'s polyether backbone to induce it to fold up into a concave ionophore.²⁶ This preorganization is evident in its binding abilities. Tetrahydropyranoid **1** was considerably more efficient at binding Li^+ and Na^+ than the unorganized triglyme dimethyl ether **2**. In fact, acyclic **1** was an even better ionophore than the cyclic 12-crown-4 (**3**).

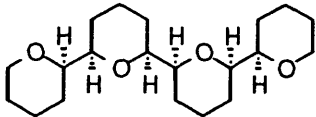
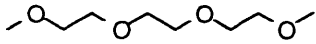
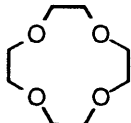
		Association Constants of Ionophores	
		Li^+	Na^+
1		3.0×10^5	4.3×10^5
2		1.2×10^4	$< 5.0 \times 10^3$
3		1.6×10^4	7.3×10^3

Figure I-3. Relative binding affinities of various cyclic and acyclic ethers.

Ionophore **1** also highlights the importance of covalent restraints. 'Tying down' the poly-ether backbone with cyclic tetrahydropyrans further restricts the receptors internal rotations. Covalent preorganization is also manifested in synthetic receptors through the generous use of rigid aromatic components.

1.5 MODULAR SYNTHESIS AND SOLUBILITY

A popular strategy for assembling synthetic receptors has been to construct them from modular components. This convergent approach enables the rapid construction of whole families of architecturally similar hosts through the use of interchangeable components. For example, appending two Kemp's triacid units

²⁶ Iimori, I.; Still, C. W.; Rheingold, A. L.; Staley, D. L. *J. Am. Chem. Soc.* 1989, 111, 3439.

to different spacers results in a variety of receptors of varying size, shape and binding selectivities (Figure I-4). Receptor 4 binds adenine with a binding constant $> 10^4 \text{ M}^{-1}$, whereas 5 has an affinity for diketopiprazines and 6 for dipeptides.^{27,28}

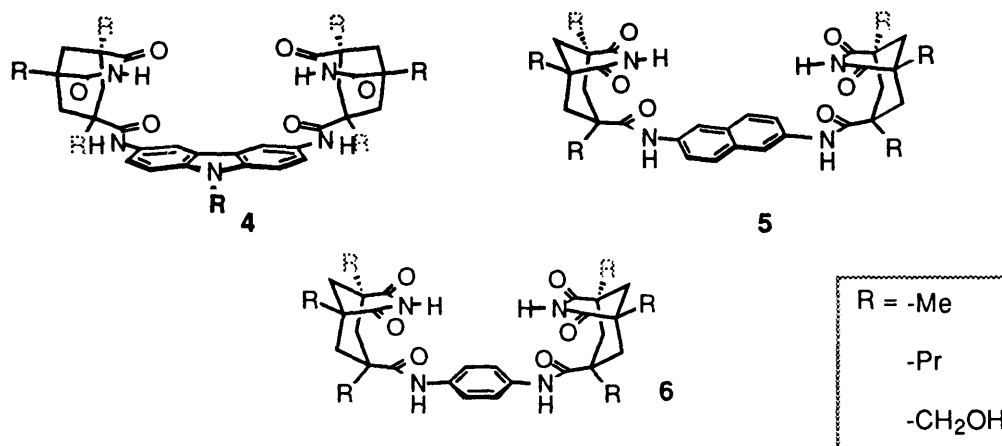


Figure I-4. Bis(Kemp's triacid) clefts of varying size and shape.

Of equal importance to the properties of these clefts were their peripheral solubilizing groups. Initially, the Kemp's triacid units were synthesized with methyl groups. However, because of poor solubility in organic solvents, a tripropyl Kemp's triacid was developed.²⁹ The increased solubility allowed the assembly of larger more complex receptors. Clefts soluble in more polar solvents were prepared by the introduction of pendant alcohols.³⁰ These water soluble clefts have allowed the evaluation and comparison of various non-covalent interactions in a variety of environments.³¹

²⁷ Conn, M. M.; Deslongchamps, G.; de Mendoza, J.; Rebek, J., Jr. *J. Am. Chem. Soc.* **1993**, *115*, 3548-3557.

²⁸ Famulok, M.; Jeong, K.-S.; Deslongchamps, G.; Rebek, J. *Angew. Chem. Int. Ed. Engl.* **1991**, *30*, 858-860.

²⁹ Jeong, K. S.; Tjivikua, T.; Muehldorf, A.; Deslongchamps, G.; Famulok, M.; Rebek, J., Jr. *J. Am. Chem. Soc.* **1991**, *113*, 201.

³⁰ Rotello, V. M.; Viani, E. A.; Deslongchamps, G.; Murray, B. A.; Rebek, J., Jr. *J. Am. Chem. Soc.* **1993**, *115*, 797-798.

³¹ Kato, Y.; Conn, M. M.; Rebek, J., Jr. *Proc. Nat. Acad. Sci. USA* **1994**, in press.

1.6 NON-COVALENT INTERACTIONS

Nature utilizes an array of non-covalent interactions often in complex combinations which has made their individual study difficult. In contrast, most synthetic hosts utilize only one or two types of interactions and can be more easily altered, manipulated, and functionalized. Not surprisingly, recent studies of non-covalent interactions have focused on synthetic receptors, leading to new insights into the nature of these interactions. This section will seek to outline the non-covalent interactions utilized in the course of this thesis, using examples of synthetic receptors from the literature.

Hydrogen bonds have been implicated as a major contributor to the specificity of enzymes, the fidelity of protein folding and the complementarity of double stranded DNA.³² For all of its apparent importance, a single hydrogen bond is still a fairly weak interaction. In solution, hydrogen bond strengths have been measured to be 0.5 to 1.8 kcal mol⁻¹; although in the gas phase they are considerably stronger (5 to 10 kcal mol⁻¹). Much of the power of hydrogen bonds results from the high specificity of the interaction. The reasons are twofold: the directionality and the two component nature of the hydrogen bond. The interaction usually occurs between a polar atom, commonly N or O, and an acidic proton. The heavy atom to heavy atom distances have been measured to be 1.7 to 3.10 Å for neutral molecules. In addition, the interaction tends to be linear with the X-H...X' angle close to 180 °.³³

Two examples of synthetic receptors which utilize hydrogen bonds as the basis for association are shown in Figure I-5. The macrocyclic host **7** from Hamilton *et al.* employs two diamido-pyridines to encircle a barbiturate with six hydrogen bonds.³⁴ Rebek *et al.* have prepared a chiral cleft **8**, which was able to

³² Fersht, A. R. *Trends Biochem. Sci.* **1987**, *12*, 3.

³³ There has been recent research that suggest that the linearity of hydrogen bonds is merely a statistical anomaly, in which the average position of the hydrogen bond acceptor tends to be on line with the X-H bond.

³⁴ Chang, S.-K.; Van Engen, D.; Fan, E.; Hamilton, A. D. *J. Am. Chem. Soc.* **1991**, *113*, 7640.

discriminate between enantiomers of diketopiprazines via hydrogen bonding (Figure I-5).³⁵

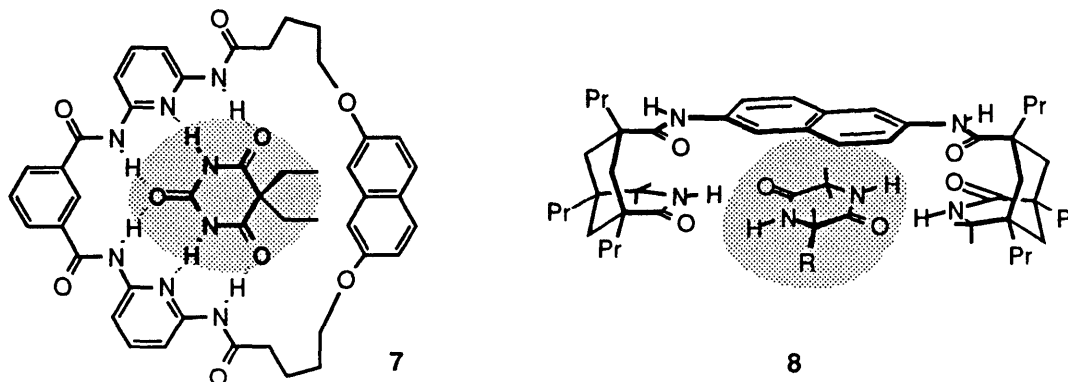


Figure I-5. Synthetic receptors utilizing hydrogen bonding arrays.

Previously, the strengths of hydrogen bonds have been shown to roughly correlate to the acidity of their proton donors and basicity of their proton acceptors.³⁶ More recently, the study of hydrogen bonding arrays in synthetic receptors has shown that the arrangement of donors and acceptors can effect the overall stability of the complex.³⁷ These 'secondary interactions' occur between adjacent donors and acceptors on opposing molecules (Figure I-6) and can either augment or detract from the existing primary hydrogen bond interactions. For example in Figure I-6a, all the secondary interactions are attractive, further stabilizing the complex.³⁸ Conversely in Figure I-6b, the cross terms are all repulsive.

³⁵ Jeong, K. S.; Muehldorf, A. V.; Rebek, J., Jr. *J. Am. Chem. Soc.* **1990**, *112*, 6144-6145.

³⁶ Pogorelyi; Vishnyakova *Russ. Chem. Rev.* **1984**, *53*, 1154.

³⁷ Jorgensen, W. L.; Pranata, J. *J. Am. Chem. Soc.* **1991**, *113*, 209.

³⁸ Jorgensen, W.; Pranata, J. *J. Am. Chem. Soc.* **1990**, *112*, 2008.

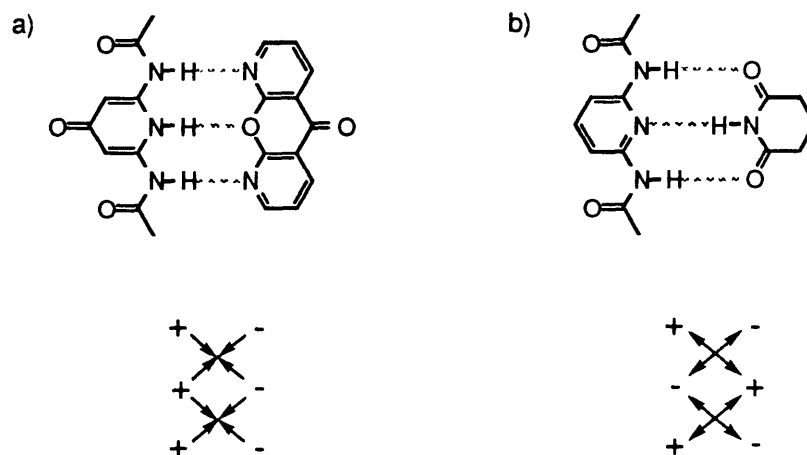


Figure I-6. a) A hydrogen bond array with stabilizing secondary interactions. b) A hydrogen bond array with destabilizing secondary interactions.

Pi-interactions take advantage of the electron rich molecular orbitals of aromatic and vinyl systems. These associations are responsible for the base stacking in DNA and intercalation of drugs between adjacent base pairs. Hunter and Sanders have recently developed a simple model to estimate the strength and geometric requirements of the aryl-aryl interactions.³⁹ The attractive forces were not attributed to pi-pi interactions, which actually repel each other due to the electron rich character of pi clouds. Instead, aryl-aryl interactions are the result of pi-sigma to pi-sigma and of polarized aryl hydrogen to pi interactions. Aryl-aryl geometries match the local polarizations in the aromatic surfaces and aryl C-H's. As a consequence, the observed energy minimums are often off-set in the 'face to face' geometries and also include 'edge to face' geometries, as shown in Figure I-7. Clearly, the aryl-aryl interaction is not merely driven by the desire to maximize orbital overlap.

³⁹ Hunter, C. A. *J. Chem. Soc, Chem. Commun.* 1991, 749-751.

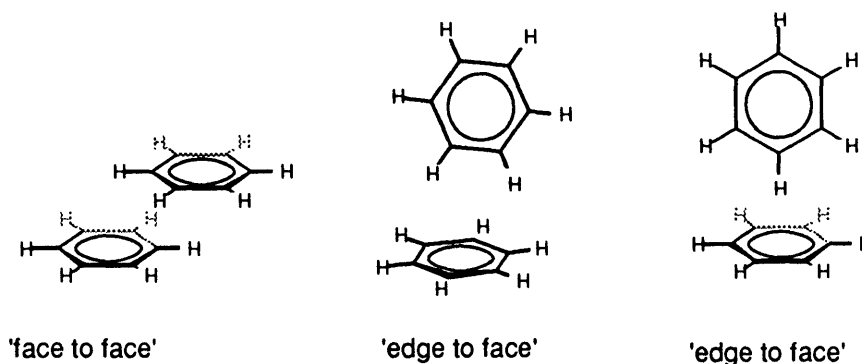


Figure I-7. Some of the more stable aryl-aryl geometries.

The most stable conformation is still subject to argument. Part of the difficulty lies in extricating the contributions of VDW's and electron-donor-acceptor interactions. Statistical examinations of crystal databases have produced a range of distances for each geometry.⁴⁰ In the 'face to face' arrangement, the two aromatic planes are separated by a distance of 3.25 to 3.6 Å. The 'edge to face' geometries had hydrogen to benzene plane distances of 2.2 to 2.6 Å.

Synthetic receptors have been made which take advantage of both 'edge to face' and 'face to face' interactions. Zimmerman's molecular tweezer **9** can sandwich a nucleoside between two rigidly held aromatic surfaces with a high degree of 'face to face' complementarity. This highly preorganized receptor binds adenine with a large binding constant of 6.0 kcal mol⁻¹ in CDCl₃.⁴¹ Whitlock *et al.* have prepared macrocycle **10** which creates an aromatic pocket.⁴² Complexation of aromatic guests was driven by both 'edge-face' and 'face-face' interactions.

⁴⁰ Burley, S. K.; Petsko, G. A. *J. Am. Chem. Soc.* **1988**, *108*, 7995.

⁴¹ Zimmerman, S.; Wu, W. *J. Am. Chem. Soc.* **1989**, *111*, 8054-8055.

⁴² Cochran, J. E.; Parrott, T. J.; Whitlock, B. J.; Whitlock, H. W. *J. Am. Chem. Soc.* **1992**, *114*, 2269-2270.

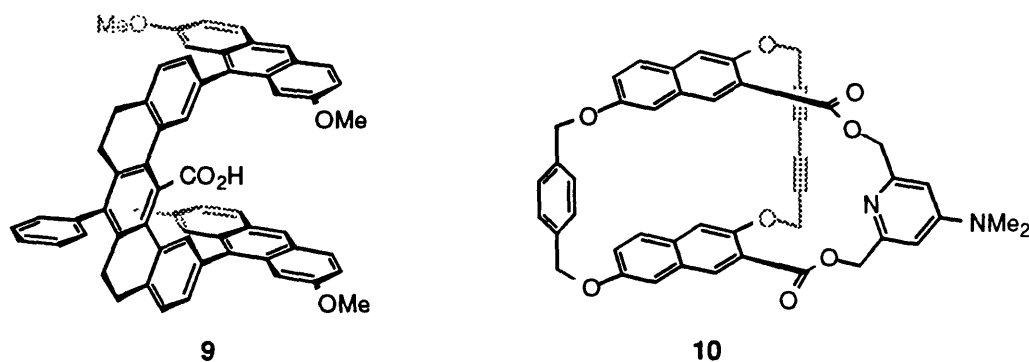


Figure I-8. Synthetic receptors utilizing aryl-aryl interactions.

Metal coordination: Metals can either act as guests or as intermediaries to bring organic components together. Because of their charged character, metal-ligand interactions tend to be stronger than neutral non-covalent interactions. A variety of arrangements are possible depending upon the metal used and the number of binding sites on the ligand. For example, Hunter *et al.* have utilized the zinc-porphyrin • pyridine interaction to assemble a variety of complex structures (Figure I-9).⁴³ Dimer 11 is particularly interesting because upon assembly, it becomes an excellent host for a third molecule. The amide -NH's are arranged on the interior surface of the assembly and can hydrogen bond to the carbonyls of a quinone. Alternatively, J.-M. Lehn has utilized metals as templates to organize organic ligands. The self-assembling system 12 consists of three Cu(I) ions and two tris(bipyridyl) ligands. While all these metal-ligand interactions are far stronger than hydrogen bonds or pi-pi interactions, they still form reversibly. This structural flexibility allows these systems to assemble into the thermodynamically most stable structure. For example, in Lehn's '3 + 2' system we can envision a variety of off-set or polymeric structures. These less stable aggregates do form but in the end the thermodynamic products shown predominate.

⁴³ Hunter, C. A.; Sarson, L. D. *Angew. Chem., Int. Ed. Engl.* 1994, 33, 2313-2316.

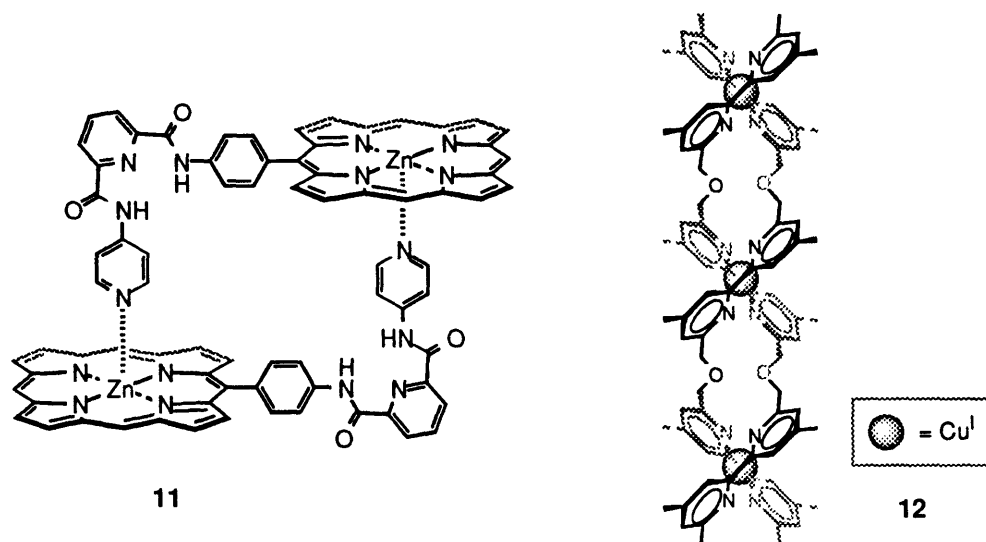


Figure I-9. Molecular recognition systems utilizing metal coordination.

Solvation plays an important and sometimes overriding role in determining the strengths of non-covalent interactions.⁴⁴ Because of the very nature of intermolecular bonds, solvent molecules also compete for the 'affections' of the host and guest. Solvents with strong attractions for either the host and/or guest will surround the(se) component(s) and obstruct complexation. Because of their overwhelming stoichiometric advantage, solvent molecules do not have to interact strongly to have dire consequences for complex formation. Alternatively, the solvent can assist and provide the driving force for complexation. For example, the hydrophobicity of host or a portion of the host (and/or guest) can actually force complexation through repulsive forces.

For example, cyclophane **13** has been shown to bind pyrene in a wide range of solvents.⁴⁵ The same non-covalent interactions are present between host and guest in every solvent, yet the binding constants varied from 3 kcal/mol in carbon disulfide to 9 kcal/mol in water. This variation is caused by the intervening solvent which augments or diminishes the apparent binding forces between host **13** and pyrene.

⁴⁴ Diederich, F. *J. Chem. Ed.* **1990**, *67*, 813-820.

⁴⁵ a) Diederich, F. *Angew. Chem., Int. Ed. Engl.* **1988**, *100*, 372-396. b) Smithrud, D. B.; Diederich, F. *J. Am. Chem. Soc.* **1990**, *112*, 339-343.

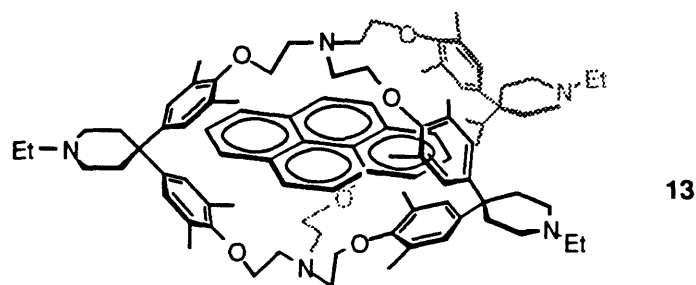


Figure I-10. Cyclophane 13 binding pyrene.

1.7 APPLICATIONS

Biomimetic systems and supramolecular devices

Carefully designed molecular recognition systems can be thought to represent information stored in a structural and temporal sense. This 'programming' enables molecular recognition systems to carry out tasks such as catalysis, communication, regulation, self-organization and replication. These seemingly elementary processes lie at the very core of what makes life so special. Understanding and mimicking the remarkable catalytic abilities of enzymes has been a major focus of molecular recognition research.⁴⁶ Synthetic catalysts and model enzymes fall into two general categories: enthalpic and entropic catalysts.

The principle of binding and stabilizing the transition state was first recognized by L. Pauling.⁴⁷ Perhaps the most powerful application of this theory has been the successful development of catalytic antibodies which are elicited from transition state analogs. The development of small synthetic receptors which bind transition states or which lower the activation energy of a reaction by introducing alternative pathways has been considerably more difficult. Only a few effective systems have been synthesized and most accelerate bond breaking reactions (e.g. hydrolysis or aminolysis). Hamilton *et al.* has prepared host 14 which assists in phosphodiester cleavage by binding to and stabilizing the

⁴⁶ Reichwein, A. M.; Verboom, W.; Reinhoudt, D. N. *Recl. Trav. Chim. Pays-Bas* 1994, 113, 1994.

⁴⁷ Pauling, L. *Nature* 1948, 161, 707.

anionic transition state.⁴⁸ Dougherty's cyclophane receptor **15** is another example of an enthalpic catalyst.⁴⁹ The aromatic pocket of **15** accelerates the methylation of quinoline by stabilizing the forming charge through the newly discovered cation- π interactions.⁵⁰ This interaction has been proposed to be present in enzymes which catalyze reactions with cationic transition states and have a high concentration of aromatic groups surrounding the active site.

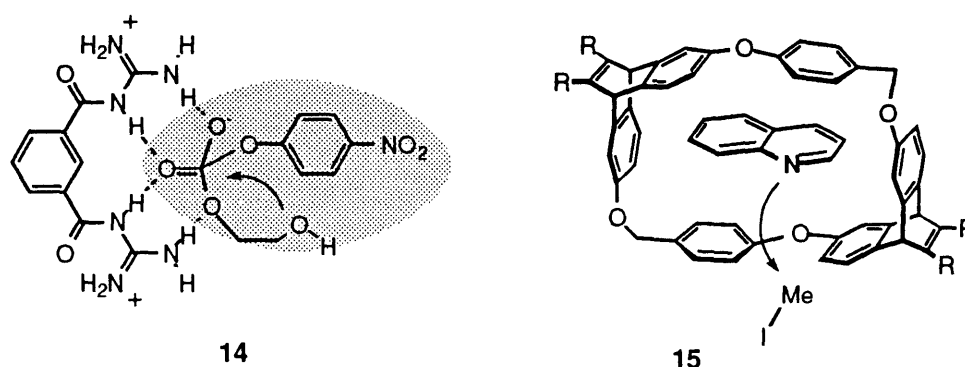


Figure I-11. Enthalpic catalysts.

Template catalysts⁵¹ which bring molecules or the reactive portions of molecules together have been far more common. These entropic catalysts have three general designs, depending upon the type of reaction being catalyzed:

- 1) Cyclization templates
- 2) Coupling templates
- 3) Interweaving or 'threading' templates

Representative examples of each type of template are shown in Figure I-12. The first is a cyclization template by Kool *et al.* based upon the associative

⁴⁸ a) Jubian, V.; Dixon, R. P.; Hamilton, A. D. *J. Am. Chem. Soc.* **1992**, *114*, 1120-1121. b) Tecilla, P.; Chang, S.-K.; Hamilton, A. D. *J. Am. Chem. Soc.* **1990**, *112*, 9586-9590.

⁴⁹ McCurdy, A.; Jimenez, L.; Stauffer, D. A.; Dougherty, D. A. *J. Am. Chem. Soc.* **1992**, *114*, 10314.

⁵⁰ Burley, S. K.; Petsko, G. A. *FEBS Lett.* **1986**, *203*, 139.

⁵¹ a) Anderson, S.; Anderson, H. L.; Sanders, J. K. M. *Acc. Chem. Res.* **1993**, *26*, 469-475. b) Hoss, R.; Vögtle, F. *Angew. Chem., Int. Ed. Engl.* **1994**, *33*, 375-384. c) Joyce, G. F. *Cold Spring Harbor Symp. Quant. Biol.* **1987**, *52*, 41-51.

interactions of triple stranded DNA (Figure I-12a).⁵² The polythymine molecule can wrap itself around a complementary poly-adenine strand, bringing its two reactive ends together and catalyzing the formation of a large polythymine macrocycle. The second type of template catalyzes a coupling reaction between two separate molecules. Kelly *et al.* has prepared a molecule with two independent binding sites (Figure I-12b).⁵³ The formation of a hydrogen bonded termolecular complex catalyzes the coupling reaction between two guest molecules. The template also properly orients the guests so that their reactive functionalities are facing each other. The third type of entropic catalyst is a 'treading' template exemplified by the Sauvage's phenanthroline systems (Figure I-12c).⁵⁴ Here, a Cu(I) ion acts as a template to bring two phenanthrolines units together. The geometry of the complex is such that after macrocyclization the resulting rings are threaded through each other, forming a catenane.

⁵² Rumney IV, S.; Kool, E. T. *Angew. Chem., Int. Ed. Engl.* **1992**, *31*, 1617-1619.

⁵³ Kelly, T. R.; Bridger, G. J.; Zhao, C. *J. Am. Chem. Soc.* **1990**, *112*, 8024-8034.

⁵⁴ Sauvage, J.-P.; Dietrich-Buchecker, C. O.; Guilhem, J.; Pascard, C. *Angew. Chem., Int. Ed. Engl.* **1990**, *29*, 1154-1156.

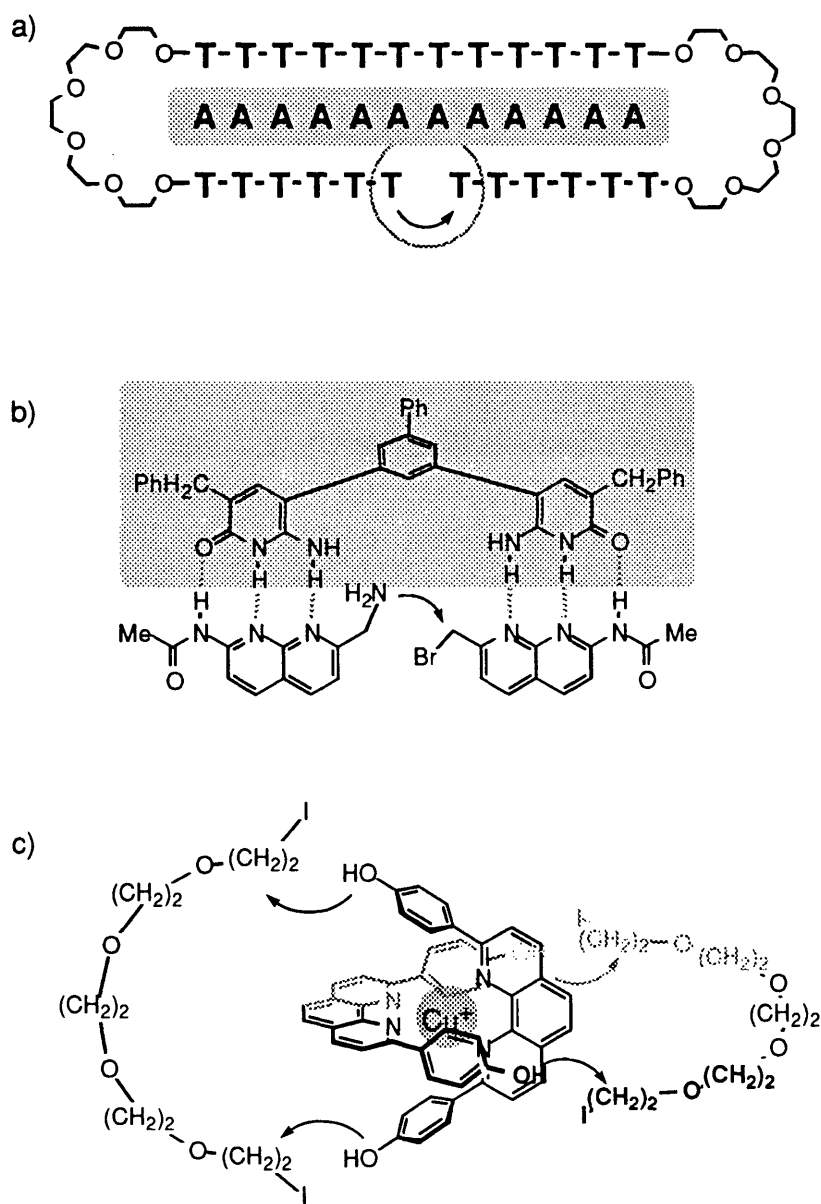
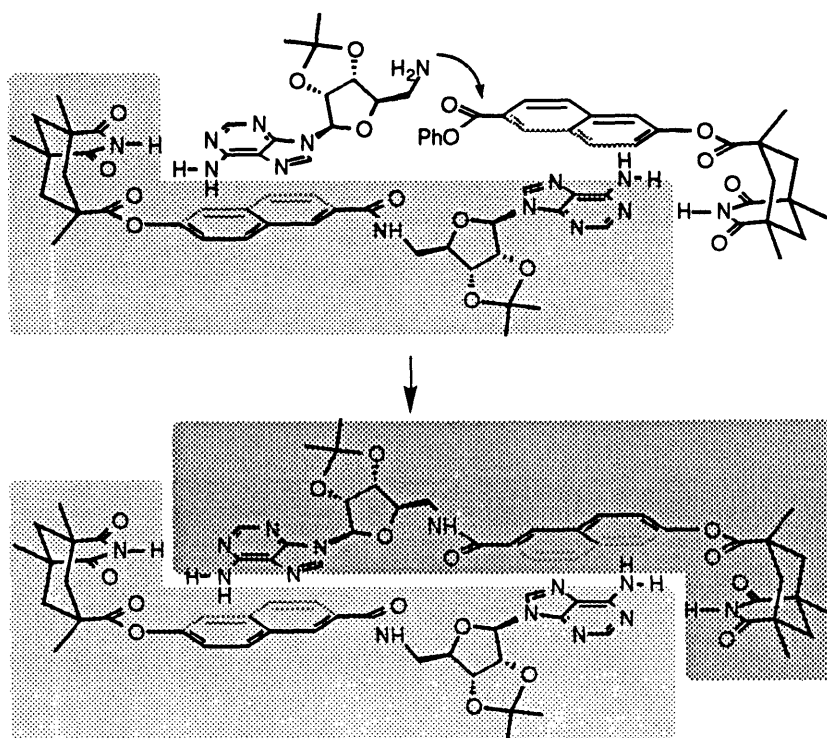


Figure I-12. Catalytic a) cyclization , b) coupling and c) interwoven templates (templates are highlighted.)

A special type of entropic catalysis is a template which can catalyze its own formation. Several synthetic systems capable of self-replication have been made

by von Kiedrowski,⁵⁵ Rebek,⁵⁶ and others.⁵⁷ Scheme I-1 shows Rebek's original replicating system composed of complementary Kemp's imides and adenosine sub-units. The success of these simple molecules is thought provoking, drawing into question the origins and definitions of life.



Scheme I-1. A self-replicating molecule.

Non-Covalent Synthesis and Self-Assembly

The most recent application of molecular recognition has been as an organizational strategy to complement classical covalent synthesis. Molecules can now be designed and 'programmed' to assemble themselves into discrete and

⁵⁵ von Kiedrowski, G.; Wlotzka, B.; Helbing, J.; Matzen, M.; Jordan, S. *Angew. Chem., Int. Ed. Engl.* **1991**, *30*, 423-426.

⁵⁶ a) Nowick, J. S.; Feng, Q.; Tjivikua, T.; Ballester, P.; Rebek, J., Jr. *J. Am. Chem. Soc.* **1991**, *113*, 8831-8839. b) Tjivikua, T.; Ballester, P.; Rebek, J., Jr. *J. Am. Chem. Soc.* **1990**, *112*, 1249-1250.

⁵⁷ For reviews see: Orgel, L. E. *Acc. Chem. Res.* **1995**, *28*, 109-118. For specific examples see: a) Li, T.; Nicolaou, K. C. *Nature* **1994**, *369*, 218-221. b) Orgel, L. E. *Science* **1992**, *358*, 203-209.

increasingly complex structures such as 'supramolecules', liquid crystals and three-dimensional crystalline lattices.⁵⁸ The advantage of non-covalent synthesis lies in the same kinetic instability, which had initially made its study difficult. The reversible formation of 'supramolecules' allow the sub-units to quickly sample all the possibilities and choose the thermodynamically most stable. The process is very similar to that of an extremely flexible peptide folding up into a well defined three-dimensional protein. Harnessing the organizational potential of non-covalent interactions is extremely appealing considering biological examples like membranes, DNA or ribosomes. This subject area is reviewed later in the introduction to Chapter VI.

Responsive Host-Guest Systems

The final area where molecular recognition has been applied is in the development of new molecules and materials which alter their properties upon application of an external stimuli. For example, systems based on azobenzenes⁵⁹ and thioindgos⁶⁰ undergo structural changes upon illumination with the correct wavelength of light. Scheme I-2 shows an example of an azobenzene system which can 'switch' its binding properties.⁶¹ In the Z-isomer, the two crown ether binding sites act independently, whereas in the E-isomer, they can bind cooperatively. Other external stimuli such as another guest,⁶² an electron,⁶³ heat or a reagent⁶⁴ have also been used to change a receptor's selectivity. Conversely, the binding of a guest can cause the host to undergo structural, color or other

⁵⁸ For reviews see: a) Whitesides, G. M.; Simanek, E. E.; Mathias, J. P.; Seto, C. T.; Chin, D. N.; Mammen, M.; Gordon, D. M. *Acc. Chem. Res.* **1995**, *28*, 37-44. b) Lindsey, J. S. *New. J. Chem.* **1991**, *15*, 153-180. c) Schneider, H. *Angew. Chem., Int. Ed. Engl.* **1991**, *30*, 1417.

⁵⁹ Bortolus, P.; Monti, S. *J. Chem. Phys.* **1979**, *83*, 648.

⁶⁰ a) Rahman, S. M. F.; Fukunishi, K. *J. Chem. Soc., Chem. Commun.* **1994**, 917-918. b) Irie, M.; Kato, M. *J. Am. Chem. Soc.* **1985**, *107*, 1024.

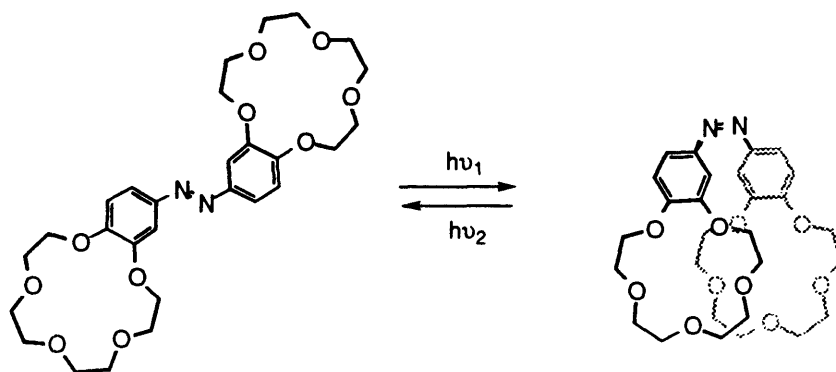
⁶¹ a) Shinkai, S.; Ogawa, T.; Jusano, Y.; Manabe, O.; Kikukawa, K.; Goto, T.; Matsuda, T. *J. Am. Chem. Soc.* **1980**, *104*, 1960. b) Shinkai, S.; Shigamatsu, K.; Sato, M.; Manabe, O. *J. Chem. Soc., Perkin Trans. I* **1982**, 2735.

⁶² Rebek, J., Jr.; Wattlely, R. V. *J. Am. Chem. Soc.* **1980**, *102*, 4853.

⁶³ Kaifer, A.; Gustowski, D. A.; Echegoyen, L.; Gatto, V. J.; Schults, R. A.; Cleary, T. P.; Morgan, C. R.; Goli, D. M.; Rios, A. M.; Gokel, G. W. *J. Am. Chem. Soc.* **1985**, *107*, 1958.

⁶⁴ Shinkai, S.; Inuzuka, K.; Hara, K.; Stone, T.; Manabe, O. *Bull. Chem. Soc., Jpn.* **1984**, *57*, 2150.

characteristic change. These molecules have potential applications as analytical sensors for the presence of a particular guest molecule.



Scheme I-2. A photoresponsive bis(crown ether).

Overall, these applications of molecular recognition have shown more potential than utility. However, many of the complexes and assemblies have unique properties and abilities, and it is these that we wish to explore with our new scaffolds. Certainly, the simplicity of most of these systems probably limits their effectiveness, and they are better suited toward demonstrating and dissecting the principles found in more complex biological systems.

Chapter II

Synthesis of C- and S-Shaped Perylene Scaffolds

2.1 INTRODUCTION

The synthesis of a new family of molecular scaffolds is introduced. The molecules share a cleft-like architecture and were assembled from two U-shaped molecules affixed to a rigid perylene spacer. The key feature of these scaffolds was their C_{aryl}-N_{imide} linkages. Restricted rotation about this bond froze out the corresponding syn- and anti- conformations which were stable at room temperature. The C-shaped scaffolds held functionality in an attractive convergent manner; whereas the S-shaped scaffolds were in an extended divergent conformation.

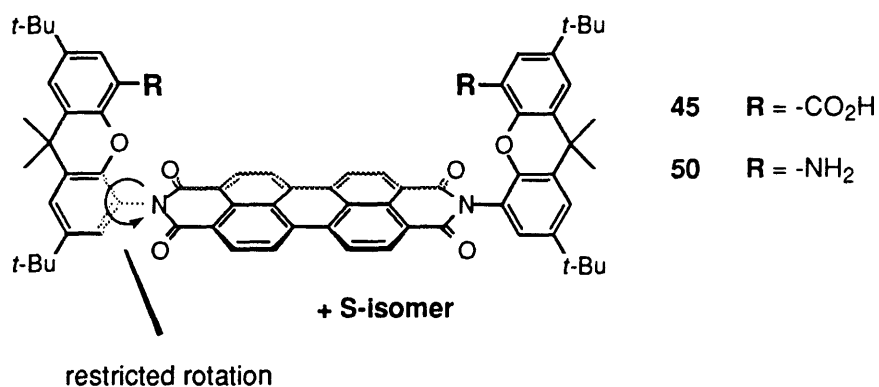


Figure II-1. The new molecular perylene scaffolds.

A particularly attractive feature of these new scaffolds was their facile and adaptable synthesis from xanthene and perylene components. The resulting rigid frameworks presented large distances between convergent functionality and possessed a spacious cavity (Figure II-1). The molecules were also easily

derivatized, further increasing their potential utility. The synthesis and functionalization of the perylene scaffolds are presented here.

2.2 BACKGROUND

In 1985, Rebek and co-workers introduced a new type of synthetic receptor to complement the existing macrocyclic structures.¹ Molecular clefts have been very successful in positioning functionality in a convergent geometry and have found applications as receptors,² transport agents,³ and catalysts.⁴ Because their cavities could be more easily functionalized, clefts were also synthetically attractive. By comparison, even well studied macrocyclic structures such as cyclodextrins still have not been efficiently derivatized on their endo surfaces.⁵ In addition, acyclic clefts were more easily assembled because they avoided low yielding macrocyclizations.

The greater synthetic flexibility of clefts and tweezers are offset by their stringent structural requirements. Cyclic molecules by their very nature focus functionality inward and create convergent binding sites. Clefts and tweezers must achieve this same preorganization through careful design, rigidity, and conformational restriction.

-
- ¹ a) Rebek, J., Jr.; Askew, B.; Islam, N.; Killoran, M.; Nemeth, D.; Wolak, R. *J. Am. Chem. Soc.* **1985**, *107*, 6736-6738. b) Rebek, J., Jr.; Nemeth, D. *J. Am. Chem. Soc.* **1985**, *107*, 6738-6739. c) Rebek, J., Jr.; Marshall, L.; Wolak, R.; Parris, K.; Killoran, M.; Askew, B.; Nemeth, D.; Islam, N. *J. Am. Chem. Soc.* **1985**, *107*, 7476-7481.
 - ² a) Askew, B.; Ballester, P.; Buhr, C.; Jeong, K. S.; Jones, S.; Parris, K.; Williams, K.; Rebek, J., Jr. *J. Am. Chem. Soc.* **1989**, *111*, 1082-1090. b) Conn, M. M.; Deslongchamps, G.; de Mendoza, J.; Rebek, J., Jr. *J. Am. Chem. Soc.* **1993**, *115*, 3548-3557. d) Jeong, K. S.; Tjivikua, T.; Muehldorf, A.; Deslongchamps, G.; Famulok, M.; Rebek, J., Jr. *J. Am. Chem. Soc.* **1991**, *113*, 201-209. e) Park, T. K.; Schroeder, J.; Rebek, J., Jr. *Tetrahedron* **1991**, *47*, 2507-2518. f) Rebek, J., Jr. *Angew. Chem. Int. Ed. Engl.* **1990**, *29*, 245-255.
 - ³ a) Andreu, C.; Galán, A.; Kobiro, K.; de Mendoza, J.; Rebek, J., Jr.; Salmeron, A.; Usman, N. J. *J. Am. Chem. Soc.* **1994**, *116*, submitted. b) Benzing, T.; Tjivikua, T.; Wolfe, J.; Rebek, J., Jr. *Science* **1988**, *242*, 266-268.
 - ⁴ Wolfe, J.; Muehldorf, A.; Rebek, J., Jr. *J. Am. Chem. Soc.* **1991**, *113*, 1453-1454.
 - ⁵ Wenz, G. *Angew. Chem., Int. Ed. Engl.* **1994**, *33*, 803.

The first molecular cleft **23** contained many of the attractive features which were copied in later structures.⁶ These included: 1) modular and interchangeable units, 2) easily modified convergent functionality and, perhaps most importantly, 3) a high degree of preorganization achieved through rigidity and conformational restriction.

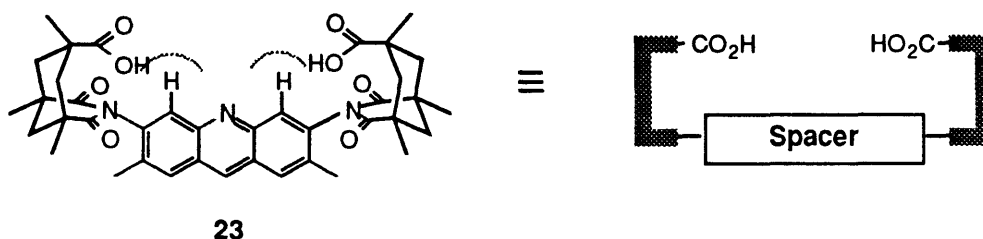


Figure II-2. Kemp's acridine diacid cleft and schematic representation. The steric bulk of the aryl hydrogens of the acridine spacer are highlighted.

This last feature has been the most difficult to incorporate into succeeding structures. The two acids of cleft **23** are sterically and covalently locked in a facing geometry. The methyl groups of the acridine spacer block rotation of the Kemp's U-turns, and the rigidity of the acridine heterocycle prevents collapse. In recent years, molecular clefts of various designs have become increasingly common, from our research group and others.⁷ Particularly popular were diacid structures; examples of which are in Figure II-3.^{7i,7b,7l} However, these new clefts all lacked the temporal preorganization of the original acridine cleft **23**. Through internal rotations, clefts **24**, **25** and **26** spend much of their time in unproductive divergent conformations.

⁶ For reviews see: a) Rebek, J., Jr. *Top. Curr. Chem.* **1988**, *149*, 189-210. b) Rebek, J., Jr. *Angew. Chem., Int. Ed. Engl.* **1990**, *29*, 245-255.

⁷ a) Rebek, J., Jr. *Angew. Chem., Int. Ed. Engl.* **1990**, *29*, 245-255. b) Adrian, J. C.; Wilcox, C. S. *J. Am. Chem. Soc.* **1989**, *111*, 8055-8057. c) Kelly, T. R.; Maguire, M. P. *J. Am. Chem. Soc.* **1987**, *109*, 6549-6551. d) Galán, A.; Andreu, D.; Echavarren, A. M.; Prados, P.; de Mendoza, J. *J. Am. Chem. Soc.* **1992**, *114*, 1511-1512. e) Tecilla, P.; Chang, S.-K.; Hamilton, A. D. *J. Am. Chem. Soc.* **1990**, *112*, 9586-9590. f) Zimmerman, S.; Wu, W. *J. Am. Chem. Soc.* **1989**, *111*, 8054-8055. g) Iimori, T.; Still, W. C.; Rheingold, A. L.; Staley, D. L. *J. Am. Chem. Soc.* **1989**, *111*, 3439-3430. h) Schmidtchen, F. P. *Tetrahedron Lett.* **1989**, *30*, 4493-4496. i) Medina, J. C.; Li, C.; Bott, S. G.; Atwood, J. L.; Gokel, G. W. *J. Am. Chem. Soc.* **1991**, *113*, 366-367. k) Bell, T. W.; Liu, J. *J. Am. Chem. Soc.* **1988**, *110*, 3673-3674. l) Güther, R.; Nieger, M.; Vögtle, F. *Angew. Chem., Int. Ed. Engl.* **1993**, *32*, 601-603.

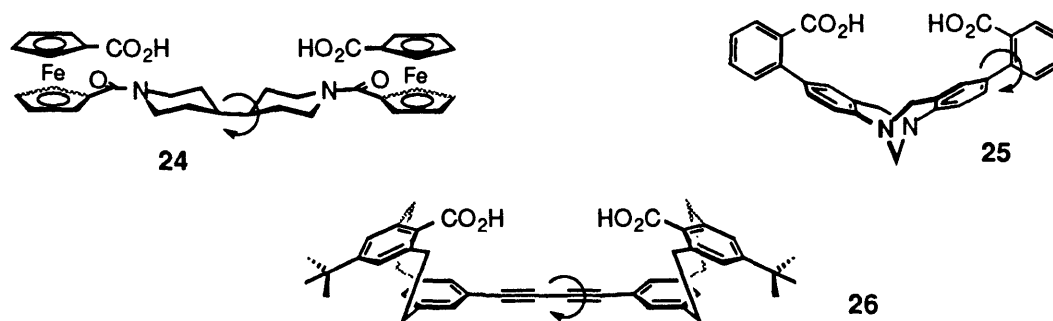


Figure II-3. Recent examples of diacid clefts pictured in a convergent conformations

Although acridine cleft **23** was very efficient in focusing functionality inward, it also possessed an extremely shallow binding pocket. The protons of the acridine spacer jut up and fill most of the binding cavity and also obstruct much of the space in front of the diacids (see Figure II-2). There has even been some question as to whether guests could simultaneously bind to both carboxylic acids,⁸ but these concerns were alleviated by crystal structures of chelated guests.⁹ Still, the fact remains that the cavity of **23** is exceedingly shallow, limiting the size of guests and making functionalization of the diacids a sterically demanding task.

The development of new molecular clefts has been driven by the desire for larger cavities, different shapes, and greater synthetic flexibility, all without sacrificing the remarkable preorganization of acridine diacid **23**. Our strategy has been to develop larger U-turn molecules which would form a deeper cavity (Figure II-4). The most successful has been xanthene diacid **27**,¹⁰ which like Kemp's triacid (**28**), has become commercially available which is the benchmark of success. Structurally, the new U-turn was akin to a similar 1,8-disubstituted xanthene developed by D. Kemp *et al.* as a covalent template to catalyze peptide bond formation.¹¹ As expected, clefts constructed from the new xanthene diacid

⁸ Jorgensen, W. L.; Boudon, S.; Nguyen, T. B. *J. Am. Chem. Soc.* **1989**, *111*, 755-757.

⁹ Pascal, R. A.; Ho, D. M. *J. Am. Chem. Soc.* **1993**, *115*, 8507-8508.

¹⁰ Nowick, J. S.; Ballester, P.; Ebmeyer, F.; Rebek, J., Jr. *J. Am. Chem. Soc.* **1990**, *112*, 8902-8906.

¹¹ Kemp, D. S.; Buckler, D. R. *Tetrahedron Lett.* **1991**, *32*, 3009-3012.

such as **29** had deeper cavities and were more easily functionalized; however, the new clefts still contained a high degree of conformational freedom. Rotations of the spacer to U-turn linkages and of the spacer itself again led to unproductive shapes.

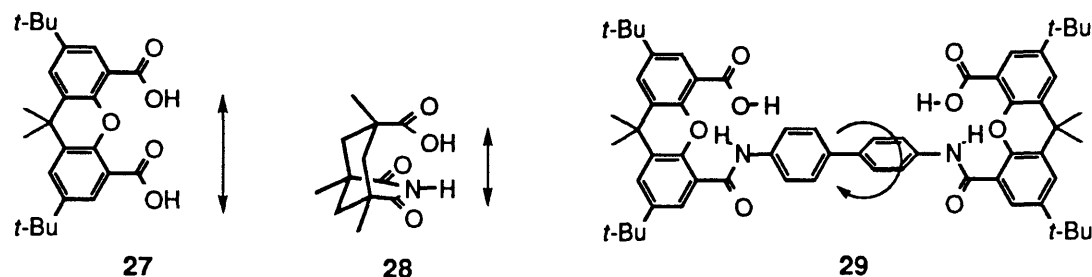


Figure II-4. Comparison of the xanthene and Kemp's triacid U-turns.

The new scaffolds presented in this thesis were designed to improve upon these previous structures. In particular, an effort was made to develop new spacers and linkages which effect greater conformational restriction. Our efforts were rewarded with the synthesis of perylene diacid **45**, shown at the beginning of this chapter. These structures retained the xanthene U-turn but replaced the flexible amide linkages of **29** with rigid cyclic imides. The choice of an aryl-imide linkage was fortuitous as all the diimide scaffolds displayed restricted rotation. The imides also twisted the perylene shelf into a perpendicular conformation well situated toward aromatic stacking. Also appealing was the commercial availability of the large polysubstituted aromatic spacer as 3,4,9,10-perylenetetracarboxylic dianhydride **30**, a brilliant red laser dye.

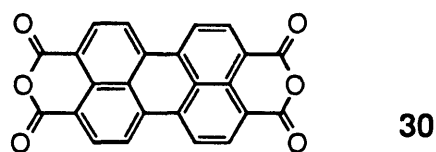


Figure II-5. New perylene dianhydride spacer.

Despite its commercial availability, only a single example was found in which perylene dianhydride **30** was incorporated into a synthetic receptor. This unproductivity can probably be attributed to its notorious insolubility. In our

own research group, Kevin Parris synthesized cleft **32**.¹² The attractive feature of a large acid-acid distance was off-set by insolubility and a lack of preorganization. Diacid **32** can access 6 different conformations of almost equal stability. The synthesis of **32** also failed to resolve the problem of how to functionalize the 3,4- and 9,10- perylene imides because the starting material already contained these linkages. Cleft **32** was synthesized from the condensation of Kemp's monoacid monoanhydride to the commercially available N,N'-bis(3-aminophenyl)-3,4,9,10-perylenetetracarboxylic diimide.

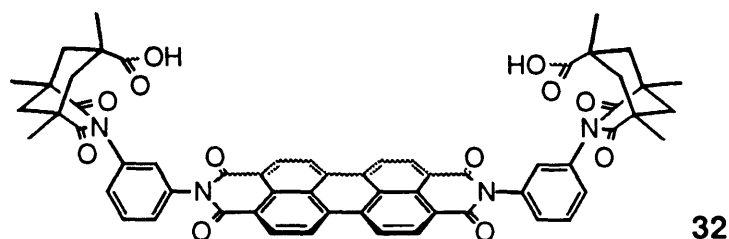


Figure II-6. Molecular receptors utilizing perylene and naphthalene dianhydrides.

2.3 SYNTHESIS OF THE XANTHENE U-TURN.

The new design of the perylene scaffolds necessitated the synthesis of an alternatively functionalized xanthene U-turn. Specifically, a xanthene was required, having an amine for connection to a spacer and a carboxylic acid binding site. Overall, the synthesis of amino-acid **34** was accomplished in 9 steps from xanthone **35** with each step proceeding in high yield. Throughout, extensive purification procedures such as chromatography or recrystallization were unnecessary and allowed multigram quantities of U-turn **34** to be readily produced. Much of the synthesis followed that of the previously reported xanthene diacid **40**,¹³ which was modified to a less expensive and more facile route. The synthesis of **34** also featured an unusual monofunctionalization

¹² Parris, K. D. Ph.D. Thesis, University of Pittsburgh, 1988.

¹³ Nowick, J. S.; Ballester, P.; Ebmeyer, F.; Rebek, J., Jr. *J. Am. Chem. Soc.* **1990**, *112*, 8902-8906.

reaction in which the xanthene 1- and 8- positions could be selectively differentiated.

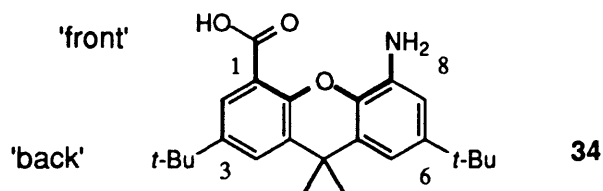
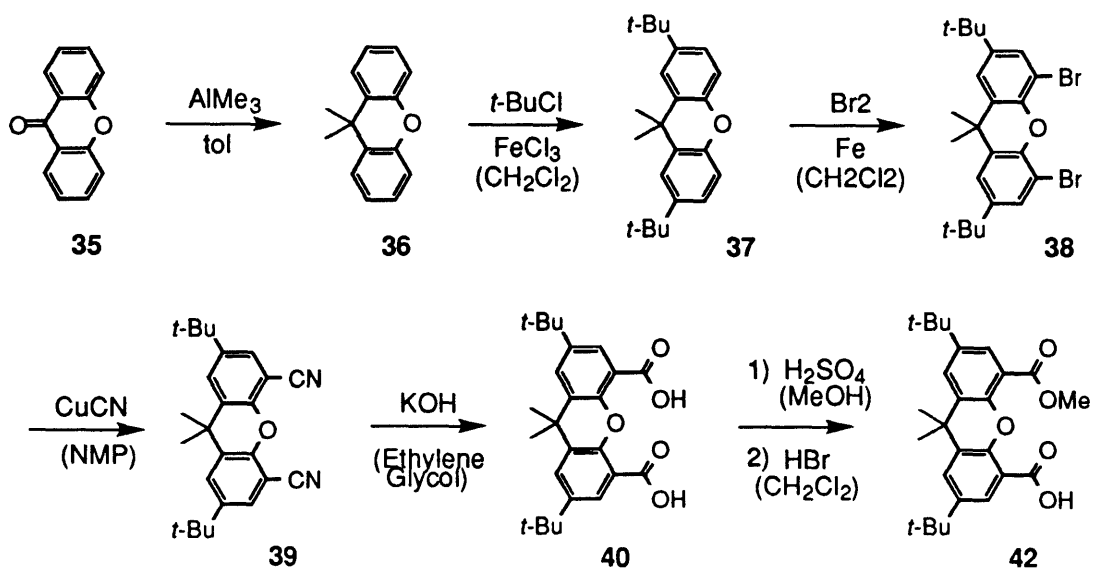


Figure II-7. Xanthene amino acid U-turn.

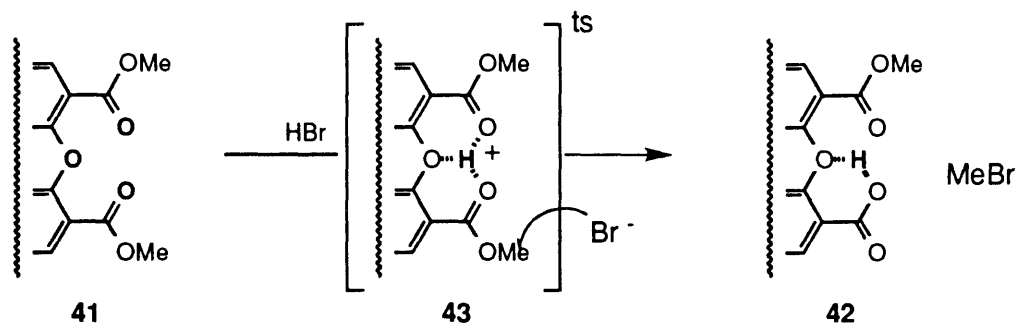
As described previously, xanthone **35** was dimethylated with AlMe_3 ,¹⁴ *t*-butylated in the 'rear' 3,6-positions and finally brominated in the front 1,8-positions. The 9,9-dimethyl groups kept the xanthene in a fairly planar conformation while also eliminating the deactivating ketone. The *t*-butyl groups considerably enhanced the solubility of the xanthene and its clefts and also blocked the more accessible rear positions. Functionality was introduced at the desired 1,8-positions by bromination which was then converted to diacid **40**. Previously, dibromide **38** had been directly transformed into the diacid via lithiation and carboxylation. On a multi-gram scale, this required large volumes of butyl lithium and anhydrous conditions. An alternative synthesis was developed, in which dibromide **38** was converted into dinitrile **39** with CuCN , followed by base hydrolysis. The new route was equally facile and rapid while still proceeding in excellent yield (96 %) for the two steps.

¹⁴ Meisters, A.; Mole, T. *Aust. J. Chem.* **1974**, *27*, 1655.



Scheme II-1. Synthesis of monofunctionalized xanthene monoacid monoester **42**.

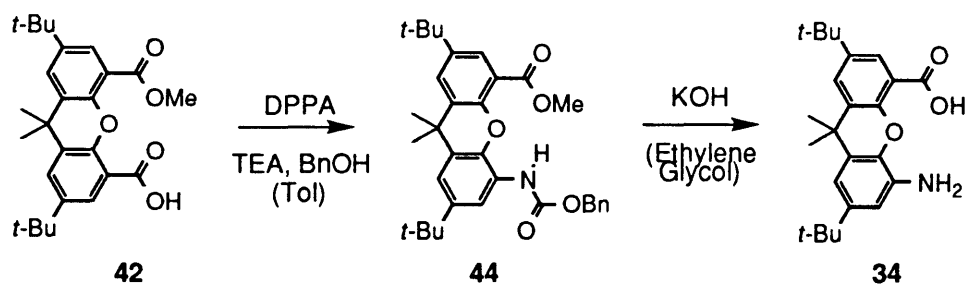
Next, the 1,8-positions of xanthene diacid **40** were differentiated. Fischer esterification of diacid **40** gave dimethyl ester **41** which on treatment with anhydrous HBr in CH_2Cl_2 led selectively to monoester monoacid **42**. The unusual lability and selectivity of the xanthene methyl esters was explained by the formation of a 'proton hole' between the diesters of **41** (Scheme II-2). Presumably, the neighboring carbonyl and ether oxygens facilitated protonation and subsequent cleavage of the ester by a bromine anion.



Scheme II-2. The proposed mechanism for the selective monodeprotection of diester **41** by the formation of a 'proton hole'.

This hypothesis is supported by three pieces of evidence. First, the esters at the 1- and 8- positions of xanthene were unusually labile. For example, a xanthene with methylesters at the 'rear' 3,6-positions was stable to the same reaction conditions.¹⁵ Clearly, some type of activation was occurring during the demethylation of **41**. Second, amides and acids in the front 1,8-positions are known to participate in intramolecular hydrogen bonding. These internally hydrogen bonded structures such as **42** demonstrate that a proton can fit between the carboxylic functionality and, in fact, has propensity to do so. Third, the proposed mechanism explains the kinetic differentiation between the first and second demethylations. The product of the initial cleavage reaction **42** is internally hydrogen bonded, effectively occupying the 'proton hole', and making the second protonation more difficult. The reason that the intermolecular hydrogen bond of **42** does not itself accelerate the second demethylation may be due to its neutral character as opposed to the more polarizing effects of a cationic proton.

Once monofunctionalized, the synthesis of xanthene U-turn **34** was completed by a Shioiri degradation.¹⁶ Treatment of monoacid monoester **42** with diphenyl phosphoryl azide (DPPA) gave *in situ* the acyl azide. Thermal rearrangement to the isocyanate, followed by quenching with benzyl alcohol, yielded benzyl carbamate **44**. A side product (~ 10 %) was the symmetrical diurea which formed from the hydrolysis of an isocyanate which then coupled to another isocyanate. The crude carbamate **44**, including the diurea impurity, was carried on as both products gave the desired xanthene amino acid **34** upon hydrolysis.



Scheme II-3. Rearrangement and hydrolysis to give xanthene U-turn **34**.

¹⁵ See last chapter of this thesis.

¹⁶ Ninomiya, K.; Shioiri, T.; Yamada, S. *Tetrahedron* **1974**, *30*, 2151-2157.

2.4 PERYLENE CLEFT ASSEMBLY.

With the xanthene U-turn in hand, condensation reactions with perylene dianhydride **30** were explored. Previous attempts in our research group to functionalize the perylene tetraacid platform centered on activating the acids as esters or acid chlorides.¹⁷ These efforts were hampered by the proximity of the acids and the insolubility of the perylene surface. Examination of the literature suggested that a more brute force approach might be more successful.¹⁸ Typically, perylene diimides were synthesized by heating dianhydride **30** with the corresponding amine as solvent.¹⁹ More applicable to our purposes were reports of condensations carried out in solvents such as quinoline or imidazole.²⁰

Using a similar procedure, xanthene amino acid **34**, perylene dianhydride **30** and Zn(OAc)₂ were heated in quinoline at 220 °C. Two nearly identical compounds were formed in approximately a 1 to 1 ratio. The products were later identified to be the stable C- and S- shaped conformers (**45c** and **45s**).²¹ Chromatography easily separated the rotational isomers and was aided by the bright red color of the perylene derivatives and insolubility of almost everything but the product.

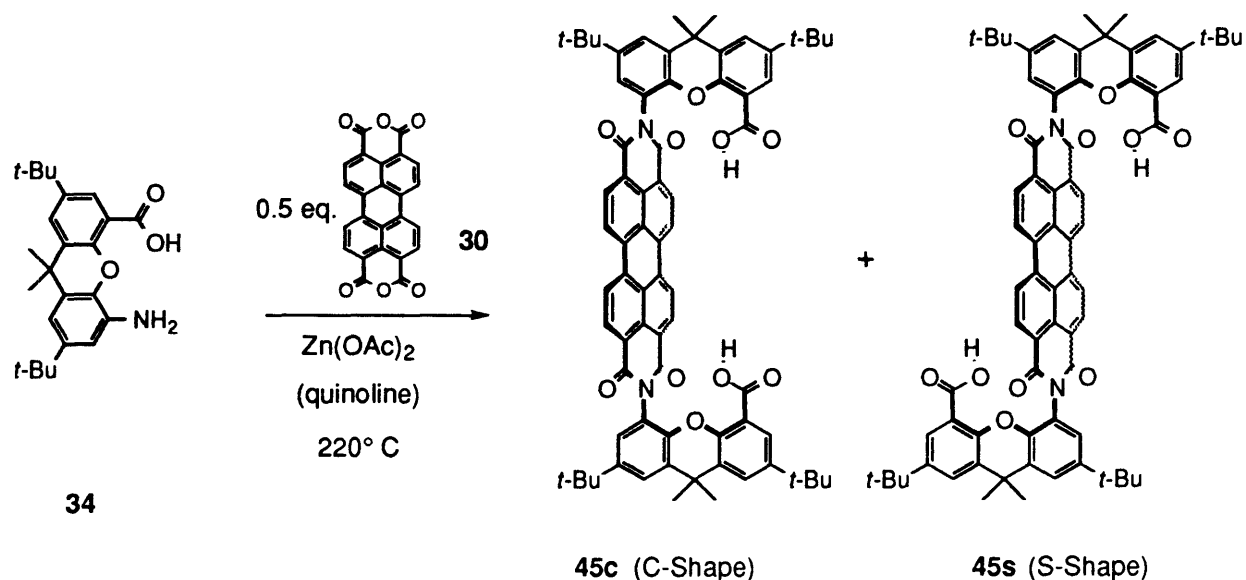
¹⁷ Personal communication. T.-K. Park

¹⁸ Langhals, H. *Chem. Ber.* **1985**, *118*, 4641.

¹⁹ a) Tamizhmani, G.; Dodelet, J. P.; Côté, R.; Gravel, D. *Chem. Mater.* **1991**, *3*, 1046. b) Petit, B.; Maréchal, E. *Bull. Soc. Chim. France* **1974**, *7-8*, 1591. c) Nagao, Y.; Ishikawa, N.; Tanabe, Y.; Misono, T. *Chem. Lett.* **1979**, 151. d) Maki, T.; Hashimoto, H. *J. Chem. Soc. Japan, Ind. Chem. Section* **1951**, *54*, 544.

²⁰ a) Rademacher, A.; Markle, S.; Langhals, H. *Chem. Ber.* **1982**, *115*, 2927 - 2934. b) Gangneux, P.; Marechal, E. *Bull. Soc. Chim. France* **1973**, *4*, 1466-1483.

²¹ The c and s following a structure's number will be used to denote the C- and S-shaped isomers through this thesis.



Scheme II-4. Assembly of the C- and S-shaped perylene scaffolds.

Yields for the condensation reaction were modest (~ 50 %); therefore, methods for improving the reaction conditions were examined. The stoichiometry, the presence of Zn(OAc)₂ and the temperature of the condensation reaction were all individually varied. First, a large excess of xanthene amino acid **34** (10 eq.) was shown to push the reaction to 90 % conversion but at the cost of valuable xanthene. A more reasonable mass balance of amino acid **34** was achieved with the use of 2.5 eq to again give 50 % yield. Surprisingly, when Zn(OAc)₂ was removed from the reaction mixture yields remained the same. The perylene condensation reactions reported by Langhals *et al.* usually achieved their best yields in the presence of Zn(OAc)₂ and often failed in its absence. Later condensations reactions were likewise shown to be dependent upon the metal catalyst for success, but this was not the case for xanthene amino acid **34**. Although, it was observed that perylene condensations performed without Zn(OAc)₂ were accompanied by large amounts of black insoluble material which complicated workups. Therefore in the preparation of perylene **45**, Zn(OAc)₂ is recommended.

A temperature of 220 °C struck the optimal balance between long reaction times and the loss of product from decarboxylation. At lower temperatures (150 °C and 180 °C) the condensation reaction was extremely sluggish. The limiting factor appears to be the solubility of dianhydride **30**, making the first

condensation the rate determining step. The monocondensation product **46** is more soluble and quickly reacts to give the diimides **45c** and **45s**. This scenario was supported by the extremely low concentrations of **46** throughout the reaction.²² In addition, more soluble anhydrides having similar substitution patterns were considerably more reactive than perylene **30** (see Chapter III). Conversely, at temperatures higher than 220 °C the greater coupling efficiencies were off-set by decarboxylation, resulting in the isolation of the mono- and di-decarboxylation products **47** and **48**. In fact, at higher temperatures both the condensation and decarboxylation reactions proceed very cleanly as evidenced by the yield of 98 % from the combination of all of the dicondensation products (**45**, **46**, **47** and **48**). Again, **47** and **48** were isolated as stable C- and S-shaped isomers. The mono decarboxylation product **47** provides access to scaffolds with different functionality at either side. This desymmetrization of the perylene scaffolds was later found to be fairly difficult (section 2.6).

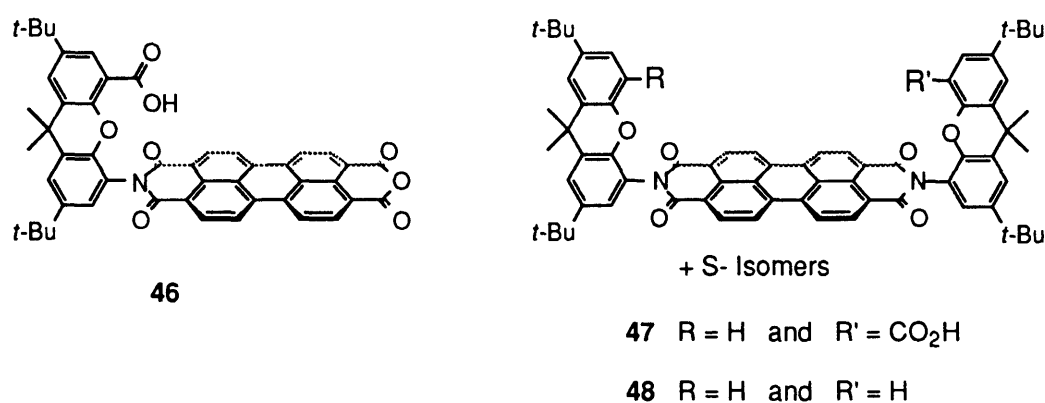


Figure II-8. Side products of the dicondensation reaction including the monocondensation and decarboxylation products.

The condensation of other aryl amines to the perylene surface was examined but again was hampered by insolubility. The coupling reactions appeared to give the corresponding diimides; however, the only confirmation that could be obtained was the disappearance of the anhydride carbonyl peak at 1759 cm⁻¹ in the IR spectra of the reaction mixture. One of the few soluble exceptions was xanthene diamine **49**. The dicondensation reaction with perylene dianhydride **30**

²² The monodecarboxylation product was determined to be a very minor impurity which by TLC fell between the C- and S- shaped isomers of the diacid clefts.

went in considerably lower yield than with xanthene amino acid **34** and was hampered by oligomerization and difficulties in isolation. In the end, the C- and S-shaped diamines **50c** and **50s** were synthesized and isolated, providing an alternatively functionalized perylene scaffold to complement diacids **45s** and **45c**.

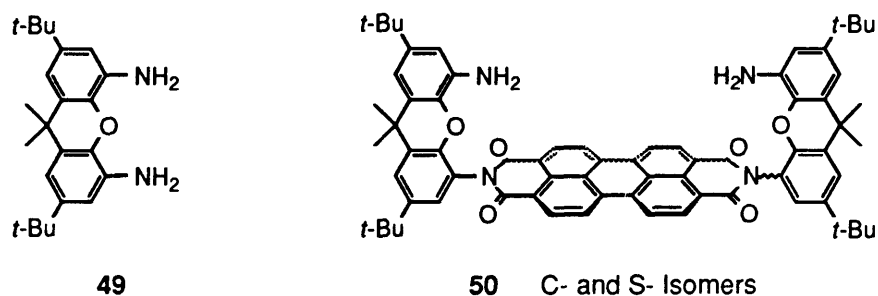


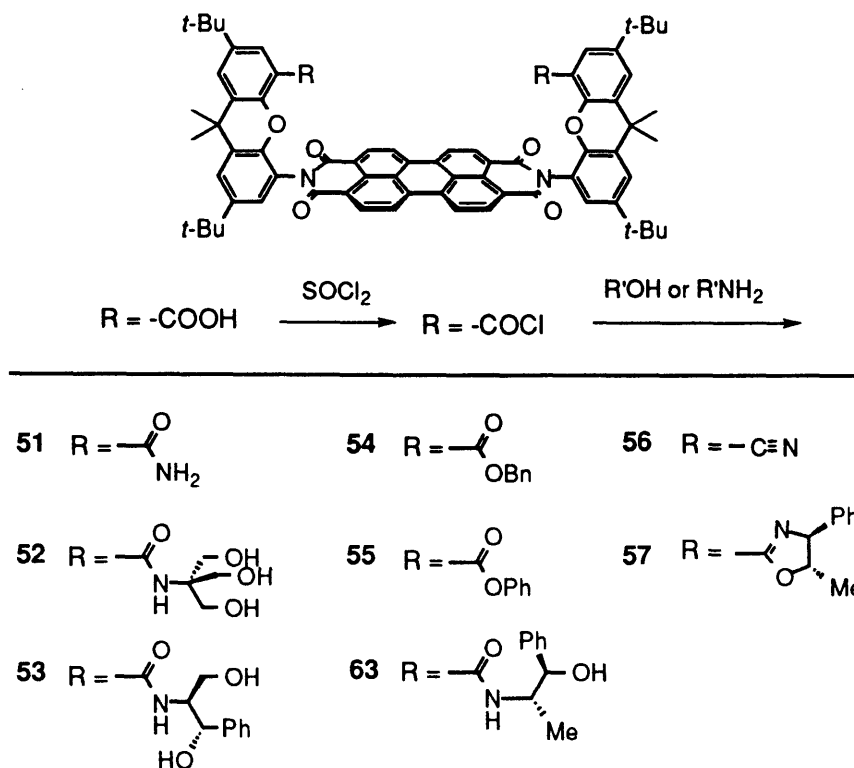
Figure II-9. Diamino xanthene and the corresponding diamino perylene scaffolds.

2.5 FUNCTIONALIZATION OF PERYLENE SCAFFOLDS

The introduction of different functionality into the perylene scaffolds was accomplished by transformation of the existing acids and amines in the assembled scaffolds. Unfortunately, a more direct approach of assembling the functionalized components with the perylene surface failed because of the harsh condensation conditions.²³ On the other hand, derivatization of the diacids of **45c** and **45s** was fairly straightforward via the diacid chloride. Treatment of either diacid with thionyl chloride followed by an amine gave cleanly the corresponding diamides (Scheme II-5). In each case, the individual rotamers were stable to the mild reaction conditions, eliminating the need for repeated separations.

From the diacid chloride, a wide array of functionality was easily accessible, including primary amides (**51**), amido alcohols (**52** and **53**) and amido esters (not shown). Perylene diesters were also synthesized from the corresponding alcohols (**54** and **55**).

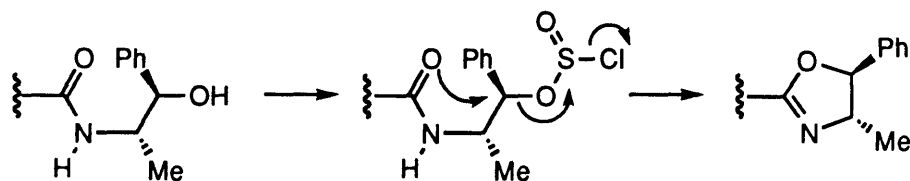
²³ For example, the condensation of xanthene monoamine monocarboxylic methyl ester with perylene dianhydride **30** gave only the hydrolyzed products **45c** and **45s**.



Scheme II-5. Derivatization of the perylene diacid via the diacid chloride.

The resulting diamides could also be converted into other useful functionalities. Dehydration of primary diamide **51** with oxalyl chloride and DMF gave in high yields dinitrile **56**. Even more attractive were chiral oxazolines which were synthesized from commercially available and chirally pure 2-aminoethanols. Perylene diamidoalcohols such as **63** were cyclized by treatment with thionyl chloride followed by a basic work up (saturated NaHCO_3) (Scheme II-6). The reaction proceeds by conversion of the alcohol into a good leaving group followed by $\text{S}_\text{N}2$ attack of the carbonyl oxygen. Inversion occurred cleanly as evidenced by the isolation of only a single diastereoisomer in cases with adjacent asymmetric centers. In addition, the measured coupling constants of the newly formed oxazoline ring of **57** were consistent with inversion. In the example below (Scheme II-6), a coupling constant of 6.0 Hz was measured. This compares

well with oxazolines from the literature which ranged from 6.0 to 6.6 Hz for the *anti*-conformer and 9.9 Hz for the *syn*-conformer.²⁴



Scheme II-6. Conversion of 2-amido-ethanols to oxazolines.

Throughout, the 'half cleft' **58** was an excellent model compound to test the reactivities of the perylene scaffolds. The compound was easily synthesized and its structure closely corresponded to the assembled scaffolds. In contrast to perylene dianhydride, the condensation reactions with 1,8-naphthalene dianhydride proceeded smoothly, under milder conditions, and in higher yields. An interesting homologue of **58** is bis(naphthalene imide) **59**. Unfortunately, the inviting aromatic shelf between the two naphthalene surfaces appears to be too small (by modeling) to slip a guest in-between. The interesting feature of diimide **59** was again conformational isomerism but in a different dimension than the perylene scaffolds. Two stable conformers were isolated; the *syn*- (**59s**) and the *anti*- (**59a**) which were easily differentiated by their contrasting ¹H NMR spectra. The *syn*- compound has a single plane of symmetry and is meso. Conversely, the *anti*- compound has C₂ symmetry and is chiral. The difference in symmetry was most evident in the 9,9-dimethyl groups of **59**. In the *syn*-isomer, two different methyl groups were observed, whereas in the *anti*-isomer the methyl groups were chemically equivalent.

²⁴ a) Meyers, A. I.; Mihelich, E. D. *Angew. Chem., Int. Ed. Engl.* **1976**, *15*, 270. b) Bölm, C.; Weickhardt, K.; Zehnder, M.; Ranff, T. *Chem. Ber.* **1991**, *124*, 1173.

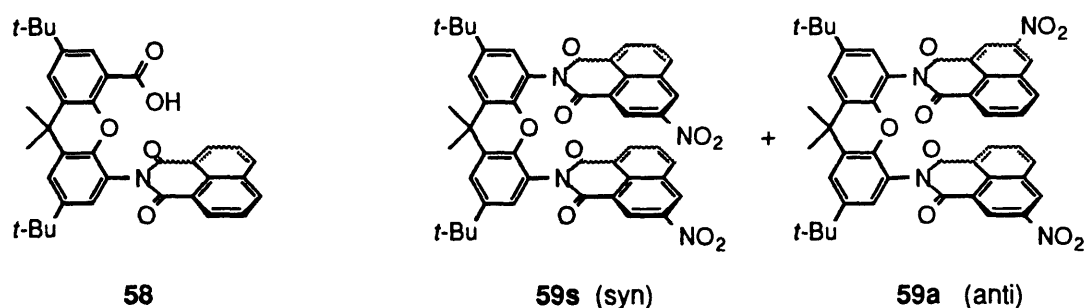


Figure II-10. The 'half cleft' model compounds.

2.6 MONOFUNCTIONALIZATION

For applications in catalysis, a cleft possessing different functionality on either end was desired. Desymmetrization of the C-shaped perylene scaffold, however, proved difficult. The literature had only a single report of a monofunctionalized perylene dianhydride surface.²⁵ In our hands, the key monoimide monoanhydride **60** was never attained. Similar attempts to form the xanthene monocondensation product **46** were equally unsuccessful. Even in an excess of perylene dianhydride, the major products were still the dicondensation products **45c** and **45s**.

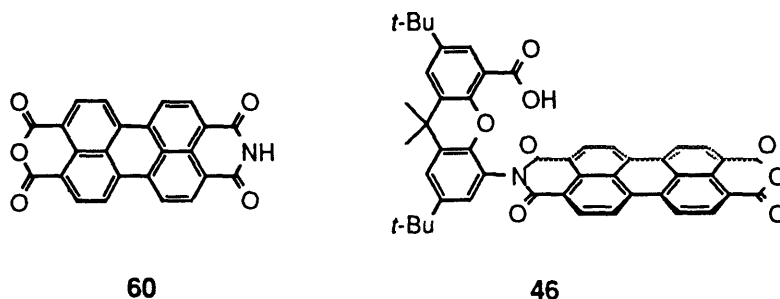


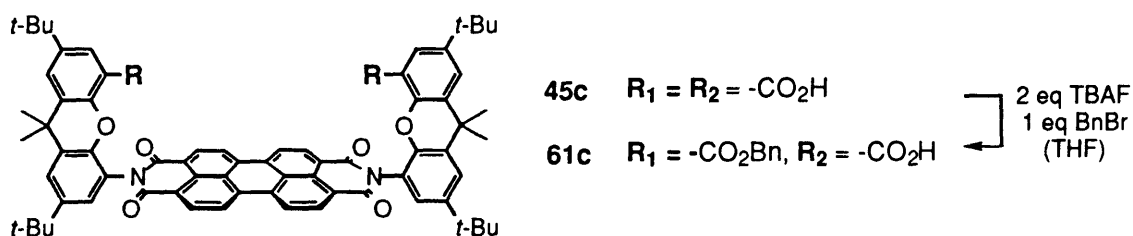
Figure II-11. New perylene and naphthalene dianhydride spacers.

An alternative strategy of acid protection and/or deprotections was pursued with limited success. Most troublesome was the differing reactivities of the functionalized C- and S-shaped perylene scaffolds. For the S-shaped isomer, the

²⁵ Kaiser, H.; Lindner, J.; Langhals, H. *Chem. Ber.* **1991**, *124*, 529.

two sites reacted independently, whereas for the C-shaped isomer, reactions at the first site affected reactions at the second, often for the worse. For example, deprotection of dibenzyl ester **54s** with HBr^{26} gave the expected statistical distribution of starting material, mono- and diacids. Deprotection of the other rotational isomer diester **54c** gave only starting material and diacid **45c** and none of the monoacid monoester **61c**.

A monoprotection strategy was developed to take advantage of the different reactivities of the perylene isomers. Treatment of diacid **45c** with tetrabutyl ammonium fluoride (TBAF, 3 eq) and 1 to 1.5 equivalent of benzyl bromide gave the monobenzyl ester monoacid **61c** in ~50 % yield. Similar alkylation conditions have been reported for phenols and amines.²⁷ This reaction is extremely mild (rt.), and proceeds rapidly even in cases with highly hindered or insoluble acids. The reaction proceeds through the sequestration of an acid proton by two TBAF's as the strongly hydrogen bonded $(\text{F}\cdots\text{H}-\text{F})^-$ anion (Scheme II-7).²⁸ The resulting carboxylate is 'naked' in organic solvents with an $\text{N}(\text{Bu})_4^+$ counterion, making it much more nucleophilic. This procedure seems considerably safer than esterifications with diazomethane while also being mild and effective.



Scheme II-7. Monoprotected C-diacid and benzylation reaction.

²⁶ Attempts at hydrolyzing the perylene diesters led to a large mixture of products perhaps due to the opening up of the imide ring.

²⁷ a) Clark, J. H. *Chem. Rev.* **1980**, *80*, 429. b) Clark, J. H.; Miller, J. M. *J. Chem. Soc., Chem. Commun.* **1976**, 229.

²⁸ Emsley, J. *Chem. Soc. Rev.* **1980**, *9*, 91.

2.7 OUTLOOK

Overall, the perylene scaffolds were easily assembled in a single step from xanthene U-turns **34** and **49** and commercially available perylene dianhydride **30**. Derivatization was straightforward making them attractive and accessible frameworks for applications in molecular recognition. As it turns out, the choice of *t*-butyl solubilizing groups on the xanthenes was an excellent one. Langhals *et al.* has extensively studied a diverse array of perylene diimides in search of a more soluble laser and printing dye.²⁹ Derivatives which disrupt the planar perylene surface were shown to be the most tractable. In particular, aryl groups with ortho- and meta- *t*-butyl groups were more effective than long alkyl chains. This observation led to the synthesis of diimide **62** which closely resembles the substitution pattern of the perylene scaffolds (Figure II-12). In fact, the newly synthesized diamides and diester derivatives of **45** appeared to be even more soluble than **62**.

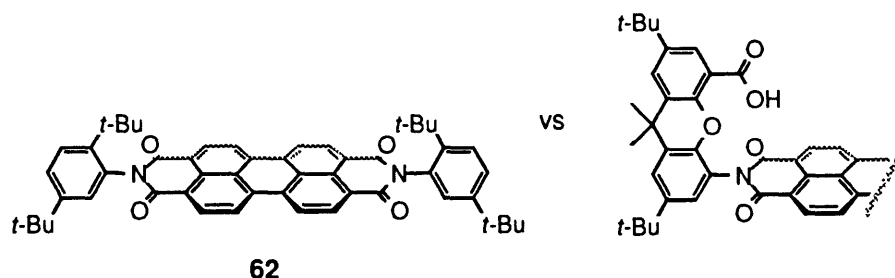


Figure II-12. Comparison of highly soluble perylene laser dye and the perylene scaffold **45**.

Continuing research on the perylene scaffolds has led to better techniques for their synthesis and derivatization. Most recently, Christian Rojas has found condensation conditions which give an overwhelming excess of the more desirable C-isomer of **45** in a (92 : 8) ratio, while giving still higher yields.³⁰ In

²⁹ a) Demmig, S.; Langhals, H. *Chem. Ber.* **1988**, *121*, 225 - 230. b) Rademacher, A.; Markle, S.; Langhals, H. *Chem. Ber.* **1982**, *115*, 2927 - 2934.

³⁰ The xanthene amino acid **34** and the perylene dianhydride were heated in NMP/xylenes for 2 days.

addition, an improved procedure for monofunctionalizing the perylene scaffolds has been developed.³¹ These developments should only enhance the utility of the large and highly organized perylene scaffold by allowing greater access and variability to their structure.

2.8 EXPERIMENTAL SECTION

Xanthene Dimethylester (41). Dibromoxanthene **38** (10.25 g, 21.35 mmol)³² and CuCN (3.92 g, 43.77 mmol)³³ was suspended in 1-methyl-2-pyrrolidinone (125 mL) and heated at a light reflux for 16 h. The reaction mixture was cooled and quenched with 2.0 N ammonium hydroxide solution (600 mL). The dinitrile **39** was filtered off and washed liberally with additional ammonium hydroxide solution until the filtrate was no longer blue. The solid was further washed with water (2 x 150 mL) and small pieces of copper metal removed: IR (KBr) 2230 cm⁻¹ (-CN); ¹H NMR (250 MHz, CDCl₃) δ 7.62 (d, 2 H, *J* = 2.1 Hz, Xan), 7.54 (d, 2 H, *J* = 2.1 Hz, Xan), 1.66 (s, 6 H, Me), 1.34 (s, 18 H, *t*-Bu).

The crude dinitrile **39** was suspended in ethylene glycol (250 mL) with KOH (8.8 g, 156 mmol) and refluxed until clear, 16 h. The solution was acidified with 1.0 N HCl and precipitated with water. The diacid **40** was filtered off as a beige solid and dried *in vacuo* (7.99 g): ¹H NMR (250 MHz, CDCl₃) δ 8.16 (d, 2 H, *J* = 2.4 Hz, Xan), 7.70 (d, 2 H, *J* = 2.3 Hz, Xan), 1.69 (s, 6 H, Me), 1.38 (s, 18 H, *t*-Bu).

The crude diacid **40** was suspended in MeOH (250 mL) with 2 mL concentrated HCl. The mixture was heated at reflux for 16 h with an attached drying tube. The solution was diluted with water (500 mL) and filtered to give a white powder (8.96 g, 96 % from the dibromide **38**): ¹H NMR (250 MHz, CDCl₃) δ 7.64 (d, 2 H, *J* = 2.4 Hz, Ar), 7.54 (d, 2 H, *J* = 2.4 Hz, Ar), 3.97 (s, 6 H, Me), 1.64 (s, 9 H). (V-13, VI-295)

Xanthene Monoacid Monomethylester (42). A 1-necked 1 L round bottom flask containing 500 mL CH₂Cl₂ was cooled in an ice bath and hydrogen bromide

³¹ The C-shaped perylene diacid **45c** was treated with 1-2 eq of [(CH₃)CCO]₂O which due to sterics reacts with only one acid. Subsequent quenching of the mixed anhydride with an amine gave the corresponding monoamide monoacid.

³² Nowick, J. S.; Ballester, P.; Ebmeyer, F.; Rebek, J., Jr. *J. Am. Chem. Soc.* **1990**, *112*, 8902.

³³ Caution should be observed with CuCN and subsequent solutions.

bubbled through the solution for 10 min. Xanthene dimethylester **41** (8.96 g, 20.4 mmol) was added and the flask sealed to atmosphere by attaching to a bubbler containing mineral oil. The reaction mixture was stirred for 1.5 h and then quenched with 500 mL of water. The organic layer was separated, washed with water (3 x 200 mL) and dried over MgSO₄, yielding an off-white crystalline solid (8.39 g, 97%): ¹H NMR (250 MHz, CDCl₃) δ 8.25 (d, 2 H, *J* = 2.5 Hz, Ar), 7.98 (d, 2 H, *J* = 2.6 Hz, Ar), 7.69 (d, 2 H, *J* = 2.5 Hz, Ar), 7.66 (d, 2 H, *J* = 2.6 Hz, Ar), 4.00 (s, 3 H, Me), 1.68 (s, 6 H), 1.33 (s, 9 H). (V-17, 31)

Xanthene Benzyl Carbamate Methyl Ester (44). Xanthene monoacid monomethylester **42** (8.39 g, 19.76 mmol), diphenylphosphoryl azide (5.1 mL, 23.71 mmol), and triethylamine (3.30 mL, 23.71 mmol) were dissolved in toluene (50 mL) under an Ar atmosphere. The solution was stirred for 10 min and then BnOH (2.87 mL, 27.66 mmol) was added. The reaction was stirred for 1 h, during which N₂ evolution was observed, and then heated at 80-85 °C for an additional 2 h. The reaction mixture was concentrated to a thick oil by rotary evaporation. The oil was taken up in 100 mL CH₂Cl₂ and washed with 1 N HCl (2 x 100 mL). The organic layer was concentrated to a clear oil under rotary evaporation. Column chromatography on silica gel (EtOAc/Hex, 10-15 %) yielded a white solid (9.72 g, 93%): mp 217-219 °C; IR (KBr) 3430, 3386, 2964, 1730, 1707, 1445, 1276, 1240, 1102, 1008, 785 cm⁻¹; ¹H NMR (250 MHz, CDCl₃) δ 8.24 (s, 1 H, Xan), 8.15 (br s, 1 H, -NH), 7.89 (d, 1 H, *J* = 2.3 Hz, Xan), 7.62 (d, 1 H, *J* = 2.2 Hz, Xan), 7.30-7.50 (m, 5 H, Ph), 7.07 (d, 1 H, *J* = 1.8 Hz, Xan), 5.28 (s, 2 H, Bn), 3.92 (s, 3 H, Me), 1.62 (s, 6 H, Me), 1.34 (s, 18 H, *t*-Bu); HRMS (EI) calcd for C₃₃H₃₉N₁O₅ 529.2831, found 529,2831.

Xanthene Amino Acid (34). Xanthene carbamate ester **44** (9.73 g, 18.38 mmol) and KOH (15.0 g) were suspended in ethylene glycol (250 mL) and refluxed under an Ar atmosphere for 3.5 h. The solution was acidified with 1.0 N HCl, diluted with H₂O (300 mL), and filtered. The wet solid was washed well with H₂O, yielding a white solid (7.20 g, 100%): mp 258-259 °C; IR (KBr) 3378, 2963, 2904, 2869, 2592, 1702, 1587, 1460, 1363, 1281, 1242, 860 cm⁻¹; ¹H NMR (CDCl₃) δ 7.95 (d, 1 H, *J* = 2.1 Hz, Xan), 7.65 (d, 1 H, *J* = 2.1 Hz, Xan), 6.81 (d, 1 H, *J* = 1.8 Hz, Xan), 6.73 (d, 1 H, *J* = 1.8 Hz, Xan), 3.40 (br s, 2 H, -NH₂), 1.63 (s, 6 H, Me), 1.35 (s, 9 H, *t*-Bu), 1.30 (s, 9 H, *t*-Bu); HRMS (EI) calcd for C₂₄H₃₁N₁O₃ 381.2304, found 381.2301.

C- and S- Perylene Diacid Cleft (45). Zinc(II) acetate 2.5 hydrate (23.5 mg, 0.107 mmol), xanthene amino acid **34** (200 mg, 0.524 mmol), and 3,4,9,10-perylene dianhydride were suspended in 7 mL of quinoline. The reaction mixture was heated at 220 °C for 1 h without a reflux condenser to allow evaporation of water and then heated an additional 15 h with a reflux condenser.³⁴ The clear dark purple reaction mixture was taken up in 100 mL of CH₂Cl₂ and washed with 1 N HCl (4 × 150 mL). The organic layer was concentrated to a dark red solid *in vacuo*. Column chromatography on silica gel (3-6% MeOH/CH₂Cl₂) yielded two isomers, S- (higher *R_f*, 63.3 mg, 24%) and C- (lower *R_f*, 60 mg, 23%), as dark red solids which fluoresce strongly. C-isomer: mp > 300 °C; IR (KBr) 3386, 2962, 1707, 1671, 1595, 1450, 1402, 1360, 1258 cm⁻¹; ¹H NMR (300 MHz, pyr-*d*₅) δ 8.82 (d, 4 H, *J* = 7.8 Hz, Per), 8.39 (d, 4 H, *J* = 8.1 Hz, Per), 8.22 (s, 2 H, Xan), 7.96 (s, 2 H, Xan), 7.78 (s, 2 H, Xan), 7.71 (s, 2 H, Xan), 1.72 (s, 12 H, Me), 1.44 (s, 18 H, *t*-Bu), 1.24 (s, 18 H, *t*-Bu); MS (FAB in 3-nitrobenzyl alcohol) calcd for C₇₂H₆₇N₂O₁₀ (M⁺H) 1119.0, found 1119.5.

S-isomer: mp > 300 °C; IR (KBr) 3385, 2965, 1707, 1673, 1594, 1451, 1360, 1359, 1265, 810 cm⁻¹; ¹H NMR (300 MHz, CDCl₃) δ 8.55 (d, 4 H, *J* = 7.8 Hz, *o*-Per), 8.51 (d, 4 H, *J* = 8.2 Hz, *m*-Per), 7.55-7.65 (m, 6 H, Xan), 7.34 (s, 2 H, Xan), 1.72 (s, 12 H, Me), 1.45 (s, 18 H, *t*-Bu), 1.24 (s, 18 H, *t*-Bu); HRMS (FAB in 3-nitrobenzyl alcohol) calcd for C₇₂H₆₇N₂O₁₀ (M⁺H) 1119.4796, found 1119.4807.

Perylene Monoxanthene imide (46). The mono condensation product **46** was isolated from the incomplete reaction of xanthene amino acid **34** (1.0 g, 2.62 mmol) and perylene dianhydride **30** (1.54 g, 3.93 mmol) in refluxing N-methyl pyrrolidinone (125 mL) for 24 h. The reaction mixture was diluted with water (300 mL) and filtered. The red solid was chromatographed (MeOH/CH₂Cl₂, 3 %): ¹H NMR (CDCl₃) δ 8.76 (d, 2 H, *J* = 8.7 Hz, Per), 8.56 (d, 2 H, *J* = 7.8 Hz, Per), 8.40 (br s, 4 H, Per), 7.86 (d, 1 H, *J* = 2.4 Hz, Xan), 7.66 (d, 1 H, *J* = 2.7 Hz, Xan), 7.62 (d, 1 H, *J* = 2.1 Hz, Xan), 7.32 (d, 1 H, *J* = 2.7 Hz, Xan), 1.76 (s, 6 H, Me), 1.41 (s, 9 H, *t*-Bu), 1.32 (s, 8 H, *t*-Bu). (VI-151).

C- and S- Perylene Scaffold (48). Isolated from the condensation reaction described for perylene diacid **45** but at higher temperatures.

³⁴ The level of the solvent was always kept above the level of the oil bath. Reactions in which the reaction flask was completely immersed showed a great deal of decarboxylated product.

S-isomer: mp > 350; ^1H NMR (300 MHz, CDCl_3) δ 8.81 (d, 4 H, $J = 8.0$ Hz, Per), 8.74 (d, 4 H, $J = 8.2$ Hz, Per), 7.58 (d, 2 H, $J = 2.2$ Hz, Xan), 7.40 (d, 2 H, $J = 2.2$ Hz, Xan), 7.24 (d, 2 H, $J = 2.2$ Hz, Xan), 7.06 (dd, 2 H, $J = 2.2, 8.5$ Hz, Xan), 6.67 (d, 2 H, $J = 8.6$ Hz, Xan), 1.73 (s, 12 H, Me), 1.40 (s, 18 H, *t*-Bu), 1.29 (s, 18 H, *t*-Bu); MS (FAB in nitrobenzyl alcohol) calc'd for $\text{C}_{70}\text{H}_{67}\text{N}_2\text{O}_6$ 1032.3 (M + H), found 1032.6.

C-isomer: ^1H NMR (300 MHz, CDCl_3) δ 8.74 (d, 4 H, $J = 8.0$ Hz, Per), 8.61 (d, 4 H, $J = 8.2$ Hz, Per), 7.55 (d, 2 H, $J = 2.2$ Hz, Xan), 7.39 (d, 2 H, $J = 2.3$ Hz, Xan), 7.33 (d, 2 H, $J = 2.3$ Hz, Xan), 7.04 (dd, 2 H, $J = 2.3, 8.6$ Hz, Xan), 6.65 (d, 2 H, $J = 8.5$ Hz, Xan), 1.72 (s, 12 H, Me), 1.35 (s, 18 H, *t*-Bu), 1.29 (s, 18 H, *t*-Bu); MS (FAB in nitrobenzyl alcohol) calc'd for $\text{C}_{70}\text{H}_{67}\text{N}_2\text{O}_6$ 1032.3 (M + H), found 1032.6.

C- and S- Perylene Diamine (50). Xanthene diamine 49³⁵ (0.203 g, 0.58 mmol) was dissolved in 10 mL quinoline with perylene dianhydride (0.113 g, 0.29 mmol) and zinc acetate dihydrate (0.44 g, 0.15 mmol). The solution was stirred and heated to 200 °C for 20 h, then allowed to cool. Most of the quinoline was removed by distillation under high vacuum, leaving a red solid. This solid was dissolved in CH_2Cl_2 , extracted with 1.0 N HCl, and dried over MgSO_4 . Rotary evaporation gave a dark red solid which was column chromatographed on silica gel (0.5-0.75% MeOH/ CH_2Cl_2). From this column was isolated a mixture of C- and S-shaped diamino clefts. These were separated further with another silica gel column (1.0-1.5% acetone/ CH_2Cl_2). The individual fractions were compared by ^1H NMR and TLC to confirm that the two isomers were separate. Some contaminants which exhibited ^1H NMR peaks at 2.0-2.5 ppm were presumably from the condensation of acetone with the free xanthene amines for the products. S-isomer: mp > 330 °C; IR (KBr) 3378, 2961, 1709, 1673, 1594, 1479, 1356, 1252, 851, 809, 746, 674 cm^{-1} ; ^1H NMR (CDCl_3) δ 8.80 (d, 4 H, $J = 8.0$ Hz), 8.73 (d, 4 H, $J = 8.0$ Hz), 7.58 (d, 2 H, $J = 1.8$ Hz), 7.25 (d, 2 H, obscured), 6.84 (d, 2 H, $J = 2.1$ Hz), 6.55 (d, 2 H, $J = 1.90$ Hz), 3.31 (br s, 4 H), 1.71 (s, 12 H), 1.40 (s, 18 H), 1.26 (s, 18 H); HRMS (EI) calc'd for $\text{C}_{70}\text{H}_{68}\text{N}_4\text{O}_6$ 1060.5139, found 1060.5129.

C-isomer: mp > 330 °C; IR (KBr) 3372, 2960, 1709, 1672, 1594, 1480, 1357, 1254, 852, 810, 746, 675 cm^{-1} ; ^1H NMR (CDCl_3) δ 8.78 (d, 4 H, $J = 7.9$ Hz), 8.68 (d, 4 H, J

³⁵ Hamann, B.; Branda, N.; Rebek, J., Jr. *Tetrahedron Letters* 1993, 34, 6837-6840.

= 8.1 Hz), 7.57 (d, 2 H, $J = 2.2$ Hz), 7.28 (d, 2 H, $J = 2.2$ Hz), 6.83 (d, 2 H, $J = 2.1$ Hz), 6.55 (d, 2 H, $J = 2.1$ Hz), 3.29 (br s, 4 H), 1.70 (s, 12 H), 1.38 (s, 18 H), 1.26 (s, 18 H); HRMS (EI) calcd for $C_{70}H_{68}N_4O_6$ 1060.5139, found 1060.5124.

C-Perylene Diamide Cleft (51c). The acid chloride was prepared by dissolving the C-isomer of the diacid cleft **45** (87 mg, 0.0777 mmol) in CH_2Cl_2 (10 mL) with 1.0 mL $SOCl_2$ and two drops of DMF. The solution was refluxed for 1.5 h and then concentrated *in vacuo* to a red solid.

The crude diacid chloride was taken up in CH_2Cl_2 (15 mL), treated with 1 mL of concentrated NH_3OH solution, and stirred for 1 h. The reaction mixture was washed with 1.0 N HCl (1 x 50 mL), H_2O (1 x 50 mL), and brine (1 x 50 mL). The organic layer was concentrated by rotary evaporation and column chromatography on silica gel (2% MeOH/ CH_2Cl_2) to yield a red solid (71.6 mg, 82%): mp > 330 °C; IR (KBr) 3492, 3399, 2961, 1709, 1673, 1594, 1449, 1357, 1253, 810 cm^{-1} ; 1H NMR ($CDCl_3$) δ 8.66 (d, 4 H, $J = 7.9$ Hz, Per), 8.45 (d, 4 H, $J = 8.2$ Hz, Per), 7.80 (d, 2 H, $J = 2.4$ Hz, Xan), 7.58 (d, 2 H, $J = 2.6$ Hz, Xan), 7.56 (d, 2 H, $J = 2.1$ Hz, Xan), 7.47 (d, 2 H, $J = 2.2$ Hz, Xan), 6.67 (br s, 2 H, -NH), 4.77 (br s, 2 H, -NH), 1.74 (s, 12 H, Me), 1.33 (s, 18 H, *t*-Bu), 1.31 (s, 18 H, *t*-Bu); HRMS (EI) calcd for $C_{71}H_{65}N_4O_8$ (M - CH_3) 1101.4802, found 1101.4798.

S-Perylene Diamide (51s). The preparation of the S-isomer is identical to the C-isomer (above) using S-diacid **45** (77 mg, 0.0688 mmol) to yield a red solid (70.4 mg, 92%): mp > 330 °C; IR (KBr) 3433, 2962, 1705, 1673, 1592, 1451, 1355, 1274, 1252, 809 cm^{-1} ; 1H NMR ($CDCl_3$) δ 8.81 (d, 4 H, $J = 8.7$ Hz, Per), 8.77 (d, 4 H, $J = 7.2$ Hz, Per), 7.81 (d, 2 H, $J = 2.4$ Hz, Xan), 7.62 (d, 2 H, $J = 2.7$ Hz, Xan), 7.59 (d, 2 H, $J = 2.4$ Hz, Xan), 7.29 (d, 2 H, $J = 2.1$ Hz), Xan, 6.86 (br s, 2 H, NH), 4.84 (br s, 2 H, NH), 1.76 (s, 12 H, Me), 1.41 (s, 18 H, *t*-Bu); HRMS (EI) calcd for $C_{71}H_{65}N_4O_8$ (M - CH_3) 1101.4802, found 1101.4798.

C-Perylene Diamide Hexol (52c). The diacid chloride (0.0474 mmol) was prepared (see **51c**) and taken up in 10 mL of CH_2Cl_2 . The amino triol, TRIS, (120 mg, 0.991 mmol) was added neat to the solution and stirred for 16 h. The reaction mixture was washed with 1.0 N HCl (1 x 50 mL) and saturated $NaHCO_3$ (1 x 50 mL) then concentrated by rotary evaporation. Column chromatography on silica gel (4% MeOH/ CH_2Cl_2) yielded a red solid (24 mg, 38%): mp > 330 °C; IR (KBr) 3394, 3167, 2960, 1708, 1671, 1594, 1449, 1403, 1360, 1257, 810 cm^{-1} ; 1H NMR ($CDCl_3/MeOD-d_4$) δ 8.54 (d, 4 H, $J = 8.1$ Hz, Per), 8.32 (d, 4 H, $J = 8.4$ Hz,

Per), 7.59 (d, 2 H, $J = 2.1$ Hz, Xan), 7.47 (d, 2 H, $J = 2.7$ Hz, Xan), 7.46 (d, 2 H, $J = 1.8$ Hz, Xan), 7.01 (d, 2 H, $J = 2.7$ Hz, Xan), 6.57 (s, 2 H, NH), 2.62 (s, 12 H, $-\text{CH}_2-$), 1.67 (s, 12 H, Me), 1.24 (s, 18 H, *t*-Bu), 1.20 (s, 18 H, *t*-Bu); HRMS (FAB in 3-nitrobenzyl alcohol) calcd for $\text{C}_{80}\text{H}_{85}\text{N}_4\text{O}_{14}$ ($M + H$) 1325.6062, found 1325.6056.

C-Perylene Diamide Tetrol (53c). The diacid chloride (0.0188 mmol) was prepared (see 51c) and taken up in CH_2Cl_2 (15 mL). Amino diol, (1*S*,1*S*)-(+)-2-amino-1-phenyl-1,3-propanediol, (54 mg, 0.323 mmol) was added neat to the solution and stirred for 16 h. The reaction mixture was washed with 1.0 N HCl (1 x 50 mL) and rotary evaporation gave a red solid. Column chromatography on silica gel (4% MeOH/ CH_2Cl_2) yielded a red solid (20 mg, 75%): mp > 330 °C; IR (KBr) 3407, 2959, 1707, 1671, 1594, 1449, 1358, 1257, 810 cm^{-1} ; ^1H NMR (CDCl_3) δ 8.64 (d, 4 H, $J = 7.8$ Hz, Per), 8.68 (d, 2 H, $J = 8.4$ Hz, Per), 8.47 (d, 2 H, $J = 9.0$ Hz, Per), 7.52 (d, 2 H, $J = 1.5$ Hz, Xan), 7.45 (d, 2 H, $J = 1.2$ Hz, Xan), 7.43 (d, 2 H, $J = 2.7$ Hz, Xan), 7.05-7.15 (m, 6 H, Xan and Ph), 6.90-7.00 (m, 4 H, Ph), 6.83 (d, 2 H, $J = 0.9$ Hz), 6.17 (d, 2 H, $J = 6.3$ Hz, NH), 4.40-4.48 (m, 2 H), 3.65-3.78 (m, 2 H), 3.30-3.42 (m, 2 H), 2.85-2.97 (m, 2 H), 2.55-2.70 (m, 2 H), 2.28-2.40 (m, 2 H), 1.70 (s, 6 H, Me), 1.68 (s, 6 H, Me), 1.38 (s, 18 H, *t*-Bu), 1.33 (s, 18 H, *t*-Bu); HRMS (FAB in 3-nitrobenzyl alcohol) calcd for $\text{C}_{90}\text{H}_{89}\text{N}_4\text{O}_{12}$ ($M + H$) 1417.6477, found 1417.6383.

C- and S-Perylene Dibenzyl Diester (54). The diacid chloride (1.31 mmol) was prepared by refluxing diacid cleft 45 (a mixture of C- and S-isomers) in 200 mL of CH_2Cl_2 with 12.0 mL of SOCl_2 for 1 h. The solution was concentrated *in vacuo* and taken up in 100 mL of CH_2Cl_2 . Benzyl alcohol (740 μL , 7.14 mmol) was added and then heated at reflux for 2 h. The solution was diluted with 100 mL of CH_2Cl_2 and extracted with 1.0 N HCl (2 x 150 mL). The organic layer was evaporated *in vacuo* to a red solid. Column chromatography on silica gel (0.0-0.25% MeOH/ CH_2Cl_2) separated the two isomers as red solids. S-isomer (0.831 g, 49 %): mp > 330 °C; IR (KBr) 2960, 1709, 1673, 1594, 1451, 1358, 1256, 1179, 810, 747 cm^{-1} ; ^1H NMR (CDCl_3) δ 8.64 (d, 4 H, $J = 8.0$ Hz, Per), 8.54 (d, 4 H, $J = 8.1$ Hz, Per), 7.63 (d, 2 H, $J = 2.2$ Hz, Xan), 7.60 (d, 2 H, $J = 2.5$ Hz, Xan), 7.58 (d, 2 H, $J = 2.0$ Hz, Xan), 7.29 (d, 2 H, $J = 2.1$ Hz, Xan), 7.09 (d, 2 H, $J = 7.0$ Hz, Ph), 7.03 (dd, 4 H, $J = 7.0$ Hz, $J = 7.5$ Hz, Ph), 6.76 (d, 4 H, $J = 7.2$ Hz, Ph), 4.38 (s, 4 H, $-\text{CH}_2-$), 1.74 (s, 12 H, Me), 1.41 (s, 18 H, *t*-Bu), 1.30 (s, 18 H, *t*-Bu); HRMS (FAB in 3-nitrobenzyl alcohol) calcd for $\text{C}_{86}\text{H}_{72}\text{N}_2\text{O}_{10}$ ($M + H$) 1299.5734, found 1299.5721.

C-isomer (0.702 g, 41%): mp>330 °C; IR (KBr) 2960, 1708, 1673, 1594, 1451, 1357, 1256, 1177, 1111, 810, 746 cm⁻¹; ¹H NMR (CDCl₃) δ 8.53 (d, 4 H, J = 7.8 Hz, Per), 8.28 (d, 4 H, J = 8.4 Hz, Per), 7.58 (s, 4 H, Xan), 7.53 (s, 2 H, Xan), 7.48 (s, 2 H, Xan), 7.01 (d, 2 H, J = 7.2 Hz, Ph), 6.92 (dd, 4 H, J = 7.2 Hz, J = 7.2 Hz, Ph), 6.52 (d, 4 H, J = 7.0 Hz, Ph), 4.13 (s, 4 H, -CH₂-), 1.72 (s, 12 H, Me), 1.33 (s, 18 H, *t*-Bu), 1.28 (s, 18 H, *t*-Bu); HRMS (EI) calcd for C₈₆H₇₈N₂O₁₀ 1298.5656, found 1298.5645; Anal. calcd for C₈₆H₇₈N₂O₁₀: C, 79.48; H, 6.05; N, 2.16. Found: C, 79.28; H, 5.85; N, 2.24.

C- Perylene Diphenylester (55c). The C-isomer of perylene diacid 45c (45 mg, 0.0403 mmol) was converted to the diacid chloride as described above (51c). The crude diacid chloride was dissolved in CH₂Cl₂ (10 mL) with phenol (35 mg, 0.37 mmol) and triethyl amine (200 μL). The reaction mixture was stirred under argon for 16 h and then diluted with CH₂Cl₂ (25 mL) and washed with 1.0 N HCl (50 mL). The organic layer was concentrated to a red solid *in vacuo* and chromatographed (EtOAc/CH₂Cl₂, 2 %). The product was isolated as a bright red solid (48 mg, 94 %): mp>330 °C; ¹H NMR (250 MHz, CDCl₃) δ 8.49 (d, 4 H, J = 8.0 Hz, Per), 8.18 (d, 4 H, J = 8.1 Hz, Per), 7.81 (d, 2 H, J = 2.3 Hz, Xan), 7.67 (d, 2 H, J = 2.3 Hz, Xan), 7.55 (d, 2 H, J = 2.2 Hz, Xan), 7.42 (d, 2 H, J = 2.1 Hz, Xan), 6.40-7.00 (m, 10 H, Ph), 1.74 (s, 12 H, Me), 1.33 (s, 18 H, *t*-Bu), 1.27 (s, 18 H, *t*-Bu).

C- Perylene Dinitrile (56c).³⁶ Oxalyl chloride (110 μL) was added to a solution of DMF (69 μL) in CH₂Cl₂ (10 mL) cooled in an ice bath. After 2 min the C-isomer of perylene diamide 51c (11 mg, 0.00985 mmol) in 5 mL CH₂Cl₂ was added. The solution was stirred for another 5 min then the pyridine (216 μL) was added. The reaction mixture was diluted with an additional 15 mL CH₂Cl₂ and then washed with 1.0 N HCl (3 x 50 mL) and brine (1 x 50 mL). The organic layer was concentrated to a red solid *in vacuo* and chromatographed (MeOH/CH₂Cl₂, 1 %) to give a highly fluorescent red solid (10 mg, 94 %): mp>330 °C; δ 8.70 (d, 4 H, J = 7.9 Hz, Per), 8.52 (d, 4 H, J = 8.1 Hz, Per), 7.59 (d, 2 H, J = 2.2 Hz, Xan), 7.53 (d, 2 H, J = 2.1 Hz, Xan), 7.49 (d, 2 H, J = 2.1 Hz, Xan), 7.29 (d, 2 H, J = 2.2 Hz, Xan), 1.70 (s, 12 H, Me), 1.33 (s, 18 H, *t*-Bu), 1.27 (s, 18 H, *t*-Bu).

³⁶ Procedure for conversion of primary amide to nitrile from: Bargar, T. M.; Riley, C. M. *Syn. Comm.* 1980, 10, 479.

C- Perylene Diamidoalcohol (63c). Perylene diacid **45c** (51 mg, 0.0455 mmol) was converted into the diacid chloride as described above (**51c**). The crude diacid chloride was dissolved in CH₂Cl₂ (15 mL) with (1R,2S)-(-)-Norephedrine (15.1 mg, 0.100 mmol) and triethyl amine (13.9 μ L, 0.100 mmol). The reaction mixture was stirred for 15 min, then washed with 1 N HCl (1 x 25 mL) and concentrated *in vacuo* to a solid. Chromatography (MeOH/CH₂Cl₂, 4 %) gave the product as a red solid (56 mg, 88 %): mp > 330 °C; ¹H NMR (CDCl₃) δ 8.58 (d, 2 H, *J* = 8.0 Hz, Per), 8.52 (d, 2 H, *J* = 8.1 Hz, Per), 8.12 (d, 2 H, *J* = 8.1 Hz, Per), 8.03 (d, 2 H, *J* = 8.0 Hz, Per), 8.58 (d, 2 H, *J* = 8.0 Hz, Per), 7.54 (d, 2 H, *J* = 2.2 Hz, Xan), 7.51 (d, 2 H, *J* = 2.3 Hz, Xan), 7.43 (d, 2 H, *J* = 2.1 Hz, Xan), 7.37 (d, 2 H, *J* = 2.3 Hz, Xan), 6.90-7.08 (m, 6 H, Ph), 6.77 (d, 4 H, *J* = 7.1 Hz, Ph), 6.28 (d, 2 H, *J* = 7.1 Hz, -NH), 4.21 (s, 2 H), 3.98 (s, 2 H), 2.95 (ddd, 2 H, *J* = 2.3, 6.8, 6.8 Hz, -CHMe), 1.76 (s, 6 H, Xan Me), 1.71 (s, 6 H, Xan Me), 1.30 (s, 32 H, *t*-Bu), 0.27 (d, 6 H, *J* = 6.9 Hz, Me). (V-125)

C- Perylene Bis(oxazoline) (57). The C-isomer of perylene diamidoalcohol **63c** (5 mg, 0.0036 mmol) was dissolved in CH₂Cl₂ (15 mL) and cooled in an ice bath. Four drops of SOCl₂ (excess) in CH₂Cl₂ (5 mL) was added to the reaction over 2 min. The solution was stirred for an additional 10 min and then worked up with saturated NaHCO₃ solution. The organic layer was concentrated and chromatographed (MeOH/CH₂Cl₂, 2 %) to give the product as a red solid (4.5 mg, 90 %): mp > 350 °C; ¹H NMR (CDCl₃) δ 8.50 (dd, 4 H, *J* = 8.0, 10.4 Hz, Per), 8.16 (dd, 4 H, *J* = 9.0, 9.0 Hz, Per), 7.65 (d, 2 H, *J* = 2.2 Hz, Xan), 7.53-7.58 (m, 4 H, Xan), 7.32 (d, 2 H, *J* = 2.1 Hz, Xan), 7.17-7.24 (m, 2 H, Ph), 7.11 (dd, 4 H, *J* = 7.3, 7.3 Hz, Ph), 6.68 (d, 4 H, *J* = 7.3 Hz, Ph), 4.04 (d, 2 H, *J* = 6.7 Hz, -CHPh), 2.25-2.45 (m, 2 H, -CHMe), 1.90 (s, 6 H, Xan Me), 1.73 (s, 6 H, Xan Me), 1.37 (s, 18 H, *t*-Bu), 1.30 (s, 18 H, *t*-Bu), 0.40 (d, 6 H, *J* = 6.6 Hz, Me). MS (Plasma Desorption) calc'd for C₉₀H₈₅N₄O₈ (M + H), 1349.6; found 1350.3.

Xanthene monoacid mononaphthalimide (58). Xanthene amino acid **34** (500 mg, 1.31 mmol), Zn(OAc)₂·2.5H₂O (57 mg, 0.31 mmol) and 1,8-naphthalic anhydride (247, mg, 1.25 mmol) were suspended in quinoline (6 mL). The reaction mixture was heated for 5 h at 220° C under argon. The clear reaction solution was taken up in 50 mL CH₂Cl₂ and washed with 1 N HCl (3 x 50 mL) and brine (1 x 50 mL). The organic layer was concentrated to a dark brown solid. Chromatography (MeOH/CH₂Cl₂, 5 %) gave the product as a clear colorless

glass (682 mg, 97 % yield): $^1\text{H NMR}$ (CDCl_3) δ 8.70 (d, 1 H, $J = 2.7$ Hz), 8.68 (d, 1 H, $J = 2.6$ Hz), 7.5 - 8.0 (m, 6 H), 7.48 (d, 1 H, $J = 2.2$ Hz), 7.38 (d, 1 H, $J = 1.9$ Hz), 1.91 (s, 6 H), 1.50 (s, 18 H). (V-63)

Xanthene monoacid mono(nitronaphthalimide) (59). Xanthene diamine **49** (145 mg, 0.411 mmol), 3-nitro-1,8-naphthalene anhydride (214 g, 0.880 mmol), and $\text{Zn}(\text{OAc})_2$ (20 mg) were heated in quinoline (6 mL) for 40 h at 160 °C. The xanthene was distilled off at reduced pressure. The resulting solid was chromatographed ($\text{MeOH}/\text{CH}_2\text{Cl}_2$, 0.25-1.0 %) to give a higher R_f anti- isomer (105 mg, 32 %) and a lower R_f syn- isomer (70 mg, 21 %). Anti-isomer: $^1\text{H NMR}$ (250 MHz, CDCl_3) δ 8.68 (d, 2 H, $J = 2.1$ Hz, Naph), 8.58 (d, 2 H, $J = 7.4$ Hz, Naph), 8.51 (d, 2 H, $J = 2.2$ Hz, Naph), 8.05 (d, 2 H, $J = 8.3$ Hz, Naph), 7.68 (d, 2 H, $J = 7.7$ Hz, Naph), 7.57 (d, 2 H, $J = 2.0$ Hz, Xan), 7.01 (d, 2 H, $J = 1.9$ Hz, Xan), 1.81 (s, 6 H, Me), 1.32 (s, 18 H, *t*-Bu); MS (EI) calc'd for $\text{C}_{47}\text{N}_{38}\text{N}_4\text{O}_9$ 802.84; found 802.1. Syn-isomer: $^1\text{H NMR}$ (250 MHz, CDCl_3) δ 8.83 (d, 2 H, $J = 2.1$ Hz, Naph), 8.72 (d, 2 H, $J = 2.2$ Hz, Naph), 8.30 (d, 2 H, $J = 6.8$ Hz, Naph), 8.05 (d, 2 H, $J = 8.1$ Hz, Naph), 7.50-7.63 (m, 4 H, Xan and Naph), 7.01 (d, 2 H, $J = 2.1$ Hz, Xan), 1.83 (s, 3 H, Me), 1.81 (s, 3 H, Me), 1.32 (s, 18 H, *t*-Bu); MS (EI) calc'd for $\text{C}_{47}\text{N}_{38}\text{N}_4\text{O}_9$ 802.84; found 802.0.

Perylene monobenzylester monoacid (61). The C-diacid **45** (100 mg, 0.0893 mmol) was dissolved in 30 mL CH_2Cl_2 with 1.0 N tetrabutylammonium fluoride in THF (270 μL , 0.267 mmol) and benzyl bromide (23 mg, 0.134 mmol). The reaction was followed by TLC and stopped when the monobenzyl product appeared to be about 50 % of the reaction mixture (~2 to 4 h). The reaction mixture was washed with 1.0 N HCl (2 x 100 mL) and dried over MgSO_4 . The organic layer was dried *in vacuo* to a bright red solid. Chromatography ($\text{MeOH}/\text{CH}_2\text{Cl}_2$, 0.5-2 %) gave the product as a red solid (49 mg, 45 % yield).

$^1\text{H NMR}$ (300 MHz, CDCl_3) δ 8.75 (d, 2 H, $J = 7.8$, Per), 8.60 (d, 2 H, $J = 8.4$, Per), 8.58 (d, 2 H, $J = 8.1$, Per), 8.49 (d, 2 H, $J = 7.5$, Per), 7.91 (d, 1 H, $J = 2.4$ Per), 7.68 (d, 1 H, $J = 2.4$ Per), 7.65 (d, 1 H, $J = 3.0$ Per), 7.61 (d, 1 H, $J = 1.8$ Per), 7.60 (d, 1 H, $J = 2.4$ Per), 7.57 (d, 1 H, $J = 1.8$ Per), 7.36 (d, 1 H, $J = 2.1$ Per), 7.34 (d, 1 H, $J = 2.1$ Per), 7.06-7.15 (m, 3 H, Ph), 6.80-6.88 (m, 2 H, Ph), 4.31 (s, 2 H, $-\text{CH}_2\text{Ph}$), 1.77 (s, 6 H, Me), 1.74 (s, 6 H, Me), 1.38 (s, 18 H, *t*-Bu), 1.33 (s, 9 H, *t*-Bu), 1.29 (s, 9 H, *t*-Bu).

Chapter III

Synthesis of C- and S-Shaped Naphthalene Scaffolds

3.1 INTRODUCTION

An attractive feature of the aryl-imide linkage was its synthetic adaptability, which allowed the assembly of different scaffolds from a small pool of components. This versatility was not fully exploited for the perylene scaffolds because of their intractable nature. However, the synthesis of diimide molecules based on 1,4,5,8-naphthalene dianhydride (**70**) produced a series of new molecular scaffolds with the desired synthetic flexibility. Like the perylene scaffolds, the smaller naphthalene scaffolds also possessed restricted rotation about their C_{aryl}-N_{imide} bonds and were likewise isolated as the corresponding C- and S-shaped isomers. Rounding out the attractive features of the new scaffolds was their greater solubility which allowed the use of milder conditions and produced higher yields.

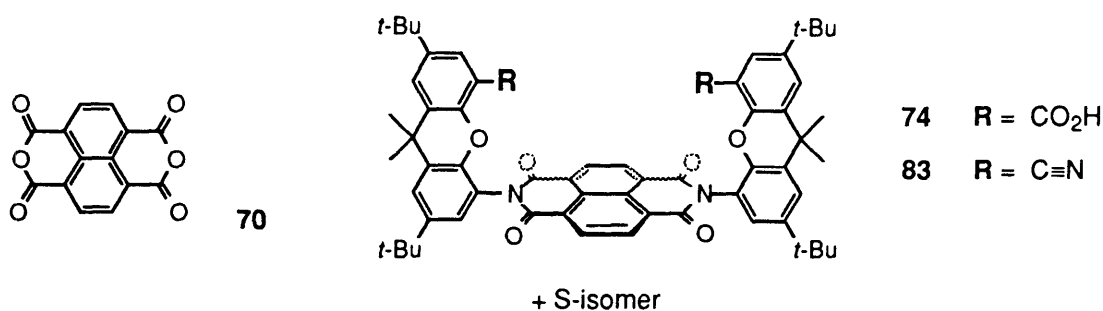


Figure III-1. The smaller naphthalene spacer and resulting bis(xanthene) scaffold.

This enhanced solubility of the naphthalene spacer also permitted the use of alternative U-turns which were more synthetically accessible. In this manner, the reaction of ortho-substituted aryl amines and the naphthalene spacer led in one

step to scaffold **72**. This framework presented functionality in a wider and more open arrangement and still had a convergent C-shape. The greater versatility of the naphthalene spacer was demonstrated by the synthesis of the 'hybrid' scaffold **73**, which gave access to scaffolds having different functionality on either end.

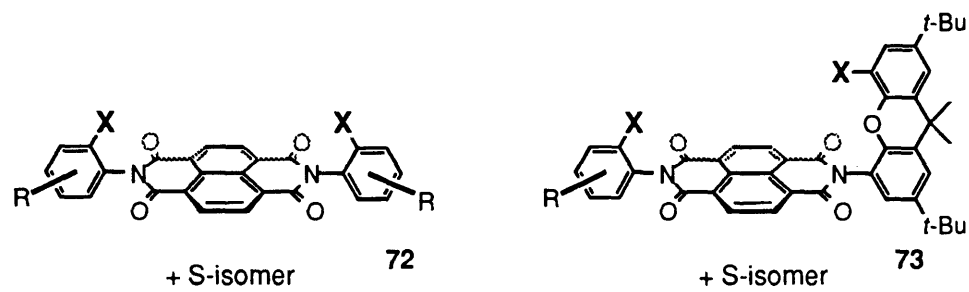


Figure III-2. New naphthalene scaffolds assembled from *o*-aryl amines.

3.2 BACKGROUND

As with perylene dianhydride, the naphthalene dianhydride was also commercially available; therefore, it was somewhat surprising that only a single report of its use in molecular recognition was found. J.-M. Lehn *et al.* prepared the macrocyclic receptor **74** from two naphthalene diimide surfaces bridged by alkyl chains.¹ Both solution and solid-state studies showed that the macrocyclic host **74** was capable of binding guests between its naphthalene surfaces. This binding process was likened to that of a drug intercalating between the base pairs of a DNA helix. The host had a particular affinity for electron poor aromatic guests which appeared to be involved in electron donor-acceptor type interactions with the naphthalene diimides. Although vastly different in design, the success of the macrocyclic receptor demonstrates the potential of the naphthalene surface in creating a rigid and well defined binding pocket.

¹ Jazwinski, J.; Blacker, A. J.; Lehn, J.-M.; Cesario, M.; Guilhem, J.; Pascard, C. *Tet. Lett.* 1987, 28, 6057.

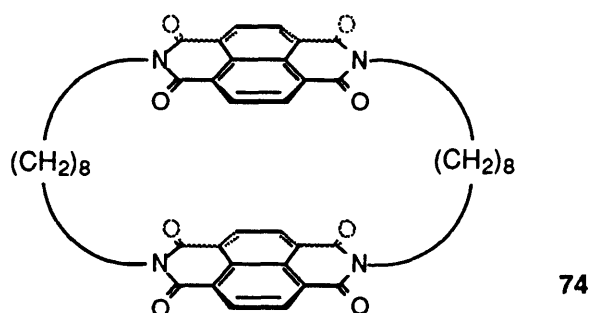


Figure III-3. New naphthalene scaffolds assembled from *o*-aryl amines.

3.3 ASSEMBLY OF THE XANTHENE DERIVED NAPHTHALENE SCAFFOLDS

Initially, the condensation of xanthene amino acid **34** and naphthalene dianhydride **70** was performed under the same conditions that were used for the perylene scaffolds. The corresponding dicondensation products were isolated as bright yellow solids in much higher yields. The C-shaped isomer was formed in 46 % yield and the S-shaped isomer in 38 % yield. Later, it was found that the condensation reaction did not necessitate such harsh conditions.² Simply heating xanthene amino acid **34** (2.2 eq) with naphthalene dianhydride **70** in DMF gave the same C- and S- shaped isomers (**74c** and **74s**). Under similar conditions the perylene dianhydride spacer had shown almost no reaction.

The slight excess of the C-shaped isomer was briefly investigated. It was found that the C- to S- ratio was dependent upon the amount of zinc acetate added: the more zinc acetate, the greater the C- to S- ratio. This was the first indication that the C-shaped naphthalene scaffold had the ability to chelate metals between its convergent functionality and is the subject of a later chapter of this thesis (Chapter V). The zinc acetate was thought to shift the C- to S- equilibrium of the dicondensation products as opposed to acting as a template for their assembly. This is because under the reaction conditions the two rotamers are rapidly interconverting and any template effect would be quickly washed out.

² Kricheldorf, H. R.; Jahnke, P. *Eur. Polym. J.* 1990, 26, 1009.

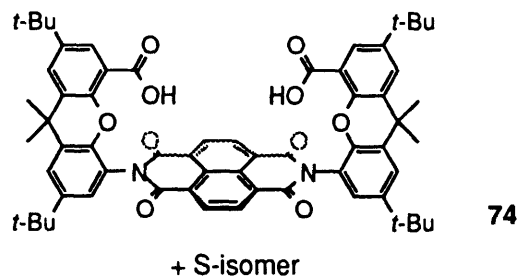


Figure III-4. The bis(xanthene)naphthalene diimide scaffolds. The corresponding S-isomer is not shown.

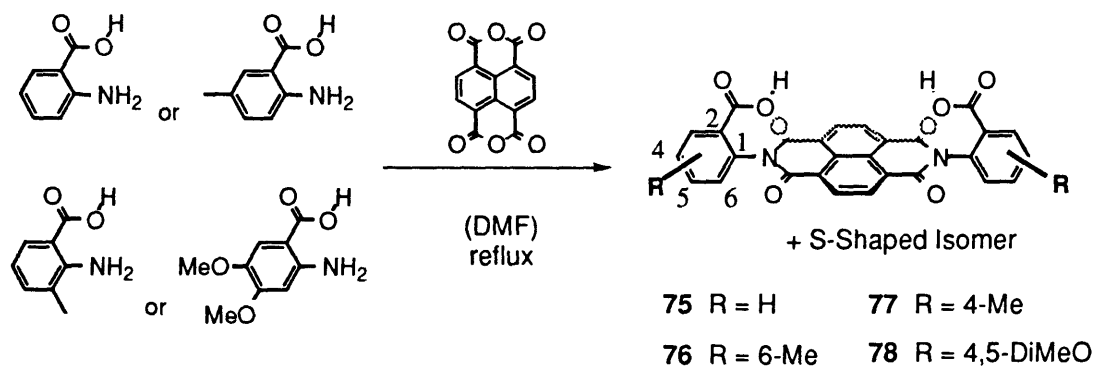
3.4 ASSEMBLY OF ANTHRANILIC ACID DERIVED SCAFFOLDS

A variety of different U-turns were also condensed to the more amenable naphthalene spacer. In particular, anthranilic acids produced scaffolds with a distinctly different shape, shallower cavity, and convergent and divergent diacids. In all the cases examined, the ortho-carboxylic acids appeared to be sufficient to prevent rotation about the $N_{\text{imide}}-C_{\text{aryl}}$ bond, as evidenced by the isolation of their individual rotamers at room temperature. The new scaffolds also had a more open geometry (Table III-1) creating a wider separation between functionality. The intermediate sized anthranilic acid scaffold **75c** nicely fills the gap between the previous bis(xanthene) scaffolds **74c** and **45c** (Table III-1).

	74c	75c	45c
~ shortest O-O dist. (R = -CO ₂ H)	4.2 Å	6.9 Å	8.3 Å

Table III-1. Schematic representations of the various C-shaped scaffolds and their corresponding acid-acid distances. The \square and \triangle shapes represent the xanthene and anthranilic acid U-turns respectively, and N and P designate the naphthalene and perylene diimide surfaces.

Perhaps most promising was the synthetic ease with which the new anthranilic acid diimides were prepared. In a single step, rigid preorganized molecules could be assembled from two commercially available components and in nearly quantitative yields. Simply heating naphthalene dianhydride **70** with an excess of anthranilic acid in DMF gave the two stable conformers of **75**. The simplest scaffold **75** was fairly insoluble and so substituted anthranilic acid scaffolds were also prepared (**76**, **77**, and **78**) with scaffold **78** being the most soluble. Only in the case of a highly electron poor dinitro-anthranilic acid did the condensation reaction fail. Interestingly, the most electron rich dimethoxy anthranilic acid was the only aryl amine in which the diconsensation reaction did not go entirely to completion. Purification was equally facile. The diacids were precipitated from the reaction mixture by dilution with 1.0 N HCl and filtered. Overall, the anthranilic acid scaffolds (**76**, **77**, and **78**) showed poor solubilities as diacids and were considerably more amenable to manipulations upon conversion to their corresponding diesters.

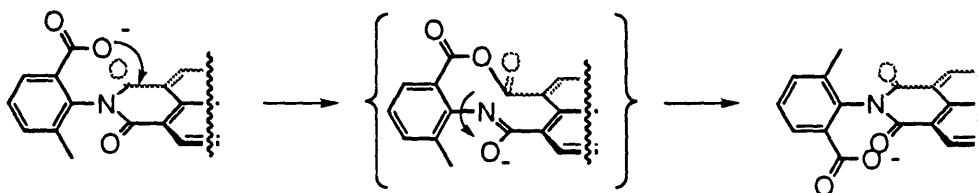


Scheme III-1. Synthesis of anthranilic acid scaffolds.

In each condensation reaction, the C- and S- shaped isomers were observed in approximately a 1 to 1 ratio. Initially, the separation of the conformers was hampered by the poor solubilities of the diacids in most chromatographic solvent systems. However, it was found that a 6 % to 7 % solution of AcOH/CH₂Cl₂ both solubilized and separated the more functionalized scaffolds **76** and **78**.

Although the precise barrier of rotation has not been determined for the bis(anthranilic acid) scaffolds, they appear to be quite stable at ambient temperatures and did not interconvert under mild reaction conditions. The sole exception was diacid **76c** which isomerized during the TBAF deprotection of its

bis(2-(trimethylsilyl)ethyl ester) derivative. This result was especially perplexing because **76** had not one but two groups ortho- to the C_{aryl}-N_{imide} linkage. Heating experiments under the usual conditions of ~ 275 °C (a heat gun) for about 1.5 min. showed no isomerization and confirmed the high thermal stability of **76**. In contrast, the previous xanthene diimides had all shown interconversion under these same conditions. A mechanism was proposed for the isomerization which avoids the direct rotation of the N_{imide}-C_{aryl} bond **76** (Scheme III-2). It is known that in the presence of TBAF, a carboxylic acid becomes considerably more nucleophilic.³ Attack of the carboxylate anion on the adjacent imide ring would form a more flexible 10 membered ring. Twisting the large ring, followed by re-closure of the cyclic imide would now place the carboxylate on the opposing side of the naphthalene.



Scheme III-2. Postulated mechanism for the pseudo rotation of **76c** in the presence of TBAF.

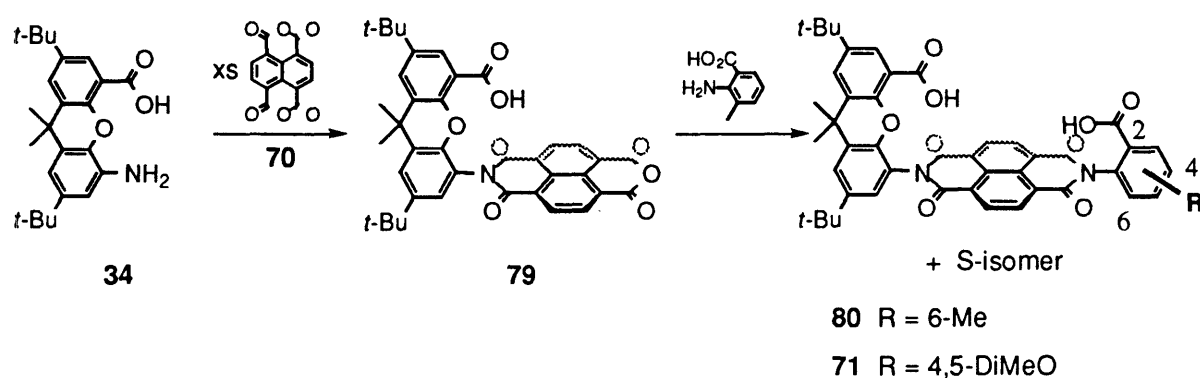
3.5 ASSEMBLY OF A HYBRID SCAFFOLD

The greater solubility of the naphthalene surface also allowed access to a desymmetrized 'hybrid' scaffold **80** which had eluded synthesis in the perylene series. The new shape adds an additional member to the growing family of diimide scaffolds. Even more attractive was that the two halves of the scaffold were now differentiated and the affixed functionality positioned at slightly different distances and orientations relative to the naphthalene spacer.

The synthesis is shown in Scheme III-3. The key step was the facile formation of monoimide monoanhydride **79**. Condensation of xanthene amino acid **34** with an excess of naphthalene dianhydride **70** in DMF gave the crude

³ See previous Chapter II, section 2.5.

monoimide monoanhydride **79**. This material was not purified, although both a ^1H NMR of the reaction mixture and the subsequent condensation products verified its formation. The converse monoimide monoanhydride was not synthesized because of concerns about its insolubility which would hamper its isolation. The greater solubility of the xanthene U-turn allowed the extraction of **79** away from its less soluble and more polar starting materials. The second condensation was equally facile and gave the hybrid scaffold **80**. Oddly, the ^1H NMR spectra of the diacid **80** was extremely broad in both polar (DMSO-d_6) and non-polar solvents (CDCl_3) and proper characterization could only be achieved by conversion into the corresponding diester. Again, these derivatives were isolated as C- and S- shaped isomers, and interestingly, one rotamer was often predominant over the other.

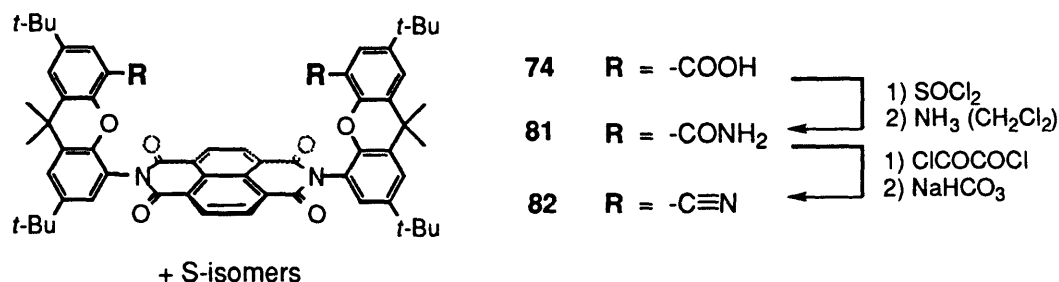


Scheme III-3. Synthesis of the hybrid scaffold.

3.6 FUNCTIONALIZATION OF NAPHTHALENE SCAFFOLDS

Functionalization of the bis(xanthene)naphthalene diimide scaffold 74 paralleled that of its larger perylene cousin. Formation of the diacid chloride followed by treatment with an amine gave cleanly the corresponding diamide. In this manner, the individual rotamers of **81** were synthesized without any interconversion. The primary diamide **81** was synthesized because modeling showed that a larger amine would already fill the smaller cavity of diacid **74**. In addition, the diamide **81** could be transformed into dinitrile **82** on treatment with DMF/oxalyl chloride followed by basic work-up. The C-shaped conformer of

the resulting dinitrile **82** possessed the unusual ability to chelate metals in a *trans*-fashion (Chapter V).



Scheme III-4. Functionalization of the smaller xanthene derived scaffold **74**.

Functionalization of the bis(anthranilic acid) and 'hybrid' naphthalene diimide scaffolds were equally facile. Esterification of the diacids was achieved by a variety of methods: 1) Fischer esterification, 2) TBAF and benzyl bromide, and 3) via the diacid chloride. In most cases, the corresponding diesters were isolated in excellent yields. The alkylation of the diacids with benzyl bromide and TBAF was particularly efficient. The Fischer esterification, however, did not proceed for the less soluble bis(anthranilic acid) scaffold.

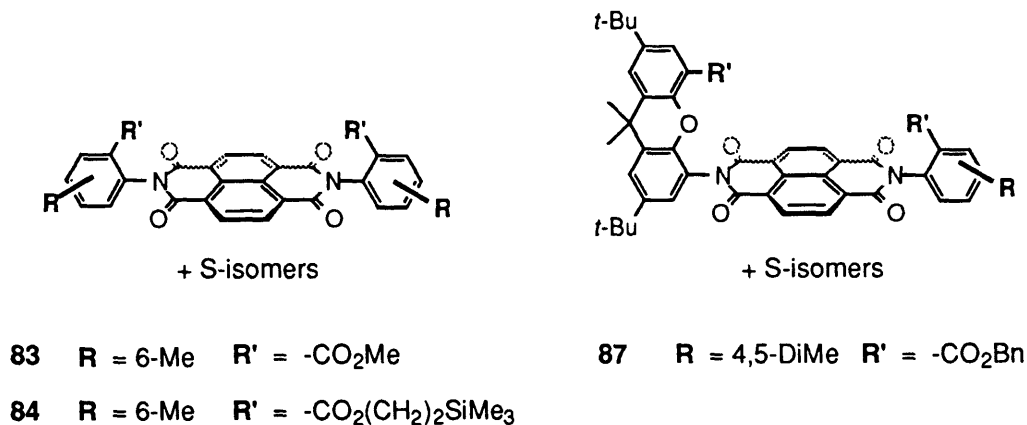


Figure III-5. Diesters of the anthranilic acid scaffolds.

3.7 OUTLOOK

As exemplified by the 'hybrid' scaffold 80, the naphthalene surface is synthetically much more adaptable. The success of monocondensation reactions considerably expands the number of different shapes and sizes that can be constructed from the available sub-units. For example, scaffold 90 creates an even larger acid-acid distance and could be assembled from just two condensation reactions from commercially available components. Preliminary tests have shown that these larger scaffolds are surprisingly soluble perhaps due to their more three-dimensional character.

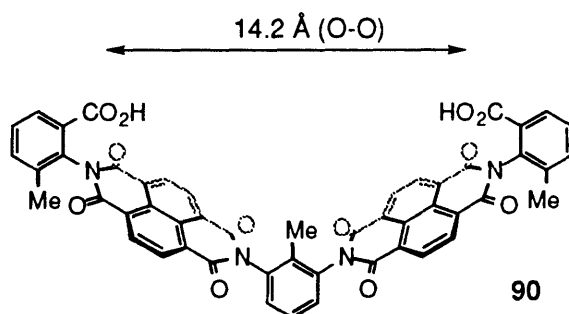


Figure III-6. A large diacid scaffold assembled from existing aryl and naphthalene units

Alternatively, other spacers and U-turns could be utilized. The 5-membered ring dianhydrides are all known.⁴ The resulting 5-membered diimides did not always form on just heating the components together and often required subsequent treatment with TFA to effect ring closure. The 5-membered aryl diimides also had a lower barrier of rotation and isomerization of the two rotamers was seen at room temperature (section 4.3). This problem was alleviated by the addition of a second ortho-aryl functionality. Other aryl amines will also quickly lead to new shapes and diacid orientations. For example, condensation of 2-amino-biaryls with naphthalene dianhydride focuses functionality inward at an angle reminiscent of diiron dicarboxylate species (Figure III-7). Other U-turns having different convergent functionality are also

⁴ Gangneux, P.; Marechal, E. *Bull. Soc. Chim. France* 1973, 4, 1466-1483.

possible such as ortho-aminophenols and should likewise display restricted rotation.

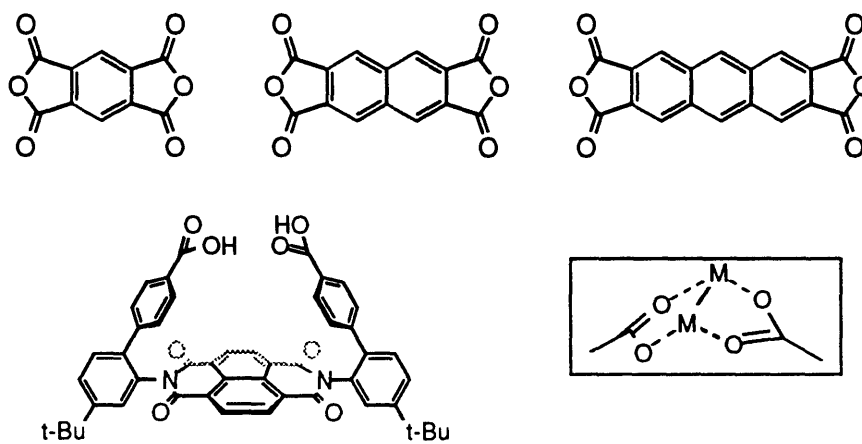


Figure III-7. Alternative spacers and U-turns.

3.8 EXPERIMENTAL SECTION

C- and S-Naphthalene Diacid Cleft (74c and 74s). Xanthene amino acid **34** (352 mg, 0.922 mmol), 1,4,5,8-naphthalenetetracarboxylic acid dianhydride (110 mg, 0.410 mmol), and $\text{Zn}(\text{OAc})_2 \cdot 2\text{H}_2\text{O}$ (45 mg, 0.205 mmol) were heated in quinoline (15 mL) for 4.5 h at 200 °C. The solution was cooled to room temperature, diluted with CH_2Cl_2 (125 mL), and washed with 1.0 N HCl (3 x 200 mL) and brine (1 x 100 mL). The organic layer was concentrated by rotary evaporation to a dark brown solid. Column chromatography on silica gel (1-3 % MeOH/ CH_2Cl_2) separated the two isomers; however the compounds eluted in the reverse of their R_f values on TLC (Kieselgel 60) as yellow crystalline solids. The C-isomer (187 mg, 46 %) had the higher R_f , and the S-isomer (153 mg, 38 %) had the lower R_f by TLC. C-isomer (74c): mp > 330 °C; IR (KBR) 3386, 2962, 2868, 1718, 1682, 1582, 1449, 1348, 1249, 768 cm^{-1} ; ^1H NMR (300 MHz, CDCl_3) δ 8.85 (s, 4 H, Naph), 7.72 (d, 2 H, $J = 0.6$ Hz, Xan), 7.62 (d, 2 H, $J = 1.5$ Hz, Xan), 7.58 (d, 2 H, $J = 2.1$ Hz, Xan), 7.40 (d, 2 H, $J = 1.2$ Hz, Xan), 1.71 (s, 12 H, Me), 1.43 (s, 18 H, *t*-Bu), 1.29 (s, 18 H, *t*-Bu); HRMS (EI) calcd for $\text{C}_{62}\text{H}_{62}\text{N}_2\text{O}_{10}$ 994.4404, found 994.4409.

S-isomer (74s): mp>330 °C; IR (KBr) 3388, 2962, 2868, 1718, 1682, 1582, 1449, 1348, 1249, 768 cm⁻¹; ¹H NMR (300 MHz, CDCl₃) δ 8.74 (s, 4 H, Naph), 7.78 (d, 2 H, J = 2.4 Hz, Xan), 7.67 (d, 2 H, J = 2.4 Hz, Xan), 7.63 (d, 2 H, J = 2.1 Hz, Xan), 7.28 (d, 2 H, J = 2.1 Hz, Xan), 1.75 (s, 12 H, Me), 1.42 (s, 18 H, *t*-Bu), 1.33 (s, 18 H, *t*-Bu); HRMS (EI) calcd for C₆₂H₆₂N₂O₁₀ 994.4404; found 994.4413.

C- and S- Naphthalene bis(6-methyl-2-benzoic acid) diimide (76).

Naphthalene dianhydride **70** (845 mg, 3.15 mmol) and 2-amino-3-methyl benzoic acid (1.00 g, 6.62 mmol) were heated at reflux in 50 mL DMF for 16 h. The reaction mixture was diluted with 250 mL 1.0 N HCl precipitating the product. The mixture of C- and S-isomers of **76** were collected as a purplish solid (1.60 g). Chromatography (AcOH/CH₂Cl₂, 6-7 %) gave the two isomers: Lower R_f (C-isomer): ¹H NMR (300 MHz, DMSO-d₆) δ 12.30 (s br, 2 H, -CO₂H), 8.77 (s, 4 H, Naph), 7.98 (d, 2 H, J = 7.5 Hz, Ar), 7.71 (d, 2 H, J = 6.9 Hz, Ar), 7.56 (dd, 2 H, J = 7.8, 7.8 Hz, Ar), 2.21 (s, 6 H, Me); MS (Plasma Desorption) calc'd for C₃₀H₁₉N₂O₈ (M + H), 535.11; found 534.3.

Higher R_f (S-isomer): ¹H NMR (300 MHz, DMSO-d₆) δ 12.35 (s br, 2 H, -CO₂H), 8.79 (s, 4 H, Naph), 7.98 (d, 2 H, J = 7.5 Hz, Ar), 7.72 (d, 2 H, J = 7.2 Hz, Ar), 7.56 (dd, 2 H, J = 7.8, 7.8 Hz, Ar), 2.19 (s, 6 H, Me).

C- and S- Naphthalene bis(4-methyl-2-benzoic acid) diimide (77).

Synthesized as above (see **76**) from 2-amino-5-methyl benzoic acid (2.17 g, 14.4 mmol) and naphthalene dianhydride (1.83 g, 6.9 mmol) in 20 mL DMF. The product was isolated as a purplish solid (3.20 g, quantitative) as a 1 to 1 mixture of C- and S-isomers: ¹H NMR (250 MHz, DMSO-d₆) δ 8.74 (s, 4 H, Naph), 8.73 (s, 4 H, Naph), 7.94 (s, 4 H, Ar), 7.61 (d, 4 H, J = 8.0 Hz, Ar), 7.46 (d, 2 H, J = 8.0 Hz, Ar), 7.42 (d, 2 H, J = 7.9 Hz, Ar), 2.46 (s, 12 H, Me). VII-91

C- and S- Naphthalene bis(4,5-dimethoxy-2-benzoic acid) diimide (78).

The diacid **78** was synthesized as described above (see **76c** and **76s**) in 85 % yield: ¹H NMR (C- and S-isomers, 300 MHz, DMSO) δ 12.78 (br s, 4 H, -CO₂H), 8.75 (s, 8 H, Naph), 7.52 (s, 4 H, Ar), 7.24 (s, 2 H, Ar), 7.20 (s, 2 H, Ar), 3.90 (s, 12 H, Me), 3.81 (s, 12 H, Me).

Naphthalene Monoxanthene imide (79). Xanthene amino acid **34** (1.0 g, 2.62 mmol) and naphthalene dianhydride **70** (1.76 g, 6.55 mmol) were heated at reflux in 100 mL DMF for 4 h. The solution was diluted with water (250 mL), filtered

and washed with 1.0 N HCl. The yellow solid was triturated with acetone (~250 mL), filtered and washed with additional acetone until the remaining solid was white. The filtrate was dried to a yellow solid *in vacuo* (1.73 g, 104 %). This crude material was used for a second condensation without purification.

$^1\text{H NMR}$ (250 MHz, Acetone- d_6) δ 8.34 (d, 2 H, $J = 8.9$ Hz, Naph), 8.78 (d, 2 H, $J = 9.2$ Hz, Naph), 7.85 (d, 1 H, $J = 2.9$, Xan), 7.78 (d, 1 H, $J = 2.7$, Xan), 7.71 (d, 1 H, $J = 2.9$, Xan), 7.51 (d, 1 H, $J = 2.9$, Xan), 1.78 (s, 6 H, Me), 1.41 (s, 9 H, *t*-Bu), 1.33 (s, 9 H, *t*-Bu).

C- and S- Naphthalene bis(xanthene diamide)diimide (81). A mixture C- and S-isomers of diacid **74** (1.16 g, 1.17 mmol), thionyl chloride (5 mL) and four drops of DMF were heated at reflux for 2.5 h. The reaction mixture dried to a yellow solid *in vacuo*. The crude diacid chloride was dissolved in 50 mL CH_2Cl_2 and treated with 10 mL of concentrated ammonium hydroxide. The mixture was stirred vigorously for 1 h and then washed with 1.0 N HCl (2 x 100 mL) and dried over MgSO_4 . Chromatography on silica gel (MeOH/ CH_2Cl_2 , 0.75 %) gave the lower R_f S-isomer **81s** (400 mg, 35 %) and the higher R_f C-isomer **81c** (462 mg, 41 %). C-isomer: $^1\text{H NMR}$ (250 MHz, CDCl_3) δ 8.85 (s, 4 H, Naph), 7.59 (br s, 2 H, Xan), 7.51 (d, 2 H, $J = 0.9$ Hz, Xan), 7.40-7.45 (m, 4 H, Xan), 7.00 (br s, 2 H, -NH), 5.68 (br s, 2 H, -NH), 1.71 (s, 12 H, Me), 1.42 (s, 18 H, *t*-Bu), 1.29 (s, 18 H, *t*-Bu); HRMS (EI) calcd for $\text{C}_{62}\text{H}_{64}\text{N}_4\text{O}_8$ (M) $^+$, 992.472416; found 992.47156.

S-isomer: $^1\text{H NMR}$ (250 MHz, CDCl_3) δ 8.87 (s, 4 H, Naph), 7.76 (d, 2 H, $J = 2.3$ Hz, Xan), 7.64 (d, 2 H, $J = 2.0$ Hz, Xan), 7.59 (d, 2 H, $J = 2.3$ Hz, Xan), 7.31 (d, 2 H, $J = 1.9$ Hz, Xan), 6.64 (br s, 2 H, -NH), 4.78 (br s, 2 H, -NH), 1.76 (s, 12 H, Me), 1.41 (s, 18 H, *t*-Bu), 1.32 (s, 18 H, *t*-Bu).

C-Naphthalene bis(xanthene nitrile) diimide (82c). Oxalyl chloride (2 mL) was added to a solution of DMF (1 mL) in CH_2Cl_2 (25 mL). After the bubbling subsided, the C-isomer (higher R_f) of naphthalene diamide **81c** (462 mg, 0.465 mmol) in 5 mL CH_2Cl_2 was added over 5 min, followed 4 mL of pyridine. The reaction mixture was stirred for 10 min, then washed with 1.0 N HCl (2 x 50 mL), and dried over Na_2CO_3 . The organic layer was concentrated *in vacuo* and chromatography (CH_2Cl_2) gave the product as a bright yellow solid (303 mg, 68 %): IR (KBr) 2228 (-CN) cm^{-1} ; $^1\text{H NMR}$ (300 MHz, CDCl_3) δ 8.89 (s, 4 H, Naph), 7.61 (d, 2 H, $J = 2.3$ Hz, Xan), 7.58 (d, 2 H, $J = 2.1$ Hz, Xan), 7.34 (d, 2 H, $J = 2.2$ Hz,

Xan), 7.34 (d, 2 H, $J = 2.2$ Hz, Xan), 1.71 (s, 12 H, Me), 1.40 (s, 18 H, *t*-Bu), 1.29 (s, 18 H, *t*-Bu). HRMS (EI) calcd for C₆₂H₆₀N₄O₆, 956.451286; found 956.45210.

C- and S- Naphthalene bis(6-methyl-2-benzoic acid methyl ester) diimide (83). A one to one C- to S- mixture of naphthalene diacid **76** (380 mg) was heated at reflux with thionyl chloride (2 mL) in methylene chloride (10 mL) for 2 h. The crude diacid chloride was concentrated *in vacuo* to a brown solid and then taken up in 10 mL MeOH and then 2 mL triethyl amine was added. The solution was concentrated and chromatography gave (MeOH/CH₂Cl₂, 0.5 % to 2.0 %) the dimethyl ester as a 1 to 1 mixture of C- and S-isomers. Most of the protons were identical for both rotamers except for the methyl singlets: ¹H NMR (250 MHz, CDCl₃) δ 8.84 (s, 8 H, Naph), 8.11 (d, 4 H, $J = 6.9$ Hz, Ar), 7.65 (d, 4 H, $J = 7.8$ Hz, Ar), 7.51 (dd, 4 H, $J = 7.7$ Hz and 7.7 Hz, Ar), 3.71 (s, 3 H, Me), 3.69 (s, 3 H, Me).

C- and S- Naphthalene bis(6-methyl-2-benzoic acid 2-(trimethylsilyl)ethyl ester) diimide (84). A mixture of C- and S-isomers of diacid **76** (500 mg, 0.936 mmol) was heated at reflux in 15 mL CH₂Cl₂ with 3 mL SOCl₂ for 5 h. The reaction mixture was concentrated *in vacuo* to a brown solid. The crude diacid chloride was taken up in 20 mL CH₂Cl₂; 2-(trimethylsilyl)ethanol (536 μL, 3.74 mmol) and 2 mL of pyridine were added and the solution refluxed overnight. The reaction mixture was washed with 1.0 N HCl (2 X 100 mL) and dried to a solid. Chromatography on silica gel (20 % - 25 %, EtOAc/Hexane) separated the two rotamers: top spot (0.161 g, 23 %) and bottom spot (0.161 g, 23 %).

¹H NMR (bottom spot, 300 MHz, CDCl₃) δ 8.84 (s, 4 H, Naph), 8.10 (d, 2 H, $J = 7.9$ Hz, Ar), 7.62 (d, 2 H, $J = 7.7$ Hz, Ar), 7.51 (dd, 2 H, $J = 7.7$ Hz and $J = 7.7$ Hz, Ar), 4.10-4.22 (m, 4 H, -CH₂-), 2.26 (s, 6 H, Me), 0.88-1.00 (m, 4 H, -CH₂-), -0.286 (s, 18 H, Me).

¹H NMR (top spot, 300 MHz, CDCl₃) δ 8.84 (s, 4 H, Naph), 8.11 (d, 2 H, $J = 7.8$ Hz, Ar), 7.64 (d, 2 H, $J = 6.9$ Hz, Ar), 7.51 (dd, 2 H, $J = 7.7$ Hz and $J = 7.7$ Hz, Ar), 4.08-4.20 (m, 4 H, -CH₂-), 2.26 (s, 6 H, Me), 0.78-0.86 (m, 4 H, -CH₂-), -0.67 (s, 18 H, Me).

C- and S- Hybrid Naphthalene Diimide Dibenzylester (87). Crude diacid **80** (122 mg, 0.150 mmol), (179 μL, 1.50 mmol) and TBAF (475 mg, 1.50) were stirred in 50 CH₂Cl₂ for 1 h. The reaction mixture was washed with 1.0 N HCl (2 x 100 mL) and dried over MgSO₄.

Chromatography (EtOAc/Hex, 33 %) separated both isomers: bottom 33 mg, top 41 mg. Bottom isomer: $^1\text{H NMR}$ (250 MHz, CDCl_3) δ 8.65 (d, 2 H, $J = 7.5$ Hz, Naph), 8.62 (d, 2 H, $J = 7.5$ Hz, Naph), 7.78 (s, 1 H, Ar), 7.71 (d, 1 H, $J = 2.4$ Hz, Xan), 7.61 (d, 1 H, $J = 2.4$ Hz, Xan), 7.58 (s, 1 H, Ar), 6.82 - 7.28 (m, 12 H), 4.97 (s, 2 H, Bn), 4.45 (s, 2 H, Bn), 4.00 (s, 3 H, Me), 3.95 (s, 3 H, Me), 1.74 (s, 6 H, Me), 1.39 (s, 9 H, *t*-Bu), 1.30 (s, 9 H, *t*-Bu).

Top isomer: $^1\text{H NMR}$ (250 MHz, CDCl_3) δ 8.67 (d, 2 H, $J = 7.6$ Hz, Naph), 8.62 (d, 2 H, $J = 7.6$ Hz, Naph), 7.83 (s, 1 H, Ar), 7.50-7.68 (m, 3 H), 7.32 (d, 1 H, $J = 2.1$ Hz, Xan), 7.08-7.22 (m, 3 H), 6.75-6.94 (m, 7 H), 6.74 (s, 1 H, Ar), 4.99 (s, 2 H, Bn), 4.39 (s, 2 H, Bn), 4.02 (s, 3 H, Me), 3.91 (s, 3 H, Me), 1.72 (s, 6 H, Me), 1.39 (s, 9 H, *t*-Bu), 1.28 (s, 9 H, *t*-Bu).

Chapter IV

Structure and Properties of the New Diimide Scaffolds

4.1 INTRODUCTION

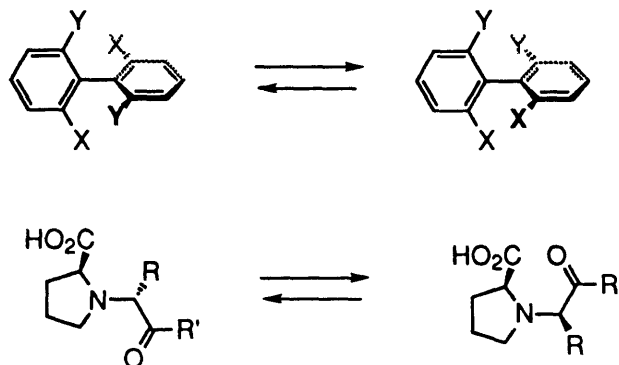
Once the new scaffolds were synthesized the question remained which isomer was which? Spectroscopically, the various C- and S- shaped conformers were virtually indistinguishable due to their similar symmetries. The rotamers, however, could be differentiated by their physical properties. Macrocyclizations of the C-shaped isomers and x-ray crystallography were used to identify the stable rotamers of the perylene and naphthalene diimide scaffolds. These experiments also gave some measure of the distance between convergent functionality in the respective C-shapes. Further conformation of the correct conformational assignments was provided by binding experiments. The C-shaped perylene scaffolds were able to complex organic molecules, whereas the smallest naphthalene scaffolds had an affinity for metal ions.

4.2 BACKGROUND

Rotational isomerism is commonly studied in textbooks as a conformational oddity which can lead to structures having unusual chirality.¹ For example in the most cited case of ortho-biaryls, restricted rotation leads to the formation of two separable enantiomers. Similarly, in our diimide scaffolds the loss of rotational freedom about the N_{imide}-C_{aryl} bond led to stabilization of the C- and S-rotamers. Restricted rotation can also have dire biological consequences. The

¹ For a review of the subject see: Oki, M. *The Chemistry of Rotational Isomers*; Springer-Verlag: New York, 1993

lowered rotational barrier of the proline amide bond² has been implicated as the rate determining step in some protein folding pathways.³



Scheme IV-1. a) Interconversion of a chiral biphenyl. b) Restricted rotation about the proline amide bond.

For isolation at ambient temperatures, a minimum barrier of rotation of ~25 kcal/mol is necessary. Rotational barriers were computed from the Eyring equation (1), assuming an ideal Arrhenius A value of $2.08 \times 10^{10} \text{ s}^{-1}\text{deg}^{-1}$.⁴ The required rate constant was generated from equation (3) using variables of $t_{1/2} \sim 1$ day and $T = 298 \text{ K}$ for the case above. Equation (3) comes from the rearrangement of the kinetic equation (2) for a first order reversible reaction in which [S] represents the concentration of starting material at times t and zero.

$$k = ATe^{-E/RT} \quad (1)$$

$$2kt = \ln \left(\frac{[S]_0}{[S]_0 - [S]_t} \right) \quad (2)$$

² Gutowsky, H. S.; Holm, C. H. *J. Chem. Phys.* **1956**, *25*, 1228.

³ Schulz, G. E.; Schirmer *Principles of Protein Structure*; Springer-Verlag: New York, 1979, pp 25, 155.

⁴ The literature reports a variety of different Arrhenius values. For example a slowly isomerizing biphenyl was estimated to have an AT value of $\sim 10^{11} \text{ s}^{-1}$, and overall for rotational isomerization the AT values tend to be slightly less than ideal. (Kistiakowsky, G. B.; Smith, W. R. *J. Am. Chem. Soc.* **1936**, *58*, 1043.) For consistency, ideal values were assumed.

$$t_{1/2} = (\ln 2)/2k \quad (3)$$

Atropisomerism has also been used to position functionality over a porphyrin surface, to change the reactivity and selectivity of the metal center.⁵ A great number of these systems have been prepared and studied and they provide an important experimental background for our work with scaffolds having restricted rotation. Recently, another interesting application of atropisomerism has been its use as a 'molecular brake' (101).⁶ Kelly *et al.* prepared a bipyridine which upon chelation of a metal ion can slow the rotation of an affixed triptycene unit.

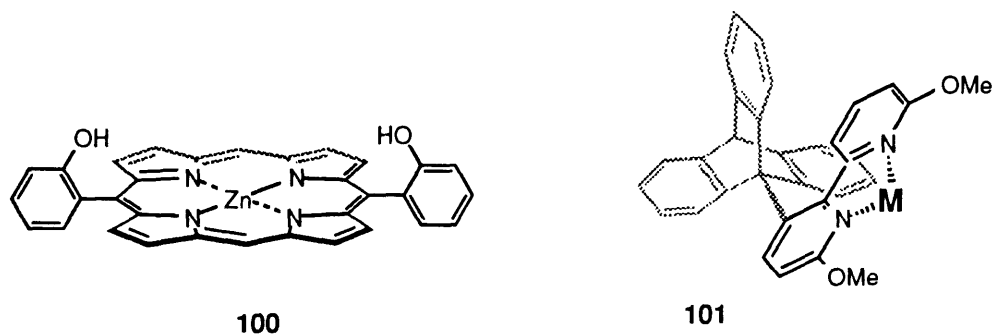


Figure IV-1. Applications of atropisomerism in synthetic porphyrins and as a 'molecular brake'.

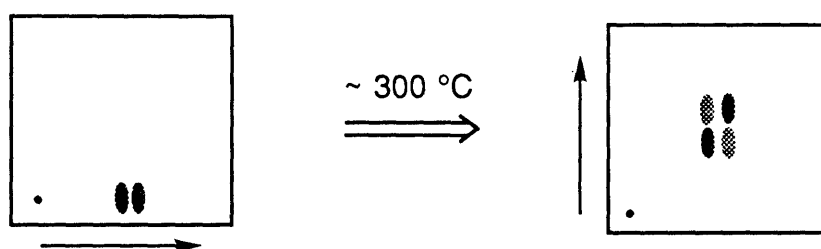
4.3 ORIGINS AND BARRIER OF RESTRICTED ROTATION

The isolation of two very similar compounds from the dicondensation reactions of aryl amines with perylene and naphthalene dianhydrides suggested

⁵ a) Freitag, R. A.; Barber, D. C.; Inoue, H.; Whitten, D. G. In *Porphyrins, Excited States and Dynamics*; M. Gouterman, P. M. Rentzepis and K. D. Straub, Ed.; American Chemical Society: Washington DC, 1986; Chapter 19. b) Aoyama, Y.; Kamohata, T.; Yamagishi, A.; Toi, H.; Ogoshi, H. *Tetrahedron Lett.* **1987**, *28*, 2143.

⁶ Kelly, T. R.; Bowyer, M. C.; Bhaskar, K. V.; Bebbington, D.; Garcia, A.; Lang, F. R.; Kim, M. H.; Jette, M. P. *J. Am. Chem. Soc.* **1994**, *116*, 3557.

that the barrier of rotation about the $C_{aryl}-N_{imide}$ bond was relatively high. Evidence of their isomeric relationship was provided by two-dimensional TLC experiments (Scheme IV-2). First, a reaction mixture was run in one direction on a square TLC plate, separating the two isomers. Heating at high temperature ($\sim 300\text{ }^{\circ}\text{C}$) for about 2 minutes led to interconversion, which was visualized by running the TLC plate in the second direction. For all the perylene and naphthalene derivatives examined, new spots were seen off of the diagonal which corresponded to its rotational isomer. The two-dimensional TLC technique also assisted in identifying the desired products. Only the dicondensation products displayed conformational isomerism. Furthermore, related isomers could easily be matched even in a complex mixture by their 'cross peaks'.



Scheme IV-2. Two dimensional TLC experiments which show interconversion of the C- and S-shaped isomers on heating.

In handling and in the reactions of the various diimides, isomerization was not observed. The stability of the C- and S- shaped isomers was both surprising and advantageous. For example, heating a bis(xanthene)perylene diimide scaffold at $70\text{ }^{\circ}\text{C}$ showed only a trace of isomerization after 15 h. Only when the temperature was raised to $110\text{ }^{\circ}\text{C}$ did the mixture reach equilibrium in a few hours. The barrier of rotation was calculated to be a quite high $\sim 29\text{ kcal/mol}$ from equations (1) and (3). For comparison, the literature reports a rotational barrier of 19.6 kcal/mol for the similar $C_{aryl}-N_{imide}$ bond of structure **102**.⁷ This lower rotational barrier equates to a half-life of only 13 seconds and is considerably lower than that observed for the xanthene scaffolds which are exemplified by structure **104**.

⁷ Verma, S. M.; Singh, N. B. *Aust. J. Chem.* **1976**, *29*, 295-300.

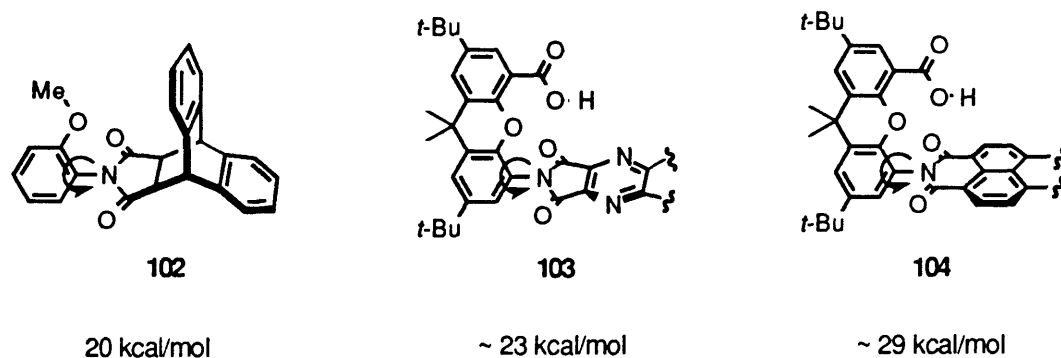


Figure IV-2. Comparisons of the barriers of rotation about several $N_{\text{imide}}-C_{\text{aryl}}$ bonds.

The discrepancy between structures **102** and **104** was hypothesized to be due to two factors. First, 5- and 6-membered imides position their carbonyls at different distances from the opposing aryl rings (Figure IV-3). The 6-membered imides push their carbonyls further out creating greater steric hindrance. Second, the cyclic ether of xanthene **104** 'buttresses' and rigidifies the ether oxygen in comparison to the acyclic ether of **102**. Support for these hypotheses was provided by the synthesis of scaffold **103**, which combined structural features of both **102** and **104**.⁸ The similarity between the three structures allowed the stepwise isolation of the variables which contributed to their three distinct rotational barriers. Scaffolds **104** and **103** differed only in the size of their respective imide rings, and this appears to account for the large 6 kcal/mol disparity in their rotational barriers. On the other end, **103** and **102** both possess less convergent 5-membered imides, but now have contrasting cyclic and acyclic ethers which leads to a further 3 kcal/mol gap.

⁸ Structure **103** is a portion of a larger C_3 symmetric triimide receptor synthesized in our group by Rene Beerli.

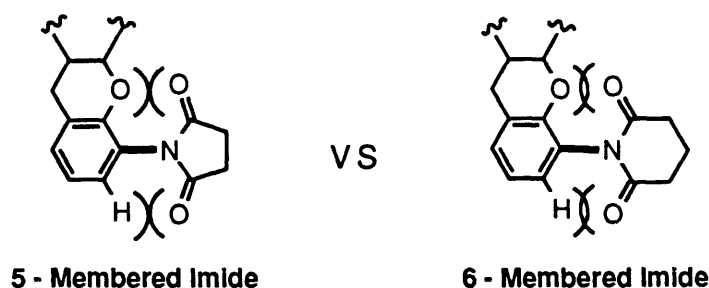


Figure IV-3. Comparisons of the different steric requirements of 5- and 6-membered imides.

Molecular modeling supports the observed increase in the rotational barrier from structures **102** to **104**. However, the forcefields, MM2, Amber and Charm did not give accurate absolute estimations of the observed rotational barriers. Modeling experiments were performed by sequentially fixing the dihedral angle about the $C_{\text{aryl}}-N_{\text{imide}}$ bond from 0° to 360° and reminimizing each structure. The rotational barriers were measured as the difference between the highest and lowest energies. Overall, the predicted rotational barriers underestimated the observed values by 20 % to 30 %. This inaccuracy was somewhat surprising, considering that rotational barriers were the subject of some of the earliest successful computational studies.⁹ Although a great deal of attention has been given to the rotational barrier of biaryls, the $N_{\text{imide}}-C_{\text{aryl}}$ bond appears to be different enough to necessitate a different model. In fact, a recent theoretical study also underestimated the rotational barriers of $N_{\text{imide}}-C_{\text{aryl}}$ bonds by a similar margin.¹⁰

4.4 ASSIGNMENT OF PERYLENE ISOMERS

Designation of the C- and S-shaped perylene isomers was more difficult than first perceived, and this uncertainty in assignment was augmented by conflicting observations. Initially, the rotamers were tentatively identified by their polarities

⁹ b) Westheimer, F. H. In *Steric Effects in Organic Chemistry*; M. S. Newman, Ed.; John Wiley & Sons, Inc.; New York, 1956, chap. 12. b) Westheimer, F. H.; Mayer, J. E. *J. Chem. Phys.* **1946**, *14*, 733.

¹⁰ Bott, G.; Field, L. D.; Sternhell, S. *J. Am. Chem. Soc.* **1980**, *102*, 5619.

as measured by their R_f 's values (silica gel, MeOH/CH₂Cl₂). This method has been used to identify the rotational isomers of aryl-porphyrins and has been successful in cases where there were up to four different conformers.¹¹ The perylene diimides followed the expected trend and their C-shapes consistently had the lower R_f values. This was verified for each new compound by isomerizing a small sample and comparing it to the original.

Heating experiments performed on perylene dibenzyl ester **54** were particularly ambiguous. Heating the higher R_f isomer (S-shape) in toluene for two days gave predominately the lower R_f isomer (C-shape) in a 2 to 1 ratio. This asymmetric partitioning was incorrectly interpreted to be caused by the benzyl groups bumping into each other in the C-shape and shifting the equilibrium toward the S-shape. Instead, the benzyl groups actually appear to attract each other, possibly through stacking interactions and making the C-shaped dibenzyl ester **54c** more thermodynamically stable.¹²

The perylene rotamers were ultimately identified by covalently spanning the convergent functionality of the C-shape. For example, the isomers of perylene diacid **45** were separately converted into their respective diacid chlorides and then treated with various diamines. For both 3,6-diaminofluorene (**109**) and 1,7-diaminoheptane (**111**), one rotamer yielded a complex mixture of products presumably due to oligomerization. The other rotamer gave cleanly a single product, which by mass spectrometry and ¹H NMR analysis were consistent with macrocyclic structures **105** and **106**. This confirmed the C-shape of the corresponding perylene starting materials. Similar experiments were performed with perylene diamine **50c**, using 4,4'-biphenyl dicarboxylic acid chloride to bridge the cavity of the C-shape, resulting in macrocycle **107**.

¹¹ Sanders, G. M.; Van Dijk, M.; Machiels, B. M.; van Veldhuizen, A. *J. Org. Chem.* **1991**, *56*, 1301-1305.

¹² An equally sound explanation is that the C-shaped isomer is less soluble than the corresponding S-shape as was seen for diacids **45c** and **45s**. The precipitation of the C-shaped isomer would shift the equilibrium in its favor.

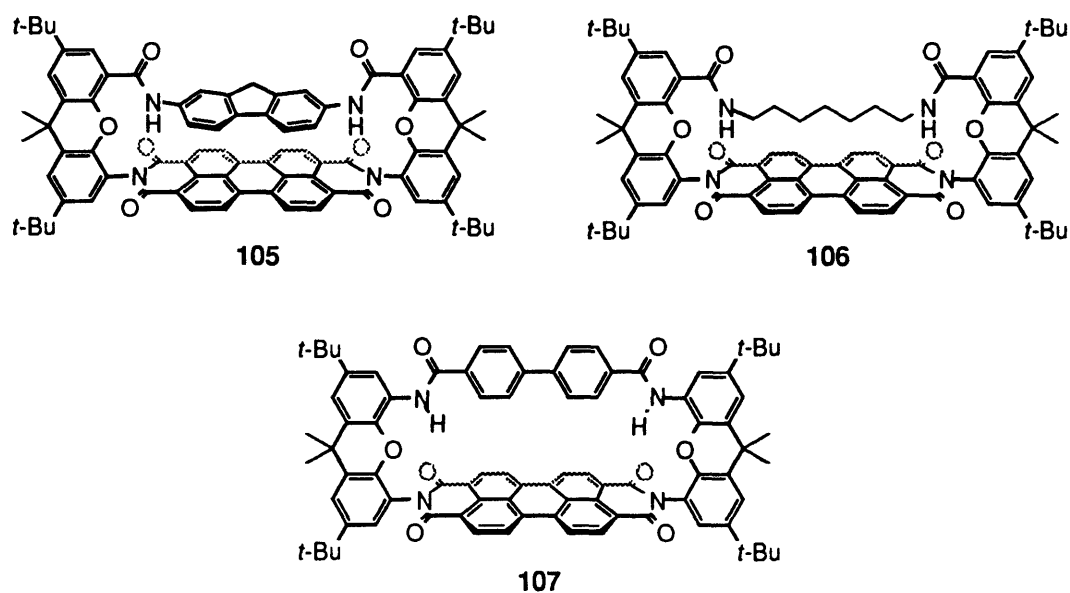


Figure IV-4. Bridged structures of the C-shaped perylene scaffolds.

The extraordinarily high yields of the macrocyclizations attest to the high degree of preorganization present in the perylene clefts. Typically, such large cyclizations proceed only under high dilution conditions or with an external template. In the case of the perylenes, no special provisions were taken. The bridged structures also provided some measure of the relative sizes of the C-shapes. In particular, bridging reactions with rigid diaminofluorene **109** left little leeway as to the distance between its two ends. In this case, molecular modeling calculated an N-N distance of ~ 7.8 Å (Figure IV-5). The equally rigid diaminoanthraquinone **108** appeared to be too long to effectively bridge the functionality of the C-shaped perylene scaffolds and gave no macrocyclized product. Conversely, the more flexible diaminoheptane **111** was able to span the C-shape even though the distance between its reactive ends was an even larger 10.0 Å in an extended conformation. The flexibility of the alkyl chain apparently adopts a shorter conformation, allowing macrocyclization. There is, however, no remedy for shortness, as bridging reactions with diaminobutane **110** and the diacid chloride of **45c** were unsuccessful.

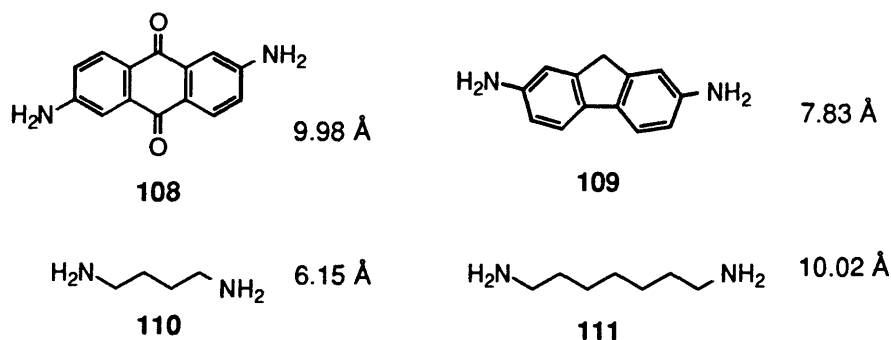


Figure IV-5. Various diamines and their calculated sizes by MM2 as implemented by Macromodel. The alkyl chains were minimized in their extended conformations. The distances were measured from amine N to N.

An intriguing molecule was isolated from the 'failed' bridging reaction of diacid 45s. The product was the least polar and the first compound off of a silica gel column. The proton spectra of this perylene displayed an unusual symmetry. The perylene surface had become desymmetrized and showed four different types of protons in the ^1H NMR spectra. Previously, this type of desymmetrization of the perylene surface was observed in structures that had two different xanthenes on either end. In this case both xanthenes were chemically equivalent. Two structures were proposed which could accommodate the observed symmetry and the S-shape of the starting materials. These are shown in Figure IV-6. The '2 + 2' product (112) consists of two perylene scaffolds and two dialkyl amines. The '1 + 1' product (113) is the strained macrocyclization product. Molecular modeling suggests that the alkyl chain of 113 can just stretch around the perylene spacer, causing significant distortions of the perylene and xanthene surfaces. The larger '2 + 2' product (112) seemed entropically less likely, although modeling suggested that it was thermodynamically more stable. This ambiguity was resolved by a plasma desorption mass spectra of the unknown compound. A $[\text{M} + \text{H}]$ peak clearly showed the '2 + 2' product at 2427.3 amu (calcd 2426.2). The observed asymmetry of the '2 + 2' product 112 suggests that the macrocycle is locked in a twisted D_{2d} conformation from which it is unable to extricate itself. This leads to a 'Möbius strip' type of chirality. Tracing the surface of the perylene spacers and edges of the xanthene U-turns leads to two independent and non-crossing paths.

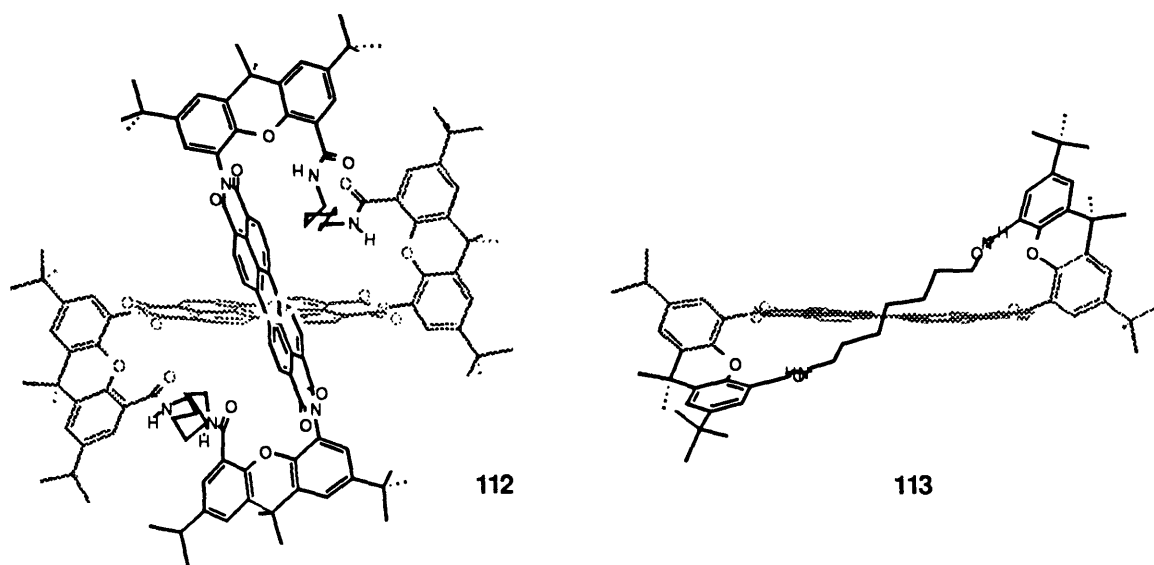


Figure IV-6. 2 + 2 product isolated from bridging experiments with perylene diacid **45s**, and less likely 1 + 1 possibility.

4.5 ASSIGNMENT OF NAPHTHALENE ISOMERS

The polarity argument proved inaccurate in identifying the rotamers of the bis(xanthene)naphthalene diimide clefts. The R_f values (by TLC) of the C- and S-shaped rotamers did not correlate with their expected dipole moments. This last stipulation is necessary because oddly, the xanthene diacids **74c** and **74s** eluted from a silica gel column in reverse of their order by TLC. This phenomenon only served to confuse the matter further.

A possible explanation for the incongruous R_f values (by TLC) of naphthalene diacid **74** is the collapse of functionality in the C-shape. A self-satisfied conformation would tie-up the diacids, making the C-shape appear less polar. Alternatively, complexation of a solvent molecule such as methanol by the C-shaped isomer would also occupy the polar carboxylic acids and produce the same overall effect. In either case, the S-shaped isomer would be unable to appease its polar diacids, leaving them dangling in space. This explanation is supported by the reversal of R_f values upon conversion to less polar and non-associating functionality as is found in dintrile **82**. Furthermore, the close

arrangement of polar functionality in **81c** and **74c** closely resembles previous examples in which atropisomers had misleading R_f values.¹³

In the end, the S-shaped isomer of naphthalene diacid **74** was definitively identified by x-ray crystallography. Crystals of the lower R_f isomer (by TLC) **74s** were collected from the slow evaporation of a methylene chloride/ethyl acetate solution. The unit cell was in the centric $P\bar{1}$ space group with an inversion center and contained a single naphthalene diacid. These data were consistent only with the S-shaped isomer (Figure IV-7). Also present in the structure were two ethyl acetates found floating over the naphthalene shelf. These solvent molecules were hydrogen bonded through their carbonyl oxygens to the xanthene carboxylic acids with an O-O distance of 2.64 Å. Interestingly, this interaction implies that the proton of the xanthene carboxylic acid is not 'tucked back' in an intramolecular hydrogen bond to the xanthene ether oxygen. Instead, the carboxylic acid proton is pointed outward toward a prospective guest.

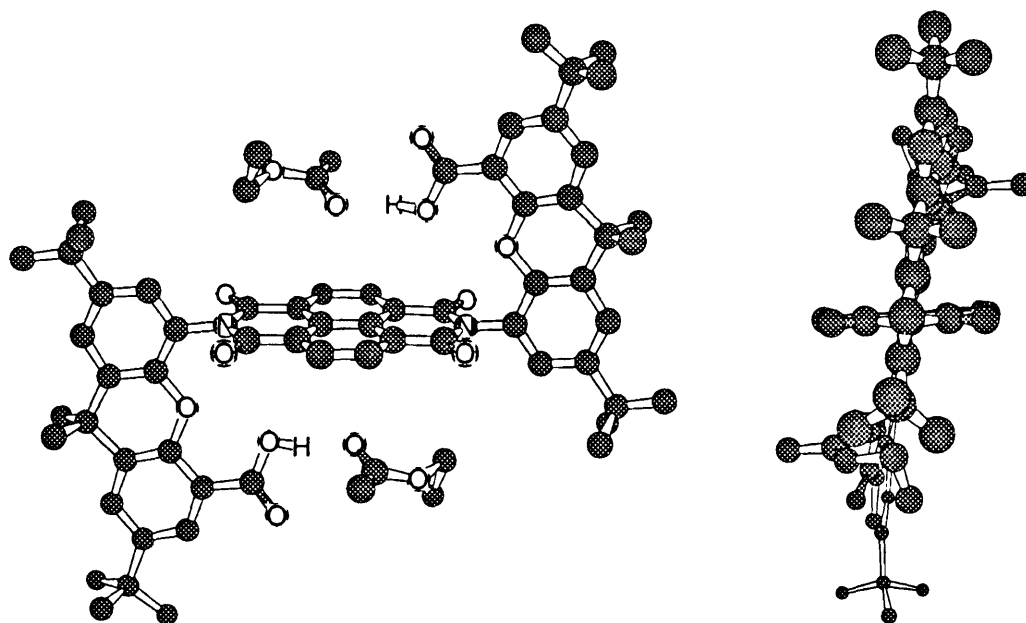
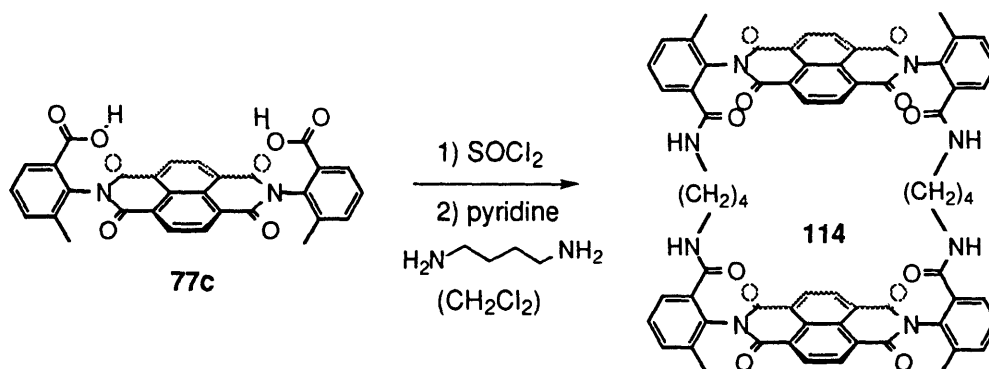


Figure IV-7. Chem 3D representations of the x-ray coordinates of the S-shaped isomer of naphthalene diacid scaffold. Side and end on views.

¹³ Sanders, G. M.; Van Dijk, M.; Machiels, B. M.; van Veldhuizen, A. *J. Org. Chem.* **1991**, *56*, 1301-1305.

The bis(anthranilic acid)naphthalene diimide scaffolds behaved more like the perylene scaffolds as opposed to their smaller naphthalene brethren. Once again, the C-shapes had the expected lower R_f value perhaps due to their wider separation between diacids than in **74c**. The C-shaped isomer of diacid **77** was identified by bridging experiments although not in the expected manner. The lower R_f isomer of **77c** was converted into its corresponding diacid chloride and then treated with 1,4-diaminobutane. A compound was isolated, which appeared by ^1H NMR to be the bridged product. However, mass spectrometry analysis gave twice the expected molecular weight, leading to the conclusion that another '2 + 2' product (**114**) had formed. The high degree of symmetry of **114**, which had led to its initial misidentification, now clearly identified it as the macrocyclization product of two C-shapes. All the protons of **114**'s spacer are chemically equivalent and were a single singlet by ^1H NMR. By contrast, the previous '2 + 2' product (**112**) which was composed of two S-isomers had a C_2 symmetry. It seems fair to assume that the other bis(anthranilic acid)naphthalene diimide scaffolds **77** and **78** will behave similarly and have their C-shapes as the lower R_f product.



Scheme IV-3. Bridging of anthranilic derived naphthalene **77c** with diaminobutane.

Initially, the 'failure' of the bridging experiment was attributed to the short length of diaminobutane. Macromodel (MM2) calculates an N-N distance of 6.2 Å for 1,4-diaminobutane, which seemed long enough to bridge the diacids of **77c** that have a predicted O-O distance of 6.9 Å. However, this simple linear analysis did not account for the angle between diacids of **77c**, which necessitates a longer

bridge to turn the corner. Bridging experiments with longer alkyl diamines and 2,7-diaminofluorene were equally unsuccessful, and no bridge products were isolated. These were in stark contrast to the high yielding macrocyclizations of the perylene scaffolds.

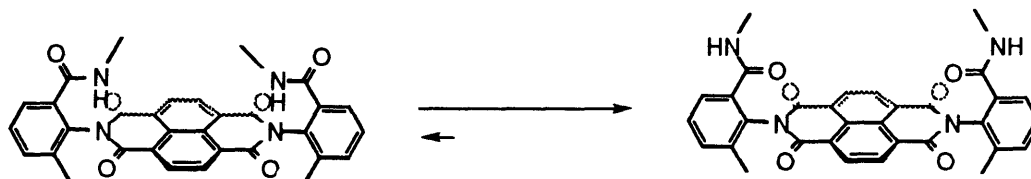


Figure IV-8. The less favored 'closed' geometry of the anthranilic diamide scaffold and the more favored 'open' geometry.

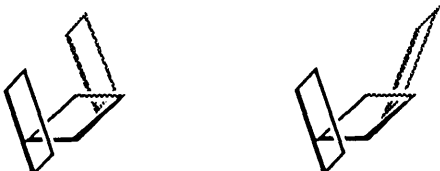
The failure to efficiently bridge the diacids of **77c** may be due to its more open and less convergent geometry. In addition, examination of the molecule's conformation by modeling suggested an additional explanation. Because of the angle between the acids of **77c**, rotation about the $C_{\text{aryl}}-C_{\text{carbonyl}}$ bond can either expand or contract the size of the cleft (Figure IV-8). For diacid **77c**, there appears to be little conformational preference, but for a diamide, the steric repulsion between the amide -NH and the naphthalene spacer favors the wider rotamer (Figure IV-8). In this 'open' conformation the functionality is not only separated by a larger distance but is also less convergent. The alkyl groups of the diamide face outward and seem better oriented toward finding a second molecule as opposed to itself.

4.6 DIMENSIONS OF THE C- SHAPED ISOMERS

The crystal structure of **74s** provided a great deal of structural information about the relationship between the xanthene U-turn and the diimide spacer. A side view shows that the xanthene surfaces remained planar but were tipped inward toward the naphthalene spacer (Figure IV-7). The tip results from a combination of two factors: 1) the slight pyramidalization of the imide nitrogen and 2) the longer C-C single bond on the outer portion of the center xanthene ring (1.58 Å) vs. the shorter C-O (1.39 Å) of the inner ether. An 'end on' view

looking down the C_{aryl}-N_{imide} bond shows that the planes of the naphthalene and xanthene were nearly perpendicular. The dihedral angle formed about the C_{aryl}-N_{imide} bond was 82.3°. Both xanthenes of 74s were leaning slightly to the right, leading to a C₂ symmetric conformation.

Because of the structural similarities between the naphthalene and perylene scaffolds, the crystal coordinates can be easily and probably accurately transformed into the more desirable C-shapes through symmetry operations. In each case, two alternative structures are possible depending upon which way the xanthenes lean relative to each other (Table IV-1). These extrapolated dimensions gave a good dynamic range for the distances between functionality in the C-shapes. In the larger perylene cleft, a sizable cavity of 8.65 Å to 9.47 Å (O-O dist.) was calculated which could easily accommodate organic guests or the introduction of additional functionality. The smaller naphthalene cleft presents its acids at a much closer distance (4.32 Å to 5.61 Å) leaving room for only a very small guest such as a metal ion.



C-Naphthalene diacid	4.32 Å	5.61 Å
C-Perylene diacid	8.65 Å	9.47 Å

Table IV-1. Acid-acid (O-O) distances of the C-shaped xanthene derived scaffolds as extrapolated from the crystal data of the S-shaped isomer of naphthalene diacid 74s.

Molecular modeling (MM2) generated very similar geometries to those extrapolated from the naphthalene crystal structure. One difference was that the MM2 calculated structures tended to tip the xanthenes even further inward, resulting in even shorter O-O distances than is given in Table IV-1 (also see section 4.8). The discrepancy may be due in part to the presence of the ethyl

acetates in the crystal structure, as it appears that the driving force for the cavity's collapse is the minimization of solvent exposed surface area. The predicted flexibility of the imide nitrogen, however, appears to be a real effect. The covalent bridging experiments of the perylene scaffold with diaminofluorene project a distance of 7.83 Å, which is somewhat shorter than the distance extrapolated from the crystal data (8.65 - 9.47 Å).

For the bis(anthranilic acid)naphthalene diimide cleft an O-O distance of 6.9 Å was calculated by modeling. As discussed earlier, this distance can widen significantly by simply rotating about the C_{aryl}-C_{carbonyl} bond to a wider conformation with an O-O distance of ~10 Å. It is not known if one rotamer is favored over the other for the acid or ester. Crystals were obtained of a dimethyl ester derivative and are currently being analyzed.

4.7 BINDING PROPERTIES OF THE PERYLENE CLEFTS

Shape imparts very different chemical properties upon the C- and S-shapes and provides additional evidence of their accurate assignments. Unfortunately, C-shaped perylene diacid **45c** was not exceedingly soluble in chloroform, making comparisons with previous diacid clefts difficult.¹⁴ The perylene diamide **51** provided a more tractable alternative. Both isomers were titrated with phenazine. The C-shape displayed regular changes in the ¹H NMR spectra (Figure IV-9) consistent with the formation of a 1:1 complex with a binding constant of 149 M⁻¹. In contrast, titration of the S-shape with phenazine showed small and irregular changes in chemical shift. The convoluted titration curve of the S-shape was attributed to a variety of association processes, which were occurring simultaneously and, thus, was easily differentiated from the C-shape.

¹⁴ Interestingly, the dicondensation reaction mixture was soluble in chloroform but after purification and removal of quinoline the C-shaped diacid became insoluble in chloroform.

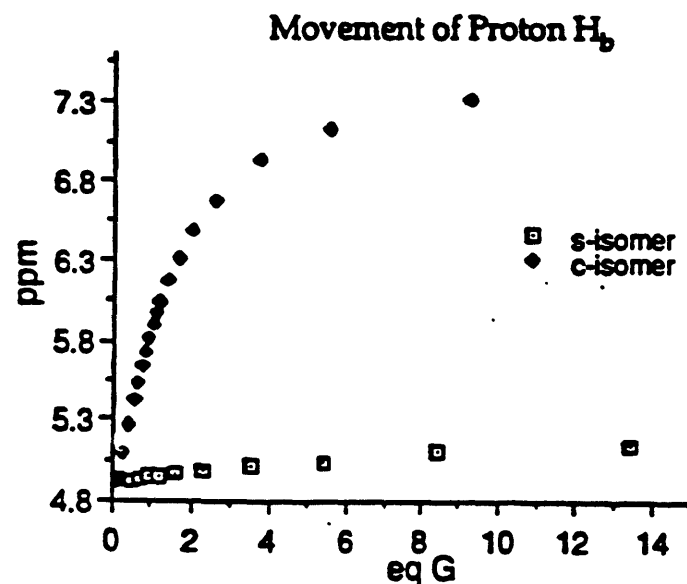
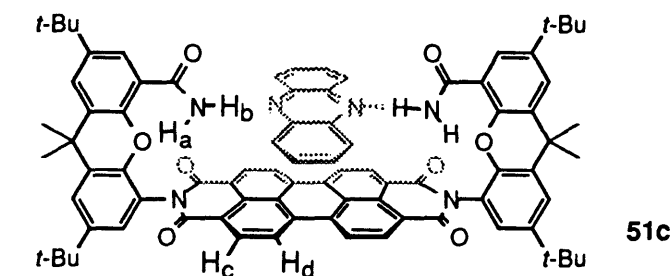


Figure IV-9. Titrations of the C- and S- shaped isomers of perylene diamide 51 with phenazine.

The chemical shifts of the C-shaped diamide 51c during titration also yielded conformational information about the complex and perylene host (Table IV-2). The most likely structure is depicted in Table IV-2 with the guest stacked over the perylene surface and hydrogen bonded to both convergent amides. Evidence for hydrogen bonding was provided by the syn- (H_b) and anti- (H_a) amide protons which were in entirely different environments. Initially, the syn-protons were shifted considerably upfield at 4.80 ppm because they point out over the perylene surface. By contrast, the anti- protons appeared to be tucked back and internally hydrogen bonded to the xanthene ether oxygens. Consequently, they were much further downfield at 6.77 ppm. During the course of the titration, the syn- proton moved 2.50 ppm downfield and passed the almost stationary anti-proton. Apparently, the syn-proton (H_b) was actively involved in complexation while the anti-proton (H_a) was preoccupied and unavailable for hydrogen-bonding to the guest. The formation of the intramolecular hydrogen bond

between the anti- amide proton and the xanthene ether oxygen restricts the rotation of C_{aryl}-C_{amide} bond and confers additional preorganization upon the perylene clefts.



	<u>H_a</u>	<u>H_b</u>	<u>H_c</u>	<u>H_d</u>
free host	6.77	4.80	8.74	8.67
phenazine complex	6.95	7.30	8.55	8.01
Δ	+ 0.18	+ 2.50	- 0.19	- 0.66

Table IV-2. ¹H NMR chemical shifts of perylene diamide **51c** upon complexation with phenazine in CDCl₃.

The presence of the phenazine guest inside the cavity can be interpreted from the changes in chemical shift of the perylene spacer. Protons H_c and H_d were shifted varying degrees upfield due to their proximity to the aromatic guest. As expected, the protons directly below the phenazine surface were influenced the most.

Other guests were also strongly complexed by the perylene C-shaped diamide **51**. Solid-liquid extractions were performed because of the insolubility of the chosen guests in chloroform. First, shaking the otherwise insoluble quinoxaline dione with the C-shape of **51** formed the corresponding 1 to 1 complex.¹⁵ This stoichiometry was determined by integration of the protons on the host and guest in their ¹H NMR spectra. Changes in chemical shift of the xanthene portion of **51c** were almost identical to those seen in the phenazine complex. Particularly diagnostic was the downfield shift of the syn- amide

¹⁵ The Aldrich catalog shows an alternate tautomer for quinoxaline dione as the diamino diphenol. IR studies suggest however that the pictured tautomer (Figure IV-9) of quinoxaline dione is the more stable.

proton (H_b). The corresponding shifts of the perylene spacer were not observed probably due to the orientation of the quinoxaline dione well above and perpendicular to the cleft floor (115). Likewise, squaric acid was also bound by perylene diamide 51c. Again the characteristic shifts in the host were observed; however the lack of protons on squaric acid prevented the definitive determination of the complex's stoichiometry (116). Due to the similar shape, size, and chemical shift data of the two guests, a very similar binding geometry is proposed in which the two amides of 51c form 4 hydrogen bonds to the guest.

Guests having similar functionality but the wrong shape and size were not bound by 51c which appears to be highly discriminating. For example, similar solid-liquid extractions with barbituric acid (118) showed no signs of extraction. Modeling shows that 118 is much larger than squaric acid or quinoxaline dione. These differences were exemplified by their different distances between amide carbonyl oxygens. The carbonyls of barbituric acid were splayed out much wider (4.66 Å) than either quinoxaline dione (2.77 Å) or squaric acid (2.33 Å).

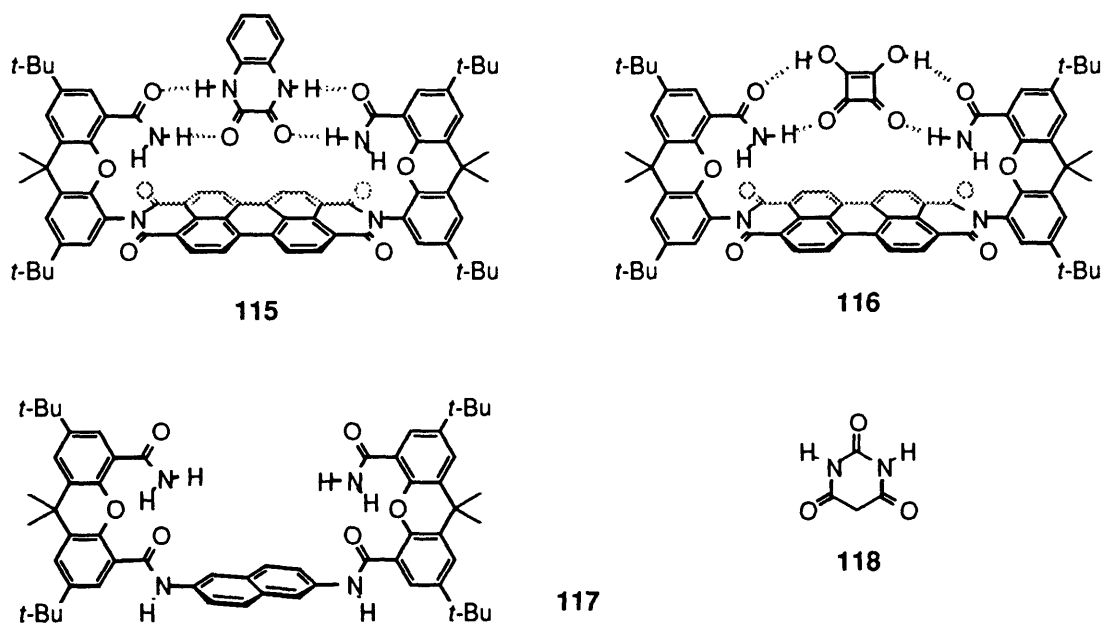


Figure IV-10. Proposed complexes between perylene diamide 51c and quinoxaline dione and squaric acid.

Some measure of the preorganization present in the new diimide clefts was provided by comparison to previous xanthene clefts which lacked restricted

rotation. Cleft 117 was also able to complex and solubilize quinoxaline dione but only with a 10 % occupancy.¹⁶ In addition, similar solid-liquid extractions were performed with the S-shaped isomers of perylene diamide 51 for each guest and again binding was not observed. The property of extractability is not solely a measure of complementarity between a host and guest but also a function of their relative solubilities and their partition coefficients in the mixed solvent system. In the case of the C- and S-shaped perylene diamides (51c and 51s), the greater complementarity of the C-shape overcomes the greater solubility of the S-shape in organic solvents.

4.8 PROPERTIES OF THE NAPHTHALENE SCAFFOLD

Both the crystal structure and computer modeling suggest that the xanthenes are able to tip inward. For the smallest diacid 74c, molecular modeling attempts to form a hydrogen bond between the opposing diacids and does so without considerable deformation of the imide nitrogen (Figure IV-11). Still, this collapsed structure was initially discounted as being the product of a gas phase calculation, which tends to overestimate non-covalent interactions. However, with the observation that the mono-anion of the C-shaped diacid 74c was particularly stable, this collapsed hydrogen bonded structure was reexamined.

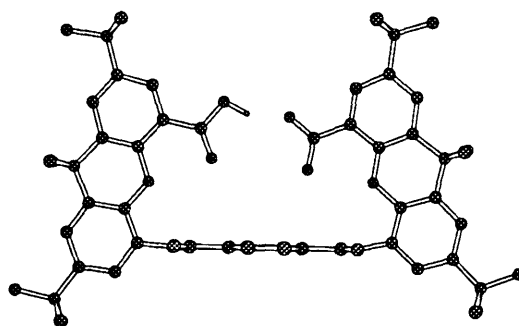


Figure IV-11. MM2 Minimized structure of monoanion of diacid 74c.

¹⁶ Notebooks of James Nowick.

The dianion of the C-shaped cleft **74c** was formed by shaking a methylene chloride solution of the diacid with 2 % $\text{Bu}_4\text{N}^+ \text{OH}^-$. The ^1H NMR spectra of the organic layer showed two equivalents of Bu_4N^+ per equivalent of diacid **74c**. On shaking the same CH_2Cl_2 solution with distilled water resulted in the corresponding mono-anion. This large disparity in pK_a 's between the two carboxylates has elsewhere been seen in structures that had a low-barrier hydrogen bond.¹⁷ Hydrogen bonds between two groups of similar basicity form extremely strong 'low barrier' hydrogen bonds, examples of which are shown in Figure IV-12.¹⁸ The presence of 'low barrier' hydrogen bonds has recently been implicated as a factor contributing to the large rate enhancements of enzymes.¹⁹

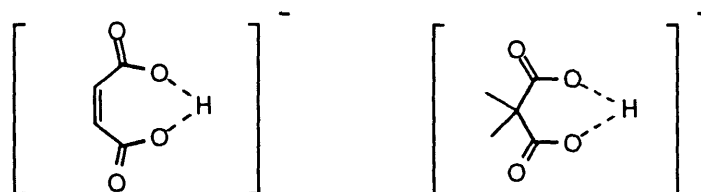


Figure IV-12 Examples of low-barrier hydrogen bonds.

The ^1H NMR of the mono-anion was taken in CDCl_3 and DMSO-d_6 and was very similar to the parent diacid. Slight upfield shifts were seen but no peaks were visible in the 10 to 25 ppm range which are characteristic of low barrier hydrogen-bonds. The observance of the acid proton is very dependent upon hydration, counterion and solvent and maybe in fast exchange with the residual water peak. Alternatively, the acids may actually be too far apart; however, it is difficult to explain such a large disparity in pK_a 's if the two groups are not somehow interacting. Clearly, this distance is not too large to be bridged by a single atom, as metal ions were bound by the dicarboxylate of **74c**.

- 17 a) Rebek, J., Jr.; Duff, R. J.; Gordon, W. E.; Parris, K. J. *Am. Chem. Soc.* **1986**, *108*, 6068. b) Yoko Kato personal communication.
- 18 a) Kreevoy, M. M.; Liang, T. M. *J. Am. Chem. Soc.* **1980**, *102*, 3315. b) Perrin, C. L.; Thoborn, J. D. *J. Am. Chem. Soc.* **1992**, *114*, 8589.
- 19 a) Robillard, G.; Shulman, R. G. *J. Mol. Biol.* **1972**, *71*, 507. b) Frey, P. A.; Whitt, S. A.; Tobin, J. B. *Science* **1994**, *264*, 1927.

4.9 OUTLOOK

The C- and S-shaped isomers of the respective perylene and naphthalene scaffolds were all assigned. Overall, the use of R_f values was found to be a valuable method for the identification of the convergent and divergent isomers; however in cases where functionality is able and willing to collapse, other methods are necessary for verification. The conformation and structure of the new diimide scaffolds were fairly accurately anticipated by molecular modeling, which should assist in the design of future analogs of these structures. Although synthetically appealing, the anthranilic acid scaffolds appear to be the least convergent especially when converted to amides. This more open geometry should lead to slightly different properties than the more convergent xanthene scaffolds.

Recently, some of the potential of these rigid molecules has been demonstrated in their application as enantioselective peracids and as decarboxylation catalysts.²⁰ The epoxidation project has brought our studies of molecular recognition full circle, as it was during attempts to control the space in front of a peracid that the first U-turn molecules were conceived and synthesized (Figure IV-13).²¹

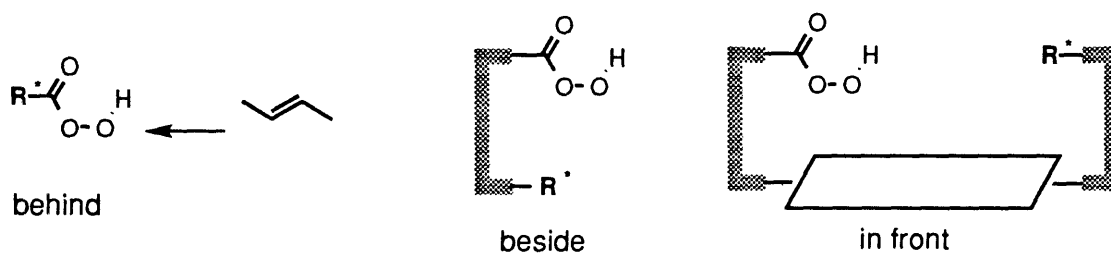


Figure IV-13. Strategy for development of an enantioselective peracid.

The perylene scaffold appears ideal to place chirality directly in front of a peracid and in the path of an attacking alkene. A monofunctionalized C-shaped

²⁰ These studies were performed by Takashi Oi and Roland Mohr.

²¹ a) Rebek, J., Jr.; Marshall, L.; McManis, H.; Wolak, R. *J. Org. Chem.* **1986**, *51*, 1649. b) Rebek, J., Jr.; Marshall, L.; Wolak, R.; McManis, J. *J. Am. Chem. Soc.* **1984**, *1984*, 1171.

perylene **120** was prepared, having a chiral amide or oxazoline on one side and a peracid on the other. Unfortunately, only highly reactive tetra- and trisubstituted alkenes could be used, which were not sterically well differentiated and probably had difficulty fitting into the cavity. Still, the chiral perylene peracids were able to effect modest enantioselectivity (Table IV-3).

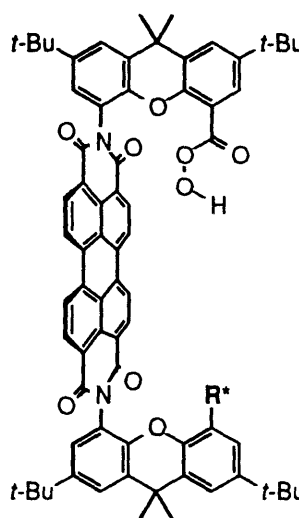
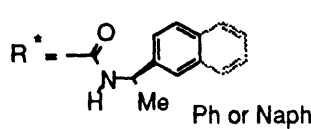
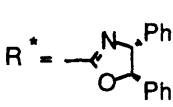
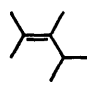
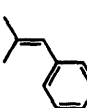
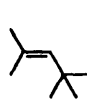
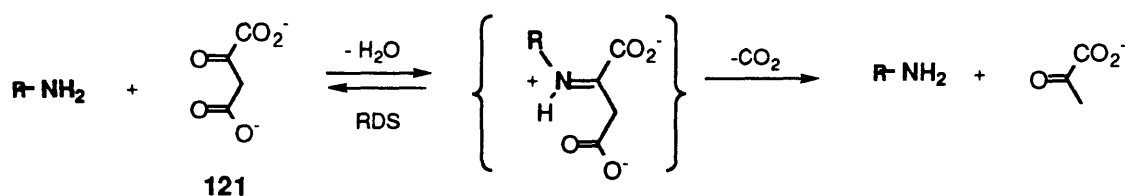
		
		20 % ee (Naph)
	7 % ee (Ph)	9 % ee
	4 % ee (Ph)	4 % ee

Table IV-3. Enantioselectivity of the C-shaped chiral peracids.

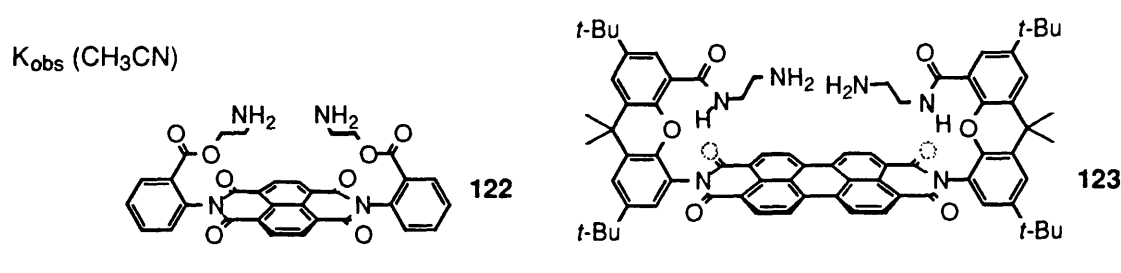
Alternatively, Roland Mohr in our research group has shown that the new diimide scaffolds are also able to catalyze reactions. The decarboxylation of ketodiacid **121** was chosen because the reaction mechanism is well understood and is known to be catalyzed by a primary amine (Scheme IV-4).²² The rate determining step (RDS) is the formation of the Schiff's base intermediate which subsequently decarboxylates. A catalyst was designed to bind the carboxylate with one amine and then bring a second amine in close proximity to the substrate, accelerating the formation of the enamine.

²² a) Hay, R. W. *Aust. J. Chem.* **1965**, *18*, 337. b) Westheimer, F. H. *Tetrahedron* **1995**, *51*, 3. c) Hoft, E. *Topics Current. Chem.* **1993**, *164*, 63.



Scheme IV-4. The amine catalyzed decarboxylation of ketodiacid **121**

Two diimide scaffolds were examined. The catalytic ability of the C-shapes were evident by comparison to their corresponding S-shaped isomers. The largest differential was observed for diamine **122c**.



C-isomer	60.0	58.8
S-isomer	8.0	35.4

Table IV-4. Rates of decarboxylation of **121** in acetonitrile.

Both examples illustrate the power of convergent functionality to alter reaction rates and selectivities in a manner reminiscent of enzymes. The C-shaped diimides would appear well suited toward application as bifunctional catalysts. For example, the active site of lysozyme and other glycolytic enzymes are known to contain two convergent carboxylic acids at varying distances from 5 to 10 Å, which act in concert to cleave polysaccharides under mild conditions.

4.10 EXPERIMENTAL

Crystallography of S-Naphthalene Diacid Cleft. Data were collected with an Enraf-Nonius CAD-4 diffractometer with Mo K α radiation ($\lambda = 0.711 \text{ \AA}$). The

structure was solved by direct methods. The non-hydrogen atoms were refined either anisotropically or isotropically. The final cycle of full-matrix least-squares refined either anisotropically or isotropically. The final cycle of full-matrix least-squares refinement was based on 1993 observed reflections ($I > 3.00\sigma(I)$) and 360 variable parameters and converged with unweighted and weighted agreement factors of $R = \sum||F_o| - |F_c|| / \sum|F_c| / \sum|F_o| = 0.098$ and $R_w = [(\sum(|F_o| - |F_c|)^2 / \omega F_o^2)]^{1/2} = 0.103$.

The data were collected from colorless plates having approximate dimensions of 0.300 x 0.400 x 0.090 mm which were obtained from the slow evaporation of an ethyl acetate/CH₂Cl₂ solution. Crystal data for C₇₀H₇₈N₂O₁₄: Mr 1171.39, space group $P\bar{1}$, $a = 13.785(1)$ Å, $b = 19.940(1)$ Å, $c = 5.993(1)$ Å, $\alpha = 98.01(2)^\circ$, $\beta = 87.01(2)^\circ$, $\gamma = 100.48(2)^\circ$, volume = 1603,6(6) Å³, $Z = 1$, $\rho(\text{calcd}) = 1.213$ g/cm³, $\mu(\text{Mo K}\alpha) = 0.78$ cm⁻¹, $T = 21^\circ\text{C}$.

Additional ORTEP views and tables of positional parameters, bond angles, bond lengths, torsional angles and anisotropic thermal factors can be found in Appendix I.

C-Perylene Fluorene Bridged Diamide (105). The diacid chloride of the lower R_f isomer of perylene diacid 45c (0.00894 mmol) was prepared as described previously (see 51c in Chapter II) and taken up in 15 mL of CH₂Cl₂. The diamine, 2,7-diaminofluorene (2.1 mg, 0.0107 mmol), and pyridine (1.7 μL, 0.0214 mmol) in 5 mL of CH₂Cl₂ were added dropwise. The reaction was stirred for 1 h and then washed with 1.0 N HCl (1 x 50 mL). Rotary evaporation of the organic layer gave a red solid. Column chromatography on silica gel (2% MeOH/CH₂Cl₂) yielded a red solid (10.2 mg, 90 %): mp > 330 °C; IR (KBr) 3408, 2959, 1708, 1673, 1593, 1445, 1366, 1259, 808 cm⁻¹; ¹H NMR (250 MHz, CDCl₃) δ 8.55 (s, 2 H, NH), 8.54 (d, 4 H, *J* = 7.5 Hz, Per), 8.34 (d, 4 H, *J* = 8.0 Hz, Per), 7.93 (d, 2 H, *J* = 2.3 Hz, Xan), 7.63 (d, 2 H, *J* = 2.4 Hz, Xan), 7.60 (d, 2 H, *J* = 2.0 Hz, Xan), 7.45 (s, 2 H, Flu), 7.31 (d, 2 H, *J* = 1.8 Hz, Xan), 6.53 (d, 2 H, *J* = 8.0 Hz, Flu), 6.18 (d, 2 H, *J* = 8.0 Hz, Flu), 3.23 (s, 2 H, -CH₂-), 1.78 (s, 12 H, Me), 1.34 (s, 18 H, *t*-Bu), 1.33 (s, 18 H, *t*-Bu); HRMS (FAB in 3-nitrobenzyl alcohol) calcd for C₈₅H₇₅N₄O₈ (N + H) 1279.5585, found 1279.5574.

C-Perylene (CH₂)₇ Diamide (106). The diacid chloride of the lower R_f isomer of perylene diacid 45c (0.0168 mmol) was prepared as described previously (see 51c in Chapter II) and taken up in 20 mL CH₂Cl₂. The diamine,

1,7-diaminoheptane (4.4 mg, 0.0335 mmol), and pyridine (2.7 μ L, 0.0336 mmol) in 15 mL of CH_2Cl_2 were added dropwise. The reaction was stirred for 1 h. The reaction mixture was washed with 1.0 N HCl (1 \times 50 mL), and then column chromatography on silica gel (2% MeOH/ CH_2Cl_2) yielded a red solid (15.1 mg, 74%): mp > 330 $^\circ\text{C}$; IR (KBr) 3435, 2960, 1710, 1673, 1594, 1446, 1357, 1254, 810, 747 cm^{-1} ; ^1H NMR (CDCl_3) δ 8.76 (d, 4 H, J = 8.1 Hz, Per), 8.62 (d, 4 H, J = 8.4 Hz, Per), 7.93 (d, 2 H, J = 2.4 Hz, Xan), 7.58 (d, 2 H, J = 2.4 Hz, Xan), 7.54 (d, 2 H, J = 2.4 Hz, Xan), 7.37 (d, 2 H, J = 2.1 Hz, Xan), 7.13 (t, 2 H, J = 5.7 Hz, NH), 2.05-2.18 (m, 4 H, $-\text{CH}_2-$), 1.73 (s, 12 H, Me), 1.55-1.70 (m, 4 H, $-\text{CH}_2-$), 1.34 (s, 18 H, t -Bu), 1.31 (s, 18 H, t -Bu), 0.20-0.40 (m, 6 H, $-\text{CH}_2-$); HRMS (FAB in 3-nitrobenzyl alcohol) calcd for $\text{C}_{79}\text{H}_{81}\text{N}_4\text{O}_8$ ($M + H$) 1213.6054, found 1213.6061.

C-Perylene Biphenyl Bridged Diamide (107). The lower R_f isomer of the diamine cleft 50c (42.0 mg) was combined with 4,4'-biphenyldicarboxylic acid dichloride (11.5 mg) in CH_2Cl_2 (5 mL) with 5 drops of pyridine. The reaction mixture was brought to reflux for 3 h and cooled overnight with a drying tube. The solvent was removed *in vacuo*. Column chromatography on silica gel (0.5-0.75% MeOH/ CH_2Cl_2) gave as the major product (24 mg) a red solid: mp > 330 $^\circ\text{C}$; IR (KBr) 3434, 2959, 1709, 1674, 1593, 1438, 1356, 1251, 809, 756 cm^{-1} ; ^1H NMR (CDCl_3) δ 8.62 (d, 4 H, J = 7.9 Hz), 8.36 (d, 4 H, J = 7.9 Hz), 8.21 (d, 2 H, J = 2.1 Hz), 8.08 (d, 2 H, obscured), 7.63 (d, 2 H, J = 2.2 Hz), 7.33 (d, 2 H, J = 2.0 Hz), 7.27 (d, 4 H, J = 8.2 Hz), 6.67 (d, 4 H, J = 8.2 Hz), 1.76 (s, 12 H), 1.39 (s, 18 H), 1.35 (s, 18 H); HRMS (FAB in 3-nitrobenzyl alcohol) calcd for $\text{C}_{84}\text{H}_{75}\text{N}_4\text{O}_8$ ($M + H$) 1267.5585, found 1267.5577.

'2 + 2' product of S-perylene bis(xanthene amide) diimide and diaminoheptane (112). The S-isomer of perylene diacid 45s (23 mg, 0.0206 mmol) was converted into the diacid chloride as described previously (see 51c in Chapter II) and taken up in CH_2Cl_2 (10 mL). Pyridine (3.3 μ L, 0.0412 mmol) and 1,7-diaminoheptane (2.7 mg, 0.0206 mmol) were added to the reaction mixture as stirred for 30 min. The solution was washed with 25 mL of 1.0 N HCl and then dried over MgSO_4 . The resulting red solid was chromatographed (MeOH/ CH_2Cl_2 , 3-4 %) to give the '2 + 2' product (5.7 mg, 23 % yield): mp > 350 $^\circ\text{C}$; ^1H NMR (CDCl_3) δ 8.78 (d, 2 H, J = 7.5 Hz, Per), 8.70 (d, 2 H, J = 8.1 Hz, Per), 8.35 (d, 2 H, J = 7.8 Hz, Per), 7.85 (d, 2 H, J = 8.4 Hz, Per), 7.63 (d, 2 H, J = 2.4 Hz, Xan), 7.60 (d, 2 H, J = 1.8 Hz, Xan), 7.55 (d, 2 H, J = 2.4 Hz, Xan), 7.37 (d, 2 H, J =

2.4 Hz, Xan), 6.45 (t, 2 H, $J = 6.2$ Hz, -NH), 2.80-2.95 (m, 2 H, -CH₂-), 2.27-2.42 (m, 2 H, -CH₂-), 1.85-2.13 (m, 2 H, -CH₂-), 1.80 (s, 6 H, Me), 1.70 (s, 6 H, Me), 1.41 (s, 18 H, *t*-Bu), 1.31 (s, 18 H, *t*-Bu), 0.54-1.20 (m, 8 H, -CH₂-); MS (plasma desorption) calc'd for C₁₅₈H₁₆₁N₈O₁₆ (M + H) 2428.1, found 2427.3.

'2 + 2' product of C-naphthathene bis(3-methyl-anthranilic amide) diimide and diaminobutane(114). The bottom isomer of diacid **76** (11.8 mg, 0.0221 mmol) was refluxed with SOCl₂ (200 μL) and a catalytic DMF (3 drops) in CH₂Cl₂ (5 mL) for 2 h. The solution was concentrated *in vacuo* to a solid. The crude diacid chloride was taken up in THF (10 mL, dried distilled) and 1,4-diamino butane (0.0265 mmol) and pyridine (0.0530 mmol) added. After 1 h, the reaction mixture was diluted with 150 mL CH₂Cl₂ and washed with 1.0 N HCl (2 x 100 mL). Chromatography (7 %, MeOH/CH₂Cl₂) on silica gel gave the product as a beige solid, which was not very soluble in CDCl₃ (2 mg, 15 % yield): ¹H NMR (300 MHz, Acetone-d₆) δ 8.81 (s, 4 H, Naph), 7.66 (d, 2 H, $J = 7.5$ Hz, Ar), 7.57 (d, 2 H, $J = 7.4$ Hz, Ar), 7.52 (t, 2 H, $J = 5.6$ Hz, -NH), 7.47 (dd, 2 H, $J = 7.7$ Hz and $J = 7.7$ Hz, Ar), 2.82 (s, 6 H, Me), 2.78-2.87 (m, 4 H, -CH₂-), 1.15-1.25 (m, 4 H, -CH₂-); MS (plasma desorption) calc'd for C₆₈H₅₂N₈O₁₂ (M + Na) 1196.2, found 1196.1.

Chapter V

Metal Binding: A Calcium Ionophore and a *trans*-Spanning Dinitrile Ligand

5.1 INTRODUCTION

The smaller C-shaped naphthalene scaffold presented functionality at the proper distances to grasp a metal atom from opposing ends. In this manner, diacid **74c** bound Ca^{2+} with a 1 to 2 stoichiometry (metal to ligand). Other binding functionality could also be introduced into the scaffold. For example, conversion of the diacids into dinitriles produced the unusual *trans*-spanning dinitrile ligand **82c**, and Au^+ , Ag^+ and PdCl_2 were all bound we believe in a rectilinear geometry. Evidence for complexation, coordination geometry and coordination number were provided by NMR and IR spectroscopy. The AuBF_4 and PdCl_2 complexes were determined to have a 1 : 1 stoichiometry (metal to ligand) and the AgBF_4 complex to have a 1 : 2 stoichiometry. For both ligands **74c** and **82c**, the extraordinary preorganization of the xanthene diimide scaffold produced stable complexes, especially when compared to their monodentate counterparts.

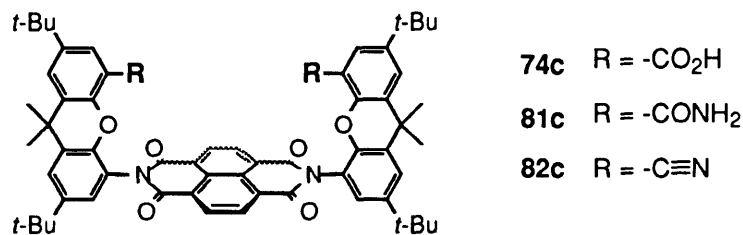


Figure V-1. Metal binding derivatives of rigid C-shaped naphthalene scaffolds.

5.2 BACKGROUND

The bis(xanthene)naphthalene diimide clefts share much in common with their Kemp's predecessors which have likewise found application as ligands. The highly convergent diacids of **125** were able to form stable diatomic iron complexes analogous to those found at the active site of methane monooxygenase and to also bind calcium.¹ Crystal structures have revealed that the Kemps' diacids are too close together to bind a metal between them. Instead, in all known cases, the metal or metals were coordinated above (Figure V-2a and V-2b) or to the side of the acid-acid plane (Figure V-2c).

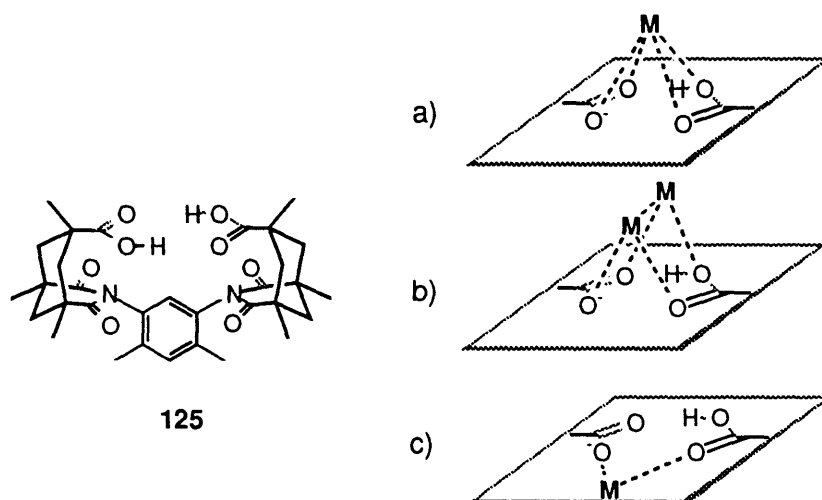


Figure V-2. Kemp's dicarboxylic acid ligand (XDK) and various binding geometries.

By comparison, the new bis(xanthene)naphthalene diimide frameworks (Figure V-1) have a larger acid-acid separation, and molecular modeling suggested that a metal ion could fit snugly in-between. In addition, the scaffolds offer other features, of a deep cavity, rigid scaffold and non-collapsing functionality also heavily favored its proficiency as bidentate ligand.

¹ a) Tanase, T.; Watton, S. P.; Lippard, S. J. *J. Am. Chem. Soc.* **1994**, *116*, 9401. b) Watton, S. P.; Masschelein, A.; Rebek, J., Jr.; Lippard, S. J. *J. Am. Chem. Soc.* **1994**, *116*, 5196. c) Parris, K. D. Ph.D. Thesis, University of Pittsburgh, 1988.

Particularly attractive was the possibility for a high degree of selectivity, as has been seen in other highly preorganized carboxylic acid ionophores. For example, the EDTA homologue **124** and the unusual *endo*-functionalized macrocycle **126** (Figure V-3) have both been shown to have a high specificity for Ca^{2+} over other alkaline earth metals.^{2,3}

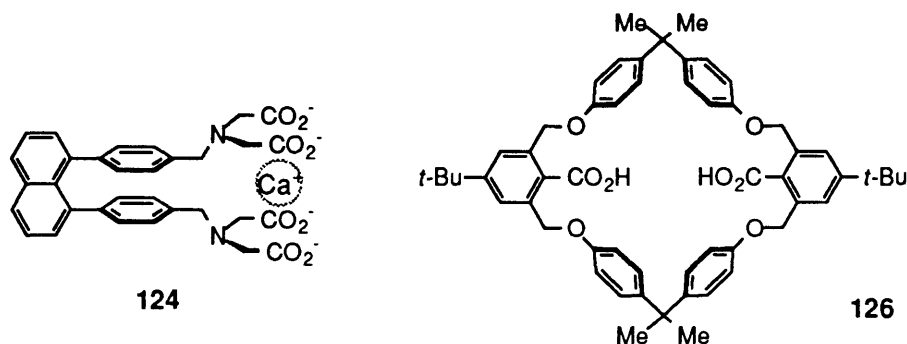


Figure V-3. Polycarboxylic acid hosts with high affinities for calcium(II) over other alkaline earth metals.

Molecules with high affinities and high selectivities toward metal ions have been sought for analytical purposes and for heavy metal sequestration and separation. These metal-ligand systems have also been used as models to probe biological systems which use metal ions as chemical signals and as catalysis. In the case of the calcium complex of diacid **74c**, we believe that it has a lot of structural homology to various calcium dependent proteins such as calmodulin,⁴ troponin and mannose-binding protein⁵ all of which chelate calcium via three to four convergent aspartate and glutamate carboxylic acids.

The rigid naphthalene scaffold also presented us with an unique opportunity to synthesize a *trans*-dinitrile ligand. Bidentate ligands which

² a) Leppkes, R.; Vögtle, F. *Angew. Chem., Int. Ed. Engl.* **1981**, *20*, 396. b) Vögtle, F.; Papkalla, T.; Koch, H.; Nieger, M. *Chem. Ber.* **1990**, *123*, 1097.

³ Glöe, K.; Stephan, H.; Heitzsch, O.; Bukowsky, H.; Uhlemann, E.; Pollex, R.; Weber, E. *J. Chem. Soc., Chem. Commun.* **1994**, 1955-1956.

⁴ Forsén, S.; Kördel, J.; Grundstrom, T.; Chazin, W. J. *Acc. Chem. Res.* **1993**, *26*, 7.

⁵ Harte, W. E., Jr.; Bajorath, J. *J. Am. Chem. Soc.* **1994**, *116*, 10394.

bind in a *trans*- or rectilinear fashion are very rare⁶ of which only a handful of examples are known. These ligands possess large bite angles and create an entirely new organization around a metal center. Recently, this coordination geometry has led to successful applications as enantioselective catalysts.⁷ Overall, two contrasting strategies have been utilized to bridge opposing sites of a metal: a kinetic and a thermodynamic. In the first, a series of blocking and isomerization reactions position a flexible ligand on opposite sides of a metal center.⁸ The resulting *trans*- complexes must be kinetically stable, a characteristic which differs greatly from metal center to metal center. Examples are shown in Figure V-4 (structures 127 and 128).⁹

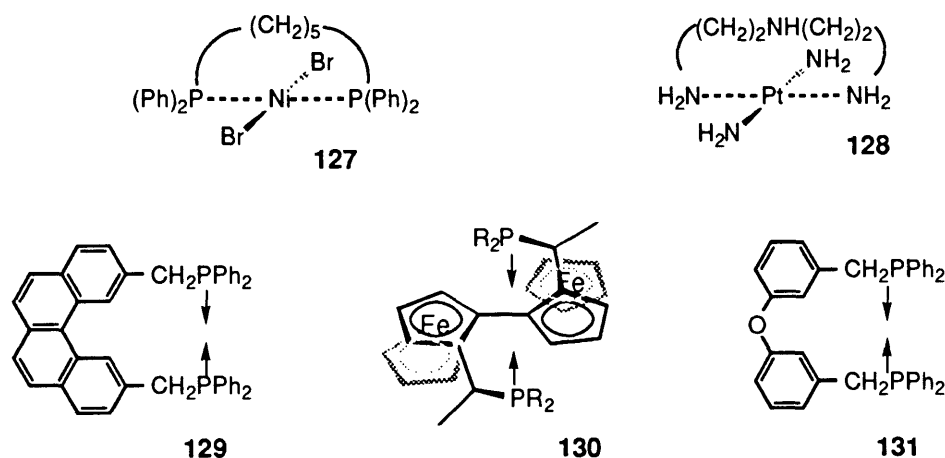


Figure V-4. Flexible (top) and rigid (bottom) *trans*- spanning ligands.

The second strategy is somewhat more general, producing a thermodynamically stable *trans*- complex, using a highly preorganized ligand. Here, the difficulty lies in constructing a framework of sufficient size, rigidity and convergency. Previous examples of rigid *trans*- ligands

- ⁶ a) Bailar, J. C., Jr. *Coord. Chem. Rev.* 1990, 100, 1. b) Ogino, H. *J. Coord. Chem.* 1987, 15, 187.
- ⁷ a) Trost, B. M.; Van Vranken, D. L. *Angew. Chem., Int. Ed. Engl.* 1992, 31, 228-230. b) Trost, B. M.; Van Vranken, D. L.; Bingel, C. *J. Am. Chem. Soc.* 1992, 114, 9327-9343. c) Sawamura, M.; Hamashima, H.; Ito, Y. *Tetrahedron Asym.* 1991, 2, 593.
- ⁸ a) Levason, W.; McAuliffe, C. A.; Murray, S. G. *J. Chem. Soc., Dalton Trans.* 1976, 2321. b) Levanson, W.; McAuliffe, C. A.; Murray, S. G. *J. Organomet. Chem.* 1975, 101, C29.
- ⁹ a) Mochida, I.; Mattern, J. A.; Bailar, J. C., Jr. *J. Am. Chem. Soc.* 1975, 97, 3201. b) Issleib, K.; Hohlfeld, G. Z. *Anorg. Allg. Chem.* 1961, 312, 170.

have been reported (129, 130, and 131);^{10,11,12} however, all bind through a tetrahedral phosphorus and possess a less convergent U-shape (Figure V-5). By contrast, *trans*- ligands which bind through sp^1 centers such as nitriles or isonitriles require a larger scaffold and a more convergent C-shape to achieve the same geometries (Figure V-5). To date, dinitrile 82c appears to be the first example of such a ligand.

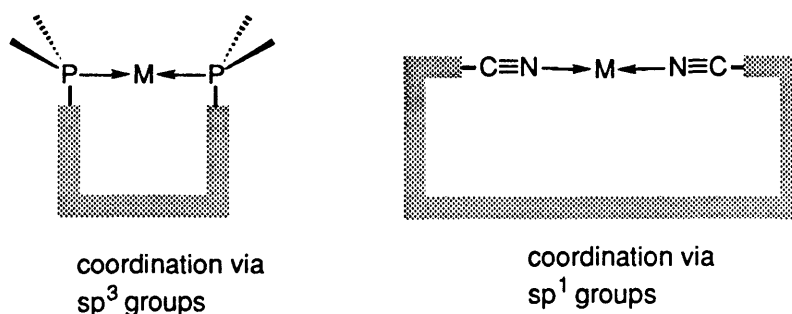


Figure V-5. Schematic representations of *trans*- ligand systems comparing relative size and shape which bind through tetrahedral and linear functional groups.

For the reasons above, multidentate nitriles are better known for their oligomeric and polymeric structures and have been successfully used to assemble three-dimensional arrays.¹³ Chelating di- and tri- nitriles and isonitriles are known but all bind to the same face of the metal as opposed to opposite sides (e.g. 132 and 133).¹⁴ An exception is ligand 134 which can form a *trans*- 2:2 Pt complex; however, in this case both nitriles do not reside on the same metal center.

- ¹⁰ a) Barrow, M.; Bürgi, H. B.; Johnson, D. K.; Venanzi, L. M. *J. Am. Chem. Soc.* **1976**, *98*, 2356. b) Leising, R. A.; Grzybowski, J. J.; Takeuchi, K. J. *Inorg. Chem.* **1988**, *27*, 1020.
- ¹¹ Sawamura, M.; Hamashima, H.; Ito, Y. *J. Am. Chem. Soc.* **1991**, *114*, 8295.
- ¹² Baltensperger, U.; Günter, J. R.; Kägi, S.; Kahr, G.; Marty, W. *Organometallics* **1983**, *2*, 571.
- ¹³ Baddley, W. H. *Inorg. Chim. Acta. Rev.* **1968**, *2*, 7.
- ¹⁴ a) Angelici, R. J.; Quick, M. H.; Kraus, G. A.; Plummer, D. T. *Inorg. Chem.* **1982**, *21*, 2178. b) Daws, C. A.; Hill, M. G.; Bullock, J. P.; Mann, K. R. *Inorg. Chem.* **1992**, *31*, 2948. c) Fehlhammer, W. P.; Schrolkamp, S.; Sperber, W. *Inorg. Chim. Acta* **1993**, *212*, 207. d) Hahn, F. E.; Tamm, M. *Angew. Chem., Int. Ed. Engl.* **1992**, *31*, 1212. e) Plummer, D. T.; Kraus, G. A.; Angelici, R. J. *Inorg. Chem.* **1983**, *22*, 3492.

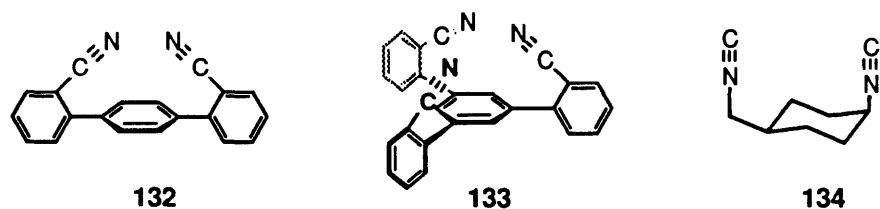


Figure V-6. Examples of di- and tri- dentate nitrile ligands.

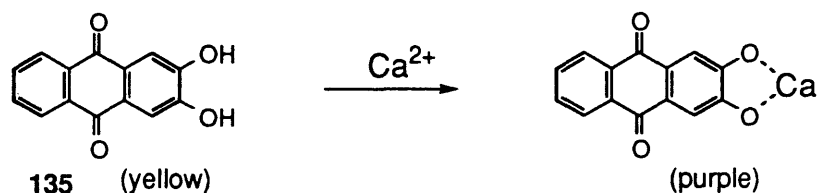
5.3 ALKALINE METAL BINDING

As noted earlier, the first indications of the possible utility of the bis(xanthene)naphthalene diimide scaffolds as ligands was during their synthesis (Section 3.3). It was observed that the C- to S- ratio would favor the convergent C-shape with the addition of more $\text{Zn}(\text{OAc})_2$. Binding experiments were performed using diacid **74c** and Zn^{+2} but no clear evidence of a well defined complex was seen. On the other hand, Ca^{+2} and **74c** formed a stable new species that was characterizable by ^1H NMR. Simply shaking a methylene chloride solution of diacid **74c** with an aqueous $\text{Ca}(\text{OH})_2$ solution gave the corresponding calcium complex in the organic layer. In contrast, the divergent diacid **74s** showed no indications of complexation. In addition, the formation of the calcium • **74c** complex was reversible. The spectra of the free ligand **74c** returned upon shaking a CDCl_3 solution of the complex with a 1.0 N HCl solution.

The stoichiometry of the new calcium complex was determined by a colorimetric method using alizarin (Scheme V-1).¹⁵ The extraction of calcium from an aqueous phase was quantified by measuring the absorbance of the purple alizarin • calcium complex at 560 nm. A test of this technique gave the expected linear response to a series of standard CaCl_2 solutions. The alizarin test also gave an accurate measure of the absolute

¹⁵ Natelson, S.; Penniall, R. *Anal. Chem.* 1955, 27, 4347. The aqueous solutions were diluted 20 fold over what was described to place the Ca concentration well below the concentration range of alizarin.

concentration of a saturated $\text{Ca}(\text{OH})_2$ solution¹⁶ which was reported to be ~23 mM.¹⁷



Scheme V-1. The chemical basis for the colorometric determinations of calcium concentrations using alizarin (135).

Various concentrations of diacid **74c** in methylene chloride (1 mL) were shaken with a saturated $\text{Ca}(\text{OH})_2$ solution (1 mL). The mixture was centrifuged and the aqueous layer analyzed. Interestingly, a blank CH_2Cl_2 solution by itself appeared to lower the Ca^{2+} concentration, but the effect was uniform and did not affect the analysis. Qualitatively, increases in the diacid concentration directly correlated to the depletion of calcium from the aqueous layer (Table V-1). A graph of $[\text{Ca}^{2+}]$ vs. [C-shaped diacid] gave a straight line with a slope of 0.45, which equates to the extraction of ~0.5 equivalents of Ca^{2+} per equivalent of diacid **74c**.

	[diacid] mM	abs @ 560 nm	[Ca ²⁺] mM
sat'd $\text{Ca}(\text{OH})_2$	0.00	0.071	21.463
blank	0.00	0.057	17.231
extraction 1	4.42	0.049	14.812
extraction 2	8.12	0.044	13.301
extraction 3	13.33	0.037	11.185

Table V-1. Data from liquid-liquid extractions of diacid **74c** in CH_2Cl_2 with a saturated $\text{Ca}(\text{OH})_2$ solution.

- ¹⁶ Saturated $\text{Ca}(\text{OH})_2$ solution was prepared by sonication and filtration. The concentration of the Ca^{++} in solution decreased on standing for several days and a white precipitate observed.
- ¹⁷ Linke, W. F. *Solubilities of Inorganic and Metal-Organic Compounds*; 4th ed.; D. Van Nostrand Company, Inc.: Princeton, NJ, 1958, pp 630. This value was reported to vary (± 1.0 mM) with the consistency of $\text{Ca}(\text{OH})_2$ used and temperature.

The formation of the 1:2 complex (Ca^{2+} to **74c**) was also observable by changes in the ^1H NMR spectra (Table V-2). Protons on only one xanthene ring moved downfield, presumably due to the electron withdrawing effects of the Ca^{2+} on the carboxylic acid. The ^1H NMR spectra of the Ca^{2+} complex also retained the symmetry of the original ligand **74c**.

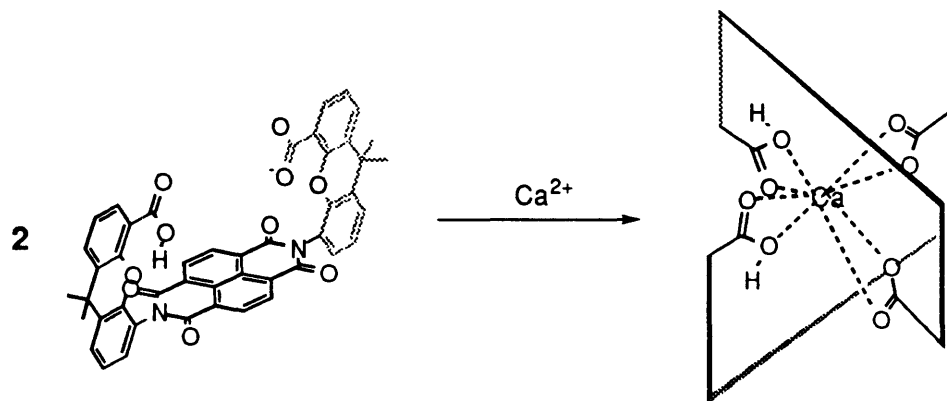
	free ligand	Ca^{2+} complex
Naph (s)	8.70	8.85
Xan (d)	~7.26 ^a	7.72
Xan (d)	7.21	7.62
Xan(d)	7.57	7.58
Xan (d)	7.35	7.40
Me (s)	1.66	1.71
<i>t</i> -Bu (s)	1.38	1.43
<i>t</i> -Bu (s)	0.99	1.29

Table V-2. Comparison of the ^1H NMR of the free and calcium complexed diacid **74c**. ^a Peak obscured by the CDCl_3 residual solvent peak.

From the above observations, the Ca^{2+} complex shown in Scheme V-2 was proposed. The metal is thought to be sandwiched in-between two diacid ligands which are off-set by 90° . This geometry is consistent with the 8-coordinate tendencies of Ca^{2+} , the observed NMR and closely resembles the binding geometries of calcium in proteins.^{4,5,18} In addition, the presence of a Ca^{2+} cation inside the cleft's cavity was supported by the 0.15 downfield shift of the naphthalene spacer. Alternative geometries could be ruled out by the observed symmetry of the calcium complex. In particular, the naphthalene spacer was observed as a singlet in the ^1H NMR spectra. Most other 1 to 2 geometries did not have such a high degree of symmetry; although, a set of quickly equilibrating asymmetric structures

¹⁸ Einspahr, H.; Bugg, C. E. In *Calcium-binding Proteins and Calcium Function*; R. H. Wasserman, R. A. Corrandino, E. Carafoli, R. H. Kretsinger, D. H. MacLennan and F. L. Siegel, Ed.; North Holland: New York, 1977.

cannot be ruled out. In fact, the proposed 1 to 2 complex in Scheme V-2 must also have a quickly exchanging carboxylic acid proton to give the observed symmetry by ^1H NMR.



Scheme V-2. Formation of the proposed 1:2 (Ca^{2+} to diacid).

The full extent of the binding properties of the C-shaped diacid cleft have yet to be determined. However, the convergent rigid framework and the acid-acid distance make **74c** an excellent candidate to selectively bind an array of divalent metals.¹⁹

5.4 A *trans*-DINITRILE LIGAND

The high degree of preorganization present in the naphthalene scaffolds was observable by the formation of stable *trans*-dinitrile complexes of dinitrile **82c**. Synthesis of the convergent dinitrile **82c** was fairly straightforward starting from the corresponding diacid **74c**, as previously described (Section 3.6). Treatment of **82c** with the appropriate metal precursor in methylene chloride gave the corresponding dinitrile complexes (Table V-3) and was accompanied by changes in the IR and ^1H NMR spectra. Conversely, the S-shaped dinitrile **82s** showed no

¹⁹ For other examples of alkali metal binding through preorganization see: Gloe, K.; Stephan, H.; Heitzsch, O.; Bukowsky, H.; Uhlemann, E.; Pollex, R.; Weber, E. *J. Chem. Soc., Chem. Commun.* 1994, 1955.

changes upon treatment with the same metal starting materials. Forcing conditions such as a large excess of ligand (usually as solvent), which are commonly necessary to drive complexation of metals with nitrile ligands, was unnecessary for dinitrile **82c**.²⁰ Ag(I), Au(I) and Pd(II) were all coordinated in a mild manner from monodentate starting materials. In each case, the resulting complex was kinetically and thermodynamically stable. For example, treatment of **82c** with less than a stoichiometric amount of metal led to the separate formation of the free and complexed ligand as opposed to rapidly equilibrating structures or no complexation.

	Metal Starting Material	IR ($\Delta -C\equiv N$) ^a	¹ H NMR (Δd) ^b	Ligand to Metal ^c
Pd(II)	PdCl ₂ (PhCN) ₂	+ 68 cm ⁻¹	$\Delta H_{(\text{Naph})} = + 0.16$ $\Delta H_{(\text{Xan})} = + 0.12$ $\Delta H_{(\text{Xan})} = + 0.10$	1 : 1
Au(I)	AuBF ₄ (CH ₃ CN) ₂	+ 53 cm ⁻¹	$\Delta H_{(\text{Naph})} = + 0.06$ $\Delta H_{(\text{Xan})} = + 0.37$ $\Delta H_{(\text{Xan})} = + 0.50$	1 : 1
Ag(I)	Ag BF ₄	+ 31 cm ⁻¹	$\Delta H_{(\text{Naph})} = + 0.06$ $\Delta H_{(\text{Xan})} = + 0.19$ $\Delta H_{(\text{Xan})} = + 0.27$	2 : 1

Table V-3. Spectroscopic changes upon treatment of dinitrile **82c**, metal starting materials, and the measured stoichiometries in solution. a) KBr, based on initial shift of 2228 cm⁻¹. b) CDCl₃, based on initial shift of H_(Naph) = 8.89, H_(Xan) = 7.57 and H_(Xan) = 7.34 ppm. c) See text for methods.

The newly formed complexes were purified according to their overall charge. The cationic Ag(I) and Au(I) complexes were purified by simply filtering off excess metal starting material and removing solvent *in vacuo* to give yellow solids. The neutral palladium complex was amazingly stable and was purified by silica gel chromatography with methylene chloride as the eluent.

²⁰ a) Storhoff, B. N.; Lewis, H. C., Jr. *Coord. Chem. Rev.* **1977**, *23*, 1. b) Walton, R. A. Q. *Rev. Chem. Soc.* **1965**, *19*, 126.

Spectroscopic changes upon complexation were consistent with the chelation of the metal between the two nitriles. The IR frequency of the nitrile ($\sim 2200\text{ cm}^{-1}$) is very sensitive to changes in the metal-nitrile geometry and lent support for the proposed 'end-on' coordination geometry.¹⁹ For each metal complex of dinitrile **82c**, the nitrile band ($\sim 2223\text{ cm}^{-1}$) was shifted $30 - 70\text{ cm}^{-1}$ to higher frequencies, which is characteristic of a linear or 'end-on' metal-nitrile arrangement (Figure V-3). By comparison, shifts to lower IR frequencies are usually attributed a 'side-on' metal-nitrile geometry. Further support for the chelation of the metal by the nitriles was provided by the downfield shifts of the protons directly conjugated to the nitrile in the ^1H NMR spectra. Only the aryl protons of the xanthene ring functionalized with the nitrile shifted; while the other xanthene protons were relatively stationary.

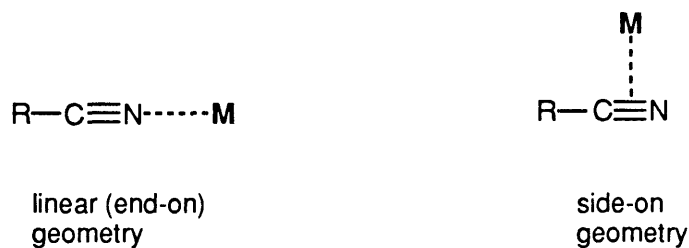


Figure V-3. Common metal-nitrile geometries.

The metal to ligand ratios in solution were measured to be 1 : 1 for both Au(I) and Pd(II), and 1 : 2 for Ag(I). These are in excellent agreement with known coordination numbers of nitrile complexes for each metal (Table V-4). The Au(I) and PdCl₂ tend to be 2-coordinate, whereas Ag(I) favors a 4-coordinate geometry. Different methods were employed to determine the individual stoichiometries, depending on the overall charge of the complexes.

Highest Coordinate Monodentate Nitrile Complex	
PdCl ₂	PdCl ₂ (PhCN) ₂ ²¹
Au(I)	AuClO ₄ (MeCN) ₂ ²²
Ag(I)	AgClO ₄ (MeCN) ₄ ²³

Table V-4. Monodentate nitrile metal complexes.

The neutral PdCl₂ complex was titrated with triphenyl phosphine (TPP) which quantitatively removed PdCl₂ from the Pd(II) complex of **82c**, forming PdCl₂(TPP)₂. During this titration, both free and complexed ligand were visible by ¹H NMR as separate species. Integrations of the corresponding naphthalene singlets showed that 2.0 eq of TPP were necessary to extract all of the PdCl₂ from the *trans*- palladium dinitrile complex (Figure V-4). The sharp break at 2.0 eq TPP and the slope of 0.5 prior to this point both implied the existence of a 1 to 1 chelate.

²¹ Adams, H.; Bailey, N. A.; Bruce, D. W.; Dunmur, D. A.; Lalinde, E.; Marcos, M.; Ridgway, C.; Smith, A. J.; Styring, P.; Maitlis, P. M. *Liquid Crystals* **1987**, *2*, 381.

²² Begerhoff, G. Z. *Anorg. Allg. Chem.* **1964**, *327*, 139.

²³ Nilsson, K.; Oskarsson, A. *Acta. Chem. Scand., Ser. A* **1984**, *38*, 79.

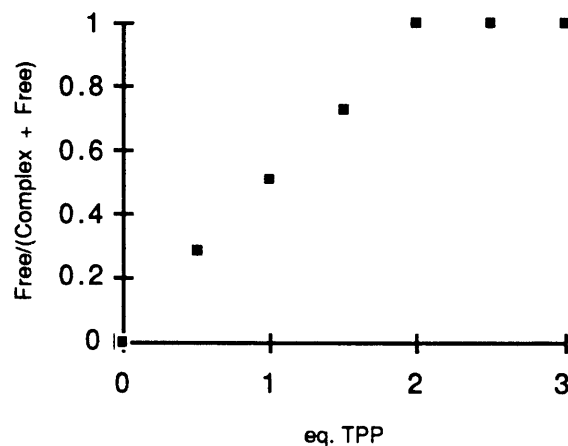


Figure V-4. Graph of the ratio of naphthalene singlets by ^1H NMR vs. the number of equivalents of triphenyl phosphine added to the $82\text{c}\cdot\text{PdCl}_2$ complex in CDCl_3 .

The cationic nature of the Ag^+ and Au^+ complexes was exploited by using their BF_4^- counter-ions to determine their stoichiometries. Fluorobenzene was added as a standard which contained both protons and fluorine. Integrations of the ligand, the standard, and the BF_4^- counter-ion in the ^1H and ^{19}F NMR spectra gave the $\text{Ph-F}/(\text{ligand } 82\text{c})$ and the $\text{BF}_4^-/\text{Ph-F}$ ratios. Combining these terms using equation (1) yielded the BF_4^- to (ligand 82c) ratios, which for Au^+ was 1.05 and for Ag^+ was 0.49. These equate to metal to ligand ratios of 1 : 1 and 1 : 2 for Au^+ and Ag^+ respectively.

$$\frac{\text{Ph-F}}{(\text{ligand } 82\text{c})} \times \frac{\text{BF}_4^-}{\text{Ph-F}} = \frac{\text{BF}_4^-}{(\text{ligand } 82\text{c})} \quad (1)$$

Comparisons of the relative shifts, in the ^1H NMR and IR spectra of dinitrile 82c upon complexation, gave further evidence for the measured stoichiometries (Table V-3). $\text{Ag}(\text{I})$ and $\text{Au}(\text{I})$ are almost identical in terms of electronegativity and size, and their complexes were expected to be spectroscopically similar. However, $\text{Au}(\text{I})$ induced shifts on the order of

twice that observed for Ag(I), which was in excellent agreement with their measured stoichiometries. In the ^1H NMR spectra, the xanthene aryl protons of **82c** moved + 0.37 and + 0.50 ppm downfield upon complexation of Au(I), whereas they moved only + 0.19 ppm and + 0.27 ppm downfield for Ag(I). Likewise, in the IR spectra of **82c**, the nitrile peak shifted + 53 cm^{-1} to higher wavelength for the Au(I) complex as compared to only + 31 cm^{-1} for Ag(I).

The proposed binding geometries are shown in Figure V-5. The 1 : 1 complex has the metal strung linearly between the two nitriles of **82c**. The 1:2 complex simply repeats this geometry twice with the two dinitrile ligands twisted by 90°. The ^1H NMR spectra of all three metal complexes were consistent with the proposed geometries in which the metal occupies the cavity of the dinitrile ligand (**82c**). In each case, the protons of the naphthalene surfaces shifted downfield, presumably from the presence of the metal center inside of the cavity. Again Au(I) induced twice the shift in the naphthalene protons than did Ag(I).

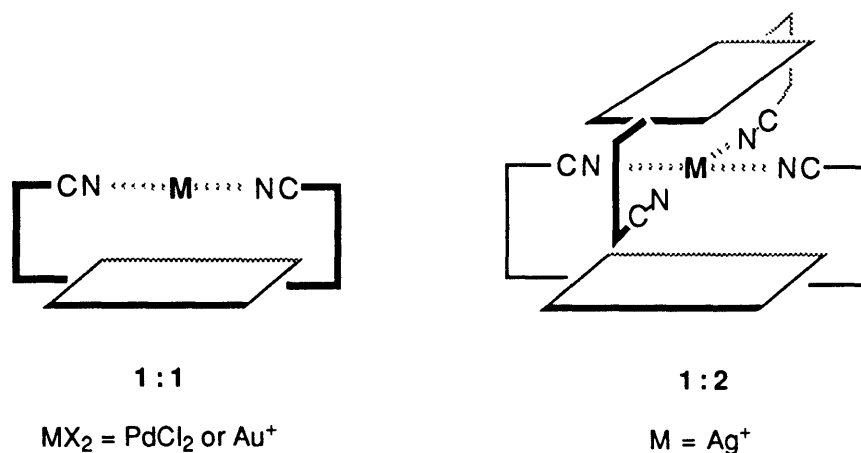


Figure V-5. Schematic representations of the proposed of metal • (dinitrile **82c**) geometries (counter ions are not shown).

Molecular modeling studies of the dinitrile complexes easily accommodated the proposed geometries and also ruled out several others. Polymeric or oligomeric structures such as those shown in Figure V-6 were sterically inaccessible due to overlapping xanthenes and *t*-butyl groups. These geometries also would have resulted in a more complex ^1H NMR

spectra because of their lower symmetries. In particular, the naphthalene protons were once again a singlet.

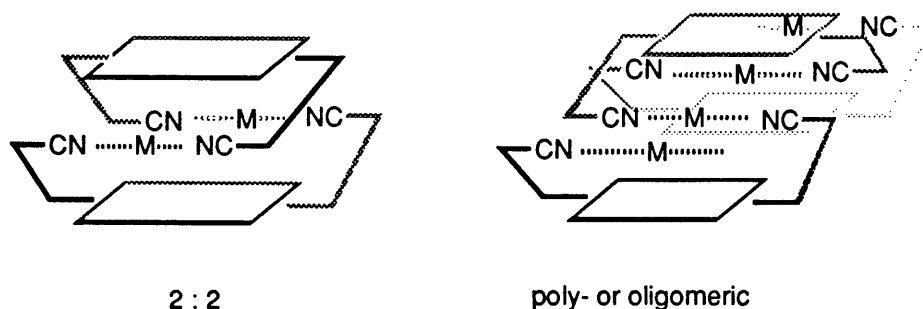


Figure V-6. Other possible coordination geometries.

In each case, a near linear -CN--M--NC- angle is proposed. Structures with bent or *cis-* geometries were discounted because of the rigid C-shape of the dinitrile. The proposed 'end-on' geometries and coordination numbers are well preceded in the monodentate versions of these complexes. PdCl_2 and Au^+ tend to form linear dinitrile complexes while Ag^+ forms tetranitrile complexes in the presence of non-complexing counter-ions such as BF_4^- and ClO_4^- (see Table V-4). One point of uncertainty is the precise geometry of the Ag(I) metal center. The shape of ligand **82c** strongly favors the formation of a square planar complex; on the other hand, Ag(I) has a propensity toward a tetrahedral geometry. A similar 'tug-of-war' is played out in Ag(I) porphyrins where a pseudo-tetrahedral geometry is observed.

Other metals were also briefly examined. Surprisingly, $\text{PtCl}_2(\text{PhCN})_2$ on treatment with dinitrile **82c** showed no complexation even on heating. This may be due to the greater kinetic stability of Pt(II) dinitrile complexes in comparison to Pd(II) . Alternatively, the selectivity may arise from the inflexibility of dinitrile **82c**. Complexation studies with Cu(I) were more successful. Treatment of the convergent dinitrile (**82c**) with $\text{Cu}(\text{MeCN})_4^+ \text{PF}_6^-$ in methylene chloride showed spectroscopic changes consistent with the previous *trans*-complexes. In fact, the shifts in the ^1H NMR spectra of

the ligand with Cu(I) were almost identical to those seen for Ag(I),²⁴ both of which have tendencies to coordinate four nitriles.

5.5 OUTLOOK

The high degree of preorganization coupled with an optimal separation between binding functionality make the naphthalene scaffolds excellent ligands. Even normally labile nitrile complexes formed under mild conditions and were fairly stable, making them easier to study than their monodentate counterparts. The convergent geometry also allows access to chelation from opposing sides of the metal center, a coordination geometry for which there are few examples.

We have also attempted to exploit the convergency of the larger perylene scaffolds in a similar fashion to create ligands which form large ring chelates. The C-shaped perylene dinitrile **56c** was treated with $\text{Rh}_2(\text{OAc})_4$ which is known to bind a nitrile on either end (Figure V-7). The distance between nitrile nitrogens in **56c** was estimated to be $\sim 6.6 \text{ \AA}$ which is very close to that reported for $\text{Rh}_2(\text{OAc})_4$ bis(nitrile) complexes (6.89 \AA).²⁵ Mixing the insoluble $\text{Rh}_2(\text{OAc})_2$ with **56c** showed no evidence of complexation. Molecular modeling suggests that the problem may lie in the peripheral methyl groups which may be too large to fit into the cavity.

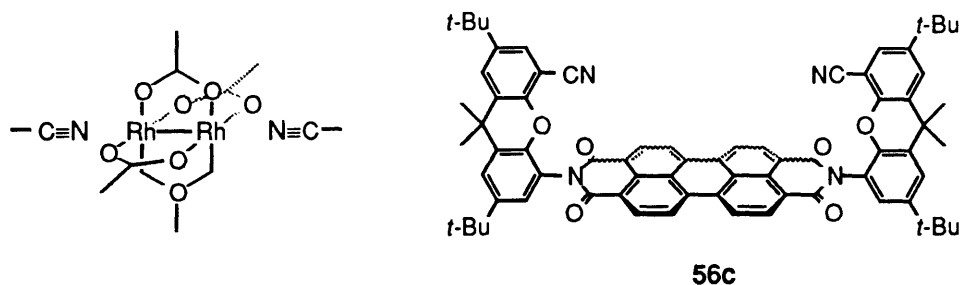


Figure V-7. Rhodium acetate dinitrile complex and perylene dinitrile **56c**.

²⁴ Shifts in the ^1H NMR spectra: $\text{H}_{\text{Naph}} = +0.036 \text{ ppm}$, $\text{H}_{\text{Xan}} = +0.183 \text{ ppm}$, $\text{H}_{\text{Xan}} = +0.273 \text{ ppm}$. Compare to those reported in Table V-3.

²⁵ a) Cotton, F. A.; Thompson, J. L. *Acta Cryst. B* **1981**, *37*, 2235. b) Doyle, M. P.; Winchester, W. R.; Hoorn, J. A. A.; Lynch, V.; Simonsen, S. H.; Ghosh, R. *J. Am. Chem. Soc.* **1993**, *115*, 9968.

More successful were binding studies with the highly preorganized hexaether **136c**, which was constructed from the condensation of cyanoethylated TRIS (**137**) and the C-shaped perylene diacid chloride. Preliminary, liquid-liquid extraction studies with alkali picrates showed that hexaether **136c** had a high affinity for metal ions, similar to that of a macrocyclic crown ether and with a certain degree of selectivity.

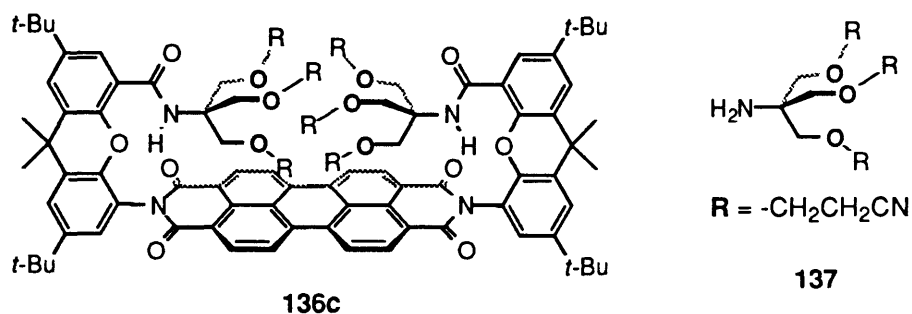


Figure V-8. The acyclic ionophore **136c**.

5.6 EXPERIMENTAL

Procedure for the colorimetric alizarin test for Ca^{2+} : Alizarin from Aldrich was refluxed in ethanol. The solids were filtered off while hot and the filtrate allowed to cool. The purified alizarin was collected as a brown solid. An alizarin solution was prepared by dissolving 20 mg in 500 mL *n*-octyl alcohol with sonication.

The analysis of an aqueous Ca^{2+} solution was performed by first diluting 20 fold to insure that the Ca^{2+} concentration remained well below the alizarin concentration. A 0.020 mL aliquot of the calcium solution was combined in a test tube with 1.0 mL distilled H_2O , 2.0 mL of 1.0 N triethanol amine, and 3.0 mL of the alizarin solution in octanol. The mixture was mechanically shaken. A 2.0 mL aliquot of the purple top (organic) layer was diluted with 3.0 mL octanol and the absorbance was measured at 560 nm. A blank was prepared to give a baseline value by repeating the above procedure substituting distilled water for the calcium solution.

A standardization graph (absorbance @ 560 nm vs. calcium concentration) was generated by measuring the absorbance of known Ca^{++} solutions. The calcium concentration was calculated by comparing measured absorbances against the standardization graph.

Procedure for the formation of $\text{Ag}^+ \cdot (\text{dinitrile})_2$ complex: The dinitrile ligand **82c** (~ 10 mg) was dissolved in 5 mL of dichloromethane. An excess of AgBF_4 was added (~ 10 mg) and the mixture was shaken well. The reaction was filtered through glass wool to remove excess AgBF_4 and the resulting solution concentrated *in vacuo* to a bright yellow solid. The silver complex appears to be light sensitive and over a period of days a silvery gray film can be seen in the sample which is presumably the result of disproportionation.

Complexation appears to occur quickly and the binding constant of the dinitrile ligand to be quite high so as little as 0.5 eq of AgBF_4 are actually necessary. Also, the exact concentrations above are only a rough guideline. Solutions of the dinitrile ligand and Ag^+ in dichloromethane which are considerably much more dilute or concentrated still result in an identical complex. IR (KBr) 2259 (-CN), 1050 (BF_4^-) cm^{-1} ; ^1H NMR (300 MHz, CDCl_3) δ 8.95 (s, 4 H, Naph), 7.76 (d, 2 H, $J = 2.3$ Hz, Xan), 7.61 (d, 2 H, $J = 2.1$ Hz, Xan), 7.61 (d, 2 H, $J = 2.2$ Hz, Xan), 7.32 (d, 2 H, $J = 2.2$ Hz, Xan), 1.74 (s, 12 H, Me), 1.40 (s, 18 H, *t*-Bu), 1.33 (s, 18 H, *t*-Bu)

Procedure for the formation of $\text{Au}^+ \cdot (\text{dinitrile})$ complex: The procedure was similar to the preparation of the silver complex above with $\text{AuBF}_4(\text{CN})_2$ substituted for AgBF_4 . $\text{AuBF}_4(\text{CN})_2$ was prepared by treatment of gold powder (250 mg) with NO^+BF_4^- (100 mg) in 1.5 mL acetonitrile. The mixture was stirred for 2 days. The reaction mixture was diluted with ether and filtered. The product Au^+BF_4^- was collected as a white crystalline solid which on standing for several days turned black. IR (KBr) 2281 (-CN), 1059 (BF_4^-) cm^{-1} ; ^1H NMR (300 MHz, CDCl_3) δ 8.95 (s, 4 H, Naph), 7.94 (d, 2 H, $J = 2.4$ Hz, Xan), 7.84 (d, 2 H, $J = 2.1$ Hz, Xan), 7.62 (d, 2 H, $J = 2.1$ Hz, Xan), 7.34 (d, 2 H, $J = 2.1$ Hz, Xan), 1.72 (s, 12 H, Me), 1.41 (s, 18 H, *t*-Bu), 1.31 (s, 18 H, *t*-Bu).

Procedure for the formation of $\text{PdCl}_2 \cdot (\text{dinitrile})$ complex: The C-shaped dinitrile **82c** (32 mg, 0.0334 mmol) and $\text{PdCl}_2(\text{PhCN})_2$ (50 mg, 0.1304) were dissolved in 10 mL CH_2Cl_2 . Immediately, TLC (CH_2Cl_2) showed full conversion

to a lower Rf product. Chromatography (CH₂Cl₂) on silica gel yielded a Pd complex as a yellow solid (33.8 mg).

IR (KBr) 2296 cm⁻¹ (-CN); ¹H NMR (300 MHz, CDCl₃) δ 9.05 (s, 4 H, Naph), 7.72 (d, 2 H, J = 2.4 Hz, Xan), 7.57 (d, 2 H, J = 2.1 Hz, Xan), 7.44 (d, 2 H, J = 2.1 Hz, Xan), 7.35 (d, 2 H, J = 2.1 Hz, Xan), 1.72 (s, 12 H, Me), 1.41 (s, 18 H, *t*-Bu), 1.31 (s, 18 H, *t*-Bu).

C- Perylene Hexaether (136c). The C-diacid (100 mg, 0.0893 mmol) was converted to the diacid chloride as previously described (see Chapter II, 51c). The crude diacid chloride was taken up in 20 mL CH₂Cl₂ with amino triether 137 (75 mg, 0.268 mmol)²⁶ and triethylamine (27 mg, 0.268 mmol) and stirred for 15 h. The reaction mixture was washed with 1.0 N HCl (2 x 100 mL), dried over MgSO₄ and dried *in vacuo* to a red solid. Gravity chromatography (CH₂Cl₂) gave the product (66 mg, 45 % yield): mp > 330 °C; ¹H NMR (250 MHz, CDCl₃) δ 8.82 (s, 8 H, Per), 7.59 (d, 2 H, J = 2.1 Hz, Xan), 7.55 (d, 2 H, J = 2.4 Hz, Xan), 7.47 (d, 2 H, J = 2.4 Hz, Xan), 7.16 (d, 2 H, J = 2.3 Hz, Xan), 6.44 (br s, 2 H, -NH), 3.36 (t, 12 H, J = 6.2 Hz, -CH₂-), 3.34 (s, 12 H, -CH₂-), 2.41 (t, 12 H, -CH₂-), 1.74 (s, 12 H, Me), 1.36 (s, 18 H, *t*-Bu), 1.33 (s, 18 H, *t*-Bu); HRMS (FAB in NBA) calcd for C₉₈H₁₀₃N₁₀O₁₄ (M+H), 1643.76552; found 1643.76052.

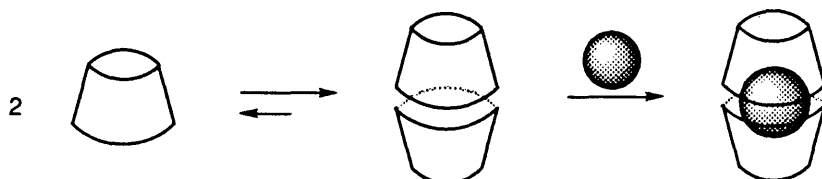
²⁶ The cyanoethyl protected TRIS was synthesized as described in the literature: Newkome, G. R.; Lin, X. F. *Synlett.* 1992, 53.

Chapter VI

A Self-Assembling Molecular-Container

6.1 INTRODUCTION

A calix[4]arene tetraurea **140** was designed to dimerize and form a completely sealed cavity **140d**.¹ The adhesive contacts were provided by four aryl ureas which upon dimerization form a cyclic array, containing up to 16 hydrogen bonds. Synthesis was completed in four steps from the previously described O,O',O'',O'''-tetrabenzylcalix[4]arene.² Evidence for assembly was provided by ¹H NMR, mass spectrometry and, most importantly, the observation of encapsulated guest molecules. The self-assembled cavity was of sufficient size to capture guests such as ethyl benzene and *p*-xylene.



¹ The **d** following a structure's number will be used to denote the formation of a dimer.

² Gutsche, C. D.; Pagoria, P. F. *J. Org. Chem.* **1985**, *50*, 5795-5802.

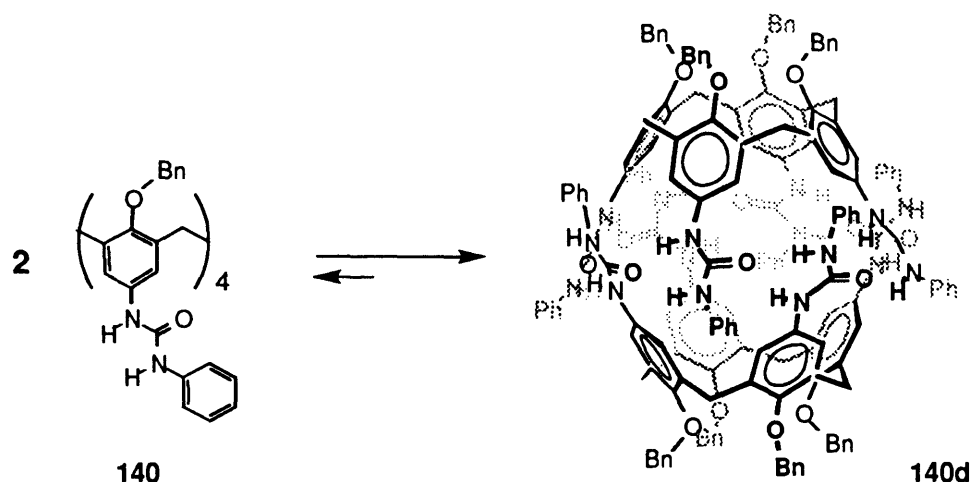


Figure VI-1. Schematic representation of calixarene tetraurea **140**, and its assembly into dimer **140d**.

6.2 BACKGROUND

Synthetic self-assembly is a relatively new field which has become an important focus of molecular recognition research.³ The commonly invoked paradigm of controlled self-assembly is the formation of the tobacco virus' capsule.⁴ In this spectacular example, more than two thousand protein units assemble about a RNA core. Indeed in biological contexts, self-assembly is an ubiquitous organizational strategy, in which modular components are held together by non-covalent interactions. Multi-molecular structures such as membranes, ribosomes and DNA attest to the importance and power of self-assembly. For the synthetic chemist, bringing molecules together with non-covalent interactions provides a promising strategy for the construction of large elaborate architectures in an equally rapid and facile manner. In addition, these new 'supramolecules' often possess unique properties and abilities that are

³ For reviews see: a) Lehn, J. M.; Rigault, A. *Angew. Chem. Int. Ed. Engl.* **1988**, *27*, 1095. b) Lindsey, J. S. *New. J. Chem.* **1991**, *15*, 153-180. c) Whitesides, G. M.; Mathias, J. P.; Seto, C. T. *Science* **1991**, *254*, 1312-1319. d) Whitesides, G. M.; Simanek, E. E.; Mathias, J. P.; Seto, C. T.; Chin, D. N.; Mammen, M.; Gordon, D. M. *Acc. Chem. Res.* **1995**, *28*, 37-44.

⁴ Branden, D.; Tooze, J. *The Structure of Spherical Viruses*; Garland Publishing: NY, 1991, Chapter 11.

totally different from their smaller components. These systems are developed upon the alluring premise that the whole can be greater than the sum of its parts.

In synthetic self-assembly, two structural patterns have emerged. In the first type, the size of the structure goes entirely unregulated. Infinite 'ribbons', 'sheets' and three-dimensional aggregates have been constructed from molecules with two, three, and four recognition surfaces respectively. Examples of each are shown in Figure VI-2. Lehn *et al.* have used chirality to direct the assembly of a polyamide ribbon or tape (Figure VI-2a).⁵ Whitesides *et al.* has utilized the two-dimensional cyanuric acid-melamine lattice as the basis for arranging large three-dimensional aggregates (Figure VI-2b).⁶ Aggregates have also been assembled using metal-ligand interactions. For example, combining a tetranitrile and a tetrahedral metal center led to the formation of an expansive three-dimensional network (Figure VI-2c).⁷

⁵ a) Brienne, M.-J.; Gabard, J.; Leclercq, M.; Lehn, J.-M.; Cesario, M.; Pascard, C.; Cheve, M.; Dutruc-Rosset, G. *Tetrahedron Lett.* **1994**, *35*, 8157. b) Lehn, J.-M.; Mascal, M.; Decian, A.; Fischer, J. *J. Chem. Soc., Perkin Trans II* **1992**, 461.

⁶ a) Mathias, J. P.; Simanek, E. E.; Whitesides, G. M. *J. Am. Chem. Soc.* **1994**, *116*, 4326.
b) Mathias, J. P.; Simanek, E. E.; Zerkowski, J. A.; Seto, C. T.; Whitesides, G. M. *J. Am. Chem. Soc.* **1994**, *116*, 4316.

⁷ Hoskins, B. F.; Robson, R. *J. Am. Chem. Soc.* **1990**, *112*, 1546.

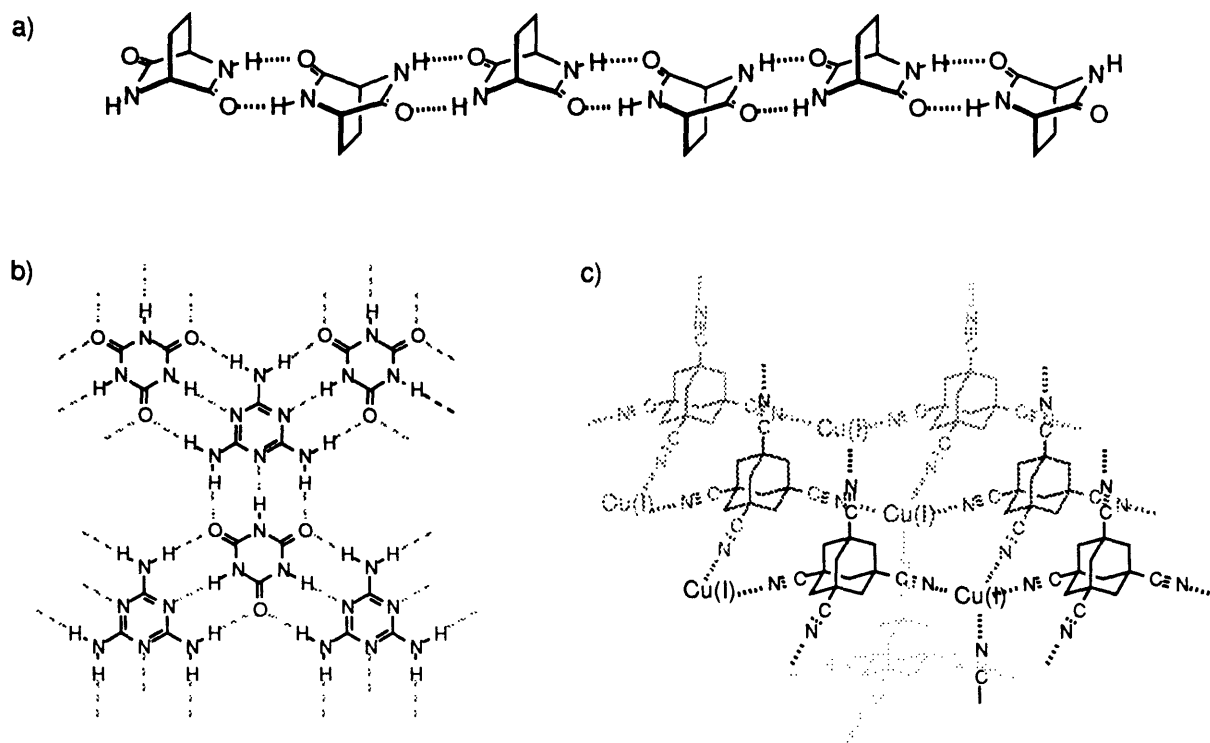


Figure VI-2. Examples of infinite assemblies: a) ribbon, b) sheet, and c) three-dimensional.

In the second type of assembly, size, and shape are well defined and predictable. These 'mesomolecular' assemblies (e.g. aggregates of 2 - 20 molecules) tend to be no longer or larger than any single component. For example, Zimmerman's cyclic trimer (Figure VI-3a) utilizes the angle between its two binding surfaces in each unit to favor the assembly of a trimer.⁸ In an extraordinary example of synthetic self-assembly, J.-M. Lehn *et al.* have brought fifteen molecules together into a metal pyridyl grid (Figure VI-3b).⁹ In this case, the size of the assembly was determined by the length of the organic ligand.

⁸ Zimmerman, S. C.; Brook, B. F. J. *Org. Chem.* **1992**, *57*, 2215-2217.

⁹ Baxter, P. N. W.; Lehn, J.-M.; Fischer, J.; Youinou, M. T. *Angew. Chem., Int. Ed. Engl.* **1994**, *33*, 2284.

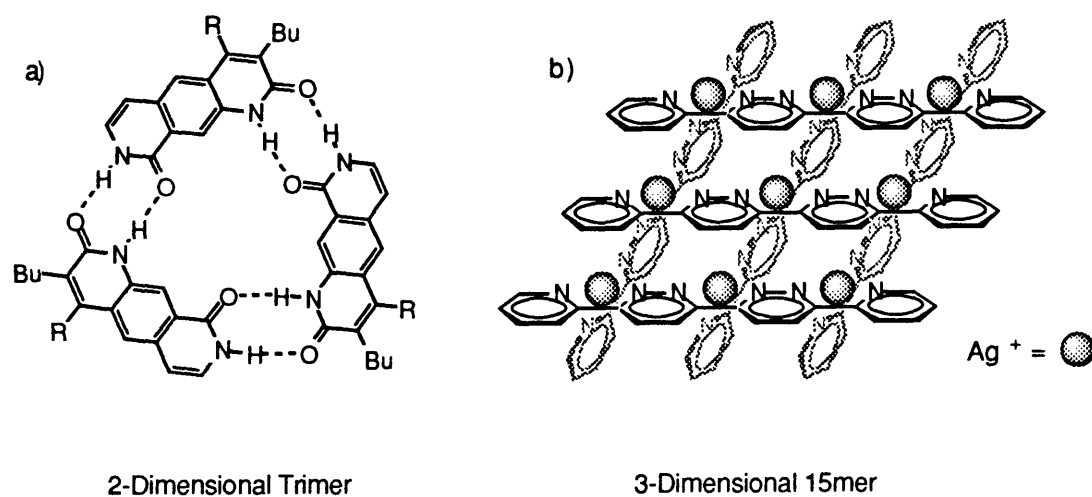


Figure VI-3. Self-assembly systems of well defined size and shape.

Recently, we have introduced a self-assembly system which dimerized to form a well defined cavity which was capable of capturing and holding guests in its interior. The 'tennis ball' (Figure VI-4) was composed of self complementary glycourils and was held together by eight hydrogen bonds. The formed cavity is fairly small, limiting its utility and potential application, as only smaller guests such as methane and its homologues could fit inside.

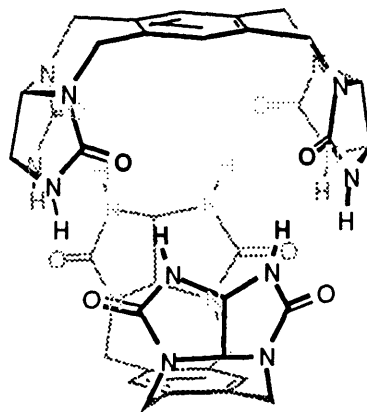


Figure VI-4. Dimeric self-assembling 'tennis ball' based upon four glycourils and eight hydrogen bonds.

The potential of these self-assembling cavities can be seen in their covalently constructed cousins. Collet *et al.* and Cram *et al.* have each synthesized molecules

composed of two halves which were sealed with covalent linkages (Figure VI-4).¹⁰ The contents or lack of contents of these spherical structures are the most fascinating aspect of these molecules. A variety of hydrocarbons and aromatic guests have been bound by these cavities, surprisingly even in apolar solvents. Cram's larger 'hemicarcerands' were even able to encapsulate and stabilize highly reactive species.¹¹ The selectivities of these covalent cavities were often limited by the size of the portals through which guests could enter the molecule, as opposed to the size and shape of their cavities.

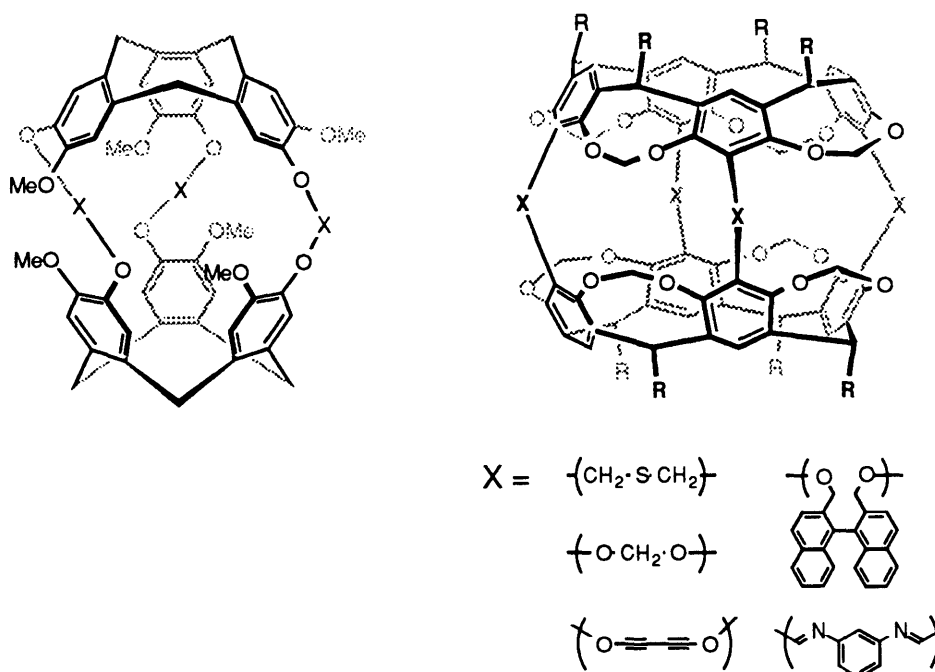


Figure VI-5. Covalently sealed molecular cavities.

¹⁰ a) Canceill, J.; Lacombe, L.; Collet, A. *J. Am. Chem. Soc.* **1985**, *107*, 6993. b) Garel, L.; Dutasta, J. P.; Collet, A. *Angew. Chem., Int. Ed. Engl.* **1993**, *32*, 1169-1171. c) Robbins, T. A.; Knobler, C. B.; Bellow, D. R.; Cram, D. J. *J. Am. Chem. Soc.* **1994**, *116*, 111-122.. d) Cram, D. J. *Nature* **1992**, 356, 29-36.

¹¹ a) Eid, C. N., Jr.; Knobler, C. B.; Gronbeck, D. A.; Cram, D. J. *J. Am. Chem. Soc.* **1994**, *116*, 8506. b) Robbins, T. A.; Cram, D. J. *J. Am. Chem. Soc.* **1993**, *115*, 12199.

6.3 DESIGN

We set forth to build a larger and synthetically more accessible self-assembling capsule. First, a new self-complementary interaction was sought. To some degree, the glycouril hydrogen bonding surface limited the size of the 'tennis ball'. Furthermore, the incorporation of the highly insoluble glycouril units onto a rigid scaffold proved to be a synthetically challenging task. Our new designs have centered on the urea-urea interaction. Much of our inspiration for utilizing ureas in self-assembly has been drawn from urea itself, which can form large cylinders, having an alkyl chain threaded through its center.¹² These beautifully chiral complexes assemble easily in the solid-state and structurally resemble larger biological assemblies such as virus sheaths. The aggregation of ureas is also pervasive, and its binding and self-association propensities extensively studied.¹³ Finally, ureas can be easily introduced into a molecular scaffold, needing only a single amine as an anchor.

When placed in a circular arrangement, ureas can be made to chase each other in a 'head to tail' fashion (Figure VI-6). X-ray crystallography has shown that this topology in which the carbonyl oxygen of one urea hydrogen bonds to both -NH's of an adjacent urea is the most common. For our purposes, the 'head-to-tail' topology is particularly advantageous because the ureas do not need to lie in the same plane and can easily adopt this circular arrangement.

¹² a) Schiessler, R. W.; Flitter, D. *J. Am. Chem. Soc.* **1952**, *74*, 1720. b) Smith, A. E. *J. Chem. Phys.* **1950**, *18*, 150. c) Schlenk, W., Jr *Liebigs Ann. Chem.* **1973**, 1145.

¹³ a) Etter, M.; Urbańczyk-Lipkowska, Z.; Zia-Ebrahimi, M.; Panunto, T. W. *J. Am. Chem. Soc.* **1990**, *112*, 8415-8426. b) Etter, M. C.; Panunto, T. W. *J. Am. Chem. Soc.* **1988**, *110*, 5896-5897.

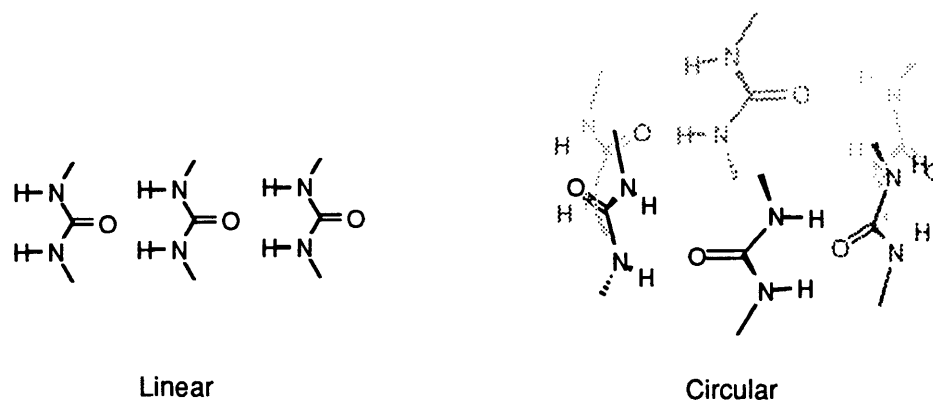
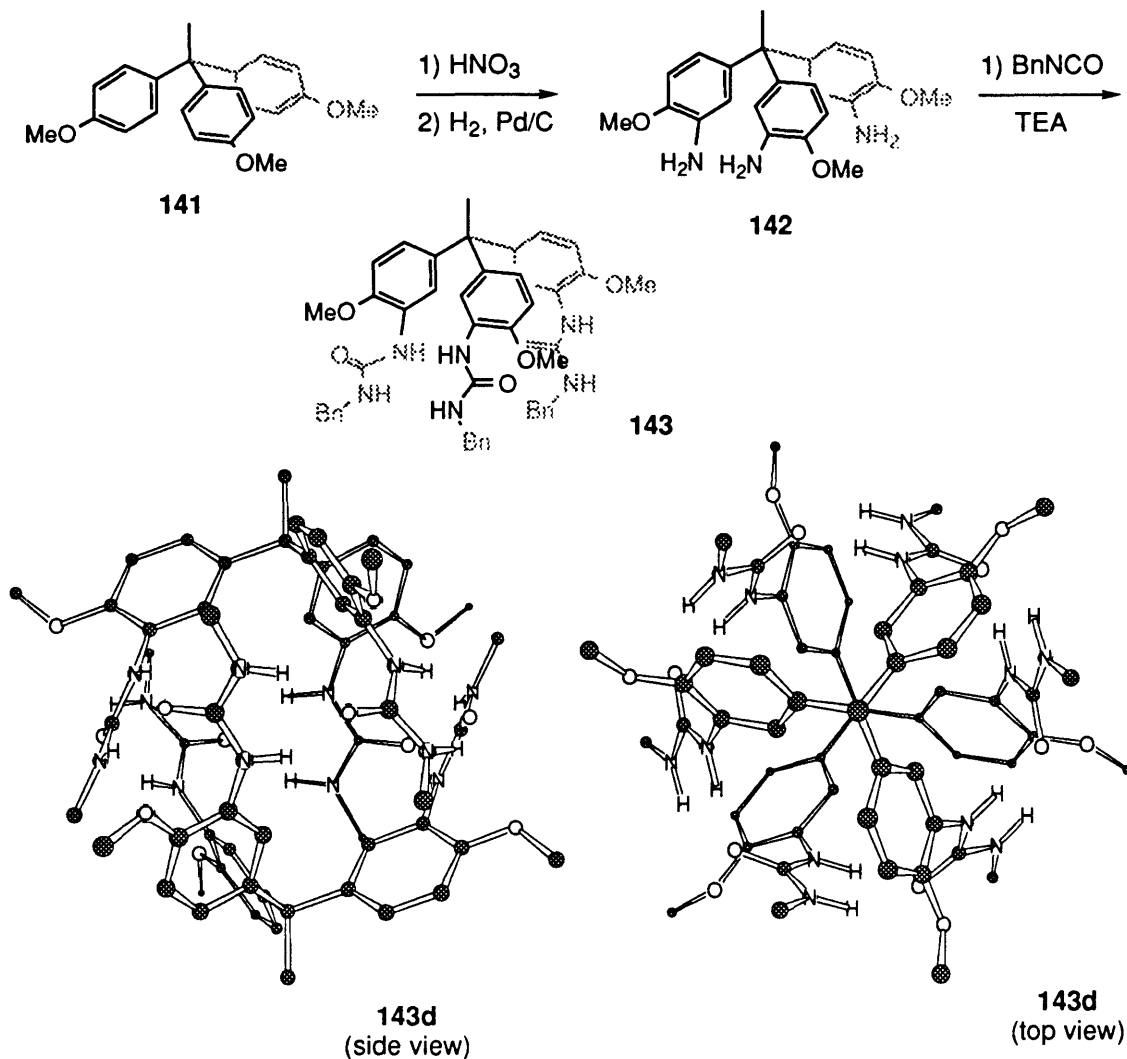


Figure VI-6. Linear and circular arrangements of ureas in a 'head to tail' topology.

Initially, a triphenyl methane scaffold was synthesized via nitration and reduction of the corresponding trimethoxytriphenyl methane (**141**). Treatment of triamine **142** with benzyl isocyanate gave the desired triurea 'chandelier' (**143**). Unfortunately, **143** showed no signs of assembly into the desired dimer **143d**. In particular, the ^1H NMR spectra did not show large downfield shifts of the urea -NH's, as the molecule appears to lack the preorganization necessary for assembly. The phenyl groups are freely rotating and the conformation in which all three ureas are pointing away from the center methyl group is present only a fraction of the time. Another problem may be the orientation of the $\text{N}_{\text{imide}}\text{-C}_{\text{aryl}}$ bond. The rotamer in which the imide carbonyl is twisted away from the adjacent methyl ether will probably be the most stable. However, the urea will also want to be coplanar and in conjugation with the attached phenyl surface. This orientation is not particularly favorable toward formation of the desired dimer.



Scheme VI-1. Synthesis of the triphenyl methane triurea **143** and the MM2 minimized structure of the desired dimer **143d**.

A more conformationally rigid scaffold was sought, and calix[4]arenes were chosen.¹⁴ The four fold symmetry of calix[4]arenes expands the circular arrangement of ureas by two, encircling an even larger cavity than **143d**. Calixarenes are well studied, both in their conformation and synthesis.¹⁵ A large

¹⁴ For another example of ureas on a calix[4]arene see: Scheer, J.; Fochi, M.; Engbersen, J. F. J.; Reinhoudt, D. N. J. *Org. Chem.* **1994**, *59*, 7815.

¹⁵ *Calixarenes; Monographs in Supramolecular Chemistry*; Gutsche, C. D., Ed.; The Royal Society of Chemistry: Cambridge, 1989.

number of derivatives have been made and synthesized in high yields. The inviting basket-like shape have also made calixarenes attractive scaffolds for molecular recognition. In fact, recent reviews of calixarene chemistry are dedicated almost entirely to applications in supramolecular chemistry.¹⁶ Of note, were previous systems designed to dimerize in a similar 'mouth to mouth' fashion to form a cavity. In our own research group, Neil Branda has developed a calix[4]arene (Figure VI-7c) based upon self-complementary amides. Unfortunately, this calixarene was not soluble in most solvent systems that favor hydrogen-bonding; although, some evidence for its dimerization in MeOH/CDCl₃ was observed.¹⁷ Elsewhere, Reinhoudt *et al.* designed a hydrogen bonding system which utilizes the dimerization of pyrrolidinones (Figure VI-7a).¹⁸ In this system, oligomerization was more prevalent than dimerization, and highlights the difficulties in designing such a system. The only highly successful calixarene dimer to date is a two component system prepared by S. Shinkai which exploits the strong pyridine-carboxylic acid association (Figure VI-7b).¹⁹ UV titrations show the formation of a 1 to 1 complex presumably in a 'mouth to mouth' geometry. Encapsulation of guests in this system was not seen probably because of the large holes in the assembly, which allow the free exchange of solvents and guests in and out of the cavity.

¹⁶ Böhmer, V. *Angew. Chem., Int. Ed. Engl.* **1995**, *34*, 713-745.

¹⁷ Branda, N. Thesis, Massachusetts Institute of Technology, 1994.

¹⁸ van Loon, J.-D.; Janssen, R. G.; Verboom, W.; Reinhoudt, D. N. *Tetrahedron Lett.* **1992**, *33*, 5125-5128.

¹⁹ Kok, K.; Araki, K.; Shinkai, S. *Tetrahedron Lett.* **1994**, *35*, 8255-8258.

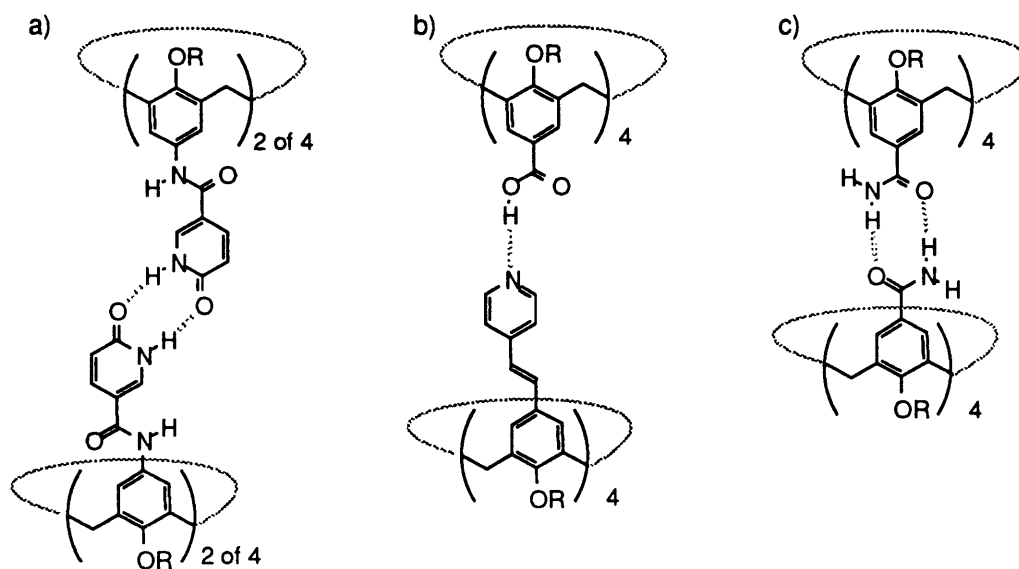


Figure VI-7. Calix[4]arenes designed to dimerize via hydrogen bonding.

Molecular modeling studies predicted that a calix[4]arene functionalized on its 'upper' rim (*para*- to the phenols)²⁰ would provide an optimal scaffold to position four ureas in the desired circular manner. In the MM2 minimized structure, the two calixarenes are offset by 45°, resulting in an interleaved structure which seals the resulting cavity (Figure VI-8a). The high symmetry of the hydrogen bonding pattern is best illustrated by a top view of the dimer (Figure VI-8b). All eight ureas are turned in the same direction, four coming from the top calixarene and the remaining four from the bottom.

²⁰ The convention 'upper' and 'lower' rim are used in this chapter to describe the calixarene in an orientation with the phenols on the bottom.

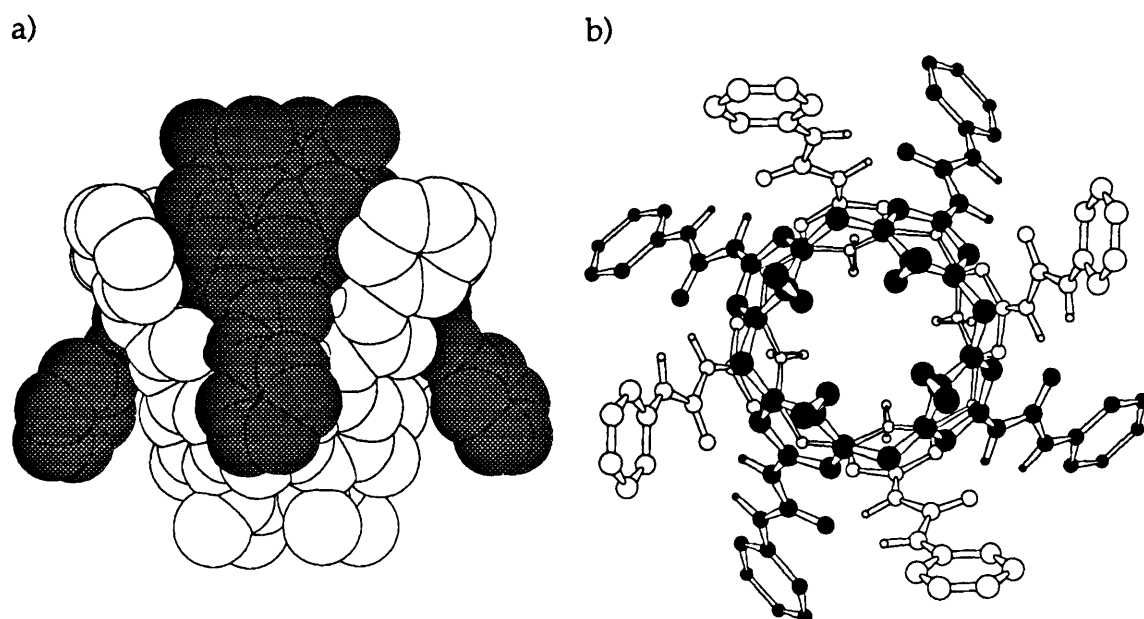


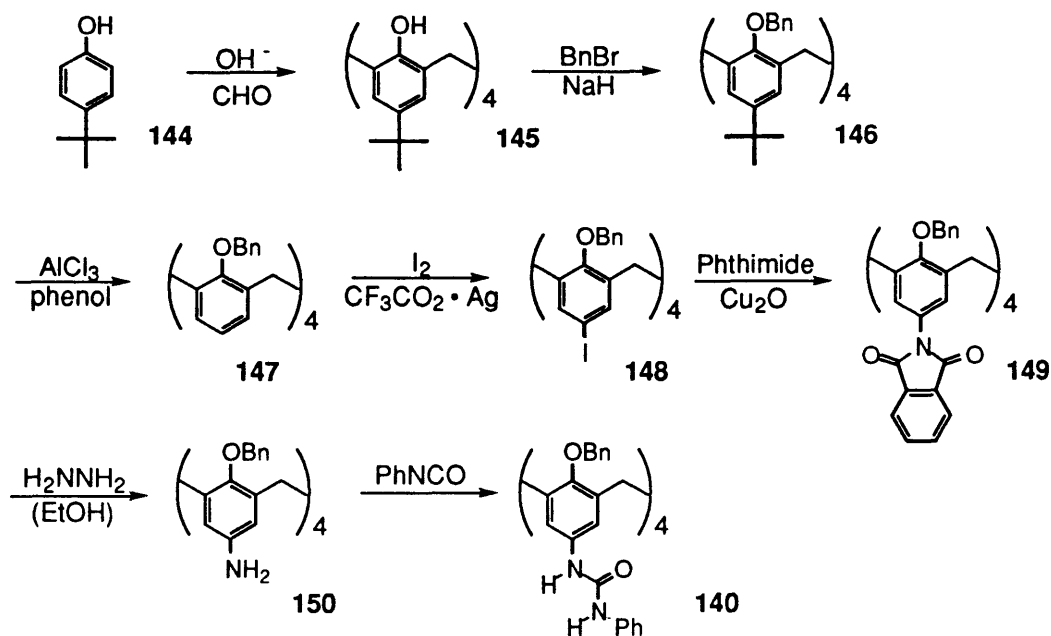
Figure VI-8. a) A CPK side view and b) a ball and stick top view of a MM2 minimized structure of calixarene tetraurea dimer 140d. The top calixarene is highlighted and the benzyl groups were removed for viewing clarity.

6.4 SYNTHESIS OF CALIX[4]ARENE TETRAUREA 140

The synthesis of a properly substituted calix[4]arene proceeded very quickly, utilizing the extensive literature on their syntheses.²¹ First, *p-t*-butyl phenol (144) was selectively macrocyclized using potassium as a template to give calix[4]arene 145.¹⁵ The phenols were capped with benzyl groups which prevent internal rotations of the calix[4]arene macrocycle and permanently fixes its conformation. Of the three possible isomers, the cone-conformer was selectively synthesized with all the benzyl groups on the same side. Finally, the *t*-butyl groups were removed with AlCl_3 and phenol.²²

²¹ a) Böhmer, V. *Angew. Chem., Int. Ed. Engl.* 1995, 34, 713-745. b) Gutsche, C. D. *Aldrichimica Acta* 1995, 28, 3-9. c) Linnane, P.; Shinkai, S. *Chem. Ind.* 1994, 811-814.

²² Aleksiuk, O.; Biali, S. E. *Tetrahedron Lett.* 1993, 1993, 4857.



Scheme VI-2. Synthesis of calixarene tetraurea **140**.

Functional groups were introduced on the 'upper rim' (*para*- to the phenol) using a modified Gabriel synthesis of amines. First, treatment of the cone conformation of **147** with iodine and silver•trifluoroacetate gave tetraiodo-calixarene **148** almost quantitatively.²³ A copper catalyzed Ullmann reaction replaced the four iodo- with four phthalimido- groups; subsequent aminolysis with hydrazine yielded calixarene tetramine **150**. The ureas were then introduced by treatment of **150** with phenyl isocyanate. The overall yield for the four functionalization steps was excellent (67 %) especially considering that each reaction had to be successful a four sites.

6.5 ASSEMBLY

The first indication that tetraaryl urea **140** was assembling was provided by its ¹H NMR spectra. In all the non-polar solvent examined so far, the ¹H NMR of

²³ Timmerman, P.; Verboom, W.; Reinhoudt, D. N.; Arduini, A.; Grandi, S.; Sicuri, A. R.; Pochini, A.; Ungaro, R. *Synthesis* **1994**, 185-189.

140 displayed an unusual symmetry (Figure VI-9a). The spectra was unlike any of **140**'s non-assembling precursors and even unlike the ^1H NMR spectra of **140** in polar solvents such as DMSO-d_6 or THF-d_8 (Figure VI-9b). The unusual ^1H NMR spectra of **140d** was attributed to the differing symmetries of the dimeric complex versus the unassociated calixarene. Typically, calix[4]arenes which are fixed in the cone-conformer have an apparent C_{4v} symmetry so that every aryl ring is chemically equivalent. In contrast, the octaurea complex **140d** possesses a S_8 symmetry in which each individual calixarene is chiral although the overall assembly is achiral (meso).

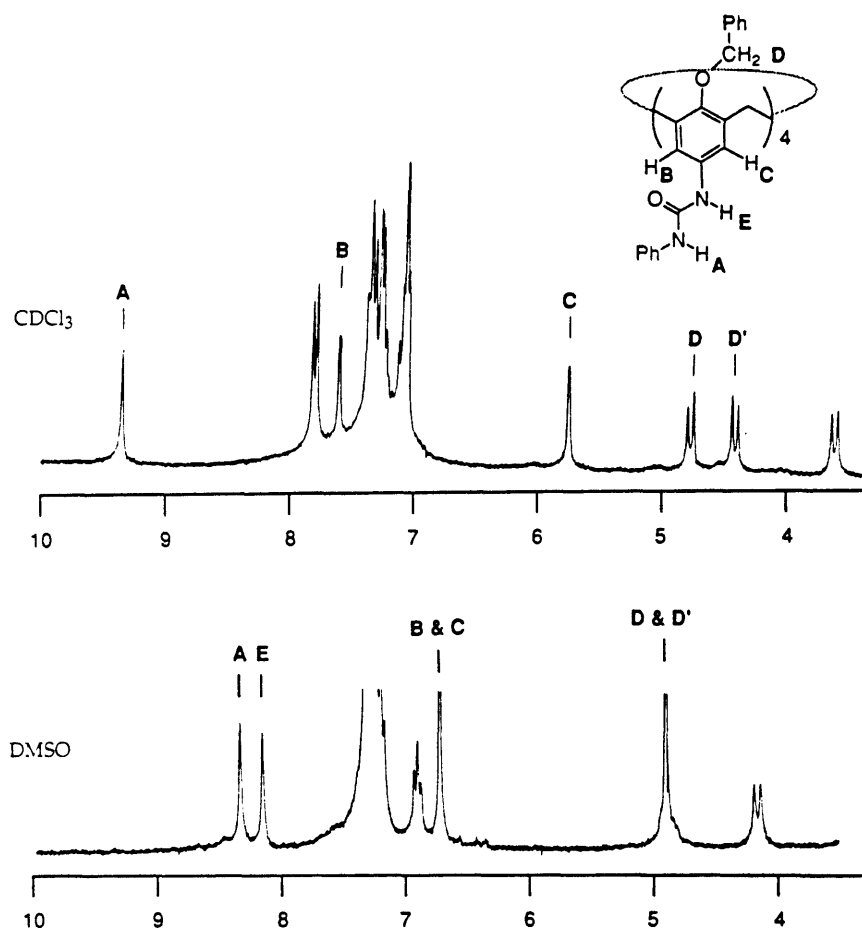


Figure VI-9. ^1H NMR spectra of **140**: a) in CDCl_3 as an assembled dimer and b) in DMSO-d_6 as an unassembled monomer.

The observed desymmetrization correlated well with the symmetry anticipated for the dimer **140d**. The calixarene aryl (H_B and H_C) and benzyl protons (H_D and $H_{D'}$), which were previously singlets, became chemically inequivalent. For example in $CDCl_3$, the aryl protons H_B and H_C of **140d** were at 7.59 ppm and 5.73 ppm respectively. Their proper assignments were clarified by the observation of *meta*-coupling (3.0 Hz) between the aryl protons. This asymmetry was also evident in the benzyl protons H_D and $H_{D'}$ of **140d**, which became diastereotopic and had a characteristically large coupling constant of 12.6 Hz. Otherwise, the 1H NMR spectra was consistent with that of previous cone-shaped calix[4]arene derivatives. In particular, the bridging methylenes ($-CH_2-$) remained a simple AB quartet with a large geminal coupling constant of ~ 12 Hz which is characteristic of the cone-conformation.²⁴

The source of the asymmetry in **140d** is apparently the slowed rotation about the aryl-urea bond for which there is precedence. Reinhoudt observed the slowed rotation about an aryl-carbamate bond in a calix[4]arene and attributed it to the formation of an intramolecular hydrogen bond.²⁵ Similarly, we propose that the circular array of ureas in the dimer (**140d**) forces all eight ureas to point in the same direction. This restricted rotation also helps to explain the significant downfield shifts of aryl protons H_B and the upfield shift of H_C from the constant proximity of the urea carbonyl and $-NH$ respectively. By contrast, in a highly competitive solvent such as DMSO, the hydrogen bonding array was disrupted, leaving the ureas free to rotate. Spectroscopically, this was seen by the collapse of the separate signals for H_B and H_C into a singlet at the intermediate value of 6.79 ppm.

Although, the dimer **140d** had a more complex symmetry than the corresponding monomer **140**, its 1H NMR spectra was still highly symmetrical and fairly well resolved. This gave additional support for the formation of a highly ordered and well defined assembly. In fact, the C_4 symmetry of the dimer was consistent only with the conformer in which all four ureas point in the same direction. Any other rotational isomer would have led to a considerably more complex 1H NMR spectra as shown in Figure VI-10.

²⁴ Conner, M.; Janout, V.; Regen, S. L. *J. Org. Chem.* **1991**, *113*, 9670.

²⁵ Timmerman, P.; Nierop, K. G. A.; Brinks, E. A.; Verboom, W.; van Veggel, C. J. M.; van Hoorn, W. P.; Reinhoudt, D. N. *Chem. Eur. J.* **1995**, *1*, 132-143.

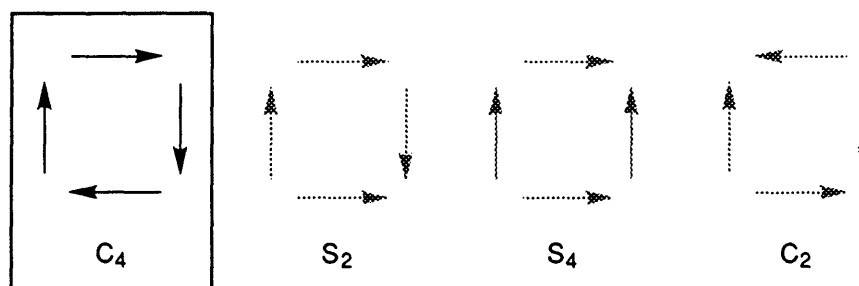


Figure VI-10. Schematic representation of possible rotamers of tetraurea 140. The arrows represent the direction of the urea carbonyls.

The ^1H NMR spectra of 140d also indicated a high degree of hydrogen bonding. In non-polar solvents, the urea protons of 140d were shifted significantly downfield in comparison to diphenyl urea (~ 6.2 ppm). Amazingly, the urea proton H_A of the dimer shifted further downfield than even the corresponding proton of the monomer in a strongly hydrogen bonding solvent such as DMSO (Figure VI-9). For example in CDCl_3 , H_A was at 9.34 ppm a full 1.0 ppm further downfield than in DMSO. The urea protons of 140d also remained downfield even when diluted to the limits of the NMR spectrometer used (~ 1 mM). In contrast, the spectra of most ureas such as diphenyl urea are highly concentration dependent. The second urea proton H_E was also shifted downfield but to a lesser extent, buried in the 7.40 - 7.00 ppm multiplet. The large 2.0 ppm difference between urea protons H_A and H_E show that they were in very different environments in the assembly. Molecular modeling of the dimer suggests that the 'inner' urea proton H_E comes in close contact with a phenyl ring of the opposing calixarene (Figure VI-11). Shielding of the urea by a phenyl group may also help to explain the large upfield shifts of the nearby calixarene aryl proton H_C . In addition, modeling predicts that the ureas -NH's will be hydrogen bonded at different angles to the C=O dipole, which would result in different hydrogen bond strengths and chemical shifts.

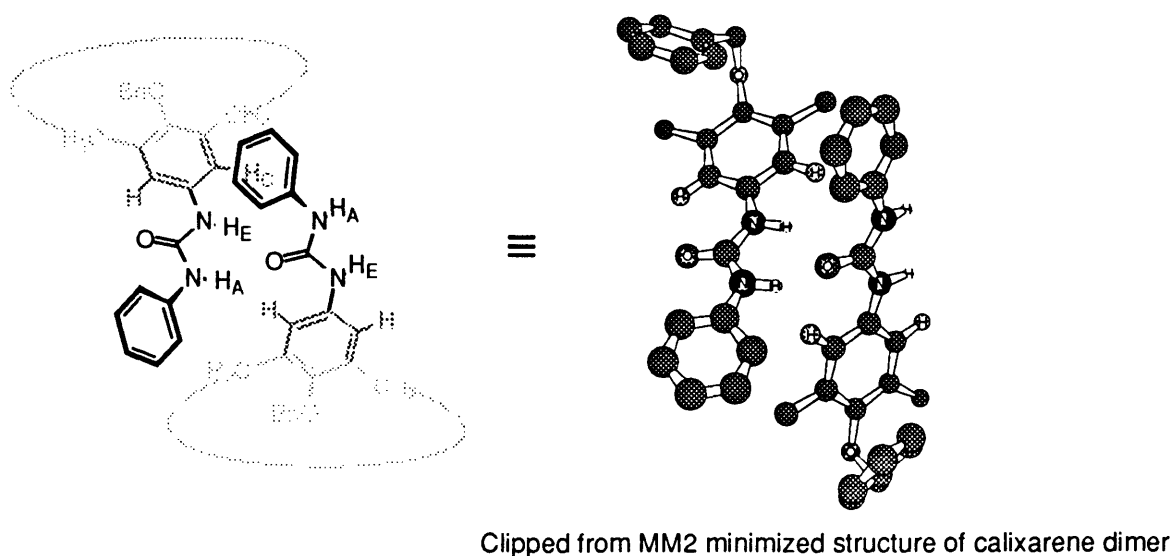


Figure VI-11. Portion of the MM2 minimized dimer, emphasizing close contacts between opposing calixarene units.

6.6 ENCAPSULATION

Perhaps the best evidence for the existence of calixarene **140** as a hydrogen bonded dimer comes from the observation of solvent molecules inside the newly formed cavity. The inclusion of guests was most apparent in mixed solvent systems where two distinct calixarene assemblies were observed by ^1H NMR. For example, the sequential addition of benzene- d_6 to a solution of assembled dimer **140d** in toluene- d_8 led to the appearance of a second calixarene species (Figure VI-12). From the similar splitting patterns, it was evident that both calixarene species were still assembled. We attributed the two different species to be assemblies containing benzene- d_6 and toluene- d_8 respectively. The addition of more benzene- d_6 shifted the equilibrium even further in favor of the benzene- d_6 encapsulated species, until it became predominant (Figure VI-12).

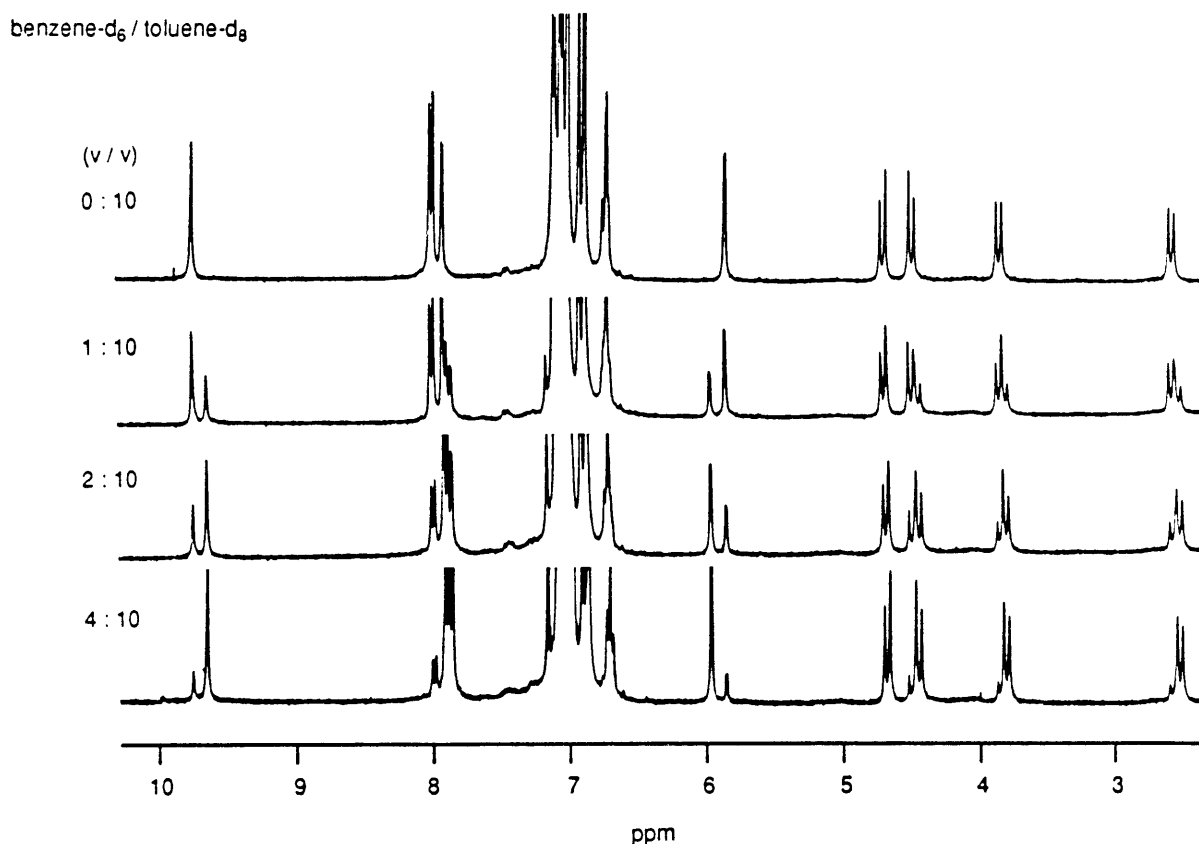


Figure VI-12. ^1H NMR spectra of 140d in toluene- d_8 (top) and followed by addition of sequential amounts of benzene- d_6 . The solvent mixture is expressed as volume to volume ratio.

Competition experiments using mixed solvent systems were also utilized to measure the relative fit of different guests. Comparisons of their relative populations in an equimolar solvent mixture led to the following series: ethyl benzene < *p*-xylene < *o*-xylene < toluene < benzene ~ chloroform. Chloroform and benzene were the best guests, whereas ethyl benzene was the worst. The series roughly corresponds to the relative van der Waals volumes of the guests with smaller molecules showing a high affinity for the assembly. Bucking the trend were ethyl benzene, *p*-xylene and *o*-xylene which all have nearly identical

volumes. These three aromatic guests were apparently differentiated by shape. So far, no solvent has been found in which the dimer **140d** appears to be empty.

Encapsulation was particularly favorable in bulky solvents that had difficulty fitting inside the cavity.²⁶ For example, a solution of **140d** in just 1 % fluorobenzene/*p*-xylene- d_{10} already showed equal populations of the two encapsulated species. In the case of fluorobenzene, the encapsulated guest was directly observable by ^{19}F NMR (Figure VI-13). A new peak appeared 5.4 ppm upfield of the bulk fluorobenzene peak at 113.1 ppm. This new peak was not visible in the absence of **140d**.

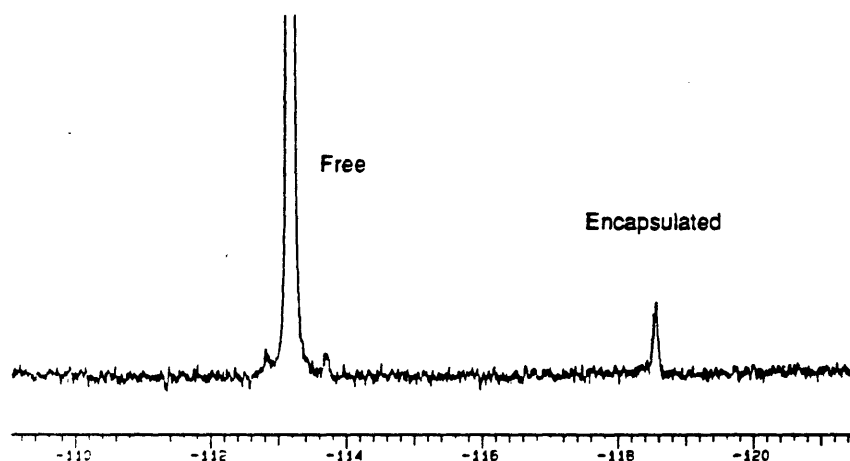


Figure VI-13. ^{19}F NMR spectra of **140d** in 1 % fluorobenzene/*p*-xylene- d_{10} , showing free and encapsulated fluorobenzene.

Unfortunately, the calculated binding constants changed considerably with concentration. Equation (1) was used to calculate the equilibrium constants for the replacement of guest 1 by guest 2 in a mixed solvent system. The actual concentrations were not measured; instead the relative ratios $[\text{HG}_1]/[\text{HG}_2]$ and $(\text{molarity } G_2)/(\text{molarity } G_1)$ were used. Even when the model was varied to account for possible differences in stoichiometry (variables n and $m \neq 1$), the K_{eq} 's could still not be made to stay constant. The problem probably arises from

²⁶ a) Chapman, K. T.; Still, W. C. *J. Am. Chem. Soc.* 1989, 111, 3075-3077. b) Whitlock, B. J.; Whitlock, H. W. *J. Am. Chem. Soc.* 1994, 116, 2301-2311.

the assumption that all of the calixarene was assembled as a well defined dimer. The broad peaks in the baseline of the ^1H NMR spectra of **140d** in CDCl_3 (Figure VI-9a) suggest that other oligomeric assemblies may be present which are not accounted for by equation (1). Interestingly, in aromatic solvents such as benzene- d_6 and toluene- d_{10} the ^1H NMR spectra was considerably sharper.

$$K_{\text{eq}} = \frac{[\text{HG}_1]^m \times [\text{G}_2]^n}{[\text{HG}_2]^n \times [\text{G}_1]^m} \quad \begin{array}{l} [\text{HG}_1] = \text{conc of host} \cdot \text{guest complex 1} \\ [\text{G}_1] = \text{conc of guest 1} \end{array} \quad (1)$$

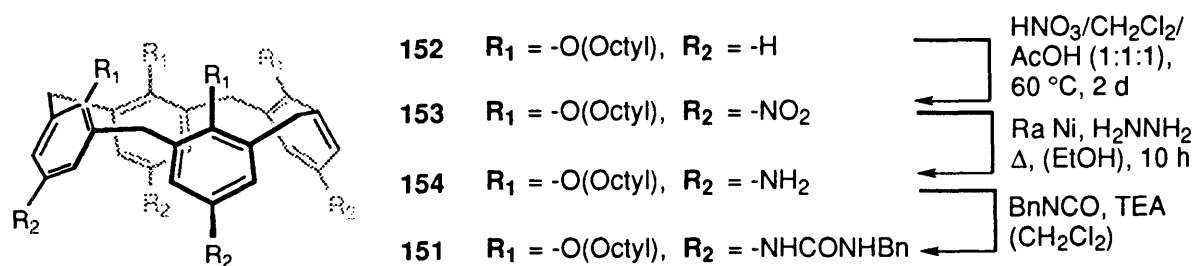
There are even indications that calixarene **140** assembles and retains encapsulated guests even in the gas phase. The use of mass spectrometry to verify the existence of complexes is still uncertain, especially for a fairly forceful ionization method like plasma desorption.²⁷ However, the observation of ternary complexes was in excellent agreement with the observed binding propensities of assembly **140d** in solution. The calixarene dimer peak $[2\text{M} + \text{Na}]$ was visible in every plasma desorption spectra of **140**. However, the presence of a ternary complex consisting of calixarene dimer plus guest $[2\text{M} + \text{guest} + \text{Na}]$ was dependent upon the last solvent used. This inclusion complex was seen only for solvents which by modeling were small enough to fit inside such as benzene, chloroform and methylene chloride. Larger solvents such as *p*-xylene or ethyl benzene, which are poor guests, showed no measurable inclusion complex.²⁸ While these observations are consistent with the encapsulation of guests inside the dimer, other structures are possible for the assembly in the gas phase.

²⁷ Recently, Lehn et. al. has shown for electrospray mass spectrometry that the observation of various complexes correlated well with their measured binding propensities in solution. This was aided by the addition of a metal binding site to allow easier ionization. Calixarenes have a built in ionophoric site in their 'lower rim' phenolic ethers and are well know to bind cation such as Na^+ and K^+ especially in the 'cone conformation'. See: Russell, K. C.; Leize, E.; Van Doorselaer, A.; Lehn, J.-M. *Angew. Chem., Int. Ed. Engl.* 1995, 32, 209.

²⁸ The relative intensities of the dimer $[2\text{M} + \text{Na}]$ peak and the encapsulated peak $[2\text{M} + \text{solvent} + \text{Na}]$ were considerably smaller (< 5 %) than the monomer $[\text{M} + \text{Na}]$ peak.

6.7 DISCUSSION

The assembly of **140** was actually somewhat surprising and occurred prematurely. Previously, a very similar calix[4]arene system **151** was prepared and appeared to aggregate as opposed to assemble. Calixarene **151** was synthesized by a different route which was altered for **140** because of the potential for over nitration of the benzyl ether protecting groups. Again the synthesis was fairly straightforward once the nitration conditions of **152** were worked out. First, the tetraoctyl calix[4]arene **152** was synthesized and fixed in the cone-conformation as previously described.²⁹ Nitration of **152** in HNO₃/CH₂Cl₂/AcOH (1:1:1) at 60 °C for 2 days gave tetranitro **153**. Interestingly, the order of nitration during this reaction was very specific and would occur first on opposing calixarene aryl rings, leading to formation of only one dinitrocalixarene species. These different mono-, di- and trinitration regioisomers were easily differentiated on the grounds of their R_f values and their unique symmetries. The synthesis was finished with reduction of **153** with Raney nickel and hydrazine in refluxing ethanol. This was followed by treatment of tetramine **154** with benzyl isocyanate to give tetrabenzyl urea **151**.



Scheme VI-3. Synthesis of calixarene tetrabenzyl urea **151**.

The ¹H NMR of **151** was extremely broad in non-polar solvents (i.e. CDCl₃), and there did not appear to be any urea -NH peaks far downfield which would have suggested complexation. However, this observation was somewhat subjective considering the lack of resolution of any of the calixarene peaks.

²⁹ Gutsche, C. D.; Lin, L. G. *Tetrahedron* 1986, 42, 1633.

Heating and cooling the NMR sample did not change the characteristics of the spectra considerably. The aggregation of **151** was attributed to the divergent C_2 conformation of the cone-conformer which would favor oligomerization as opposed to dimerization. Although, the NMR spectra of calix[4]arene implies that it is C_{4v} symmetric, this is merely a consequence of a rapid dynamic process shown in Figure VI-14. In fact, the C_{4v} conformation is a high energy transition state between the two divergent C_{2v} conformations. A number of researchers have mentioned that the inaccessibility of the C_{4v} symmetric cone-conformer may have hindered the success of similar molecular recognition systems which were anchored to the 'upper rim'.³⁰

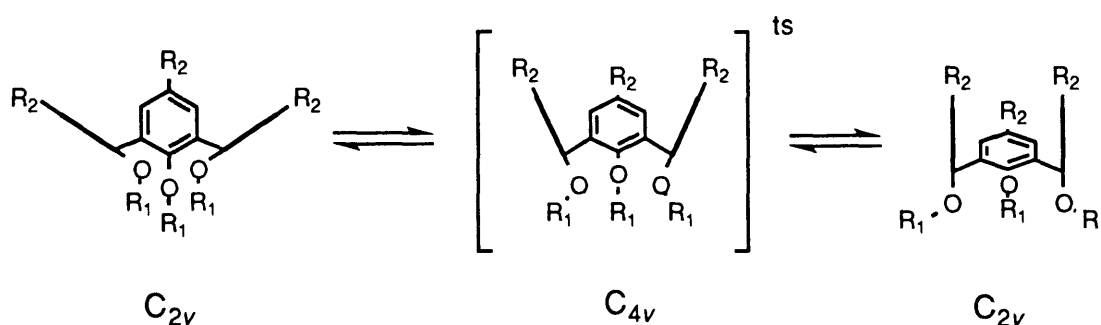


Figure VI-14. The equilibrium between C_{2v} symmetric conformations of calix[4]arenes in the cone-conformer. The equilibrium is fairly rapid resulting in a dynamically symmetric C_{4v} NMR of calix[4]arenes. Note that the C_{4v} symmetric conformation is actually a transition state.

To remedy this problem, calix[4]arenes were sought which could access the C_{4v} symmetric cone conformation. Hydrogen bonding (Figure VI-15a) or chelation of Na^+ (Figure VI-15b) on the 'lower rim' have both been shown to freeze out the C_{4v} symmetric conformation.³¹ Calixarene **151** with its octyl protected phenols was not amenable to further functionalization or defunctionalization on the 'lower rim', and for this reason, the benzyl ether groups were introduced into the synthesis of **140**. Even before these protecting groups were removed, tetraurea **140** was observed to assemble; however

³⁰ van Loon, J.-D.; Janssen, R. G.; Verboom, W.; Reinhoudt, D. N. *Tetrahedron Lett.* **1992**, *33*, 5125-5128.

³¹ a) Arduini, A.; Fanni, S.; Pochini, A.; Sicuri, A. R.; Ungaro, R. *Tetrahedron* **1995**, *51*, 7951-7958.
b) Gleave, C. A.; Sutherland, I. O. *J. Chem. Soc., Chem. Commun.* **1994**, 1873.

continuation of the original plan may further enhance the ability of **140** to assemble. Although, the dimer **140d** has up to 16 hydrogen bonds, it does not show the corresponding stability. For example, the 'tennis ball', which has 8 hydrogen bonds, can assemble in DMF whereas **140** does not. This lower dimerization energy maybe due, in part, to the necessary formation of the unstable C_{4v} cone conformer.

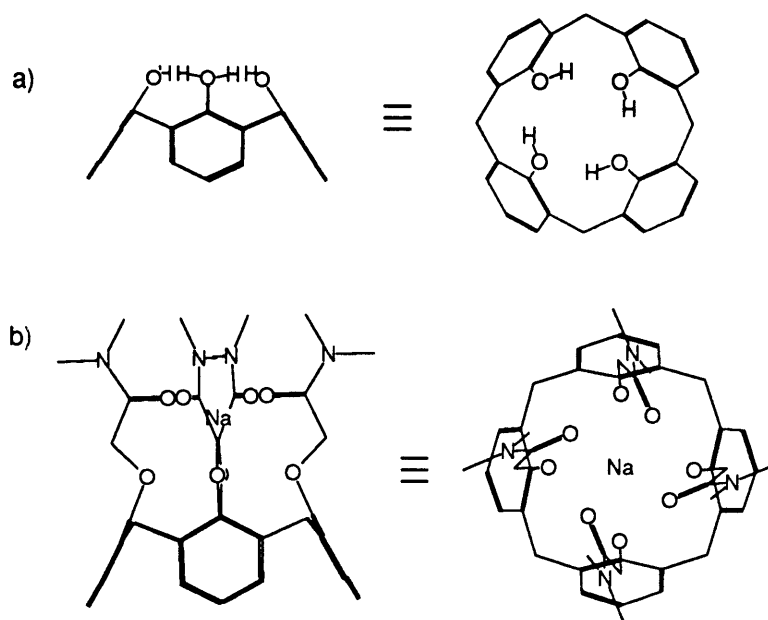


Figure VI-15. Stabilization of the C_{4v} symmetric cone conformation by a) hydrogen bonding and b) metal chelation on the 'lower rim'.

Clearly, the line separating assembled, not assembled and aggregated is fairly fine when one compares the unsuccessful triphenylmethane triurea **143** and calixarene **151** versus the successful **140**. In particular, the starkly different behavior of the calixarene tetraureas **140** and **151** was puzzling considering their structural homology. The unintentional choice of phenyl isocyanate over benzyl isocyanate may have been particularly fortuitous. As described previously (section 6.5), both modeling and upfield shifts in ^1H NMR spectra of **140d** imply that its urea phenyl groups are actively involved in stabilizing aryl-aryl and polarized hydrogen to aryl interactions. Aryl ureas are also considerably more

acidic than alkyl ureas and are known to form stronger hydrogen bonds,³² and this combination of factors may have been just enough to push the equilibrium toward assembly.

6.8 CAVITY SHAPE AND SIZE

Due to the interleaved geometry of dimer **140d**, the shape of the resulting cavity is difficult to visualize. One possible geometric simplification is shown in Figure VI-16. Each calix[4]arene is represented by a square pyramid with its triangular facets corresponding to the *endo*-aromatic surfaces. In the complex, the pyramids are offset by 45°, and the corners cut off to represent the 8 interleaved ureas which encircle the equator of dimer **140d**.

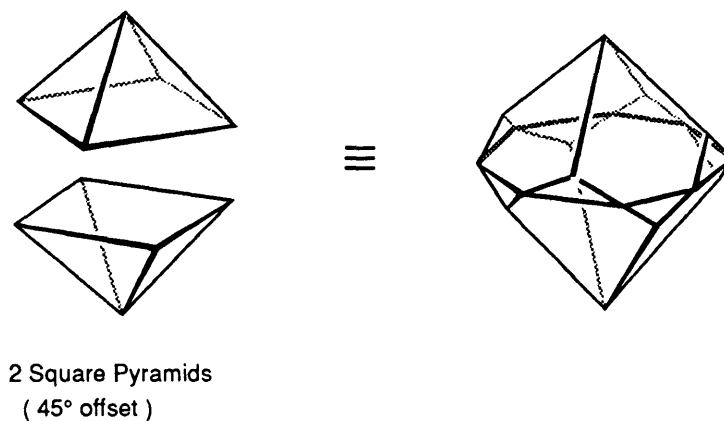


Figure VI-16. Schematic representations of the cavity formed by the dimerization of tetraurea **140**. The two square pyramids on the left represent the separate calix[4]arenes, and the geometric figure on the right the assembled cavity.

Cross sections of the molecular model are in agreement with the gem-like geometric representation (Figure VI-17). A horizontal slice through the plane of the ureas yields an octagonal cavity. While a vertical slice gives the characteristic diamond shaped cavity, having different angles and lengths for the top and bottom sections. Overall the cavity has a height of ~ 10 Å and a width of 7-8 Å

³² Etter, M. C. *Acc. Chem. Res.* 1990, 23, 120.

which was measured from VDW surface to VDW surface. The model easily accommodated such guests as benzene, cyclohexane, and chloroform. Larger guests like *p*-xylene or a formic acid dimer fit more snugly in the cavity in a lengthwise orientation.

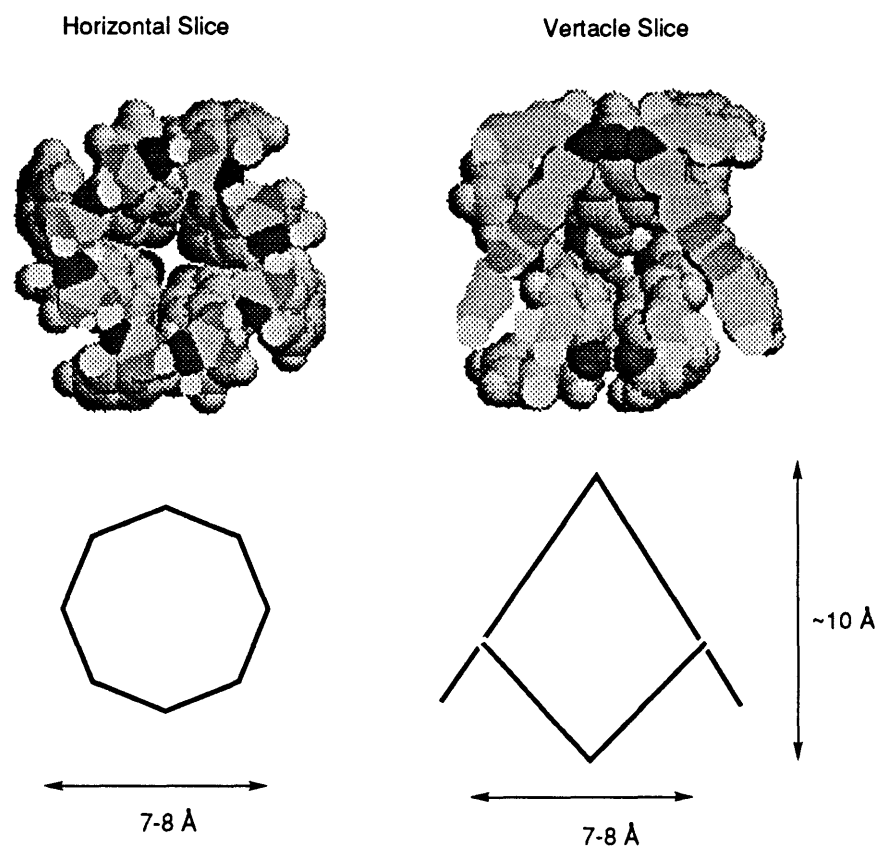


Figure VI-17. Vertical and horizontal cross sections of VDW's representations of the calixarene 140 dimer. Note in each representation half of the dimer has been cut away.

The determination of negative volumes inside of a molecule have been particularly difficult to estimate.³³ Often low tech methods such as physically building a model and measuring the amount of plaster that can be pressed into its interior have been used.³⁴ However, it was found that the modeling program

³³ a) Branda, N. Thesis, Massachusetts Institute of Technology, 1994. b) Kleyweht, G. J.; Jones, T. A. *Acta. Cryst.* **1994**, *D50*, 178.

³⁴ Eid, C. N., Jr.; Cram, D. J. *J. Chem. Ed.* **1993**, *70*, 1993.

MacroModel could accurately measure the negative volume of a cavity through a series of manipulations. The key was that MacroModel can calculate the positive volume of a molecule and does so without calculating overlapping volumes twice (Figure VI-18). First, the volume that the host occupied was measured. (MacroModel does not add on the extra volume for negative space of the cavity). Second, the cavity was filled with smaller overlapping molecules so that no unoccupied space remained inside the cavity, and the volume was measured again. Care must be taken so that none of the 'stuffing' penetrates the outer VDW's surface of the capsule. Subtraction of the second volume from the first gave the volume of the enclosed cavity.

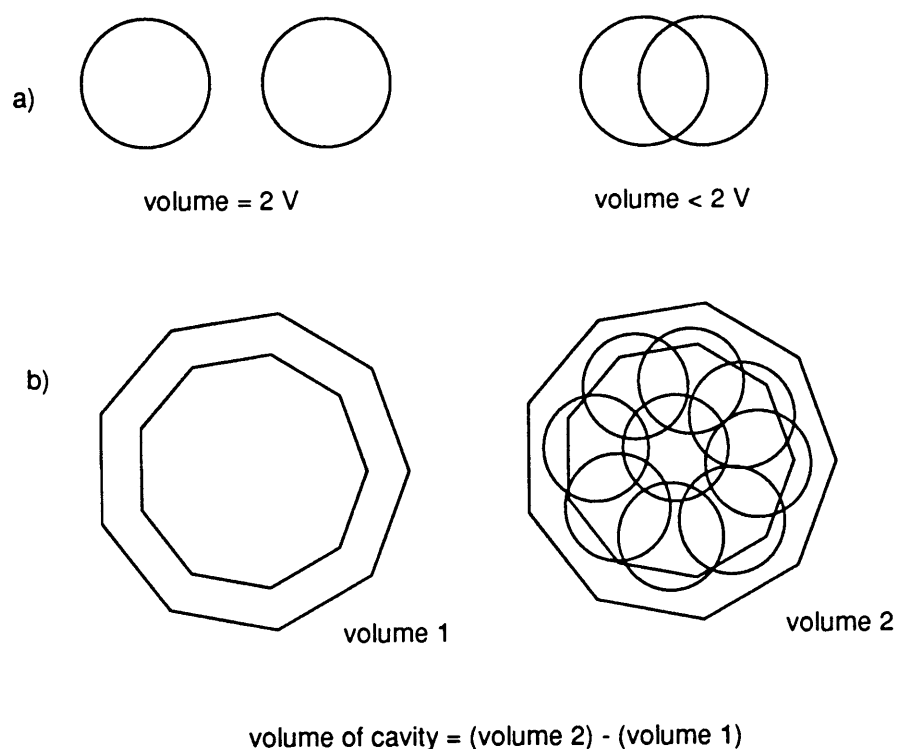


Figure VI-18. a) MacroModel's rules for calculating overlapping volumes. b) Method for determining the volume of a cavity.

In this manner, the volume of the cavity was determined to be $\sim 210 \text{ \AA}^3$. In addition, the volumes of several guests were measured for comparison and are listed in Table VI-1. These measurements show that most guests appear to fill

~50% or less of the available space in the cavity. By comparison, in a liquid 70 % of space is filled.

guest	volume (Å ³)	longest axis ^a
benzene	83	7.4
chloroform	77	6.4
dichloromethane	61	
toluene	99	
<i>m</i> -xylene	118	
<i>p</i> -xylene	117	9.2
<i>o</i> -xylene	118	

Table VI-1. Volume and size of various guests. The longest axis was measured from VDW surface to VDW surface (Å).

6.9 OUTLOOK

In conclusion, we have prepared a highly self-complementary calix[4]arene **140**. The large size and ease of synthesis make **140** an attractive self-assembling system. In non-polar solvents, the calixarene dimer **140d** forms via an unique circular array of eight ureas which are hydrogen bonded in a head-to-tail fashion. The resulting assembly also possesses a sizable cavity which was capable of capturing and imprisoning guest molecules. Future applications for self-assembling capsules of this sort include the transport of guests, the stabilization of high energy species³⁵ and use as 'high pressure' reaction chambers.

Variations on this new self-assembly system can easily be made by treatment of tetraamino calixarene **150** with other readily available isocyanates. For example, isocyanates having fluorine atoms could be used to quantify the precise

³⁵ Cram, D. J.; Tanner, M. E.; Thomas, R. *Angew. Chem., Int. Ed. Engl.* **1991**, *30*, 1024-1027.

stoichiometry of fluorinated guests by ^{19}F NMR. Alternatively, the effect of different aryl ureas on assembly could also be explored.

Like the large perylene clefts, space fills up quickly in the self-assembling dimer. When the VDW radii of the calixarene surfaces are taken into account, the cavity becomes considerably smaller than is suggested by stick-figure representations. Figure VI-18 shows how a good and poor guest fill the cavity. In each structure, part of the cavity wall is cut-away so that the guest can be seen.

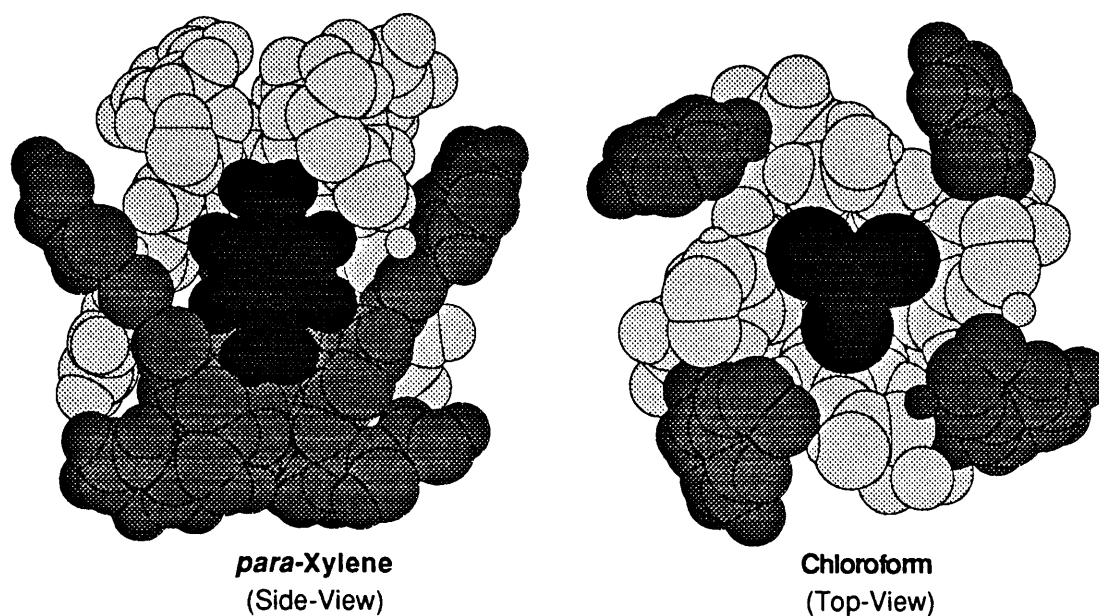


Figure VI-18. Cut-away views of CPK representations of the dimer with encapsulated *p*-xylene and chloroform from side- and top-views respectively.

6.10 EXPERIMENTAL

General

Throughout, reagent grade solvents were used except where noted. Chloroform and methylene chloride were dried over molecular sieves. Melting points were measured on an Electrothermal 9100 melting point apparatus. NMR spectra were taken on a Varian XL-300 (300 MHz) and a Bruker WM-250 (250 MHz) spectrometers. ^{19}F NMR spectra were reported as positive values corresponding to upfield shift from CCl_3F (0.00 ppm). IR spectra were obtained

on a Mattson Sygus 100 FT IR spectrometer. High resolution mass spectra were obtained on a Finnegan Mat 8200 instrument. Plasma desorption mass spectra were obtained on a BioIon 20 instrument with a ^{252}Cf source. Samples prepared by dissolution of **140** in the specified solvents and deposited on a nitrocellulose matrix target. The plasma desorption mass spectra of **140** showed a $[\text{M} + \text{Na}]$ peak as the major peak for all calixarene species. A $[\text{M} + \text{H}]$ peak was visible for some species but in much lower amounts. Molecular modeling experiments were performed on the Macromodel program with a MM2 force field.

Synthesis

2,2,2-Tris(4-methoxyphenyl)ethane (141): Methyl iodide (12.4 mL, 199 mmol), 2,2,2-tris(4-hydroxyphenyl)ethane (20 g, 65.3 mmol) and K_2CO_3 (28.9 g, 209 mmol) were heated at reflux in acetone (250 mL) for 15 h with a drying tube. The reaction mixture was diluted with H_2O (250 mL) and 1.0 N HCl (200 mL). The white precipitate was collected. The white solid was suspended in Et_2O (300 mL) and THF (50 mL) and then wash with 2.5 N NaOH solution (3 x 200 mL). The organic layer was concentrated down to a white solid, which was triturated with MeOH. Filtration gave the product as a white crystalline solid (9.87 %, 40 % yield). ^1H NMR (300 MHz, CDCl_3) δ 7.00 (d, 6 H, $J = 9.0$ Hz), 6.79 (d, 6 H, $J = 9.0$ Hz), 3.79 (s, 9 H), 2.11 (s, 3 H).

2,2,2-Tris(4-methoxy-3-aminophenyl)ethane: 2,2,2-Tris(4-methoxyphenyl)ethane **141** (49 mg, 0.141 mmol) was stirred vigorously in 5 mL HNO_3 . The solution turned red. After 5 min the reaction mixture was diluted with 100 mL H_2O and filtered. The crude product was collected as a bright yellow solid. ^1H NMR (250 MHz, CDCl_3) δ 7.59 (d, 3 H, $J = 2.7$ Hz), 7.22 (dd, 3 H, $J = 8.9$ Hz, 2.6 Hz), 7.04 (d, 3 H, $J = 9.0$ Hz), 3.97 (s, 9 H), 2.17 (s, 3 H).

The crude trinitro product was taken up in EtOH (40 mL) with 50 mg 5 % Pd/C and stirred under H_2 for 5-6 h. The catalyst was filtered off and washed with THF. The solution was concentrated *in vacuo* to a brown solid.

The crude triamine **142** was taken up in THF (35 mL) and treated with benzyl isocyanate (100 μL). After 1 h, the solution was quenched with 30 mL saturated NaHCO_3 and stirred for an additional 1 h. The THF layer was separated and concentrated *in vacuo* to a brown solid. Chromatography (MeOH/ CH_2Cl_2 , 4 - 5

%) gave the product (30 mg). $^1\text{H NMR}$ (300 MHz, DMSO-d_6) δ 8.05 (s, 3 H, -NH), 7.93 (s, 3 H, -NH), 7.05-7.45 (m, 15 H), 6.77 (d, 6 H, $J = 8.3$ Hz), 6.36 (d, 6 H, $J = 8.6$ Hz), 4.23 (s, 6 H, $-\text{CH}_2\text{Ph}$), 3.78 (s, 9 H, -OMe), 1.91 (s, 3 H, Me).

Cone-conformer of O,O',O'',O'''-tetrabenzyl-4,4',4'',4'''-tetraiodocalix[4]arene (148): Silver trifluoroacetate (1.20 g, 6.37 mmol) was refluxed for 15 min. in 100 mL of dry CHCl_3 under argon. The cone-conformer of O,O',O'',O'''-tetrabenzylcalix[4]arene, **147** (1.00 g, 1.24 mmol)³⁶ in 30 mL of CHCl_3 was added dropwise and the solution refluxed for an additional 15 min. Iodine (1.62 g, 6.37 mmol) was placed in the elbow of a Y-tube and the solution refluxed over it, slowly delivering the I_2 into the reaction flask. After 30 min, the addition was complete and the reaction mixture was bright purple. The solution was washed with 1.0 M sodium thiol sulfate (2 X 100 mL) and brine (1 X 100 mL), dried over MgSO_4 and concentrated *in vacuo* to a white solid (1.63 g, 100 %): m.p. = 285-6 °C; IR (KBr) 3028, 2913, 1561, 1456, 1191, 980, 862, 834, 746, 697 cm^{-1} ; $^1\text{H NMR}$ (250 MHz, CDCl_3) δ 7.40 - 7.10 (m, 20 H, Ph), 6.91 (s, 8 H, Ar), 4.88 (s, 8 H, $-\text{CH}_2\text{Ph}$), 3.91 (d, 4 H, $J = 13.6$ Hz, $-\text{CH}_2-$), 2.70 (d, 4 H, $J = 13.6$ Hz, $-\text{CH}_2-$); HRMS (FAB, nitrobenzyl alcohol) calcd for $\text{C}_{56}\text{H}_{45}\text{I}_4\text{O}_4$ (M + H), 1288.949693; found, 1288.94845.

Cone-conformer of 4,4',4'',4'''-tetraamino-O,O',O'',O'''-tetrabenzylcalix[4]arene (150): Tetraiodo calixarene **148** (623 mg, 0.484 mmol), phthalimide (569 mg, 3.87 mmol) and Cu_2O (830 mg, 5.80 mmol) were heated in 2 mL N-methyl-2-pyrrolidinone (NMP) at 200 °C for 16 h. The solution was cooled, diluted with 150 mL CH_2Cl_2 and filtered. The filtrate was concentrated to an oil (mostly NMP) by rotary evaporation and then triturated with 1.0 N HCl solution (300 mL). The suspension was sonicated and the crude product **149** collected as a brown solid containing some excess phthalimide: $^1\text{H NMR}$ (250 MHz, CDCl_3) δ 7.60 - 7.10 (m, 36 H, Ph and Phth), 6.88 (s, 8 H, Ar), 5.00 (s, 8 H, $-\text{CH}_2\text{Ph}$), 4.30 (d, 4 H, $J = 13.4$ Hz, $-\text{CH}_2-$), 3.08 (d, 4 H, $J = 13.5$ Hz, $-\text{CH}_2-$).

The entire sample of tetraphthalimido calixarene **149** was suspended in 20 mL EtOH and 4.5 mL hydrazine hydrate. The solution was refluxed for 3 h and then diluted with H_2O . The mixture was extracted repeatedly with CH_2Cl_2 (4 x 100 mL). The organic layers were combined, dried over Na_2CO_3 and

³⁶ For synthesis see: Gutsche, C. D.; Pagoria, P. F. *J. Org. Chem.* 1985, 50, 5795-5802.

concentrated *in vacuo* to a brown solid (409 mg, 100 % from the tetraiodo calixarene **148**): m.p. = 148 °C; IR (KBr) 3405, 3345, 3038, 1608 (br), 1473, 1212, 992, 756, 868 cm⁻¹; ¹H NMR (250 MHz, CDCl₃) δ 7.40 - 7.00 (m, 20 H, Ph), 5.98 (s, 8 H, Ar), 4.83 (s, 8 H, -CH₂Ph), 4.05 (d, 4 H, *J* = 13.5 Hz, -CH₂-), 3.05 (s, 8 H, -NH₂), 2.70 (d, 4 H, *J* = 13.5 Hz, -CH₂-); HRMS (FAB, nitrobenzyl alcohol) calcd for C₅₆H₅₃N₄O₄ (M + H), 845.406681; found, 845.40740.

Cone-conformer of 4,4',4'',4'''-tetrakis(phenyl urea)-O,O',O'',O'''-tetrabenzylcalix[4]arene (140). Phenyl isocyanate (150 μL) and tetraamino calixarene **150** (95 mg, 0.122 mmol) were dissolved in 15 mL CH₂Cl₂ and stirred for 1 h. The solution was concentrated *in vacuo* to a beige solid. Chromatography on silica gel (13 % - 15 %, EtOAc:CH₂Cl₂) gave a white solid. The product was taken up in toluene and reconstituted *in vacuo* to remove EtOAc and CH₂Cl₂ (99 mg, 67 %): m.p. = 195-6 °C (dec.); IR (KBr) 3383, 3033, 2928, 1670, 1598, 1566, 1542, 1498, 1473, 1442, 1315, 1206, 750, 696 cm⁻¹; ¹H NMR (250 MHz, CDCl₃) δ 9.34 (s, 4 H, -NH), 7.79 (d, 8 H, *J* = 6.9 Hz, *o*-Ph), 7.59 (d, 4 H, *J* = 3.0 Hz, Ar), 7.40 - 7.00 (m, 36 H, Ph and -NH), 5.73 (d, 4 H, *J* = 3.0 Hz, Ar), 4.74 (d, 4 H, *J* = 12.6 Hz, -CH₂Ph), 4.39 (d, 4 H, *J* = 12.6 Hz, -CH₂Ph), 3.57 (d, 4 H, *J* = 12.3, -CH₂-), 2.26 (d, 4 H, *J* = 12.6, -CH₂-); HRMS (FAB, nitrobenzyl alcohol) calcd for C₈₄H₇₃N₈O₈ (M + H), 1321.55514; found, 1321.55323.

Cone-conformer of 4,4',4'',4'''-tetranitro-O,O',O'',O'''-tetraoctylcalix[4]arene (153). The cone-conformer of O,O',O'',O'''-tetraoctylcalix[4]arene **152** (600 mg) was stirred in 60 mL HNO₃/CH₂Cl₂/AcOH (1:1:1) at 60 °C for 2 days. The solution was diluted with 200 mL CH₂Cl₂ and washed with water (3 x 200 mL) and saturated NaHCO₃ solution (1 x 200 mL). The organic layer was dried over K₂CO₃ and dried *in vacuo* to a brown solid. Chromatography (CH₂Cl₂) gave the product (505 mg). ¹H NMR (250 MHz, CDCl₃) δ 7.57 (s, 8 H), 4.01 (d, 4 H, *J* = 14.0 Hz), 3.97 (t, 8 H, *J* = 7.4 Hz), 3.40 (s, 4 H, *J* = 14.1 Hz), 1.75-2.00 (m, 8 H), 1.10-1.50 (m, 40 H), 0.80-0.95 (m, 12 H).

Cone-conformer of 4,4',4'',4'''-tetrakis(benzylurea)-O,O',O'',O'''-tetraoctylcalix[4]arene (151). The tetranitro calixarene **153** (100 mg) was suspended in 50 mL EtOH with hydrazine (0.5 mL) and Raney nickel (200 mg) and heated at reflux for 10 h. The solution was diluted with CH₂Cl₂ (250 mL)

and washed with water (2 x 200 mL) and concentrated to a brown solid. The crude material appeared to be binding Ni which would precipitate out slowly.

The crude tetraamine calixarene **154** (80 mg) was dissolved in CH₂Cl₂ (50 mL) and treated with an excess of benzyl isocyanate (5 eq) and triethyl amine (5 eq). The solution was stirred for 2 h and then washed with 1.0 N HCl (2 x 100 mL). Chromatography (EtOAc/CH₂Cl₂, 33 %) gave the desired product in 85 % yield. ¹H NMR (250 MHz, CDCl₃) δ 7.12-7.38 (m, 20 H, Ph), 6.67 (s, 8 H, Ar), 4.41 (d, 4 H, *J* = 13.2 Hz), 4.30 (s, 8 H, -CH₂Ph), 3.84 (t, 8 H, *J* = 7.5 Hz, CH₂O), 3.08 (d, 4 H, *J* = 13.5 Hz), 1.80-2.00 (m, 8 H), 1.18-1.44 (m, 40 H), 0.80-0.95 (m, 12 H).

Binding Studies

Typically, the calixarene tetraurea **140** was taken up in one solvent (~5 mM). The second solvent was added in aliquots and the new calixarene species observed by ¹H NMR. This was done so that the respective encapsulated species could be properly assigned. The solution was diluted with the second solution until the first encapsulated species disappeared or until 3 or 4 fold of the second solvent was added.

Chapter VII

A Selectively Functionalizable Molecular Scaffold with Four Carboxylic Acid Sites

7.1 INTRODUCTION

9,9-Dimethylxanthene-1,3,6,8-tetracarboxylic acid **160** is a tetrafunctional building block, suitable for use in molecular receptors and combinatorial libraries. The unique structure of the xanthene ring system permits the regioselective functionalization of tetraacid **160**. Carboxyl groups in the 'front' 1- and 8- positions were efficiently differentiated from each other and from the carboxyl groups in the 'rear' 3- and 6- positions. This chapter describes the efficient synthesis of **160** in 4 steps and 87% yield from xanthone. In addition, the selective functionalization of its carboxyl groups is presented.¹

7.2 BACKGROUND

Molecules which present functional groups in specific orientations serve as scaffolds in molecular recognition² and in peptidomimetics.³ Notable examples

¹ This work was done with James Nowick.

² a) Kelly, T. R.; Maguire, M. P. *J. Am. Chem. Soc.* **1987**, *109*, 6549-6551. b) Iimori, T.; Still, W. C.; Rheingold, A. L.; Staley, D. L. *J. Am. Chem. Soc.* **1989**, *111*, 3439-3430. c) Bell, T. W.; Liu, J. *J. Am. Chem. Soc.* **1988**, *110*, 3673-3674. d) Schmidtchen, F. P. *Tetrahedron Lett.* **1989**, *30*, 4493-4496. e) Zimmerman, S. C.; Wu, W. *J. Am. Chem. Soc.* **1989**, *111*, 8054-8055. f) Adrian, J. C.; Wilcox, C. S. *J. Am. Chem. Soc.* **1989**, *111*, 8055-8057. g) Rebek, J., Jr. *Angew. Chem., Int. Ed. Engl.* **1990**, *29*, 245-255. h) Tecilla, P.; Chang, S.-K.; Hamilton, A. D. *J. Am. Chem. Soc.* **1990**, *112*, 9586-9590. i) Medina, J. C.; Gay, I.; Chen, Z.; Echegoyen, L.; Gokel, G. W.; *J. Am. Chem. Soc.* **1991**, *113*, 365-366.

³ For recent reviews, see: a) Hölzemann, G. *Kontakte* **1991**, 3-12. b) Hölzemann, G. *Kontakte* **1991**, 55-63. c) Olson, G. L.; Bolin, D. R.; Bonner, M. P.; Bös, M.; Cook, C. M.; Fry, D. C.; Graves, B. J.; Hatada, M.; Hill, D. E.; Kahn, M.; Madison, V. S.; Rusiecki, V. K.; Sarabu, R.;

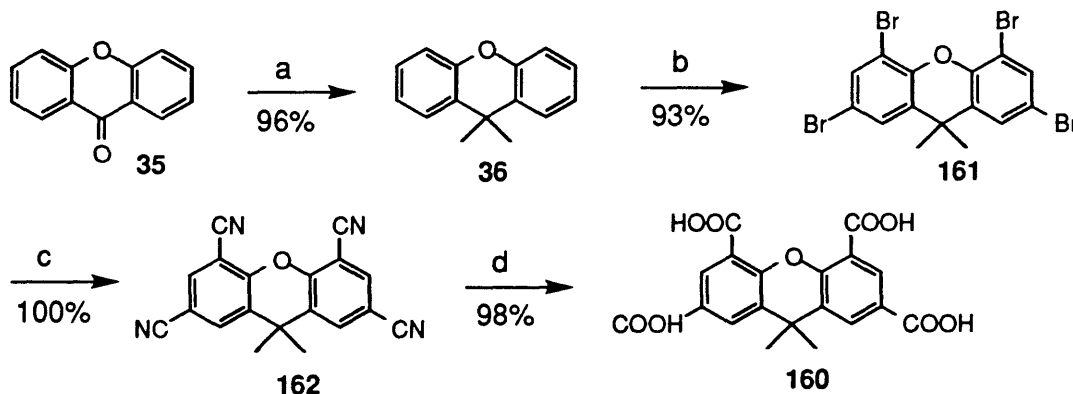
include Kemp's triacid,⁴ 4,6-disubstituted phenoxathiin derivatives,⁵ 4,6-disubstituted dibenzofurans,⁶ 3,6-di-*t*-butyl-9,9-dimethylxanthene-1,8-dicarboxylic acid⁷ and diurea derivatives of 1,2-diaminoethane and 1,3-diaminopropane.⁸ Recently, Rebek and coworkers introduced 1,3,6,8-tetracarboxylic acid (**160**) as a core molecule for a solution based strategy toward combinatorial libraries.⁹

7.3 SYNTHESIS

Tetraacid **160** was readily prepared as illustrated in Scheme VII-1. Xanthone was converted to 9,9-dimethylxanthene (**36**) by treatment with trimethylaluminum.^{7a} Bromination of **36** with 4.0 eq of Br₂ generated 1,3,6,8-tetrabromide **161**. Reaction of **161** with CuCN, followed by hydrolysis of the resulting tetranitrile **162** afforded **160** in 87% overall yield.

Sepinwall, J.; Vincent, G. P.; Voss, M. E. *J. Med. Chem.* **1993**, *36*, 3039-3049. d) Gante, J. *Angew. Chem., Int. Ed. Engl.* **1994**, *33*, 1699-1720.

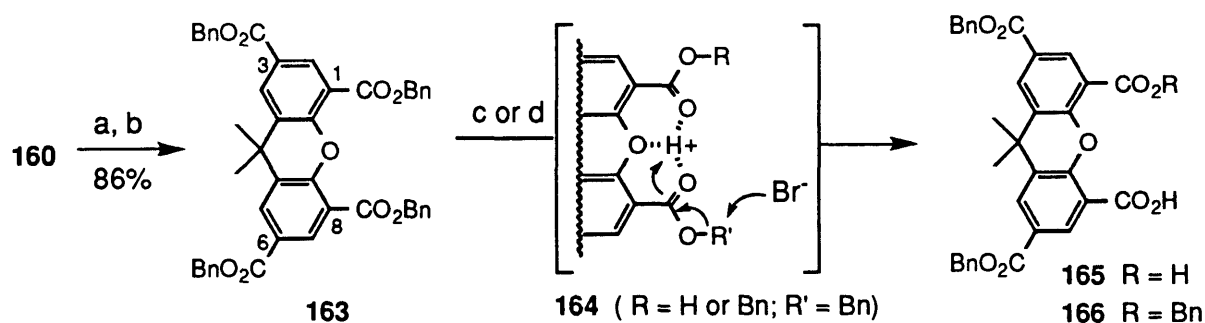
- 4 a) Rebek, J., Jr.; Marshall, L.; Wolak, R.; Parris, K.; Killoran, M.; Askew, B.; Nemeth, D.; Islam, N. *J. Am. Chem. Soc.* **1985**, *107*, 7476-7481. b) Rebek, J., Jr.; Askew, B.; Killoran, M.; Nemeth, D.; Lin, F. *J. Am. Chem. Soc.* **1987**, *109*, 2426-2431. c) Jeong, K. S.; Tjivikua, T.; Muehldorf, A.; Deslongchamps, G.; Famulok, M.; Rebek, J., Jr. *J. Am. Chem. Soc.* **1991**, *113*, 201-209.
- 5 Feigel, M. *J. Am. Chem. Soc.* **1986**, *108*, 181-182. b) Feigel, M. *Liebigs Ann. Chem.* **1989**, 459-468. c) Wagner, G.; Feigel, M. *Tetrahedron* **1993**, *49*, 10831-10842.
- 6 a) Diaz, H.; Kelly, J. W. *Tetrahedron Lett.* **1991**, *32*, 5725-5728. b) Diaz, H.; Tsang, K. Y.; Choo, D.; Kelly, J. W. *Tetrahedron* **1993**, *49*, 3533-3545. c) Tsang, K. Y.; Diaz, H.; Graciani, N.; Kelly, J. W. *J. Am. Chem. Soc.* **1994**, *116*, 3988-4005.
- 7 a) Nowick, J. S.; Ballester, P.; Ebmeyer, F.; Rebek, J., Jr. *J. Am. Chem. Soc.* **1990**, *112*, 8902-8906. b) Shimizu, K. D.; Dewey, T. M.; Rebek, J., Jr. *J. Am. Chem. Soc.* **1994**, *116*, 5145-5149. c) Galán, A.; Sutherland, A. J.; Ballester, P.; Rebek, J., Jr. *Tetrahedron Lett.* **1994**, *35*, 5359-5362.
- 8 a) Nowick, J. S.; Powell, N. A.; Martinez, E. J.; Smith, E. M.; Noronha, G. *J. Org. Chem.* **1992**, *57*, 3763-3765. b) Nowick, J. S.; Abdi, M.; Bellamo, K. A.; Love, J. A.; Martinez, E. J.; Noronha, G.; Smith, E. M.; Ziller, J. W. *J. Am. Chem. Soc.*, in press.
- 9 a) Carell, T.; Wintner, E. A.; Bashir-Hashemi, A.; Rebek, J., Jr. *Angew. Chem., Int. Ed. Engl.* **1994**, *33*, 2059-2061. b) Carell, T.; Wintner, E. A.; Rebek, J., Jr. *Angew. Chem., Int. Ed. Engl.* **1994**, *33*, 2061-2064.



Scheme VII-1. a) AlMe₃, toluene; b) Br₂, Fe, CH₂Cl₂; c) CuCN, *N*-methyl pyrrolidone; d) KOH, H₂O.

The proximity of the 1,8-positions and the xanthene ether oxygen permits the regioselective functionalization of tetraacid **160**. The carboxyl groups at the 1- and 8- positions are differentiated from each other and from carboxyl groups at the 3- and 6- positions (Scheme VII-2). Treatment of the benzyl or alkyl tetraester of **160** with anhydrous HBr or HI led to selective mono- and di- deprotection. In this manner, tetrabenzyl ester **163** was readily converted to either tribenzyl ester **165** or dibenzyl ester **166**. Treatment of **163** with HBr for 1 h at -23 °C cleaved only a single benzyl ester at the 1- and 8- positions to afford **165** with greater than 95% selectivity. Alternatively, treatment of **163** with HBr for 1.5 days at 25 °C cleaved both 'front' benzyl esters to afford **166** with comparable selectivity. We attributed the selectivity to the coordination of a proton by the 1- and 8- carboxyl groups and the ring oxygen atom as illustrated for structure **164**.^{7a,10}

¹⁰ Also see chapter II (section 2.3).



Scheme VII-2. a) oxalyl chloride, cat. DMF, CH_2Cl_2 ; b) BnOH , pyridine, CH_2Cl_2 ; c) HBr , CH_2Cl_2 , 25°C , 1.5 d (89%); d) HBr , CH_2Cl_2 , -23°C , 1.0 h (88%).

7.4 OUTLOOK

The ease and efficiency with which tetraacid **160** was regioselectively functionalized permitted the preparation of derivatives in which the carboxyl groups were highly differentiated. For example, triester **167** was prepared from **160** in 53% overall yield by the following sequence of steps: 1) conversion of **160** to the 1,3,6,8-tetraiodopropyl ester (via the tetraacid chloride); 2) cleavage of the ester at the 1- and 8- positions (HI , CH_2Cl_2 , 8 d); 3) formation of the 1,8-dibenzyl-3,6-diiodopropyl ester (via the diacid chloride); and 4) selective cleavage of one of the benzyl ester with HBr . Triester **167** was then converted to water-soluble molecular cleft **168** as follows: The carboxylic acid of **167** was converted to the acid chloride and coupled with 1,4-phenylenediamine. The benzyl ester was cleaved with HBr . And the resulting diacid was treated with trimethylamine to afford **168** in 51% overall yield.

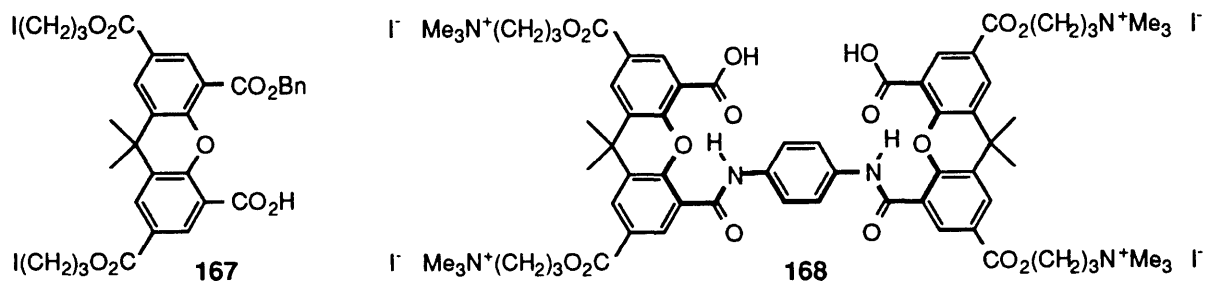


Figure VII-1.

In summary, the ease of preparation and selective functionalization of tetraacid **160** makes it an ideal building block for the creation of complex molecular architectures. The success of **160** as a core molecule may lie in its shape. The molecule presents functionality in a variety of different relationships simultaneously. More symmetric polyfunctional molecules present functionality in redundant orientations and sample less three-dimensional space.

7.5 EXPERIMENTAL

9,9-Dimethyl-1,3,6,8-tetrabromoxanthene (161). A 50 mL, one-necked flask fitted with an addition funnel was charged with Br₂ (14.97 g, 93.67 mmol) in 25 mL of CH₂Cl₂ and cooled in an ice bath. 9,9-Dimethylxanthene (**36**)^{7a} (4.92 g, 23.4 mmol) was added over 10 min. After 45 min, Fe powder (0.030 g, 0.54 mmol) was added and the reaction mixture was allowed to warm to 25 °C over 2.5 h. The flask was fitted with a condenser attached to a mineral oil bubbler and heated at reflux until the condensate became colorless. The reaction was monitored by ¹H NMR and additional aliquots of Br₂ were added as necessary. The addition of large excesses, however, should be avoided due to the possibility of over bromination.¹¹ The resulting solution was extracted with 30 mL of H₂O, dried over MgSO₄, filtered, and concentrated to afford a white solid. The solid was boiled with 30 mL of ethanol, and the resulting suspension allowed to cool to 25 °C. Filtration, followed by drying of the precipitate under vacuum afforded **160** (11.48 g, 93%) as a white solid: mp 152-154 °C (dec); IR (KBr) 2990, 2951, 1576, 1428, 1256, 1092, 859 cm⁻¹; ¹H NMR (500 MHz, CDCl₃) δ 7.64 (d, *J* = 2.0 Hz, 2 H), 7.44 (d, *J* = 2.5 Hz, 2 H), 1.60 (s, 6 H); HRMS (EI) calcd for C₁₅H₁₀⁷⁹Br₄O, 521.7476; found, 521.7465.

9,9-Dimethylxanthene-1,3,6,8-tetranitrile (162). A suspension of **161** (34.6 g, 65.8 mmol) and CuCN (25.9 g, 289 mmol) in 100 mL of *N*-methyl pyrrolidone was heated at reflux for 6 h. The mixture was cooled to 25 °C, and filtered, and the precipitate was washed with water. The precipitate was then stirred

¹¹ If the bromination has stopped, additional quantities may be necessary.

vigorously in 400 mL of a 20% nitric acid solution at 25 °C for 4 h and at 70 °C for 12 h. (CAUTION: USE HOOD. HCN and NO₂ are evolved.) The green mixture was filtered, and the precipitate was washed with water and dried under vacuum to afford 20.36 g (100%) of tetranitrile **162** as a tan solid: mp 352 °C; IR (KBr) 3059, 2999, 2240, 1610, 1590, 1436, 1271, 1248, 924, 848, 755 cm⁻¹; ¹H NMR (CD₃SOCD₃) δ 8.55 (d, *J* = 1.9 Hz, 2 H), 8.47 (d, *J* = 1.9 Hz, 2 H), 1.66 (s, 6 H); HRMS (CI, NH₃) calcd for C₁₉H₁₀N₄O, 310.0855; found, 310.0858.

9,9-Dimethylxanthene-1,2,6,8-tetracarboxylic acid (160). A suspension of xanthene tetranitrile **162** (5.00 g, 16.1 mmol) in 50 mL of 1.6 M aqueous NaOH solution was heated at reflux for 14 h. The clear brown solution was acidified to pH 0 with 2.0 M HCl, and the aqueous layer was extracted with three 100-mL portions of a THF/EtOAc (1:1) solution. The combined organic portions were dried over Na₂SO₄ and concentrated under vacuum, to afford 6.13 g (98%) of tetraacid **160** as a tan solid: mp > 350 °C; IR (KBr) 3117, 2985, 2639, 2538, 1715, 1684, 1610, 1405, 1275, 1248, 928, 766, 614 cm⁻¹; ¹H NMR (CD₃SOCD₃) δ 13.19 (br s, 4 H), 8.25 (d, *J* = 2.0 Hz, 2 H), 8.15 (d, *J* = 2.0 Hz, 2 H), 1.66 (s, 6 H); HRMS (CI, NH₃) calcd for C₁₈H₁₁O₉ (M - CH₃), 371.0403; found, 371.0402.

Xanthene-1,2,6,8--tetracarboxylic acid, tetrabenzyl ester (163). An ice-cooled, 100-mL, one-necked, round-bottomed flask, equipped with a magnetic stirring bar and a reflux condenser fitted with a drying tube, was charged with tetraacid **160** (3.10 g, 8.02 mmol), 49 mL of dry THF, oxalyl chloride (8.7 mL, 100 mmol), and 20 μL of DMF. After 30 min, the ice bath was removed. The solution was stirred for 3 h at 25 °C and then heated at reflux for 30 min. The reaction mixture was concentrated under vacuum to afford the tetraacid chloride as a brown solid. A solution of benzyl alcohol (5.15 mL, 49.8 mmol) and dry pyridine (4.02 mL, 49.7 mmol) in 15 mL of CH₂Cl₂ was added to the tetraacid chloride. After 2 h, the reaction mixture was extracted with three 50-mL portions of 1.0 M HCl solution, dried over MgSO₄, and concentrated by rotary evaporation to afford a dark brown oil. Trituration with methanol followed by filtration and drying of the resulting solid under vacuum gave 5.13 g (86%) of tetraester **163** as a white solid: mp 151-152 °C; IR (KBr) 3038, 2960, 1728, 1711, 1597, 1440, 1245, 1119, 760, 733, 696 cm⁻¹; ¹H NMR (CDCl₃) δ 8.35 (d, *J* = 2.0 Hz, 2 H), 8.28 (d, *J* =

2.0 Hz, 2 H), 7.26 - 7.45 (m, 20 H), 5.44 (s, 4 H), 5.37 (s, 4 H), 1.69 (s, 6 H); HRMS (CI, NH₃) calcd for C₄₇H₃₉O₉ (M + H), 747.2593; found, 747.2595.

Xanthene-1,2,6,8--tetracarboxylic acid, 1,8-dibenzyl ester (165). Hydrogen bromide was bubbled through a solution of tetraester **163** (3.03 g, 4.06 mmol) in 180 mL of dry CH₂Cl₂ for 15 min, and the solution stirred for 1.5 d in a stoppered flask. Argon was bubbled through the solution for 15 min, and then the solution was concentrated by rotary evaporation to give an oily white solid, which was triturated with hexane and dried under vacuum to afford 2.04 g (89%) of diacid **165** as a white solid: mp 238 °C (dec); IR (KBr) 3125, 2640, 2558, 1720, 1700, 1612, 1256, 1122, 762, 696 cm⁻¹; ¹H NMR (CDCl₃) δ 11.90 (br s, 2 H), 8.64 (d, *J* = 2.0 Hz, 2 H), 8.39 (d, *J* = 2.0 Hz, 2 H), 7.3 - 7.5 (m, 10 H), 5.41 (s, 4 H), 1.73 (s, 6 H); HRMS (CI, NH₃) calcd for C₃₃H₂₇O₉ (M + H), 567.1655; found, 567.1649.

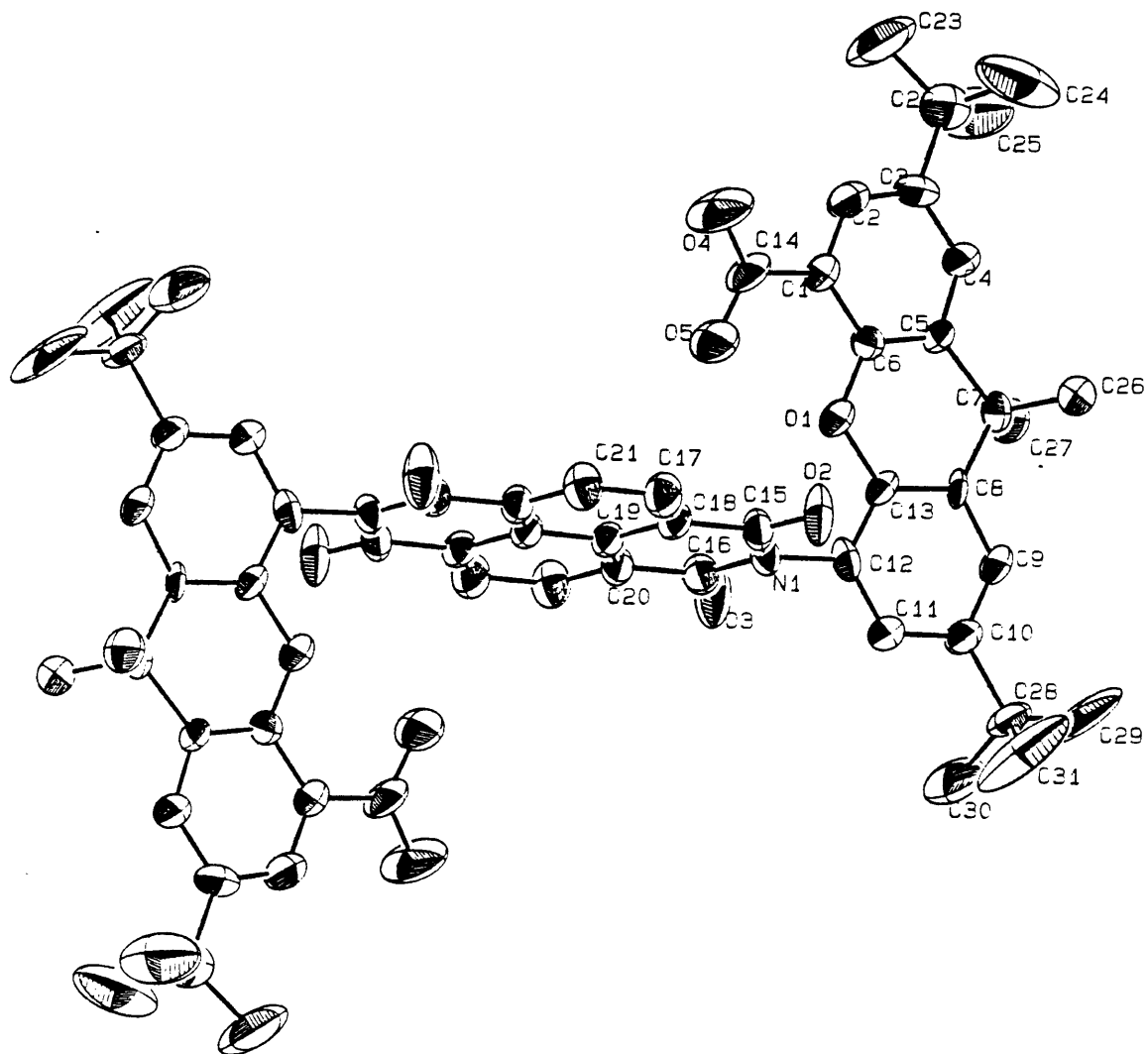
Xanthene-1,2,6,8-tetracarboxylic acid, 3,6,8-tribenzyl ester (166). A solution of HBr in CH₂Cl₂ was prepared by bubbling HBr vigorously into a flask of 160 mL CH₂Cl₂ for 10 min. The solution was then cooled to -23 °C in a CCl₄/dry ice bath, a solution of tetraester **163** (1.91 g, 2.56 mmol) in 10 mL of CH₂Cl₂ was added, and the flask was stoppered. After 1 h the reaction mixture was extracted with three 100-mL portions of H₂O and 100 mL of saturated aqueous NaCl solution. The organic phase was concentrated to afford a yellow oil, which solidified on standing. Column chromatography on silica gel (5% CH₃OH/CHCl₃) afforded 1.47 g (88%) of **166** as a white solid: mp 95-96 °C; IR (KBr) 3316, 2971, 1720, 1611, 1599, 1440, 1257, 1119, 761, 697 cm⁻¹; ¹H NMR (CDCl₃) δ 11.83 (br s, 1 H), 8.94 (d, *J* = 2.0 Hz, 1 H), 8.70 (d, *J* = 2.2 Hz, 1 H), 8.40 (d, *J* = 2.4 Hz, 1 H), 8.38 (d, *J* = 2.2 Hz, 1 H), 7.30 - 7.60 (m, 15 H), 5.46 (s, 2 H), 5.402 (s, 2 H), 5.398 (s, 2 H), 1.71 (s, 6 H); HRMS (CI, NH₃) calcd for C₄₀H₃₃O₉ (M + H), 657.2124; found, 657.2127.

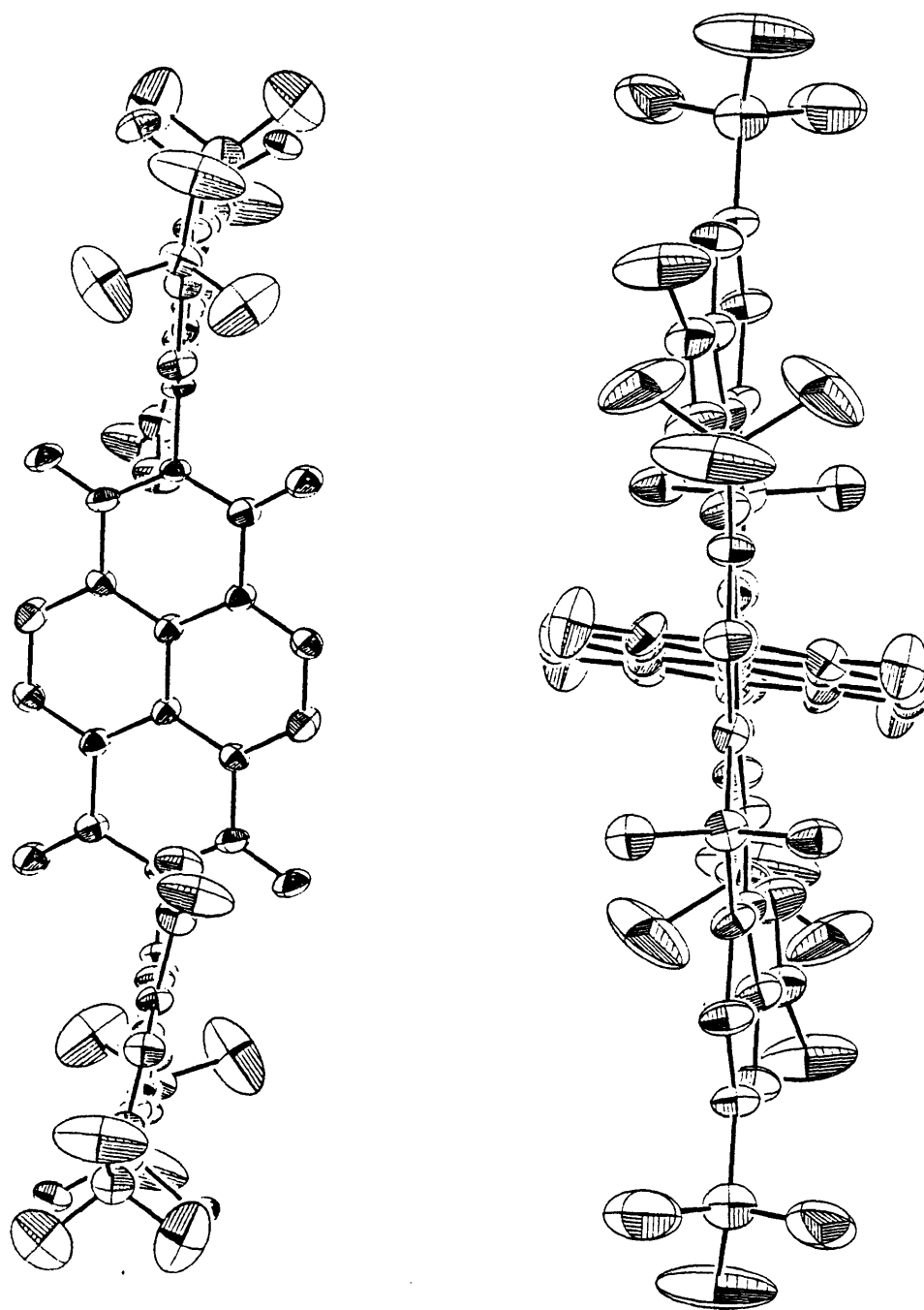
Appendix I

POSITIONAL PARAMETERS FOR S-DIACID 74s

atom	X	Y	Z	B(eq)
O1	0.0169(5)	0.2416(3)	0.487(1)	3.6(3)
O2	-0.0332(5)	0.2027(4)	-0.034(1)	5.3(4)
O3	-0.1713(6)	0.0836(4)	0.523(1)	5.9(4)
O4	0.3060(6)	0.2239(5)	0.425(2)	10.1(6)
O5	0.1577(5)	0.1757(4)	0.340(1)	5.5(4)
O6S	0.7573(7)	0.9255(5)	0.860(2)	7.9(2)
O7S	0.6327(8)	0.9692(6)	1.011(2)	11.6(3)
N1	-0.1043(5)	0.1421(4)	0.245(1)	2.9(4)
C1	0.1822(7)	0.2782(5)	0.611(2)	3.4(5)
C2	0.2482(7)	0.3217(6)	0.746(2)	4.3(5)
C3	0.2245(7)	0.3751(5)	0.895(2)	4.0(5)
C4	0.1290(7)	0.3856(5)	0.894(2)	4.0(5)
C5	0.0583(6)	0.3440(5)	0.756(2)	3.2(5)
C6	0.0842(7)	0.2892(5)	0.620(2)	2.9(5)
C7	-0.0483(7)	0.3625(5)	0.760(2)	3.2(5)
C8	-0.1128(6)	0.3086(4)	0.604(2)	2.5(4)
C9	-0.2112(7)	0.3125(5)	0.573(2)	3.5(5)
C10	-0.2734(7)	0.2647(5)	0.433(2)	3.5(5)
C11	-0.2373(7)	0.2080(5)	0.326(2)	3.7(5)
C12	-0.1409(8)	0.2017(5)	0.352(2)	3.4(5)
C13	-0.0795(6)	0.2523(5)	0.486(2)	2.6(4)
C14	0.2193(8)	0.2236(6)	0.456(2)	4.3(6)
C15	-0.0464(7)	0.1489(5)	0.050(2)	3.4(5)
C16	-0.1232(7)	0.0843(5)	0.351(2)	3.6(5)
C17	-0.0548(7)	-0.0929(5)	0.241(2)	4.2(6)
C18	-0.0035(6)	0.0894(5)	-0.050(2)	2.9(5)
C19	-0.0215(6)	0.0291(5)	0.050(2)	2.8(5)
C20	-0.0799(7)	0.0238(5)	0.245(2)	3.1(5)
C21	-0.0971(7)	-0.0353(5)	0.341(2)	4.0(5)
C22	0.3005(9)	0.4235(7)	1.049(2)	5.5(7)
C23	0.3930(1)	0.3960(1)	1.070(3)	14.0(1)
C24	0.3250(1)	0.4905(9)	0.961(3)	12.0(1)
C25	0.2570(1)	0.4389(9)	1.288(3)	10.0(1)
C26	-0.0384(7)	0.4324(5)	0.681(2)	4.7(5)

C27	-0.0908(7)	0.3652(5)	0.997(2)	4.2(5)
C28	-0.3814(7)	0.2721(6)	0.402(2)	4.2(5)
C29	-0.4130(1)	0.3290(1)	0.547(3)	15.0(1)
C30	-0.4500(1)	0.2071(8)	0.461(4)	12.0(1)
C31	-0.3960(1)	0.2760(1)	0.155(3)	13.0(1)
C32S	0.6810(1)	0.9150(1)	0.988(3)	9.3(4)
C33S	0.6490(1)	0.8618(8)	1.121(3)	9.4(4)
C34S	0.6610(1)	1.0370(1)	0.905(3)	11.6(5)
C35S	0.6060(2)	1.0150(1)	0.713(4)	15.0(7)
H1	0.3147	0.3148	0.7410	4.9
H2	0.1105	0.4241	0.9904	4.5
H3	-0.2378	0.3509	0.6522	4.1
H4	-0.2788	0.1743	0.2300	4.5
H5	-0.0663	-0.1339	0.3104	4.7
H6	-0.1365	-0.0386	0.4741	4.2
H7	0.3759	0.3547	1.1339	18.7
H8	0.4368	0.4288	1.1617	18.7
H9	0.4213	0.3872	0.9234	18.7
H10	0.3515	0.4834	0.8145	14.9
H11	0.3706	0.5202	1.0580	14.9
H12	0.2657	0.5085	0.9601	14.9
H13	0.3055	0.4706	1.3727	12.0
H14	0.2426	0.3972	1.3476	12.0
H15	0.2003	0.4578	1.2762	12.0
H16	-0.0131	0.4302	0.5295	5.4
H17	0.0056	0.4658	0.7747	5.4
H18	-0.1012	0.4462	0.6863	5.4
H19	-0.1562	0.3741	0.9987	4.5
H20	-0.0514	0.4001	1.0944	4.5
H21	-0.0920	0.3217	1.0482	4.5
H22	-0.3749	0.3706	0.5187	17.0
H23	-0.4063	0.3222	0.7008	17.0
H24	-0.4811	0.3283	0.5224	17.0
H25	-0.5165	0.2108	0.4351	13.7
H26	-0.4429	0.2031	0.6141	13.7
H27	-0.4335	0.1681	0.3680	13.7
H28	-0.3572	0.3163	0.1167	15.4
H29	-0.4636	0.2753	0.1356	15.4
H30	-0.3764	0.2366	0.0705	15.4





Intramolecular Distances

atom	atom	distance	ADC(*)	atom	atom	distance	ADC(*)
O1	C6	1.39(1)	1	C8	C9	1.40(1)	1
O1	C13	1.385(9)	1	C8	C13	1.38(1)	1
O2	C15	1.23(1)	1	C9	C10	1.38(1)	1
O3	C16	1.20(1)	1	C9	H3	0.965	1
O4	C14	1.20(1)	1	C10	C11	1.38(1)	1
O5	C14	1.30(1)	1	C10	C28	1.54(1)	1
O6S	C32S	1.28(2)	1	C11	C12	1.38(1)	1
O7S	C32S	1.36(2)	1	C11	H4	0.944	1
O7S	C34S	1.56(2)	1	C12	C13	1.38(1)	1
N1	C12	1.43(1)	1	C15	C18	1.46(1)	1
N1	C15	1.39(1)	1	C16	C20	1.49(1)	1
N1	C16	1.37(1)	1	C17	C18	1.37(1)	2
C1	C2	1.35(1)	1	C17	C21	1.42(1)	1
C1	C6	1.40(1)	1	C17	H5	0.953	1
C1	C14	1.48(1)	1	C18	C19	1.39(1)	1
C2	C3	1.37(1)	1	C19	C19	1.44(2)	2
C2	H1	0.950	1	C19	C20	1.39(1)	1
C3	C4	1.37(1)	1	C20	C21	1.36(1)	1
C3	C22	1.54(1)	1	C21	H6	0.949	1
C4	C5	1.39(1)	1	C22	C23	1.50(2)	1
C4	H2	0.958	1	C22	C24	1.48(2)	1
C5	C6	1.36(1)	1	C22	C25	1.53(2)	1
C5	C7	1.58(1)	1	C23	H7	0.939	1
C7	C8	1.51(1)	1	C23	H8	0.938	1
C7	C26	1.52(1)	1	C23	H9	0.953	1
C7	C27	1.51(1)	1	C24	H10	0.939	1

Distances are in angstroms. Estimated standard deviations in the least significant figure are given in parentheses.

Intramolecular Distances				(cont)			
atom	atom	distance	ADC(*)	atom	atom	distance	ADC(*)
C24	H11	0.945	1				
C24	H12	0.946	1				
C25	H13	0.944	1				
C25	H14	0.937	1				
C25	H15	0.939	1				
C26	H16	0.955	1				
C26	H17	0.953	1				
C26	H18	0.952	1				
C27	H19	0.948	1				
C27	H20	0.947	1				
C27	H21	0.956	1				
C28	C29	1.45(2)	1				
C28	C30	1.53(2)	1				
C28	C31	1.52(2)	1				
C29	H22	0.924	1				
C29	H23	0.962	1				
C29	H24	0.955	1				
C30	H25	0.960	1				
C30	H26	0.944	1				
C30	H27	0.944	1				
C31	H28	0.936	1				
C31	H29	0.946	1				
C31	H30	0.944	1				
C32S	C33S	1.40(2)	1				
C34S	C35S	1.39(2)	1				

Distances are in angstroms. Estimated standard deviations in the least significant figure are given in parentheses.

Intermolecular Distances

atom	atom	distance	ADC(*)	atom	atom	distance	ADC(*)
O1	H5	2.807	55602	O5	C32S	3.48(2)	66602
O1	O2	3.09(1)	55601	O5	C21	3.56(1)	55602
O2	H21	2.620	55401	O6S	H6	2.788	66501
O2	C6	3.09(1)	55401	O6S	C14	3.36(1)	66602
O2	C5	3.27(1)	55401	O6S	C20	3.44(1)	66601
O2	C13	3.30(1)	55401	O6S	C19	3.50(1)	66601
O2	C27	3.45(1)	55401	O6S	C21	3.50(1)	66601
O2	C8	3.57(1)	55401	C1	H14	3.002	55401
O3	C34S	3.28(2)	44501	C1	H5	3.113	55602
O3	C35S	3.35(2)	44501	C2	H14	3.005	55401
O3	H5	3.401	55602	C3	H14	3.362	55401
O3	C17	3.45(1)	55602	C4	H14	3.583	55401
O3	C18	3.51(1)	55601	C5	H14	3.566	55401
O4	H25	2.513	65501	C6	H5	3.144	55602
O4	O6S	3.22(1)	66602	C6	H14	3.318	55401
O4	H24	3.300	65501	C8	H21	3.372	55401
O4	H7	3.313	55401	C9	H21	3.488	55401
O4	C32S	3.47(2)	66602	C10	H21	3.466	55401
O4	C30	3.47(1)	65501	C11	H21	3.317	55401
O4	C33S	3.55(2)	66702	C12	H21	3.164	55401
O4	C33S	3.56(2)	66602	C13	H21	3.159	55401
O4	H29	3.597	65501	C14	H5	2.943	55602
O5	H5	2.552	55602	C14	H14	3.563	55401
O5	O6S	2.64(1)	66602	C16	H5	3.304	55602
O5	H6	3.054	55602	C16	C17	3.51(2)	55602
O5	C17	3.32(1)	55602	C20	H6	3.440	55602

Contacts out to 3.60 angstroms. Estimated standard deviations in the least significant figure are given in parentheses.

Intermolecular Distances				(cont)			
atom	atom	distance	ADC(*)	atom	atom	distance	ADC(*)
C20	C21	3.52(1)	55602	H1	H24	3.031	65501
C21	C21	3.34(2)	55602	H1	H14	3.338	55401
C21	H6	3.454	55602	H2	H18	3.027	56702
C23	H29	3.449	65601	H2	H17	3.092	56702
C23	H11	3.485	66702	H2	H16	3.578	55601
C24	H8	3.481	66702	H3	H28	3.259	55601
C24	H13	3.510	55401	H3	H12	3.450	56702
C25	H18	3.401	56702	H7	H29	2.946	65601
C25	H10	3.410	55601	H7	H24	3.277	65601
C26	H16	3.125	56602	H8	H11	2.980	66702
C26	H15	3.378	56702	H8	H10	3.117	66702
C26	H20	3.449	56702	H8	H24	3.497	65601
C26	H20	3.492	55401	H8	H29	3.556	65601
C26	H2	3.511	56702	H9	H24	2.906	65501
C26	H17	3.587	56602	H9	H23	3.073	65501
C26	H17	3.595	56702	H9	H11	3.115	66702
C27	H16	3.415	55601	H9	H29	3.372	65601
C27	H17	3.467	56702	H10	H13	2.718	55401
C29	H9	3.374	45501	H10	H14	3.340	55401
C29	H11	3.529	56702	H11	H22	3.099	56702
C29	H28	3.588	55601	H11	H23	3.232	56702
C31	H23	3.014	55401	H11	H28	3.598	56602
C31	H26	3.403	55401	H12	H19	2.986	56702
C33S	H26	3.323	56702	H12	H18	3.195	56702
C33S	H25	3.484	56702	H12	H13	3.534	55401
C34S	H4	3.130	66601	H12	H28	3.577	56602

Contacts out to 3.60 angstroms. Estimated standard deviations in the least significant figure are given in parentheses.

Intermolecular Distances

(cont)

atom	atom	distance	ADC(*)	atom	atom	distance	ADC(*)
H13	H22	3.123	56702				
H13	H18	3.574	56702				
H15	H18	2.528	56702				
H15	H16	3.238	55601				
H15	H17	3.501	56702				
H16	H20	2.649	55401				
H16	H16	2.809	56602				
H16	H17	2.930	56602				
H16	H18	3.084	56602				
H16	H21	3.447	55401				
H17	H20	2.648	56702				
H17	H17	2.861	56702				
H17	H18	3.552	56602				
H18	H20	3.513	56702				
H19	H28	2.896	55601				
H23	H28	2.637	55601				
H23	H29	2.916	55601				
H23	H30	3.065	55601				
H26	H30	2.876	55601				
H26	H29	3.276	55601				

Contacts out to 3.60 angstroms. Estimated standard deviations in the least significant figure are given in parentheses.

Torsion or Conformation Angles

(1)	(2)	(3)	(4)	angle	(1)	(2)	(3)	(4)	angle
O1	C6	C1	C2	-177.0(9)	N1	C16	C20	C21	-179.0(9)
O1	C6	C1	C14	6(1)	C1	C2	C3	C4	-3(2)
O1	C6	C5	C4	175.3(9)	C1	C2	C3	C22	179(1)
O1	C6	C5	C7	-5(1)	C1	C6	O1	C13	-177.6(8)
O1	C13	C8	C7	-4(1)	C1	C6	C5	C4	-4(1)
O1	C13	C8	C9	176.5(8)	C1	C6	C5	C7	175.2(9)
O1	C13	C12	N1	5(1)	C2	C1	C6	C5	3(2)
O1	C13	C12	C11	-176.2(9)	C2	C3	C4	C5	2(2)
O2	C15	N1	C12	-5(1)	C2	C3	C22	C23	-17(2)
O2	C15	N1	C16	-179.8(9)	C2	C3	C22	C24	106(1)
O2	C15	C18	C17	1(1)	C2	C3	C22	C25	-138(1)
O2	C15	C18	C19	-179.2(9)	C3	C2	C1	C6	1(2)
O3	C16	N1	C12	3(1)	C3	C2	C1	C14	179(1)
O3	C16	N1	C15	178(1)	C3	C4	C5	C6	2(2)
O3	C16	C20	C19	-178(1)	C3	C4	C5	C7	-177(1)
O3	C16	C20	C21	2(2)	C4	C3	C22	C23	166(1)
O4	C14	C1	C2	-11(2)	C4	C3	C22	C24	-71(2)
O4	C14	C1	C6	166(1)	C4	C3	C22	C25	45(2)
O5	C14	C1	C2	172(1)	C4	C5	C7	C8	-177.6(9)
O5	C14	C1	C6	-10(2)	C4	C5	C7	C26	63(1)
O6S	C32S	O7S	C34S	0(2)	C4	C5	C7	C27	-57(1)
N1	C12	C11	C10	179(1)	C5	C4	C3	C22	179(1)
N1	C12	C13	C8	-176.0(9)	C5	C6	O1	C13	3(1)
N1	C15	C18	C17	-179.7(9)	C5	C6	C1	C14	-175(1)
N1	C15	C18	C19	0(1)	C5	C7	C8	C9	-179.1(9)
N1	C16	C20	C19	2(1)	C5	C7	C8	C13	2(1)

The sign is positive if when looking from atom 2 to atom 3 a clockwise motion of atom 1 would superimpose it on atom 4.

Torsion or Conformation Angles					(cont)				
(1)	(2)	(3)	(4)	angle	(1)	(2)	(3)	(4)	angle
C6	O1	C13	C8	2(1)	C12	C11	C10	C28	180(1)
C6	O1	C13	C12	-178.9(8)	C13	C8	C7	C26	120(1)
C6	C5	C7	C8	3(1)	C13	C8	C7	C27	-119(1)
C6	C5	C7	C26	-117(1)	C13	C12	N1	C15	-79(1)
C6	C5	C7	C27	124(1)	C13	C12	N1	C16	96(1)
C7	C8	C9	C10	-180(1)	C15	N1	C16	C20	-2(1)
C7	C8	C13	C12	176.9(9)	C15	C18	C17	C21	-179.9(9)
C8	C9	C10	C11	3(2)	C15	C18	C19	C19	-180(1)
C8	C9	C10	C28	-179(1)	C15	C18	C19	C20	0(1)
C8	C13	C12	C11	3(1)	C16	N1	C15	C18	1(1)
C9	C8	C7	C26	-61(1)	C16	C20	C19	C18	-1(1)
C9	C8	C7	C27	60(1)	C16	C20	C19	C19	179(1)
C9	C8	C13	C12	-2(1)	C16	C20	C21	C17	-179.2(9)
C9	C10	C11	C12	-2(2)	C17	C18	C19	C19	0(2)
C9	C10	C28	C29	-5(2)	C17	C18	C19	C20	-180(1)
C9	C10	C28	C30	-124(1)	C17	C21	C20	C19	0(1)
C9	C10	C28	C31	120(1)	C18	C17	C21	C20	0(2)
C10	C9	C8	C13	0(1)	C18	C19	C19	C20	0(2)
C10	C11	C12	C13	0(2)	C18	C19	C20	C21	180(1)
C11	C10	C28	C29	172(1)	C19	C18	C17	C21	0(1)
C11	C10	C28	C30	54(2)	C19	C19	C20	C21	0(2)
C11	C10	C28	C31	-62(2)	C32S	O7S	C34S	C35S	92(2)
C11	C12	N1	C15	102(1)	C33S	C32S	O7S	C34S	172(1)
C11	C12	N1	C16	-83(1)					
C12	N1	C15	C18	175.7(8)					
C12	N1	C16	C20	-176.6(8)					

The sign is positive if when looking from atom 2 to atom 3 a clockwise motion of atom 1 would superimpose it on atom 4.

Intramolecular Bond Angles

atom	atom	atom	angle	atom	atom	atom	angle
C6	O1	C13	118.3(7)	C8	C7	C26	110.4(8)
C32S	O7S	C34S	128(1)	C8	C7	C27	110.2(8)
C12	N1	C15	117.5(8)	C26	C7	C27	109.9(8)
C12	N1	C16	117.2(8)	C7	C8	C9	121.4(8)
C15	N1	C16	125.1(9)	C7	C8	C13	122.6(8)
C2	C1	C6	118(1)	C9	C8	C13	116.0(9)
C2	C1	C14	117(1)	C8	C9	C10	123.8(9)
C6	C1	C14	124(1)	C8	C9	H3	118.87
C1	C2	C3	123.6(9)	C10	C9	H3	117.32
C1	C2	H1	119.12	C9	C10	C11	117.8(8)
C3	C2	H1	117.29	C9	C10	C28	121.6(9)
C2	C3	C4	116.5(9)	C11	C10	C28	120.5(9)
C2	C3	C22	123(1)	C10	C11	C12	120.4(9)
C4	C3	C22	121(1)	C10	C11	H4	119.49
C3	C4	C5	122.7(9)	C12	C11	H4	120.08
C3	C4	H2	119.03	N1	C12	C11	120.3(9)
C5	C4	H2	118.23	N1	C12	C13	119.7(9)
C4	C5	C6	118.4(8)	C11	C12	C13	120.0(9)
C4	C5	C7	118.8(9)	O1	C13	C8	124.2(9)
C6	C5	C7	122.9(9)	O1	C13	C12	113.9(8)
O1	C6	C1	116.9(9)	C8	C13	C12	121.9(9)
O1	C6	C5	122.7(8)	O4	C14	O5	118(1)
C1	C6	C5	120.4(9)	O4	C14	C1	122(1)
C5	C7	C8	109.0(8)	O5	C14	C1	120(1)
C5	C7	C26	107.4(8)	O2	C15	N1	120.6(9)
C5	C7	C27	109.7(8)	O2	C15	C18	122(1)

Angles are in degrees. Estimated standard deviations in the least significant figure are given in parentheses.

Intramolecular Bond Angles (cont)

atom	atom	atom	angle	atom	atom	atom	angle
N1	C15	C18	117.3(9)	C22	C23	H8	108.82
O3	C16	N1	121(1)	C22	C23	H9	108.16
O3	C16	C20	122(1)	H7	C23	H8	111.49
N1	C16	C20	116.9(9)	H7	C23	H9	110.17
C18	C17	C21	120.8(9)	H8	C23	H9	110.27
C18	C17	H5	119.76	C22	C24	H10	108.69
C21	C17	H5	119.46	C22	C24	H11	108.04
C15	C18	C17	120(1)	C22	C24	H12	108.11
C15	C18	C19	120.0(9)	H10	C24	H11	110.89
C17	C18	C19	119.8(9)	H10	C24	H12	110.74
C18	C19	C19	119(1)	H11	C24	H12	110.27
C18	C19	C20	121.5(8)	C22	C25	H13	107.64
C19	C19	C20	119(1)	C22	C25	H14	107.15
C16	C20	C19	119.2(9)	C22	C25	H15	108.07
C16	C20	C21	120(1)	H13	C25	H14	111.17
C19	C20	C21	120.9(9)	H13	C25	H15	110.99
C17	C21	C20	120.0(9)	H14	C25	H15	111.60
C17	C21	H6	119.51	C7	C26	H16	109.79
C20	C21	H6	120.53	C7	C26	H17	110.26
C3	C22	C23	114(1)	C7	C26	H18	109.98
C3	C22	C24	109(1)	H16	C26	H17	108.82
C3	C22	C25	111(1)	H16	C26	H18	108.89
C23	C22	C24	110(1)	H17	C26	H18	109.07
C23	C22	C25	108(1)	C7	C27	H19	109.65
C24	C22	C25	106(1)	C7	C27	H20	110.13
C22	C23	H7	107.83	C7	C27	H21	108.62

Angles are in degrees. Estimated standard deviations in the least significant figure are given in parentheses.

Intramolecular Bond Angles (cont)

atom	atom	atom	angle	atom	atom	atom	angle
H19	C27	H20	109.97	H29	C31	H30	110.32
H19	C27	H21	109.17	O6S	C32S	O7S	110(2)
H20	C27	H21	109.28	O6S	C32S	C33S	131(2)
C10	C28	C29	114.5(9)	O7S	C32S	C33S	118(2)
C10	C28	C30	108.7(9)	O7S	C34S	C35S	96(1)
C10	C28	C31	108.5(9)				
C29	C28	C30	106(1)				
C29	C28	C31	112(1)				
C30	C28	C31	107(1)				
C28	C29	H22	110.55				
C28	C29	H23	107.59				
C28	C29	H24	108.47				
H22	C29	H23	110.72				
H22	C29	H24	111.33				
H23	C29	H24	108.05				
C28	C30	H25	108.82				
C28	C30	H26	109.38				
C28	C30	H27	109.86				
H25	C30	H26	109.14				
H25	C30	H27	109.08				
H26	C30	H27	110.53				
C28	C31	H28	108.47				
C28	C31	H29	107.77				
C28	C31	H30	107.93				
H28	C31	H29	111.04				
H28	C31	H30	111.19				

Angles are in degrees. Estimated standard deviations in the least significant figure are given in parentheses.